

Springer Aerospace Technology

Markus G. R. Sause
Elena Jasiūnienė
Editors

Structural Health Monitoring Damage Detection Systems for Aerospace

OPEN ACCESS

 Springer

Springer Aerospace Technology

Series Editors

Sergio De Rosa, DII, University of Naples Federico II, NAPOLI, Italy

Yao Zheng, School of Aeronautics and Astronautics, Zhejiang University,
Hangzhou, Zhejiang, China

Elena Popova, Air Navigation Bridge Russia, Chelyabinsk, Russia

The series explores the technology and the science related to the aircraft and spacecraft including concept, design, assembly, control and maintenance. The topics cover aircraft, missiles, space vehicles, aircraft engines and propulsion units. The volumes of the series present the fundamentals, the applications and the advances in all the fields related to aerospace engineering, including:

- structural analysis,
- aerodynamics,
- aeroelasticity,
- aeroacoustics,
- flight mechanics and dynamics
- orbital maneuvers,
- avionics,
- systems design,
- materials technology,
- launch technology,
- payload and satellite technology,
- space industry, medicine and biology.

The series' scope includes monographs, professional books, advanced textbooks, as well as selected contributions from specialized conferences and workshops.

The volumes of the series are single-blind peer-reviewed.

To submit a proposal or request further information, please contact:

Mr. Pierpaolo Riva at pierpaolo.riva@springer.com (Europe and Americas)
Mr. Mengchu Huang at mengchu.huang@springer.com (China)

The series is indexed in Scopus and Compendex


More information about this series at <http://www.springer.com/series/8613>


Markus G. R. Sause • Elena Jasiūnienė
Editors

Structural Health Monitoring Damage Detection Systems for Aerospace

 Springer

Editors

Markus G. R. Sause 
Institute of Materials Resource
Management
University of Augsburg
Augsburg, Germany

Elena Jasiūnienė 
Prof. K. Baršauskas Ultrasound Research
Institute
Kaunas University of Technology
Kaunas, Lithuania



ISSN 1869-1730

ISSN 1869-1749 (electronic)

Springer Aerospace Technology

ISBN 978-3-030-72191-6

ISBN 978-3-030-72192-3 (eBook)

<https://doi.org/10.1007/978-3-030-72192-3>

© The Editor(s) (if applicable) and The Author(s) 2021. This book is an open access publication.

Open Access This book is licensed under the terms of the Creative Commons Attribution 4.0 International License (<http://creativecommons.org/licenses/by/4.0/>), which permits use, sharing, adaptation, distribution and reproduction in any medium or format, as long as you give appropriate credit to the original author(s) and the source, provide a link to the Creative Commons license and indicate if changes were made.

The images or other third party material in this book are included in the book's Creative Commons license, unless indicated otherwise in a credit line to the material. If material is not included in the book's Creative Commons license and your intended use is not permitted by statutory regulation or exceeds the permitted use, you will need to obtain permission directly from the copyright holder.

The use of general descriptive names, registered names, trademarks, service marks, etc. in this publication does not imply, even in the absence of a specific statement, that such names are exempt from the relevant protective laws and regulations and therefore free for general use.

The publisher, the authors and the editors are safe to assume that the advice and information in this book are believed to be true and accurate at the date of publication. Neither the publisher nor the authors or the editors give a warranty, expressed or implied, with respect to the material contained herein or for any errors or omissions that may have been made. The publisher remains neutral with regard to jurisdictional claims in published maps and institutional affiliations.

This Springer imprint is published by the registered company Springer Nature Switzerland AG
The registered company address is: Gewerbestrasse 11, 6330 Cham, Switzerland

Preface

Why do we need structural health monitoring? Structural health monitoring (SHM) is a significant technology that would help avoid failures/accidents and improve the safety of various structures because it continuously monitors a structure's health and can immediately identify critical damage. SHM can also help reduce maintenance costs because it continuously monitors a structure's health and identifies the need for maintenance, thereby enabling the replacement of the schedule type maintenance with condition-based maintenance. Accordingly, research in the SHM field has been continuously increasing in the last years.

However, while SHM looks to be a promising technology, it is still not widely used in practical applications and is limited to lab applications because not all issues/drawbacks/limitations are solved.

The scope of this publication is the definition of the current state of the art in SHM applications in aerospace. Within the COST ACTION 18203—Optimized Design for Inspection (ODIN), experts from the field of structural health monitoring were asked to compile the current state of the art and put it into a closed form. This current document shall form the starting point for future SHM investigations and serve as a reference for the current state of the art in 2020. The publication focuses on SHM application in the field of aviation, the associated challenges, as well as the technical regulations and restrictions that go along with them.

The publication shall provide an overview for newcomers and experienced users alike for the use of different condition monitoring systems. The focus is on a clear presentation of the fundamentals and basics and the elaboration of the current challenges. Wherever possible, reference is made to standard literature in the field and current application examples that already exist in the field.

The work is divided into 10 chapters. It starts with a short introduction to the topic, a definition of structural health monitoring in the context of aerospace applications, and a presentation of typical defects, followed up by a discussion of

the specific requirements in the aviation sector. The main focus is on different structural health monitoring methods and signal reduction and processing methods. Finally, the current state of the art is evaluated and summarized.

Augsburg, Germany
Kaunas, Lithuania

Markus G. R. Sause
Elena Jasiūnienė

Acknowledgment

This publication is based upon work from COST Action 18203—Optimized Design for Inspection (ODIN), supported by COST (European Cooperation in Science and Technology).

Contents

1	Introduction	1
	Markus G. R. Sause, Elena Jasiūnienė, and Rhys Pullin	
2	Monitoring Tasks in Aerospace	5
	Shashank Pant, Zahra Sharif Khodaei, and Mohamad Ghazi Droubi	
3	Defect Types	15
	Nadimul Faisal, Ömer Necati Cora, Muhammed Latif Bekci, Romana Ewa Śliwa, Yehuda Sternberg, Shashank Pant, Richard Degenhardt, and Anil Prathuru	
4	Aerospace Requirements	73
	Zahra Sharif Khodaei and Stephen Grigg	
5	Ultrasonic Methods	87
	Vykintas Samaitis, Elena Jasiūnienė, Pawel Packo, and Damira Smagulova	
6	Vibration Response-Based Damage Detection	133
	Maria Pina Limongelli, Emil Manoach, Said Quqa, Pier Francesco Giordano, Basuraj Bhowmik, Vikram Pakrashi, and Alfredo Cigada	
7	Acoustic Emission	175
	Dimitrios G. Aggelis, Markus G. R. Sause, Pawel Packo, Rhys Pullin, Steve Grigg, Tomaž Kek, and Yu-Kun Lai	
8	Strain Monitoring	219
	Steve Vanlanduit, Mario Sorgente, Aydin R. Zadeh, Alfredo Güemes, and Nadimul Faisal	

9 Data Reduction Strategies 243
Basuraj Bhowmik, Said Quqa, Markus G. R. Sause,
Vikram Pakrashi, and Mohamad Ghazi Droubi

10 Conclusions 273
Elena Jasiūnienė, Markus G. R. Sause, Vykintas Samaitis,
Dimitrios G. Aggelis, Maria Pina Limongelli, and Steve Vanlanduit

Contributors

- Dimitrios G. Aggelis** Vrije Universiteit Brussel, Brussels, Belgium
- Muhammed Latif Bekci** Karadeniz Technical University, Trabzon, Turkey
- Basuraj Bhowmik** University College Dublin, Dublin, Ireland
- Alfredo Cigada** Politecnico di Milano, Milano, Italy
- Ömer Necati Cora** Karadeniz Technical University, Trabzon, Turkey
- Richard Degenhardt** German Aerospace Center (DLR), Braunschweig, Germany
- Mohamad Ghazi Droubi** Robert Gordon University, Aberdeen, UK
- Nadimul Faisal** Robert Gordon University, Aberdeen, UK
- Pier Francesco Giordano** Politecnico di Milano, Milano, Italy
- Stephen Grigg** Cardiff University, Cardiff, UK
- Alfredo Güemes** Technical University of Madrid, Madrid, Spain
- Elena Jasiūnienė** Prof. K. Baršauskas Ultrasound Research Institute, Kaunas University of Technology, Kaunas, Lithuania
- Tomaž Kek** University of Ljubljana, Ljubljana, Slovenia
- Yu-Kun Lai** Cardiff University, Cardiff, UK
- Maria Pina Limongelli** Politecnico di Milano, Milano, Italy
- Emil Manoach** Institute of Mechanics, Bulgarian Academy of Sciences, Sofia, Bulgaria
- Pawel Packo** AGH University of Science and Technology, Krakow, Poland
- Vikram Pakrashi** University College Dublin, Dublin, Ireland
- Shashank Pant** National Research Council Canada, Ottawa, ON, Canada

Anil Prathuru Robert Gordon University, Aberdeen, UK

Rhys Pullin Cardiff University, Cardiff, UK

Said Quqa University of Bologna, Bologna, Italy

Vykintas Samaitis Kaunas University of Technology, Kaunas, Lithuania

Markus G. R. Sause Institute of Materials Resource Management, University of Augsburg, Augsburg, Germany

Zahra Sharif Khodaei Imperial College London, London, UK

Romana Ewa Śliwa Rzeszow University of Technology, Rzeszow, Poland

Damira Smagulova Kaunas University of Technology, Kaunas, Lithuania

Mario Sorgente Optics 11, Amsterdam, The Netherlands

Yehuda Sternberg Israel Aerospace Industries Ltd, Ben Gurion, Israel

Steve Vanlanduit University of Antwerp, Antwerp, Belgium

Aydin R. Zadeh Optics 11, Amsterdam, The Netherlands

Chapter 1

Introduction



Markus G. R. Sause, Elena Jasiūnienė, and Rhys Pullin

The aerospace industry is aiming for a cleaner means of transport. One way to achieve this is by making transportation lighter, thus directly improving fuel efficiency and reducing environmental impact. A further aim, of the industry, is to reduce maintenance time to lessen operating costs, which can result in a reduction of air transport costs, benefitting both passenger and freight services. Current developments to support these aims include using advanced materials, with the current generation of aerospace structures being 50% composite materials. These materials offer a weight reduction whilst maintaining adequate stiffness; however, their damage mechanics are very complex and less deterministic than those of metals. This results in an overall reduced benefit. Structures are manufactured thicker using additional material to accommodate unknown or unpredictable failure modes, which cannot be easily detected during maintenance. A way to overcome these issues is the adoption of a structural health monitoring (SHM) inspection system.

Structural health monitoring (SHM) is understood to be the continuous or periodic and automated method for determining and monitoring the condition of a monitored object within condition monitoring (according to DIN ISO 17359). This is conducted through measurements with permanently installed or integrated transducers and the analysis of the measurement data. Its purpose is to detect damage, for example, cracks or deformations, at an early stage to initiate countermeasures. A frequently quoted example for SHM is the human skin, whose pain receptors provide

M. G. R. Sause (✉)

Institute of Materials Resource Management, University of Augsburg, Augsburg, Germany
e-mail: markus.sause@mrm.uni-augsburg.de

E. Jasiūnienė

Prof. K. Baršauskas Ultrasound Research Institute, Kaunas University of Technology,
Kaunas, Lithuania

R. Pullin

Cardiff University, Cardiff, UK

© The Author(s) 2021

M. G. R. Sause, E. Jasiūnienė (eds.), *Structural Health Monitoring Damage Detection Systems for Aerospace*, Springer Aerospace Technology,
https://doi.org/10.1007/978-3-030-72192-3_1

spatially resolved and timely information about both physical stress and state of health.

An SHM system comprises the monitoring object with transducers, signal acquisition and transfer units and data storage devices, the data processing system and the (automated) diagnostic system. The determination of the status of the monitored object can be conducted in various degrees of detail. This can include the current recording of the stress (e.g. as a result of an acting load or environmental influences), damage detection and the determination of the type of damage up to the assessment of the effects (the integrity of the monitored object, stability and load-bearing capacity). Objects to be monitored are primarily structures with load-bearing properties and/or frequently statically supported structures.

In the case of aerospace applications, these structures are landing gears, wing boxes, tails, struts and other load-bearing primary structures of the aircraft. For helicopters, rotor blades and their attachment structures, as well as the life cell of the helicopter, are the primary targets for SHM applications.

The knowledge about the existence of critical internal defects stems from their relevance during the operation of aerospace structures. Usually, tests of components are conducted according to fixed times in intervals regulated by flight safety standards. The inspection intervals must be selected in such a way that damage is detected with a given certainty before total failure of the structure occurs.

In contrast to this (classical) approach, the SHM method provides characteristic values at any time, which results in information on whether or not the damage is present. Airlines expect to save up to 40% in maintenance time through this determination alone. Additionally, to the sole knowledge about the damage, the second step is to determine the location and size of the damage, so that in the third step, a statement can be made as to what influence the damage has on the properties of the structure and whether or not it is necessary to replace the component immediately.

Acoustic emission (AE) and acousto-ultrasonics (AU) (10–1000 kHz) based SHM systems that utilize energy harvesting for power generation and wireless sensor networks for communication are being increasingly demonstrated to be effective in monitoring damage in simple plates and aerospace components in a laboratory setting. AE is a passive system that detects and locates stress waves as a structure undergoes damage. AU is an active system that sends out waves and monitors, periodically, for changes in the received wave to identify structural damage. Batteries are currently not allowed within aerospace structures, and the addition of cables to power a system or transfer data adds increased weight to the aircraft, removing any benefit. Hence, energy harvesting and wireless communication are essential for any aerospace SHM system as schematically outlined in Fig. 1.1. Furthermore, the large data sets produced need reliable analysis to deliver prognosis and methods of interpretation that non-specialists can understand. Additionally, vibration-based monitoring methods have been developed with a certain degree of maturity for civil engineering applications. The transfer of the established approaches to aerospace structures has been demonstrated on the lab scale and seems promising for SHM in aerospace structures as well. Finally, the use of strain

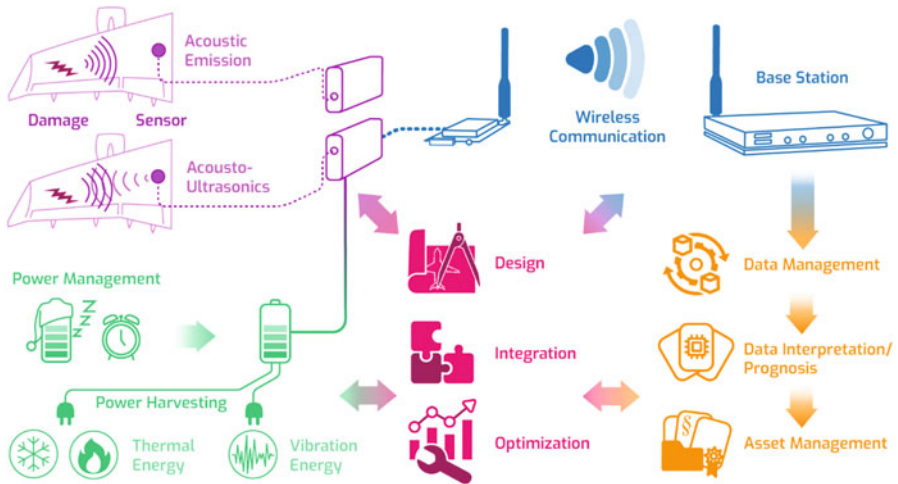


Fig. 1.1 Schematic for the operation of SHM system in aerospace applications

measurement systems in aerospace structures is existent for decades. Modern methods using optical fiber system are emerging in this field and provide an interesting portfolio of applications exceeding the performance and drawbacks of the classical strain gage-based monitoring methods.

COST action ‘Optimizing design for inspection’ (ODIN) CA18203 brought together experts in the fields of NDE/SHM, energy harvesting and wireless sensor networks to integrate these in an aircraft structure, designed and optimized for the implementation. This COST action aims to advance Europe’s position of strength in the aerospace industry through the development of optimized intelligent structures integrated at the design inception phase. The objective of this action is to develop an integrated framework for optimized self-sensing structures capable to diagnose damage as envisioned in Fig. 1.2. The idea is to develop in-service, continuous monitoring of critical aerospace structures by integrating non-destructive evaluation, energy harvesting and wireless sensor technologies at the design phase. This should improve the maintenance effectiveness, by reducing operating costs and, at the same time, increasing safety. To achieve the main objective, the state of the art of the SHM damage detection systems, including sensing technologies, reliability/durability and data acquisition, must be reviewed; methods for delivering the improvement of damage detection need to be identified. Furthermore, the state of the art of the current signal processing techniques must be evaluated. Signal processing techniques, which can identify/classify damage characteristics and parameters, need to be determined.

Within this publication, this network of experts compiled the current status of SHM systems as existent in 2020. Subsequent to this introduction, Chap. 2 will provide an overview of the typical targets of SHM applications in aerospace alongside a definition of its understanding throughout this work. Chapter 3 will

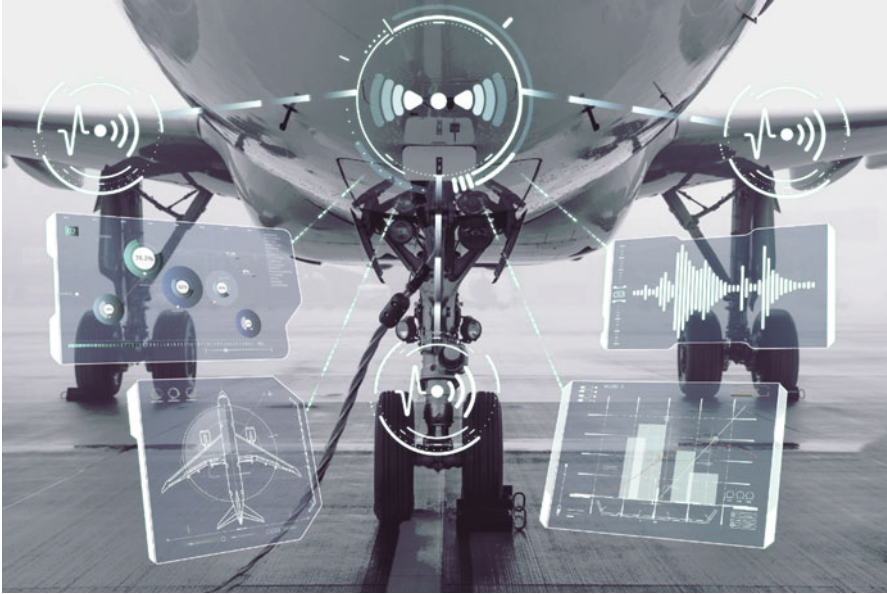


Fig. 1.2 Vision of SHM integration in future aircraft solutions

introduce the typical defects encountered in the materials that are used for primary aerospace structures. Chapter 4 will then set the aerospace requirements for the implementation, operation and reliability of SHM systems. Various techniques that are currently applied in aerospace applications are introduced and elaborated throughout Chaps. 5 to 8. Chapter 9 has its focus on the use data reduction strategies and the use of wireless sensing systems in this context. The work closes with a conclusion in Chap. 10 on the current state of the art of SHM systems to provide an up-to-date reference for future developments.

Open Access This chapter is distributed under the terms of the Creative Commons Attribution 4.0 International License (<http://creativecommons.org/licenses/by/4.0/>), which permits use, duplication, adaptation, distribution and reproduction in any medium or format, as long as you give appropriate credit to the original author(s) and the source, a link is provided to the Creative Commons license and any changes made are indicated.

The images or other third party material in this chapter are included in the work's Creative Commons license, unless indicated otherwise in the credit line; if such material is not included in the work's Creative Commons license and the respective action is not permitted by statutory regulation, users will need to obtain permission from the license holder to duplicate, adapt or reproduce the material.



Chapter 2

Monitoring Tasks in Aerospace



Shashank Pant, Zahra Sharif Khodaei, and Mohamad Ghazi Droubi

Abstract Approximately up to one-fifth of the direct operating cost of a commercial civilian fixed-wing aircraft is projected to be due to inspection and maintenance alone. Managing aircraft health with minimal human intervention and technologies that can perform continuous or on-demand monitoring/evaluation of aircraft components without having to take the aircraft out of service can have a significant impact on increasing availability while reducing maintenance cost. The ambition of these monitoring technologies is to shift aircraft maintenance practice from planned maintenance (PM), where the aircraft is taken out of service for scheduled inspection/maintenance, to condition-based maintenance (CBM), where aircraft is taken out of service only when maintenance is required, while maintaining the required levels of safety. Structural health monitoring (SHM) techniques can play a vital role in progressing towards CBM practice. Therefore, this chapter aims to provide the reader with a brief overview of the different SHM techniques and their use, as well as, challenges in implementing them for aircraft applications.

Aircraft structures are typically designed using safe-life (designed to surpass the required service life through rigorous fatigue testing), fail-safe (having multiple load paths in case one of the components fail) or damage tolerance (discontinuities are assumed to exist from initial manufacturing; thereby, requiring periodic inspections and maintenance to detect and repair such discontinuities before they reach a critical size). These practices in aircraft structural design and long-term performance require a high level of understanding of material performance in both durability and damage

S. Pant (✉)
National Research Council Canada, Ottawa, ON, Canada
e-mail: shashank.pant@nrc-cnrc.gc.ca

Z. Sharif Khodaei
Imperial College London, London, UK

M. G. Droubi
Robert Gordon University, Aberdeen, UK

tolerance. This knowledge and sophisticated structural design tools are enabling newer generations of aircraft to be designed and built using newer and less material to tighter margins, resulting in improved performance in terms of increased operational capability (distance flown and cargo capacity).

Aircraft operators are always seeking ways to improve their existing fleet operation by increasing aircraft availability and reducing overall costs. Keeping the aircraft flying longer, increases the inspection and maintenance requirement. As described in (IATA 2018), the increase in civilian aircraft aging related maintenance cost can be attributed to three main causes: (i) due to increase in routine maintenance driven by scheduled maintenance program; (ii) due to non-routine maintenance, which can be discovered during routine maintenance actions or by unexpected faults and failures; and (iii) due to compliance with the mandatory maintenance actions as called out by airworthiness directives (ADs) and service bulletins (SBs). ADs and SBs can have one-time cost, where the solution is implemented and no addition cost is incurred thereafter or can have an ongoing cost, where permanent fix is not available, thereby requiring repetitive additional inspections (IATA 2018). In the military domain, operators around the world are flying aging aircraft way past their nominal designed life through service life extension programs to fulfill current and future requirements (Maksimović et al. 2015). One of the best example of the service life extension is Boeing B-52 bomber, which first entered in-service in the 1950s and has been continuously upgraded to be flown until 2050s (Collins Aerospace 2020). Extending the life of a component often entails increasing the inspection requirement, which in turn increases the cost and reduces the aircraft availability. There is also a rise in cost due to an increase in periodic inspection to maintain aircraft whose service life has been extended past the optimal designed life. Accurate estimation of overall maintenance cost is challenging as it varies from aircraft to aircraft (narrow-body, wide-body, rotorcraft, etc.) and operator to operator (civilian, military, etc.). As reported by (Heisey 2002), for commercial airline industry, depending on airplane age, type, and range, maintenance costs can represent between 10 and 20% of the overall direct operating cost, which includes cost of ownership, flight crew, fuel, maintenance, and others.

As the number of inspection and maintenance increases so may the number of potential maintenance-related damages such as accidental tool-drops, improper repairs, etc. Some of these maintenance-related damages can be catastrophic at times, such as in the case of China Airlines Flight 611, where fatigue cracks began from a damage due to tail strike incident that was not repaired following the original equipment manufacturer (OEM) suggested procedure. The fatigue cracks grew under the repaired doubler and went undetected, which led to the in-flight breakup of the aircraft killing all on board (IASA 2005). A similar example can be found in Japan Airlines Flight 123, where a poorly repaired rear pressure bulkhead gave way in flight that caused explosive decompression killing 520 passengers (Aircraft Accident Investigation Report 1985). These catastrophic failures due to human errors are very rare; nonetheless, they can still occur. Manual inspection plays a major role in maintaining aircraft safety; however, there are limitations in terms of the detectable size of damage in composite structure with the current non-destructive



Fig. 2.1 Aircraft health management (SAE ARP6461 2013)

inspection (NDI) techniques. In particular, barely visible impact damage (BVID) if not detected, may cause catastrophic failure and is the main reason for conservative damage tolerant design of composite structure. Therefore, the current scheduled based maintenance have two main disadvantages: (i) the cost of the manual inspection and the loss in aircraft availability/revenue and (ii) the reliability of maintenance which depends on the technician skills; both of which can be reduced by implementing automated inspection techniques. In civilian domain operators are only allowed to use the aircraft within their given type certificate; however, for military aircraft, the actual flown mission profiles oftentimes vary from their initially OEM designed profiles. The actual mission profiles as flown by the military operators are difficult to track and mostly rely on flight crews' input and processing data from the operation load monitoring and flight data recorder (FDR) systems. Therefore, components that are designed using a safe-life approach may not be optimally utilized as they may be retired prematurely due to the difference in actual versus designed flight profiles. Conversely, if the aircraft is flown in severe missions than initially designed, the components may fail prematurely and can be detrimental for flight safety. This also highlights the interest in operation monitoring for an aircraft, where load levels can be recorded to inform the operators about the remaining useful life (RUL) at the aircraft level, as well as, optimization of the maintenance and operation at the fleet level.

Aircraft operators both civil and military are always looking for ways to reduce cost and increase availability by optimizing the use of aircraft components through the aircraft health management (AHM) approach, which is shown in Fig. 2.1.

Managing aircraft health with minimal human intervention and having to take the aircraft out of service for maintenance only when required can have a significant impact on increasing availability and reducing maintenance cost. This can be achieved through structural health monitoring (SHM) technique, which is an element of the structural health management, a subset of the aircraft health management, as

shown in Fig. 2.1. SHM aims to shift aircraft maintenance practice from planned maintenance (PM), where the aircraft is taken out of service for scheduled inspection/maintenance to condition-based maintenance (CBM) without compromising safety. However, this decision comes with a cost and higher complexity to the maintenance program.

There are several definitions of SHM. For example, in the military domain (MIL-STD-1530D 2016), United States Air Force (USAF) defines SHM as “a nondestructive inspection process or technique that uses in-situ sensing devices to detect damage”; whereas in the civilian domain (SAE ARP6461 2013), the Society of Automotive Engineers (SAE) (established in 1905 and now covers all types of transport vehicles including aircraft) defines SHM as “the process of acquiring and analyzing data from on-board sensors to determine the health of a structure,” which divides SHM into damage monitoring (DM) and operation monitoring (OM). Conversely, researchers from NASA have defined SHM as “a continuous assessment of structural integrity to increase safety and performance within design constraints to meet operational requirements” (Seshadri et al. 2014). Despite different definitions, common themes among all SHM systems are that they process the acquired data, whether from permanently installed onboard sensors or from other sources such as FDR with advanced data/signal processing techniques.

Currently, there are no certification standards for SHM to be integrated into a maintenance strategy for civil aircraft. There are only guidelines, one of which recommends following the SAE-APR6461 for implementation of SHM onboard civilian aircraft. Depending on how the inspection is carried out, an SHM system can be broken down into scheduled SHM (S-SHM) and automated SHM (A-SHM). The following are the differences between the two: A-SHM system does not have a pre-determined interval and relies on the system to inform the operator when and if any maintenance action is required; whereas, S-SHM system is set to run and acquire data at pre-determined fixed schedule regardless of damage presence (SAE ARP6461 2013).

Application of the SHM system can be widely divided into condition monitoring (CM), OM, and DM.

2.1 Condition Monitoring

Aircraft parts operate under harsh environments and with very strict airworthiness requirements for each part; therefore, their conditions are monitored thoroughly.

The CM system is designed to collect, process, integrate and transmit the information from electro-mechanical systems to avionics systems. The gathered information is then used to monitor the condition of the component.

For example, an aircraft engine constitutes the heart of the aircraft and is expected to work reliably under harsh operational conditions (e.g., high rotation speed, high temperature and pressure). A network of sensors monitors the temperature, pressure,

and gas flow within the engine and thus can assess whether the engine parameters are within the operational range in real-time.

Among the available methodologies, one of the promising technologies is prognostics and health management (PHM), which has been successfully applied in avionics and engines. PHM can in general be classified into three classes:

- Model-based method: for a system that can be represented by a mathematical model;
- Experience-based method: building stochastic models, not applicable to complex systems; and
- Data-driven method: based on sensor data and historical operation/test data. This is the only class that requires sensors.

PHM can be applied to different parts of the aircraft such as engines and structures. The data gathered from each system can also serve as input into the scheduled maintenance of the component.

2.2 Operation Monitoring (OM)

Operation monitoring are indirect methods that contribute to the evaluation of a structure's condition or utilization. The usage evaluation can lead to modifying inspection intervals as a function of aircraft use.

Some examples of operational monitoring include:

- Fatigue monitoring: evaluate the structural fatigue response based on related parameters such as flight hours and strain measurement.
- Exceedance monitoring: when the in-service load exceeds the design spectra.
- Environmental monitoring: temperature, humidity, etc. These data can contribute to the increase or decrease in inspection intervals when the environmental conditions vary significantly from the design criteria.

The output of the OM is based on information processed from the recorded data to provide a health assessment of the aircraft structure. The main difference between OM and CM is that operation monitoring records data during flight to assist an operator to identify, quantify, assess and address operational risk but does not provide any diagnosis in terms of the condition of the aircraft and whether a maintenance action is required. In addition, the OM output can be used to support a range of airworthiness and operational safety tasks to the fleet and the process is a subset of safety management system (SMS) of an airline. CM results in diagnosis (whether damage exists and if immediate action needs to be taken) for an aircraft in operation.

Load profiles recorded during operation can be used as an essential parameter to calculate accumulated life and to predict the remaining useful life. They can be monitored either using conventional strain gauges or by calculating the resulting load sequence from recorded flight parameters (e.g., speed, altitude and maneuver).

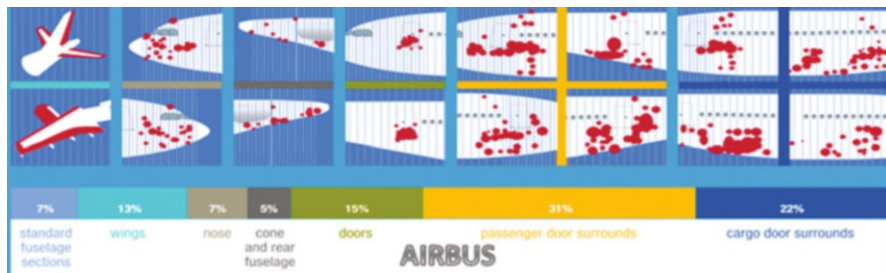


Fig. 2.2 Probable locations of impact damage within an aircraft (Favre and Morteau 2011)

With the recent developments in SHM techniques, load monitoring has also become an integrated part of the SHM, where the permanently installed sensors can record the load levels during the flight (Nicolas et al. 2016). Fiber optic sensors have gained a lot of interest in load monitoring due to their many advantages such as multiplexing, lightweight, immunity from electro-mechanical interference and high strain sensitivity (García et al. 2015).

Another application of OM is by monitoring and recording impact events (locations that are susceptible to impact damage are shown in Fig. 2.2) during the service-life of the aircraft. The current practice for designing aircraft composite structures is based on probable impacts and their energy levels. For each probable impact (e.g. bird impact at nose, debris impact at lower fuselage), the impact energy levels that is used in the composite structural design is based on metallic structures, where impact events during the service life of an aircraft leaves dents in the structure. By measuring the dents (size and depth), impact energies are estimated. However, this is a conservative approach which is adopted in designing a composite structure. A possible benefit of SHM in the context of OM is to record impact events for each aircraft to estimate the actual impact energy levels. By having a better estimation of the impact energy levels, design of the composite aircraft structures can be optimized, thus resulting in weight savings.

2.3 Damage Monitoring (DM)

In a typical damage monitoring system, permanently attached onboard sensors can be used to monitor aircraft structures continuously or at desired intervals. Processing and evaluation of data acquired from the sensors can be performed onboard or at a ground control station. The evaluation results can be used by the operators to locate and identify damage types, as well as, severity, such that proper maintenance action could be taken. The intent is to reduce the associated cost of performing NDI in areas that are prone to damage and are difficult to access, requiring disassembly of some components. A reliable DM system can also increase the service life of a structure or drive changes to the structural design allowing for a lighter structure.

DM can be classified based on the following sensor technologies:

- Piezoelectric transducers
- Optical fibers
- Micro-electro-mechanical system
- Eddy current foil sensor
- Comparative vacuum monitoring
- Hybrid systems

DM can also be classified based on the following techniques:

- Vacuum or pressure based: monitoring drop in vacuum pressure due to air leakage caused by cracks, defects, etc.
- Ultrasonic guided wave based: analyzing changes in propagation characteristics of guided waves using different algorithms for detecting damage, such as damage index approach, or detecting and localizing based on probability-based approach together with imaging technique such as delay and sum.
- Fiber optics: based on reflectivity shift, spectrum distortion or backscattering.
- Acoustic emission: monitoring release of energy due to impact, crack and damage formation.
- Vibration-based: monitoring change in modal parameters such as natural frequencies, mode shapes and damping due to the presence of damage.
- Conductive medium: measure change in electrical resistance or continuity.
- Data-driven methods: outlier analysis, machine-learning, advanced signal processing, etc., which could be applied to any DM techniques listed above.

Current DM systems span a wide range of technology readiness levels (TRLs), where some are commercially approved for use in United States commercial transport fleet such as comparative vacuum monitoring (CVM) (Swindell et al. 2017). Another example is the use of a conductive medium to detect tail strikes, developed and used by Airbus on its long-haul aircraft. The system consists of two sensors with two conductive mediums (crack wires) on each sensor, which indicates tail strikes to the flight crew. It was also mentioned that the system has “enabled Airbus designers to achieve a significant weight saving by integrating the tail strike system capabilities into the structural design” (Wenk and Bockenheimer 2014). These are two examples of SHM systems that are currently being used in aircraft; however, others are currently being developed and evaluated by OEMs, aircraft operators, research institutes, etc. Table 2.1 shows the examples of some of the most commonly used DM techniques; some of which are discussed in detail in the later chapters of this book.

2.4 Challenges

The use of the SHM system on an aircraft has been envisioned to minimize cost, time and human errors. There has been a significant advancement in research and development of novel sensors, advanced signal processing techniques, signal

Table 2.1 Summary of commonly used DM techniques

Method	Principle of operation	Detectable damage type	Strengths	Weaknesses
Comparative Vacuum Monitoring (CVM)	Cracks on the specimen surface create a leak within the vacuum. This can be tracked via a monitoring device.	Cracks, corrosion, debonding, delamination.	No need for electrical excitation. Can be performed off-line.	Hot-spot/local analysis. Sub-surface crack that do not interact with the vacuum gallery cannot be detected.
Acoustic Ultrasonic (AU)	The propagation properties of an ultrasonic guided wave depend on the state of the medium they travel through.	Cracks, change in thickness (corrosion), composite damage, delamination/debonding, etc.	Covers large distances, lightweight sensors, multi-modal, sensitive to various damage types based on the excitation modes.	Baseline is required (baseline free techniques exist but they have low reliability and cannot be generalized); sensitive to environmental effect (load and temperature) which can be mistaken for damage.
Eddy Current Foil Sensors	Inducing eddy currents in the specimen and observing the interaction to find damage	Cracks, corrosion.	Can be mounted on interfaces between structural parts and can be tailored to work on different shapes. Can be used in locations that are difficult to reach.	Sample material must be conductive. Mainly used for thin materials as thick materials will have penetration constraints.
Acoustic Emission (AE)	Collection and analysis of waves generated by the impact, fretting, rubbing, formation of a new surface, etc.	Impact damage, corrosion formation, crack/damage propagation.	Allows for in-situ monitoring of large areas. Allows for source localization.	Requires active source and real-time monitoring. Prone to background noise.
Fibre Bragg Grating (FBG)	Gratings on the fiber core are subjected to strains. These can be caused by a change in temperature or a local material strain transmitted to the fiber.	Overloads, impacts, and delamination.	Monitors cracks whilst loaded/in-flight (online). Can be embedded in layers of composites during manufacturing. Suitable for networking. The sensor has a	Adds complexity to the manufacturing process. Provides only local damage. Extremely fragile requires extra care during

(continued)

Table 2.1 (continued)

Method	Principle of operation	Detectable damage type	Strengths	Weaknesses
			lifetime close to fiber reinforced polymer composites. Immune to electromagnetic interference.	installation and operation.

transmission, etc. for SHM application. Despite all the advancements, OEMs and aircraft operators are still reluctant in accepting SHM systems for widespread use. Thus, maintenance conducted at a specified number of flight hours and/or calendar days remains the method of choice until the SHM system can meet the same level of damage detectability/reliability as set by the current methods. These challenges include the ability of SHM system manufacturers to minimize/eliminate false calls and to ensure proper operation of these sensors over their useful lifespan. Furthermore, certification authorities may require the SHM system manufacturers to provide the same level of probability of detection (PoD) as is needed for current NDI techniques. Currently, guidelines to develop PoD curve for NDI are provided in (MIL-HDBK-1823A 2009), but may not be generalized in its entirety for SHM application. PoD curves have been developed for SHM application but for specific cases (Roach 2015) (Meeker et al. 2019). Developing a PoD curve for a general SHM sensor setup would likely require a large experimental program with multiple reference samples, with and without damages, in a representative environment translating into a very costly effort. One way to reduce this cost is to implement a robust model-assisted PoD methodology, in which one uses high-fidelity digital models to reduce the number of expensive experimental evaluations. A significant challenge lies in increasing the TRLs of these SHM systems to ensure long-term in-service performance and reliability.

Some of the SHM systems are required to be powered using onboard power supply, as batteries may not be permitted in certain cases. These wired systems may add weight, which in turn may increase fuel consumption. Therefore, energy harvesting, printed circuits and wireless technologies need to be developed to ensure that the benefit of using SHM can be maximized (Chuw et al. 2016).

References

Aircraft Accident Investigation Report (1985) Aircraft accident investigation commission ministry of transportation. Online: https://www.mlit.go.jp/jtsb/eng-air_report/JA8119.pdf. Accessed July 2020.

Chew ZJ, Ruan T, Zhu M (2016) Strain energy harvesting powered wireless sensor node for aircraft structural health monitoring. *Procedia Eng* 168:1717–1720

- Collins Aerospace (2020) B-52 bomber preparing to fly into 2050. November 2020, Online: B-52 bomber preparing to fly into 2050 (collinsaerospace.com). Accessed January 2021
- Faivre V, Morteau E (2011) Damage tolerant composite fuselage sizing. Airbus FAST magazine – Flight Airworthiness Support Technology (48), pp. 10-16.
- García I, Zubia J, Durana G, Aldabaldetrekú G, Illarramendi MA, Villatoro J (2015) Optical fiber sensors for aircraft structural health monitoring. *Sensors* 15(7):15494–15519
- Heisey R (2002) 717-200: low maintenance costs and high dispatch reliability. *AERO*, No 19. July 2002.
- IASA (2005) China Airlines Flight CI-611 crash report released. Online: http://www.iasa.com.au/folders/Safety_Issues/FAA_Inaction/CI-611finalreport.html. Accessed July 2020.
- IATA (2018) Maintenance costs for aging aircraft, 1st ed. ISBN 978-92-9229-637-7
- Maksimović S, Vasić Z, Došić R (2015) Service life extension program for aircraft structures. *Scientific Technical Review* 65(3):46–54
- Meeker WQ, Roach D, Kessler SS (2019) Statistical methods for probability of detection in structural health monitoring. International Workshop on Structural Health Monitoring, April 2019.
- MIL-HDBK-1823A (2009) Nondestructive evaluation system reliability assessment. Department of Defense Handbook
- MIL-STD-1530D (2016) Department of Defense Standard Practice – Aircraft Structural Integrity Program (ASIP)
- Nicolas MJ, Sullivan RW, Richards WL (2016) Large scale applications using FBG sensors: determination of in-flight loads and shape of a composite aircraft wing. *Aerospace* 3(3) mdpi.com
- Roach D (2015) Calculating probability of detection for SHM systems using one-sided tolerance intervals – Applications & Limitations. Sandia National Labs.
- SAE ARP6461 (2013) Guidelines for implementation of structural health monitoring on fixed wing aircraft aerospace industry steering committee on structural health. SAE International, <https://doi.org/10.4271/ARP6461>.
- Seshadri B, Krishnamurthy T, Ross R (2014) Integrated structural health monitoring and management of in-flight damaged aircraft structure. In: Proceedings of the 2014 Aircraft Airworthiness and Sustainment Conference. Baltimore, MD
- Swindell P, Doyle J, Roach D (2017) Integration of structural health monitoring solutions onto commercial aircraft via the Federal Aviation Administration structural health monitoring research program. AIP conference proceedings, 43rd annual review of progress in quantitative nondestructive evaluation, vol 36, p 1806. <https://doi.org/10.1063/1.4974616>.
- Wenk L, Bockenheimer C (2014) Structural Health Monitoring – a real-time on-board ‘stethoscope for Condition-Based Maintenance. Airbus Technical Magazine, No. 54.

Open Access This chapter is distributed under the terms of the Creative Commons Attribution 4.0 International License (<http://creativecommons.org/licenses/by/4.0/>), which permits use, duplication, adaptation, distribution and reproduction in any medium or format, as long as you give appropriate credit to the original author(s) and the source, a link is provided to the Creative Commons license and any changes made are indicated.

The images or other third party material in this chapter are included in the work’s Creative Commons license, unless indicated otherwise in the credit line; if such material is not included in the work’s Creative Commons license and the respective action is not permitted by statutory regulation, users will need to obtain permission from the license holder to duplicate, adapt or reproduce the material.



Chapter 3

Defect Types



**Nadimul Faisal, Ömer Necati Cora, Muhammed Latif Bekci,
Romana Ewa Śliwa, Yehuda Sternberg, Shashank Pant,
Richard Degenhardt, and Anil Prathuru**

Abstract This chapter provides an overview of the common types of defects found in various structural materials and joints in aircraft. Materials manufacturing methods (including large-scale production) have been established in the aircraft industry. However, as will be seen in this chapter, manufacturing defects and defects during in-service conditions are very common across all material types. The structural material types include metals, composites, coatings, adhesively bonded and stir-welded joints. This chapter describes the defect types as a baseline for the description of their detection with the methods of Chap. 5 to 8. Based on the understanding of the defect types, there is great expectation for a technical breakthrough for the application of structural health monitoring (SHM) damage detection systems, where continuous monitoring and assessment with high throughput and yield will produce the desired structural integrity.

N. Faisal (✉) · A. Prathuru
Robert Gordon University, Aberdeen, UK
e-mail: n.h.faisal@rgu.ac.uk

Ö. N. Cora · M. L. Bekci
Karadeniz Technical University, Trabzon, Turkey

R. E. Śliwa
Rzeszow University of Technology, Rzeszow, Poland

Y. Sternberg
Israel Aerospace Industries Ltd, Ben Gurion, Israel

S. Pant
National Research Council Canada, Ottawa, ON, Canada

R. Degenhardt
German Aerospace Center (DLR), Braunschweig, Germany

© The Author(s) 2021

M. G. R. Sause, E. Jasiūnienė (eds.), *Structural Health Monitoring Damage Detection Systems for Aerospace*, Springer Aerospace Technology, https://doi.org/10.1007/978-3-030-72192-3_3

3.1 Metallic Materials

Load bearing aircraft structure is assembled and built using several major components such as fuselage, wings, engines and landing gear, as shown in Fig. 3.1. Among material types, metallic materials used in the aircraft structure manufacturing and assembly include aluminium, high-strength steel, titanium and superalloys (nickel, iron–nickel and cobalt-based alloys) with each possessing certain qualities that make them ideal for this use. Aluminium alloys have been the main airframe material. The attractiveness of aluminium alloys is that it is relatively low cost, lightweight, easily heat-treated to high strength levels and most easily fabricated with low costs. Titanium alloys can often be used to save weight by replacing heavier steel alloys in the airframe and superalloys in the low-temperature parts of gas turbines, and they are used instead of aluminium alloys when the temperature requirements exceed aluminium capabilities or when fatigue or corrosion has been a recurring problem. High-strength steels (HSS) are used for highly critical parts such as landing gear components. The main advantages of HSS are their high strengths and stiffness, but they are of high density and susceptible to brittle fracture. Super-alloys are used extensively in jet turbine engines, when the temperature of exploitation excess 80% of the incipient melting temperatures while exhibiting high strength, good fatigue, creep resistance, good corrosion resistance and ability to work at high temperatures.

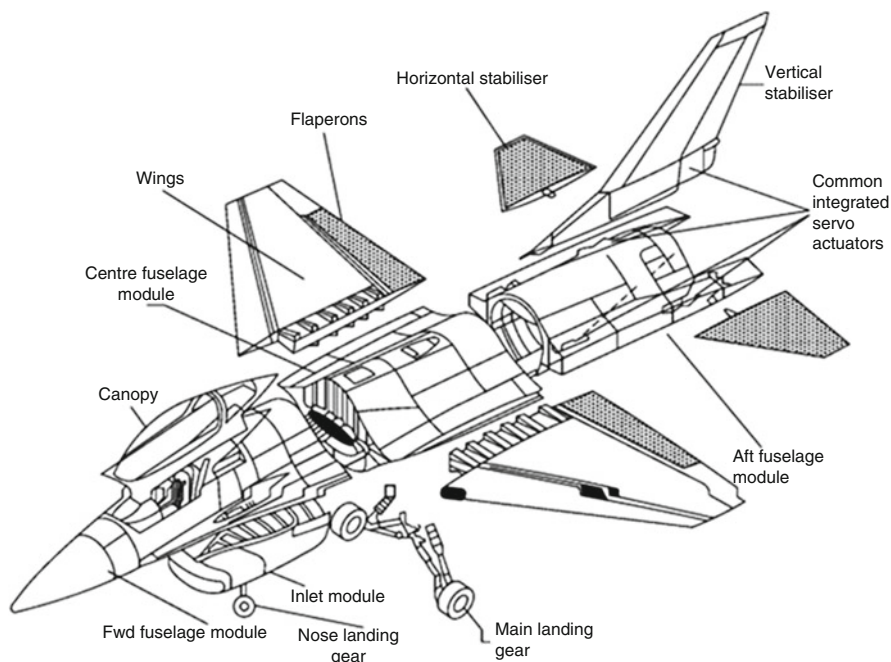


Fig. 3.1 Main structural components of a modern military aircraft (Mouritz 2012a, 2012b, 2012c)

Both magnesium and beryllium alloys as extremely lightweight materials (competitive on specific strength and specific modulus) are considered for applications. In the case of magnesium alloys, the biggest obstacle to use them is their extremely poor corrosion resistance; hence, the products require special solutions for protection. Beryllium alloys represent an attractive combination of properties, but they must be processed using powder metallurgy technology with the requirement for controlled manufacturing environments and the concern for safety during the repair/service of deployed structures (Śliwa et al. 2016; Peel and Gregson 1995; Campbell 2006; Śliwa et al. 2017).

Note that safety-critical aircraft structure demands metallic materials that are both durable and lightweight, as well as being able to withstand severe structural stress at various altitudes and temperatures, including fatigue and wear resistance. High-quality material requirements for aeronautical applications make the defect detection and inspection techniques of prime importance, both in manufacturing and in-service operation. The following subsections describe the major defects encountered in metallic materials.

3.1.1 Defects During the Manufacturing Process

Metallic materials or their alloys are a class of elementary materials, such as aluminium, steel, titanium and nickel alloys, all of which are crystalline when solid. Given pure metals, some of the important defect types can be point defect, line defect and plane defect (Gilbert 2020). A point defect involves only a single particle (called a lattice point). A line defect is limited to a row of lattice points. A plane defect involves an entire plane of lattice points in a crystal. A vacancy occurs where an atom is missing from the crystalline array, constituting a tiny void in the middle of a solid.

There are four fundamental mechanisms for introducing a point defect into the structure of a solid (Hiroshi 2014; Fang 2018), such as (a) when a particle is missing at one or more lattice sites, a vacancy is attained; (b) when a particle forces its way into a hole between lattice sites, interstitial impurity is attained; (c) substitutional impurities result from replacing the particle that should occupy a lattice site with a different particle and (d) dislocations are unidirectional defects caused by holes that are not large enough to be a vacancy.

When a fraction of the original materials are replaced by impurities, a solid solution can be attained. Alloys are examples of solid solutions. Lattice distortions of the crystalline materials often occur when impurities are added to a solid. Thus, point defects often determine the properties of a material. Point defects can change the mechanical properties, such as strength, malleability or ductility. Dissolving a small percentage of carbon in pure iron (i.e. making it a steel) makes it stronger than iron; however, higher percentages of carbon can make the steel harder and more brittle.

A dislocation mechanism (screw or edge dislocation types) can weaken a metal, as it allows planes of atoms in a solid to move one row at a time. Interestingly, they can also strengthen a metal when work hardened during heating, hammering, cooling, reheating and reworking. In the course of the work hardening process, intersecting dislocations (i.e. when planes of atoms move one row at a time) that impede the movement of planes of atoms are created.

Most metallic materials are polycrystalline in nature (i.e. structure with many crystallites of varying size and orientation), whereas a group of crystals is called grains. Crystal grains in polycrystalline metallic materials deform by slips on specific slip systems. The place where two grains meet is called a grain boundary. The movement of a deformation through a solid polycrystalline tends to stop at a grain boundary. Therefore, managing the grain size in solids is necessary to obtain a desirable mechanical property, and fine-grained polycrystalline materials are usually stronger than coarse-grained ones.

3.1.2 Defects During In-service Conditions

From early aircraft to the most advanced ones, different types of materials are used in the aerospace industry. Metals have been the most preferred materials and served as the primary choice of materials for many years because of its versatile features and properties. Although the use of advanced composites is continuously increasing in aircraft, metallic materials still constitute 45% of the total weight (20% aluminium, 15% titanium and 10% steel) of the Boeing 787 aircraft. Aluminium is exploited in wings and tail leading edges; titanium is primarily exploited on engine parts and fasteners while steel is used in several places including landing gears, leading edge of the wings, engine pylons, hinges, cables, fasteners, etc.. Airbus A350 has a similar material distribution, 20% Al, Al–Li alloys, 14% titanium and 7% steel by weight (Criou 2007).

Defects and its prevention in aerospace materials are uttermost concerns since undetectable flaws can cause catastrophic consequences for aircraft and passengers. The defects can be categorized, from the origin point of view, under four headings: (a) due to manufacturing, (b) during assembly, (c) during transport and (d) during service. This subsection is intended to shed light on the in-service related defects of aerospace materials. Defects during in-service mainly occur because of either inadequate material specification; in other words, inappropriate material choice and operation beyond the intended design parameters (Archer and McIlhagger 2015).

The common characteristic of in-service damage is that they occur unexpectedly, and it might be difficult to predict and diagnose it. Table 3.1 shows the most common causes of failure. The following subsections describe the major defects or failure types encountered in metallic structures.

Table 3.1 Percentage of the failures in aircraft components (Brooks and Choudhury 2002; Findlay and Harrison 2002)

Failure type	Percentage (%) of failures
Fatigue	55–61
Corrosion	3–16
Overload	14–18
Stress-corrosion-cracking/corrosion fatigue/hydrogen embrittlement	7–8
Wear	6–7
High-temperature corrosion	2
Creep	1

Table 3.2 Fatigue causes for some aircraft accidents (Tiffany et al. 2010)

Fatigue causes	Numbers of accidents	
	Airframes	Engine discs
Unanticipated high local stresses	11	-
Manufacturing defect or tool mark	3	2
Material defect	2	1
Maintenance deficiencies	6	-
Abnormally high fan speed	-	1

3.1.2.1 Fatigue

Fatigue is the primary reason for failure in aerospace metals that occurs under repeated loads leading to premature failure of structural parts. If it is not detected in the early stages, it can cause catastrophic failures. It is usually characterized as the initiation and propagation of cracks to an unaccepted size. Fatigue is mostly controlled with stress history, material properties, chemical environment and manufacturing quality (Arrieta and Striz 2005). Table 3.2 shows a summary of the common fatigue causes observed in aircraft that have led to accidents, whereas Fig. 3.2 shows the structural areas prone to fatigue damage in early Airbus A300 design.

The frequency, sign, sequence and magnitude of repeated loads affect the fatigue rate, its initiation and growth. Besides these, corrosive environment, loading rate and temperature may play role in fatigue. Several early aircraft accidents were related with stress concentration that initiated cracks under operational loads. These stress concentrations were not detected until the accidents occurred. Stress concentration was not the only reason for early aircraft accidents, but several other factors including the use of high strength material with low fatigue crack resistance and tolerance (very short final crack size) and manufacturing process, material-oriented defects are involved. In August 29, 1948, Martin 202-type aircraft belonging to Northwest Airlines crashed near in Winona, Minnesota, during a Chicago–Minneapolis scheduled flight killing all 37 persons aboard. The accident caused by

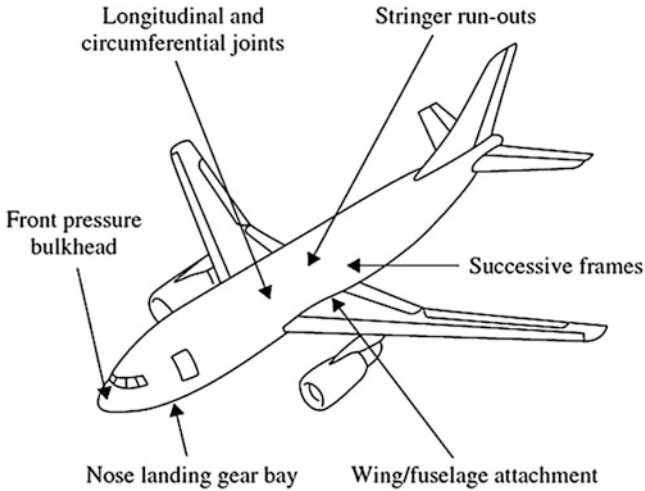


Fig. 3.2 Common fatigue failure zones for Airbus A300 (Brand and Boller 1999)

the left-wing separation from the aircraft during thunderstorm related turbulence conditions. Investigations conducted by Civil Aeronautics Board revealed that a fatigue crack caused the detachment of outer wing (made of AA 7075-T6 alloy) from the rest of the wing. The aircraft design was not based on fail-safe approach at that time and this accident along with other Comet type aircraft failures led to the development of “Fail-Safe Design” approach (Tiffany et al. 2010; Ruth 1973). This approach is regarded as the extension of the safe-life concept in which the component or system is designed in a way that it will not fail within a specified period. After this period, the part is removed from the service. In Fail-Safe approach, however; in case of specific type of failure, the component or system should carry an honourable service load even after one of its components fail. In this approach, different from Safe-Life, the failure for specific part is possible, yet the system design prevents or at least mitigates the unsafe consequences of the system’s catastrophic failure. In other words, the part may fail yet it does not trigger the failure of other parts and, it remains as safe as it was before the failure (Mills et al. 2009; McBrearty 1956). Figure 3.3 shows the schematic for the wing root assembly failure for a Martin 202 aircraft.

More recently, Rebhi et al. examined the reason for the fracturing of the ADF antenna placed just behind the cockpit of a military aircraft (Rebhi et al. 2018). Figure 3.4a shows the ADF antenna location on the aircraft while Fig. 3.4b shows where it breaks. Note that the upper portion of the antenna was fractured because of the fatigue initiated by the corrosion pits. The crack origin was found to be at the outer surface on the antenna by tracing back the beach mark Fig. 3.5.

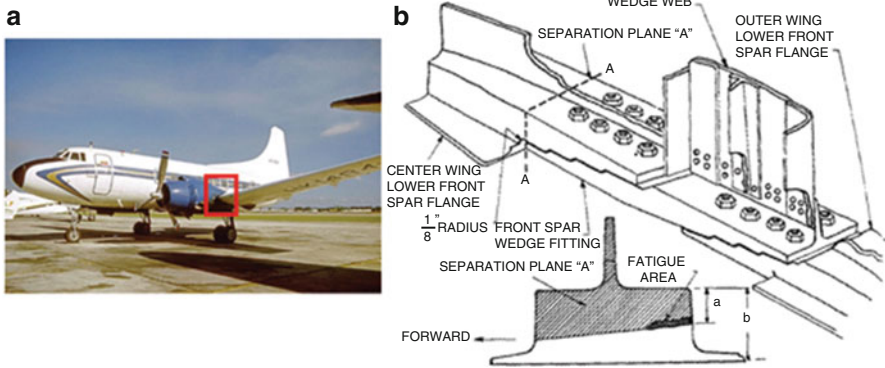


Fig. 3.3 (a) A typical Martin 202 aircraft (produced by Glenn L. Martin Company during 1947–1948) with approximate fatigue location (in red box) (Ruth 1973), (b) schematic section of separation of lower flange showing fatigue are and also sudden increase of depth of flange ‘a’ to approximately twice the depth as indicated by ‘b’ (after Civil Aeronautics Board 1949)

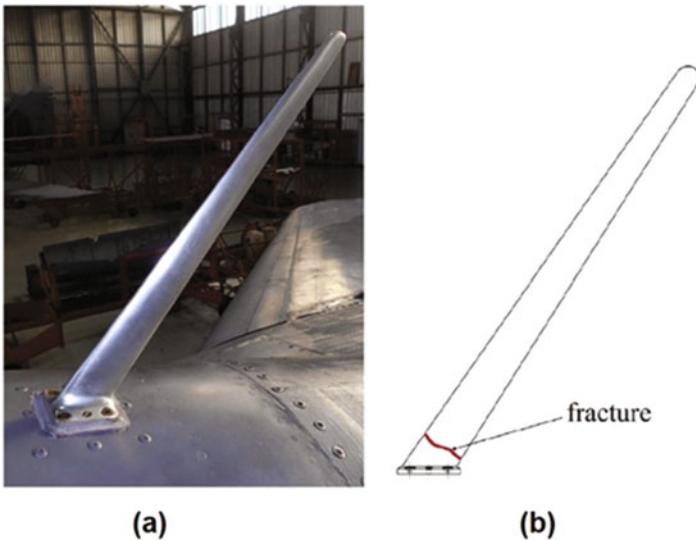


Fig. 3.4 Fractured ADF antenna of a military aircraft (a) location of antenna, (b) breaking line (Rebhi et al. 2018)

3.1.2.2 Corrosion

Any metallic part in an aircraft is prone to corrosion. Corrosion, generally, can be defined as deterioration of metals by electrochemical reaction with surrounding environment and gradual material loss. It is one of the serious concerns especially for older aircraft and responsible for 25% of the metallic component failures.

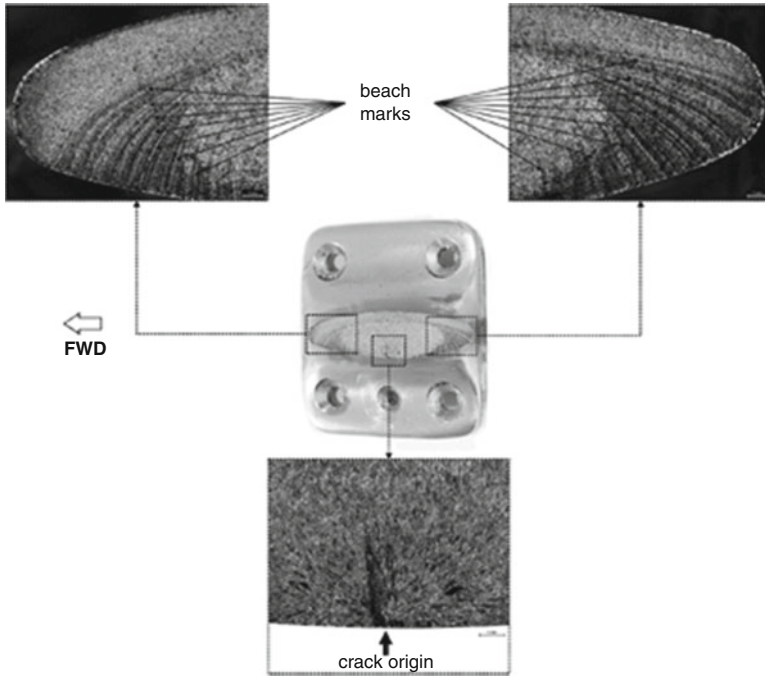


Fig. 3.5 Fractured surface of the ADF antenna (Rebhi et al. 2018)

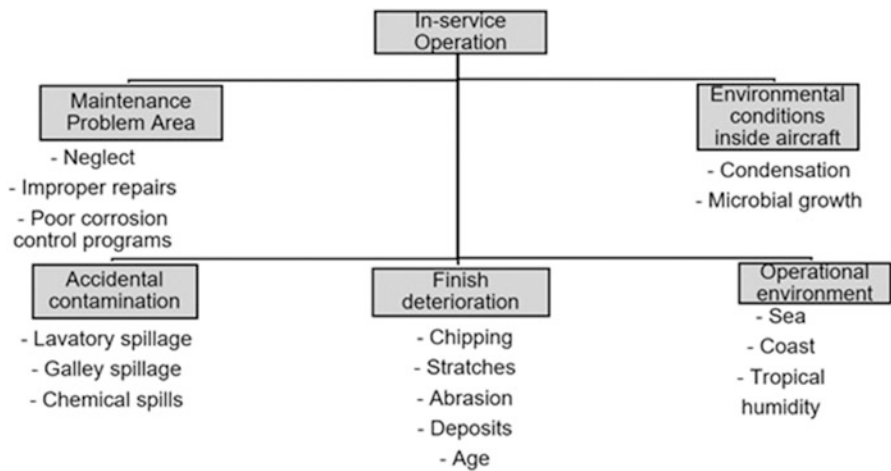


Fig. 3.6 Common sources of corrosion during in-service operation of aircraft (after Mouritz 2012a)

Corrosion-related expenses are estimated as big as 2.2 billion USD (Mouritz 2012a). It is commonly agreed that if corrosion issues are eliminated, maintenance of aircraft can be simplified. Many sources are available for corrosion during in-service phase of aircraft as illustrated in Fig. 3.6.

Three conditions should be available for corrosion: (i) availability of a reactive metal anode that corrodes and a passive metal cathode (does not corrode), (ii) a metal connector between cathode and anode and (iii) an electrode such as water. Preventing these conditions is quite challenging as it may not be practical, functional and hence feasible to eliminate them. For example, dissimilar metal contact cannot be prevented due to lightweighting, cost and functionality problems. Nevertheless, corrosion potential can be reduced by using surface enhancements such as painting, plating and sealing (Banis et al. 1999). Corrosion types can be categorized as follows:

- a. Concentration cell (or crevice, deposit) corrosion: In this type of corrosion, water, moisture or any other pollutant trapped in between two surfaces (e.g. under loose paint, within a delaminated bond line or in an unsealed joint) may lead to pitting or exfoliation corrosion, depending on the alloy, temper and corroded material. Lapped skin joints or rivets on an oil-stained belly are primary spots to notice this type of corrosion.
- b. Pitting corrosion: It occurs due to local loss of material. Although small amount of metal is removed, the pits can act as stress concentrators that may result in fatigue failure in critical load paths. Aluminium, magnesium and steel used in aircraft are vulnerable to this type of corrosion.
- c. Stress corrosion: This is also referred to as stress corrosion cracking (SCC) or environmentally assisted stress corrosion that occurs rapidly and follows the grain boundaries in aluminium alloys. SCC arises from three factors: susceptible metals and alloys, corrosive environment and residual tensile stress. It is observed on highly stressed parts such as engine crankshafts or landing gears and may originate from a scratch or surface corrosion. SCC occurs in a variety of aerospace metals with the presence of corrosive environment. High-strength steels, heat-treated steels and aluminum alloys are known to be affected by the salt solutions and sea water, and these can cause stress corrosion cracking. Methyl alcohol-hydrochloric acid solutions are reported to cause stress corrosion cracking for some titanium alloys. Magnesium alloys, on the other hand, may stress corrode with moisture in air. It is also reported that sulfur from surrounding environment (e.g., air, dust, or lubricant) can initiate the SCC especially in hot parts (Rossman, 2020). Fig. 3.7f shows SCC failure in 7XXX alloy aircraft wing structure. Reducing the residual and assembly stresses and application of protective coatings are suggested to increase the corrosion resistance and to delay the initiation of SCC for aluminum alloys (Wanhill and Amsterdam, 2010).
- d. Exfoliation corrosion: Similar to stress corrosion it follows the grain boundaries and causes a leaf-like separation of the metal grain structure (Fig. 3.7d). It reduces the load-carrying capacity of aircraft parts, and the best way to combat with it is to use material with grain structure resistant to exfoliation.
- e. Filiform corrosion: It results from poorly prepared polyurethane paints and appears as worm-like lines under the paint that eventually lead to bubbling and flaking (Fig. 3.7b).

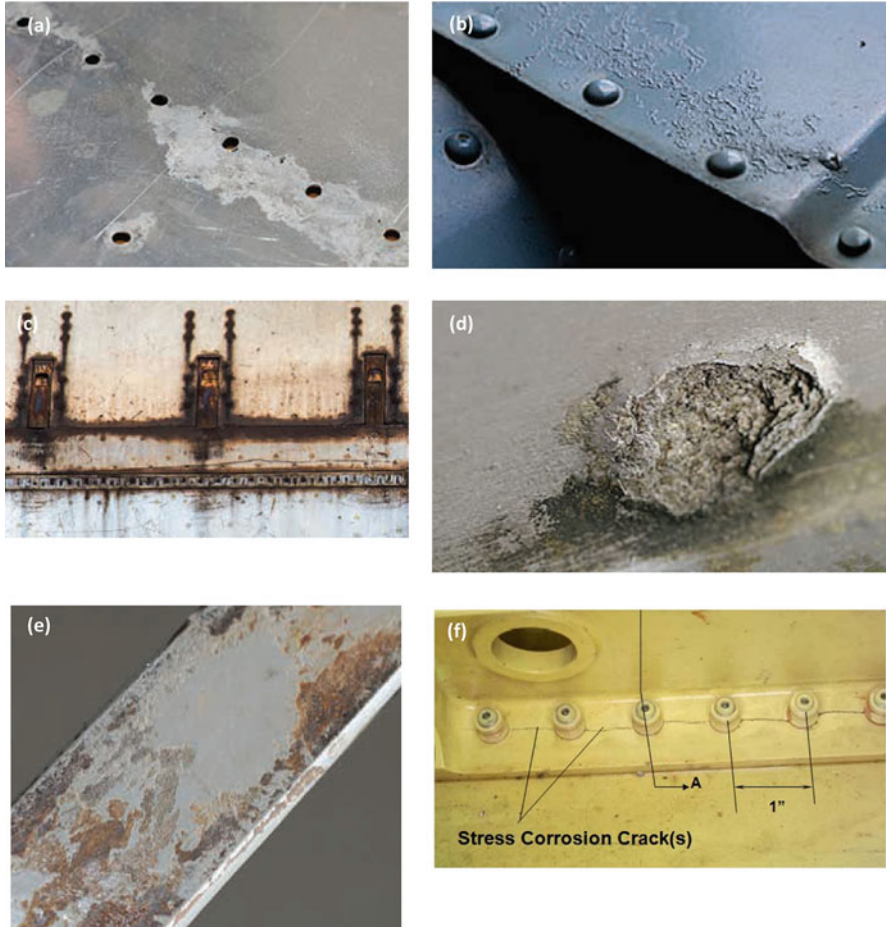


Fig. 3.7 Different forms of corrosion: (a) general surface corrosion, (b) filliform corrosion, (c) galvanic corrosion, (d) exfoliation corrosion, (e) fretting corrosion (Aeronautics Guide, Forms of Corrosion 2019), and (f) stress corrosion cracking (Snyder, 2014)

- f. Galvanic corrosion: This type of corrosion occurs by when two metals having different electric potentials are electrically connected via an electrolyte. It can be observed on aluminium–nickel–bronze bushing in an aluminium fitting in macro-scale, whereas one can notice it at the surface of an aluminium–copper intermetallic in micro-scale (Fig. 3.7c).
- g. Fretting corrosion: It is a corrosive attack when two mating surfaces have relative motion with each other, normally at rest. It is characterized by pitting of the surfaces and the generation of fine debris. As the restricted movements of the two surfaces prevents the debris from escaping easily, a highly localized abrasion occurs (Fig. 3.7e).

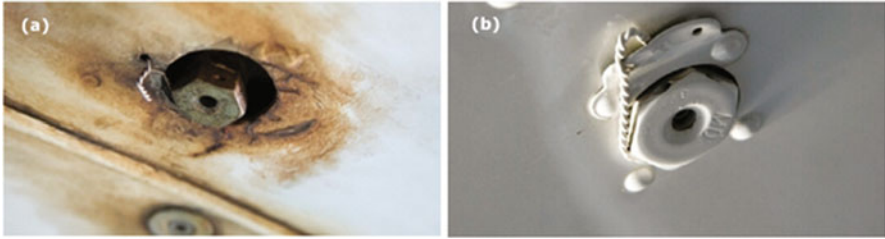


Fig. 3.8 Corrosion marks on different metal parts (a) rust around steel bolt, (b) whitish/gray dulling on an aluminium surface (Aircraft Owners and Pilots Association [n.d.](#))

- h. General surface corrosion: It is the least destructive type of corrosion and also named as uniform surface attack (Fig. 3.7a). As the name implies, the metal is removed from surface uniformly and slowly in this case. Nevertheless, if it is not controlled for a long period, general corrosion may lead to structural failures (Aircraft Owners and Pilots Association [n.d.](#); Mouritz [2012a](#); Banis et al. [1999](#)).

The visible sign of corrosion for aluminium and steel are quite different (Fig. 3.8). The steel surfaces are covered with reddish colored rust usually while aluminium corrosion is characterized as a whitish or gray 'dulling', which may lead to severe pitting and eventual destruction of the metal.

Trifkovic et al. investigated a failed combat jet aircraft rudder shaft which is a component of the vertical stabilizer (Trifkovic et al. [2011](#)). The function of the vertical stabilizer is to prevent the yawing motion of the aircraft's nose. The components of the vertical stabilizer with rudder shaft are shown schematically in Fig. 3.9.

The rudder shaft made of high strength St. 1.7784 steel failed because of pitting corrosion. Figure 3.10a shows the broken two pieces of the rudder shaft. To see the depth of the pits, the shaft sectioned from the longitudinal crack (shown with number 1), Fig. 3.10b. In Fig. 3.10c, corrosion pits formed in the inner wall are shown with arrows. It can be seen that these pits act as stress concentrators and result in early fracture of the shaft.

Although aluminium alloys provide high strength and fairly high stiffness at a low weight and have been exploited in aircraft structures for years, they are more prone to corrosion and fatigue than any other aerospace material. Corrosion can be minimized, If not avoided, with the selection of the appropriate material, surface finishing operation and the use of drainage, sealants and corrosion inhibitors.

3.1.2.3 Creep

Creep is defined as a process that involves the gradual visco-elastic and/or visco-plastic deformation growth of a material over time, and for metals it occurs at elevated temperature and below the yield strength of the material. The process of creep occurs in three stages: primary creep, secondary creep and tertiary creep.

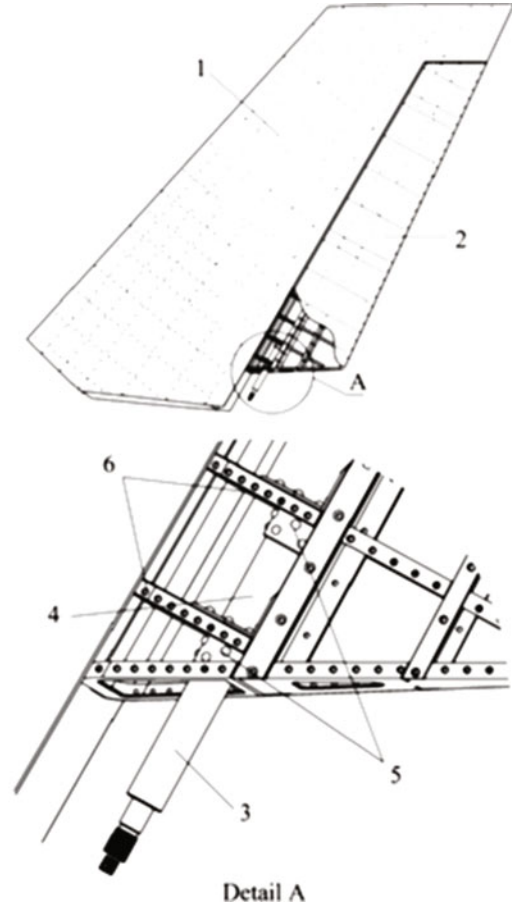


Fig. 3.9 Empennage of an aircraft (on the left) and schematic illustration of the vertical stabilizer-rudder assembly (on the right): 1. Vertical stabilizer; 2. rudder; 3. rudder shaft; 4. torsional tube; 5. flange; 6. rib (Trifkovic et al. 2011)

These stages have distinct behaviours with the function of the time and are illustrated in Fig. 3.11.

Creep is among the encountered failure types in aircraft engine components since those are exposed to extreme temperatures. If a rotating component in the aircraft engine is damaged, it will cause unbalance and lead to high vibration. This sudden increase in vibration can cause destruction in the engine in a very short time. Ejaz et al. conducted a study on the broken aircraft engine. They examined a low-pressure turbine blade made of Udimet 500 (a nickel–chromium–cobalt alloy) and found that primary cracking was initiated on the trailing edge of the blade due to creep; see Fig. 3.12 (Ejaz et al. 2011).

Fig. 3.10 (a) Broken rudder shaft, (b) longitudinal crack formed on the outer surface and (c) sectioned view of the rudder shaft (Trifkovic et al. 2011)

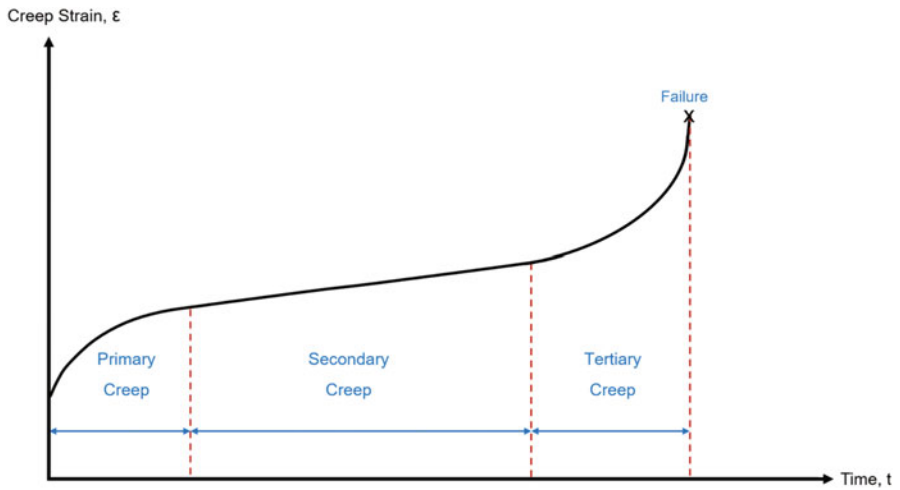
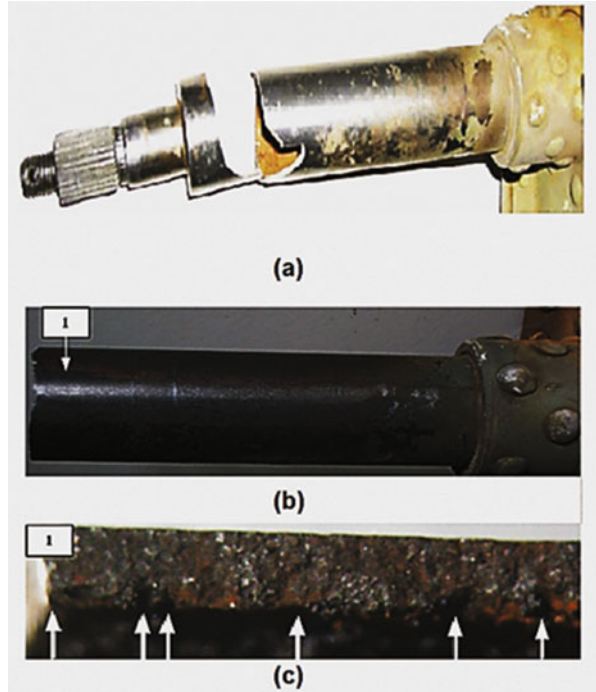


Fig. 3.11 A typical creep curve and its progress

Fig. 3.12 Fractured low-pressure turbine blade due to creep (Ejaz et al. 2011)

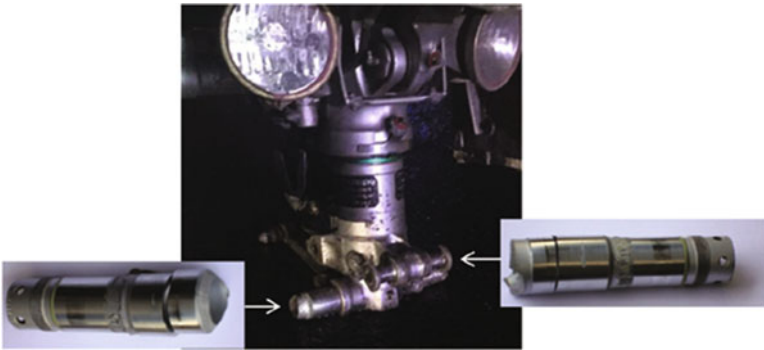
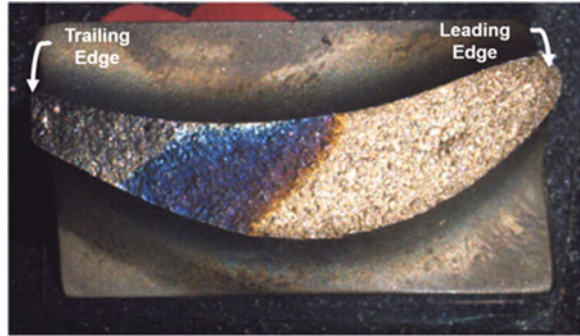


Fig. 3.13 Fractured landing gear (Freitas et al. 2019)

3.1.2.4 Operational Overload

Operational overload failure means that fast fracture of a material when stresses exceed the design stress of a material. Landing gears are the essential parts that undercarriage of an aircraft and are used for both takeoff and landing. It is well known that they are exposed to very high loads, especially at the time of landing. Freitas et al. (2019) showed a failed landing gear in Fig. 3.13. In this case, the aircraft experienced a hard landing due to the severe weather conditions, and the nose landing gear fractured into three pieces. Microscopic examination revealed ductile fracture characterized with dimples on the fractured surfaces (Fig. 3.14). These dimples are the main characteristics of the overloading failures and are due to the coalescence of microvoids during plastic deformation (Freitas et al. 2019).

In aviation, another operational overload type is known as foreign object damage. The sizes of these objects can range from a small solid particle to a wild large bird. Aircraft suffers from bird strikes during any time of flight. This situation is usually attributed to overload damages due to its devastating consequences on the aircraft. It may cause considerable danger to both aircraft and passengers, which can also lead to various major accidents. The number of reported bird strikes to commercial

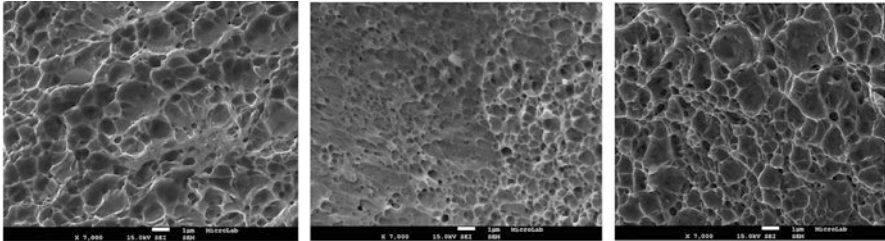


Fig. 3.14 SEM fractographs of the dimples on the fractured surfaces (×7000) (Freitas et al. 2019)

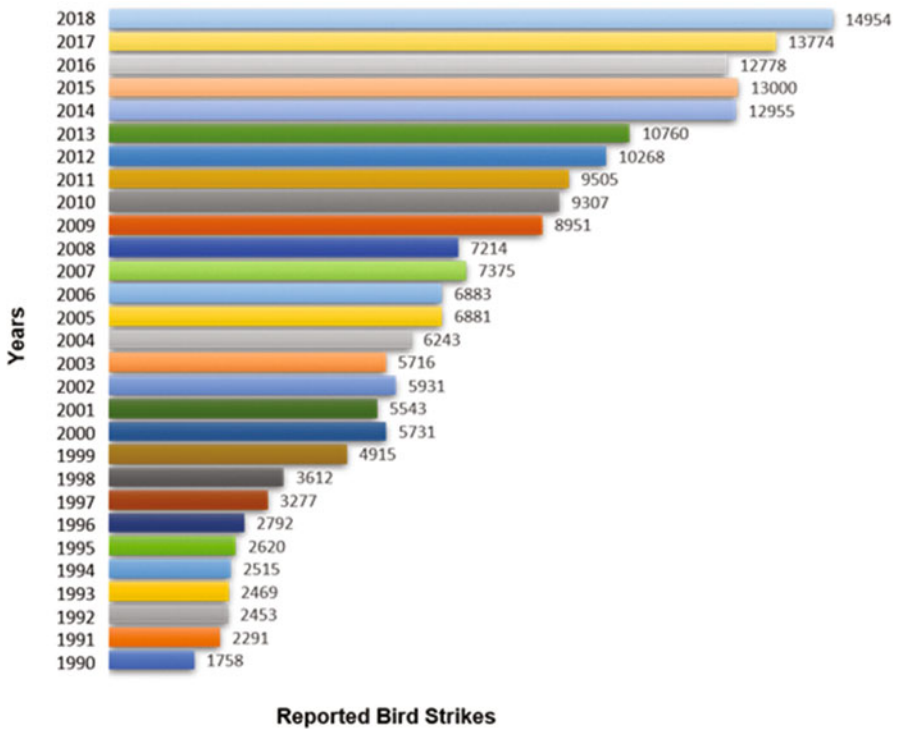


Fig. 3.15 Reported bird hits to civil aircraft from 1990 to 2018 in the USA (Dolbeer et al. 2019)

aircraft between 1990 and 2018 in the United States is given in Fig. 3.15. The number has been increasing over the years. In total, 202,472 bird strikes reported between 1990 and 2018, and almost 16% of these strikes damaged the aircraft (Dolbeer et al. 2019). The specific regions of planes that are susceptible to bird strikes are given in Fig. 3.16.

Figure 3.17 shows some bird strike cases that happened in 2007 and caused significant damages to the aircraft. A black vulture crashed into the nose cone of

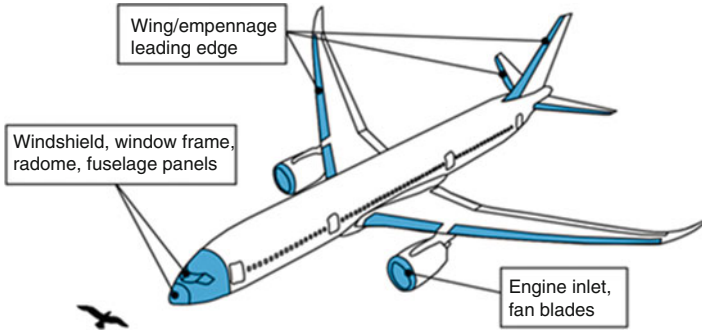


Fig. 3.16 Risky regions for bird strikes (Heimbs 2012)

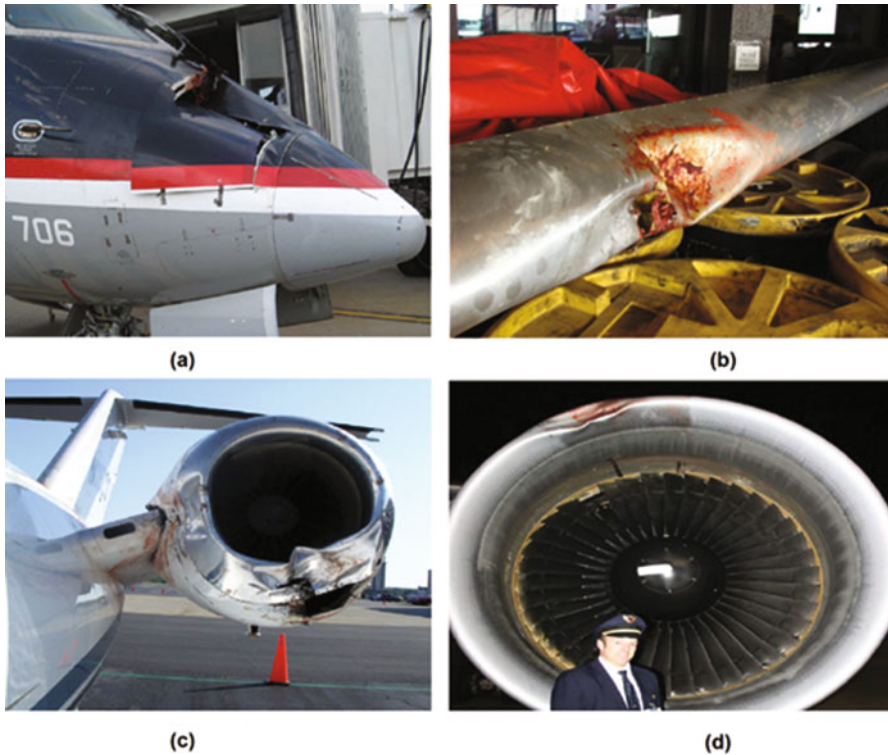


Fig. 3.17 Examples of bird strike aircraft accidents: (a) CRJ Jet crashed by a black vulture, (b) the leading edge of the left wing of a B-737 hit a great blue heron, (c) A Cessna 525 en-route at 5000 feet above ground level was hit by a flock of white-winged scoters and (d) a Boeing 767 was struck by a flock of canvasback ducks at 800 feet (Dolbeer and Wright 2008)

CRJ-700 on the final leg to the airport and caused severe damage as it can be seen in Fig. 3.17a. In another instance, a great blue heron struck to the left wing leading edge of the Boeing 737 on approach to the airport (Fig. 3.17b). A flock of white-winged scoters struck to both engines of Cessna 525 at 1500 m altitude (~5000 feet), and engine casing was damaged (Fig. 3.17c). In another instance, a flock of canvasback ducks hit to engines of Boeing 767 at 800 feet. The visual inspection revealed that fan and compressor blades in Engine #1 were seriously damaged (Fig. 3.17d) (Dolbeer and Wright 2008).

3.1.2.5 Wear

Wear is simply defined as some degree of material loss from the surface. These are adhesive, abrasive, fatigue, impact, chemical (corrosive), electrical-arc-induced wear and fretting wear. Erosion is examined under the impact wear and occurs by impingement of sand, rain, volcanic ash and other particles to the aircraft during service. It gradually reduces the life cycle of the components. Particular regions of planes are more prone to erosion on air. Figure 3.18 illustrates these regions. The regions indicated by the smaller dots are exposed to lower speed object impacts and bigger dots are for the medium speed object impacts. The hatched region (nose of aircraft) corresponds to objects with higher speeds (Kutyinov and Ionov 1996).

In engineering applications, bolted parts, shrink and press fits, couplings and bearings are particularly vulnerable to fretting wear. In the aircraft, the most commonly encountered fretting wear occurs in engine components and riveted structural connections. Lee et al. analyzed the failed first-stage compressor blade shown in Fig. 3.19a. In this case, an emergency landing was made due to an engine problem.

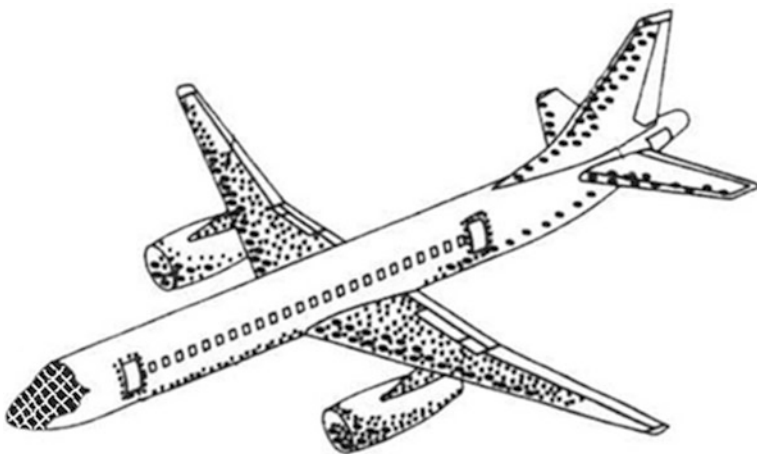


Fig. 3.18 Critical regions for erosion on a commercial aircraft (Kutyinov and Ionov 1996)

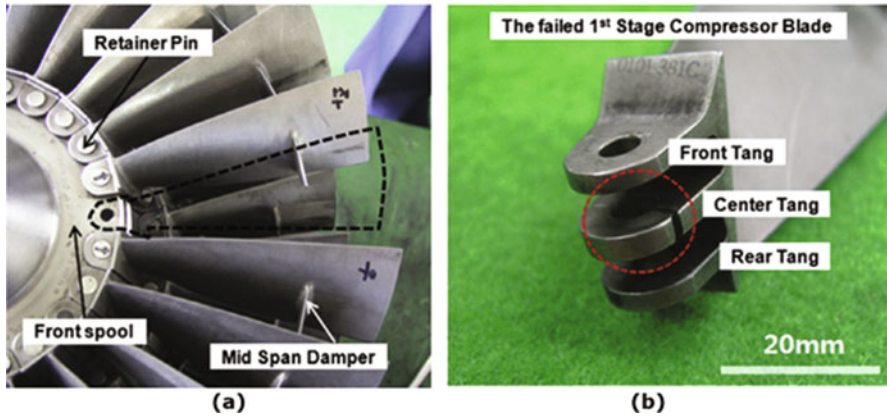


Fig. 3.19 (a) Failed compressor blade and (b) detailed view of the fractured pinhole lug (Lee et al. 2011)

After a detailed inspection, it was observed that the center tang of a pinhole lag was fractured due to fretting wear induced fretting fatigue (Fig. 3.19b) (Lee et al. 2011).

3.1.2.6 Extreme Weather Conditions

Weather conditions such as low cloud, fog and rain, snowfall, frost, icing, heavy storms (e.g. thunderstorms) and lightning can significantly hamper airline operations, functions of aircraft components and even cause catastrophic damages. Severe weather conditions usually cause increased drag and weight and reduced lift and thrust effect. This section will focus on two of those weather conditions, namely icing and lightning.

Ice is collected primarily on antennas, propeller blades, horizontal stabilizers, rudder and landing gear struts, and it disrupts the function of wings, control surfaces and propellers, windscreens and canopies, radio antennas, pitot tubes, static vents and air intakes. Turbine engines are especially vulnerable as ice forming on the intake cowling constricts the air intake (US National Oceanic and Atmospheric Administration n.d.). Figure 3.20 shows various forms of icing conditions on aircraft parts and a typical deicing operation, which is usually performed by applying heated glycol diluted with water.

Conversely, a lightning strike is an atmospheric discharge of electricity and can cause no damage to significant damage that requires extensive inspection and repair. Today, lightning strikes to airplanes is common yet those rarely result in significant problems due to the lightning protection measures, proper inspection and repair procedures implemented. According to the statistics, a plane can be struck by lightning on average every 1000 to 3000 flight hours. It is equivalent to one strike per commercial aircraft per year (Sweers et al. 2014).

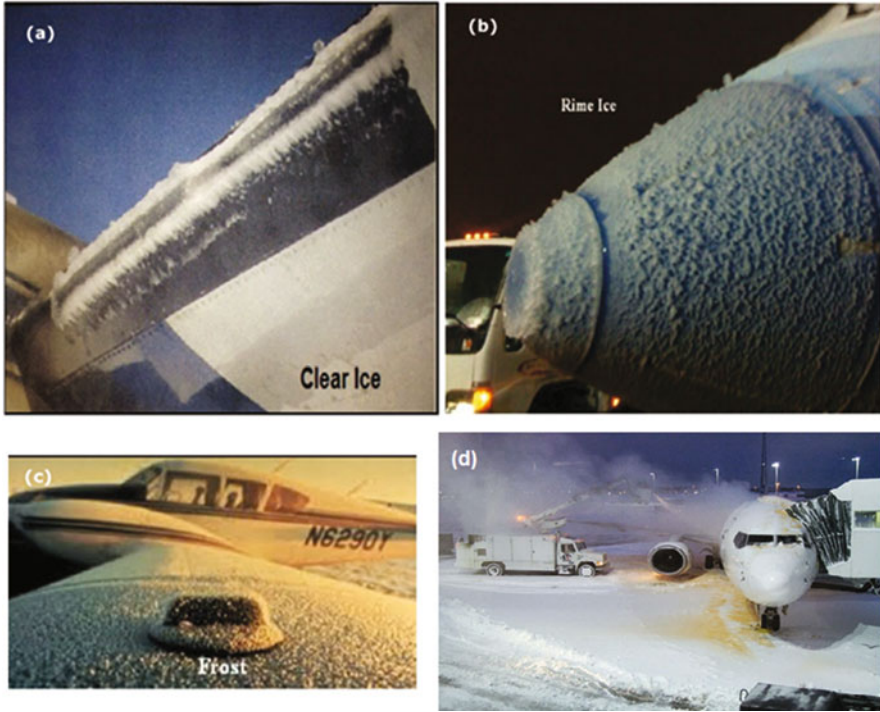


Fig. 3.20 Examples of effect of extreme weather conditions on aircraft: (a) clear ice formation on the leading edge of an aircraft wing, (b) rime ice on radome of an aircraft, (c) frost formation on a wing (US National Oceanic and Atmospheric Administration n.d.) and (d) deicing of an aircraft (Hartman 2008)

In 1967, Pan American Airlines Flight 214 was a Boeing 707 flying from San Juan in Puerto Rico to Philadelphia with a stop in Baltimore. The aircraft suffered a lightning strike upon taking off from Baltimore heading to Philadelphia, in which lightning-ignited vapours in the fuel tank led to an inflight explosion, totally destroying the aircraft and killing all aboard. Since then, lightning protection techniques have been improved tremendously. Nowadays, airplanes should be certified to verify the safety of their designs against lightning. As aircraft materials vary, their response to lightning differ. For example, Aluminium is a highly conductive material and, even in the worst-case scenario, the 200,000 A jolt can be quickly conducted away. However, for less-conductive materials such as carbon fibre composites or non-conductive fibreglass, lightning strike protection becomes more critical (Sweers et al. 2014; Black 2013; Rupke 2006). Figure 3.21 shows a lightning damage to a regional jet fuselage.



Fig. 3.21 Lightning strikes damage to a regional jet (Alemour et al. 2019)

3.1.2.7 Miscellaneous Defect Types in Metals

Fuselage materials need good resistance against fatigue cracking owing to pressurization and depressurization of the fuselage with every flight (Mouritz 2012a). During pressurization and depressurization of the fuselage, it is highly likely that the materials should be able to carry bending moments, shear forces and torsional loads. If these loads reach a critical limit, the material could have initiation and propagation of cracks leading to catastrophic failure of the fuselage structure. Overall, fuselage materials require a combination of properties that include light-weight, high elastic modulus and yield strength and resistance against fracture, fatigue and corrosion. Among metallic materials, high strength aluminium alloy is the most common fuselage materials. The new generation of Al-Li alloys is a modern metallic material used in the production of aircraft parts, such as fuselage sub-assemblies or floor bearing elements (e.g. A380). These alloys are characterized by attractive mechanical properties in comparison to conventional aluminium type alloys. The Al-Cu 2xxx series alloys, characterized by high strength and low-density properties, as well as Al-Zn 7xxx series alloys characterized by high corrosion resistance, are used for structural applications, such as aircraft wings. The development of light-weight materials and fabricating parts/sub-assemblies of substantially large dimensions has become a major issue for the aerospace industry, which has boosted the development of more advanced materials with high specification properties. Recent aluminium alloy developments are based on achieving superior fatigue crack growth resistance, better corrosion resistance, lower density etc. Standard manufacturing techniques, such as welding and casting or extrusion, are ought to be developed to find a beneficial solution allowing structural weight reduction.

Aluminium alloys used in aircraft applications possess several extraordinary properties that make them suitable for use in the manufacture of the structural parts of aircraft. Extrusion as a manufacturing process of these materials allows for

the obtaining of the required quality of the specific geometrical parameters, macro- and micro-structure, properties (including mechanical ones) but also creating structural elements of very complex cross-sections, whose manufacture is usually impossible or more costly with the use of other techniques. Another main advantage of this process is its ability to select optimum shapes of extruded blanks used to manufacture parts maximally similar to the theoretical profile of the final part. Aluminium is the most commonly extruded material. Examples of products include profiles for the following aircraft parts: brackets, levers, fasteners, frames, liners, window frames, rails and cargo (Pawłowska and Śliwa, 2015). Although profiles production in extrusion runs smoothly and easily most often, several repeated faults might occur during the extrusion process and some distinct patterns of faults and defects can be seen on the surface of the produced profiles (Al-Jabbouli et al. 2015). To avoid possible defects in the extruded profiles (e.g. damage of the finished surface, internal or external cracks, banding of extruded profiles) the extrusion rates have to be selected not to cause any damage to the finished surface, which would prove the disturbance of the extrusion process or negative structural phenomena in the material (e.g. hot cracking).

Wings are designed to carry bending, shear and tension loads. During take-off, flight and landing stages, the bending action on the aircraft wing, which is a combination of tension and compression forces, including fluctuation of loads can induce fatigue damage. Among metallic materials, aluminium alloy is used to make wings, whereas the wing-box and wing connections are highly loaded structures built into the fuselage that are constructed of composite material or titanium alloy (Mouritz 2012a).

Undercarriage materials (e.g. landing gear) are expected to have high static and dynamic strength, fracture toughness, including fatigue strength. Arguably, the most used materials for load bearing part in aircraft is high-strength steel. The critical components of one of the largest landing gear assembly in commercial service (Airbus Industrie A330 and A340 passenger aircraft) are made from tempered martensite (Bhadeshia 2006). As an example, Fig. 3.22 contains the micro-structure

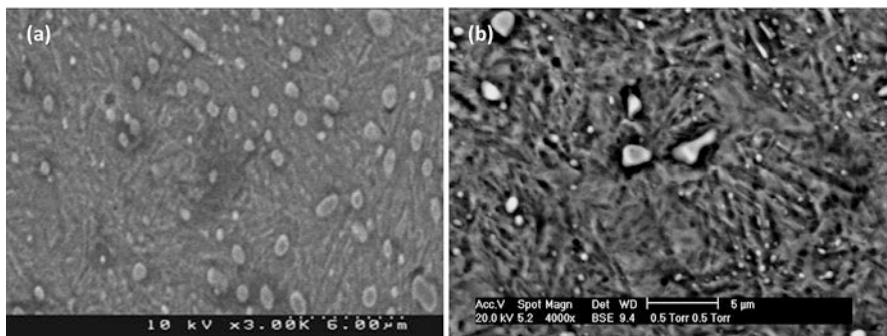


Fig. 3.22 Martensitic steel surface (polished and etched surface) showing lathes and coarse carbides, with dark zones or microvoids between carbide particles and martensitic matrix (Faisal et al. 2011b)

of the high strength hardened steel showing spheroidal carbide particles dispersed in a martensite matrix phase, which itself probably contains some smaller temper carbides. Small spheroidal carbides observed in Fig. 3.22 or many high-carbon martensite structures are considered routine (Faisal et al. 2011a). However, grain-boundary carbides, massive carbides that occur on edges and corners are deemed detrimental to mechanical properties and should be avoided. While carbides are harder than the surrounding matrix (martensite/austenite), they do not always have an appreciable effect on micro-hardness (e.g. Vickers or Rockwell). Carbides are known to enhance wear resistance.

In the high-strength hardened steel, the carbides are much harder than the tempered martensitic surrounding matrix so that any plastic deformation gets concentrated in the surrounding matrix and is impeded by the carbides (Blaha et al. 2002), leading to an accommodation mechanism including plastic deformation and carbide cracking (Girodin et al. 2002). The details of this failure mechanism may not be visible at the microscopic magnifications normally used in conventional material testing and optical analysis, although some evidence of failure at the carbide–matrix interface can be visible for some of the larger particles using acoustic emission (AE) sensors during contact mechanics study (Faisal et al. 2011a) (e.g. Fig. 3.22).

Since no macro-cracks can easily be detected on the surface around the stressful zones (tensile or compressive during contact mechanics), it is expected that the fine distribution of the brittle phase leads to generate micro-cracking in the areas of highest tensile stress (Faisal et al. 2011b). Since the stress is tensile over the entire contacting edge (e.g. indentation loading), it is expected that micro-cracking will initiate or be present in these areas.

Materials used in gas turbine engines are required to operate under high stress and temperature conditions for long periods of time (Mouritz 2012a). Engine materials require a combination of properties that includes high strength, toughness, fatigue resistance and creep strength at elevated temperature. Engine materials must also resist damage from oxidation and hot corrosive gases. The material of choice for the hottest engine components are nickel-based superalloys.

3.2 Composite Materials

Composites are of growing importance in aeronautics. They offer explicit weight saving in comparison with metal parts together with high quality and resistance to fatigue and corrosion. The modern, optimized composite aircraft structures require careful monitoring and inspections to identify damage and take corrective action as needed to ensure continued safe operation. The constant aggravation in quality requirements for aeronautics makes the defect detection and NDI techniques of prime importance, both in manufacturing and in-service inspection.

All the main types of composites such as polymer, ceramic and metal matrix composites (PMC,CMC, MMC), hybrid composite and structural composites (laminar composites, sandwich panels) demonstrate different mechanical and structural

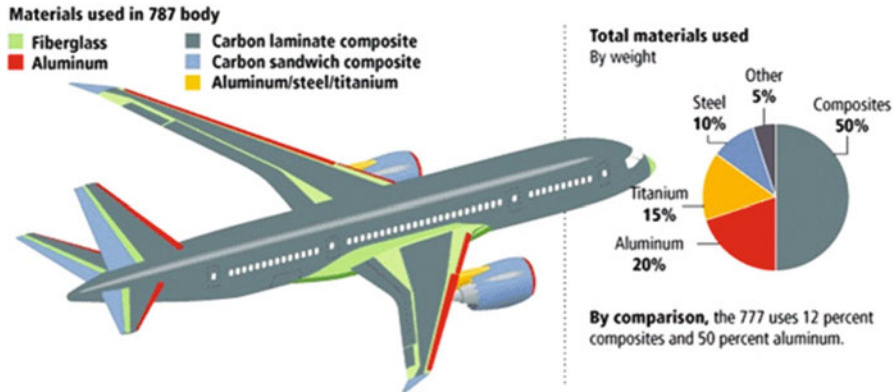


Fig. 3.23 Composites and other structural materials used in aircraft construction. Example: Boeing 787 body (Rosato 2013)

behaviour in special current and future applications in the aerospace industry. Recently, fibre-reinforced polymer composites are developed and used in the aerospace, especially carbon- and glass-fibre-reinforced plastic (CFRP and GFRP respectively) that consist of carbon and glass fibres, both of which are stiff and strong (for their density), but brittle, in a polymer matrix, which is tough but neither particularly stiff nor strong. Metal and ceramic matrix composites remain important materials, e.g. fiber metal laminates, in particular glass fiber reinforced aluminium laminates (GLARE) of high fatigue performance or carbon-carbon (CC) composites as ceramic matrix composite for high temperature applications. An example of *use of composites in aircraft design* is presented in Fig 3.23.

Composite materials have been used in the aerospace industry in primary and secondary structural parts, including rocket motor casings, radomes, antenna dishes, engine nacelles, horizontal and vertical stabilizers, centre wing boxes, aircraft wings, pressure bulkheads, landing gear doors, engine cowls, floor beams, tail cones, flap track panels and so on. The use of advanced composite materials in the aerospace sector is growing due to several advantages of composites over metals, such as composites light weight, high strength, corrosion resistance and superior fatigue and fracture properties, as well as multifunctional performances such as SHM and self-healing.

The major aspects related to quality control during composites manufacturing and their maintenance, testing and repairing in services: visual, ultrasonic, X-ray, back light and moisture detectors are some of the techniques reviewed as the main methods commonly used to detect damages, e.g. in sandwich structures that are applied in aerospace and aircraft parts. Major manufacturing damage and defects usually include delamination, resin starved and resin-rich areas, cracks, blisters and air bubbles, wrinkles, voids and thermal decomposition.

The following subsections describe the major defects encountered in composites. For each defect, we will explicitly indicate whether it is a manufacturing, an in-service or both a manufacturing and in-service defect.

3.2.1 Disbonds

Disbonds are both manufacturing and in-service defects. They are defined as unplanned non-adhered or unbonded areas within a bonded interface. They can be caused by adhesive or cohesive failure and may occur at manufacturing or at any time during the life of the structure. Disbond is generally a result of misprocessing during manufacturing such as incorrect initial surface cleaning, pressure/vacuum fail or an excessive load of the structure during service. Actually, this type of damage is dependent on the integrity of the adhesive layer and is affected by the presence of manufacturing defects as well as in-service loads. Manufacturing defects include a wide range of misprocesses such as poor surface preparation, contamination, improper curing, inaccurately applied pressure, the geometrical mismatch between the adherends and trapped air/moisture in the adhesive mixture.

Poor surface preparation is one of the leading causes of adhesively bonded joint failures. The creation of porosity and voids can also degrade the adhesive properties, as well as, create stress concentration during loading. During service, disbond can occur due to excessive stress applied at the bonding interface, impact damage, environmental degradation such as moisture ingress and aging of the adhesive layer (US Department of Transportation, FAA-AR-09-4 2009 (Tomblin, Seneviratne and Pillai, 2009)). Disbond can be found in any bonding surface, some of the examples include laminate/metal or laminate/laminate bonding surface, laminate skin to core (honeycomb or foam) bonding surface in sandwich structure and core to the core in multiple sandwich structure. Typical disbonds are shown in Figs. 3.24, 3.25, 3.26, and 3.27.

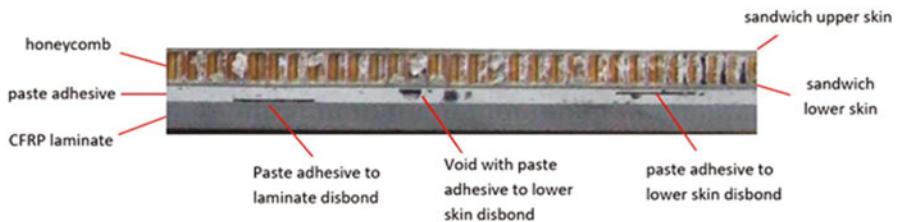


Fig. 3.24 Section of honeycomb sandwich structure bonded to CFRP laminate (either spar or rib) by paste adhesive showing several disbond issues

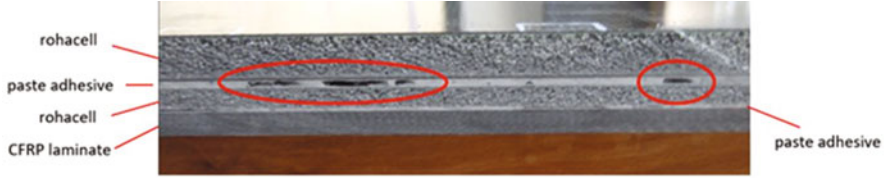


Fig. 3.25 Section of ROHACELL[®] foam blocks bonded together showing several disbond defects at the interface line

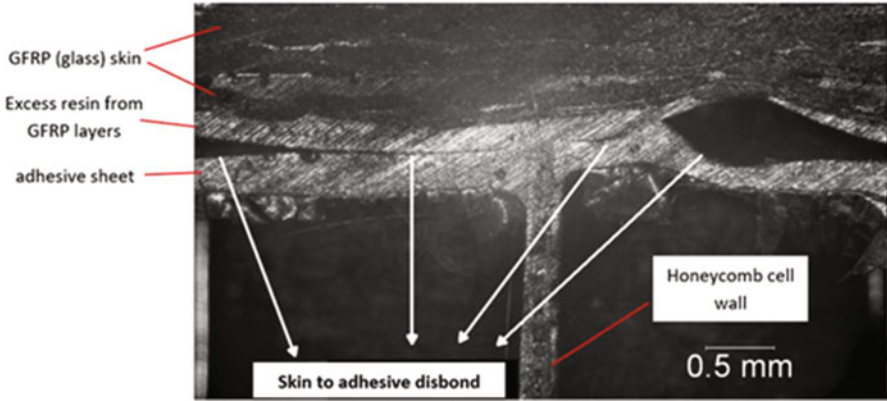


Fig. 3.26 Honeycomb sandwich structure—disbond between the adhesive layer and the GFRP skin

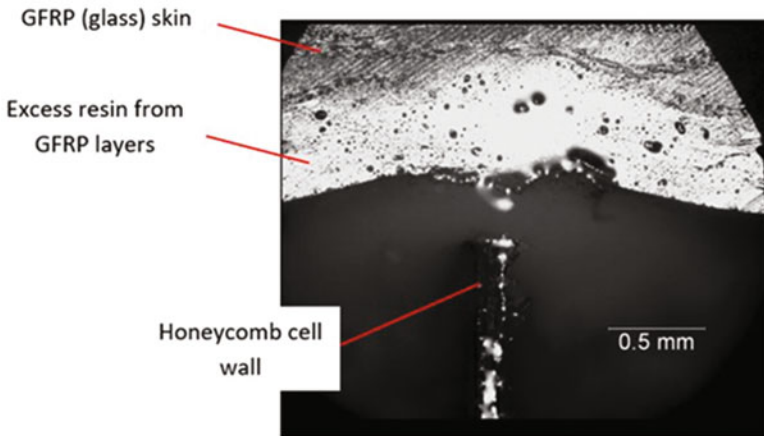


Fig. 3.27 Honeycomb sandwich structure - disbond between the honeycomb cell wall and the GFRP skin, and porosity bubbles are also visible within the excess resin

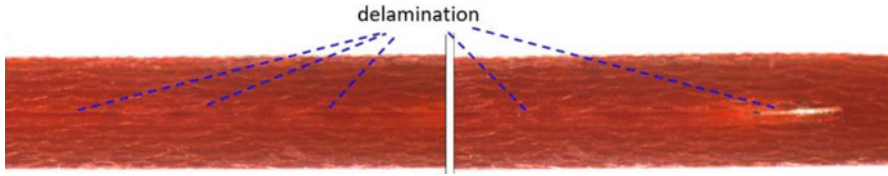


Fig. 3.28 Stereoscopic microscopic view of delamination within a GFRP laminate

3.2.2 *Delamination*

Delaminations are both manufacturing and in-service defects. In composites, they can be defined as a local failure in the adhesion between two successive layers causing the two layers to separate from one another at that location. Delamination can be caused by misprocessing during manufacturing (such as pressure/vacuum failure) or by impact damage or excessive load during in-service. Delamination is caused due to matrix properties having lower fracture toughness, strength and resistance against inter-laminar shear and transverse tension as compared to the reinforcement constituent. During the manufacturing process, thermal stresses and resin cure shrinkage can give rise to residual/inter-laminar stresses. These stresses can be high enough to cause delamination due to the mismatch between the properties of two adjacent layers (Bolotin 1996).

In-service delamination may be due to temperature cycling, local loads, impacts and fatigue. Failure due to delamination often initiates from free edges, surface defects and stress concentration points, which leads to the loss of overall stiffness/strength and under compressive loading leads to reduced buckling load limits (Vorontsov et al. 1990). Delaminations can also occur at free edges, in which a local three dimensional stress state phenomena plays an important role. Mainly explained by the mismatch of the elastic material properties between two adjacent dissimilar laminate layers, the free-edge effect is characterized by the concentrated occurrence of three-dimensional and singular stress fields at the free edges in the interfaces between two layers of composite laminates (Mittelstedt and Becker 2007). Several delamination cases are shown in Figs. 3.28, 3.29, and 3.30.

Defects in the composites may also occur during other processes, e.g. during drilling (Figs. 3.31 and 3.32), where delamination and extracted fibres are visible (Tyczynski, Śliwa, Ostrowski 2015).

3.2.3 *Foreign Inclusion*

Foreign inclusion is a typical manufacturing defect. It stands for the presence of a foreign body within the composite structure. Generally, foreign inclusions are pieces of material that have inadvertently not been removed from the surface before bonding. Most foreign inclusions in composites are the remains of unremoved pieces of: (a) protective sheets of prepregged plies, either paper, nylon or teflon sheets,

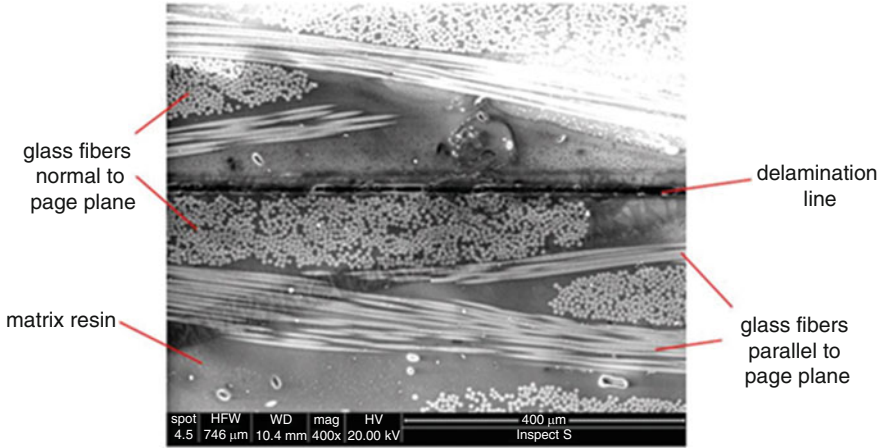


Fig. 3.29 SEM view of delamination within a GFRP plain weave laminate; Average fibre diameter is 5–7μm

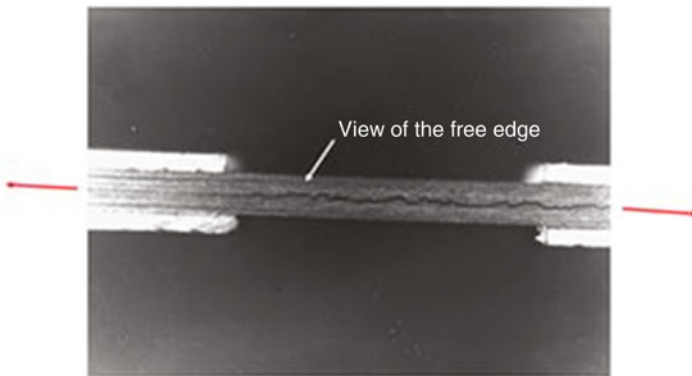


Fig. 3.30 Free edge delamination of a $[0_2, +45, 0_2, -45, 0, 90]_s$ laminate under tension loading

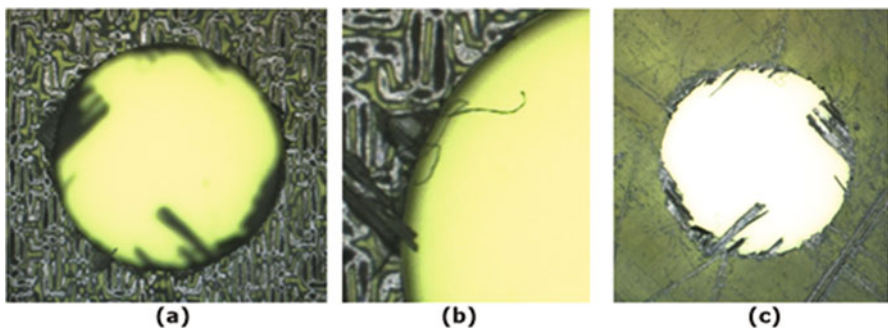


Fig. 3.31 Drilling of composite GFRP: Input (a, b) and output (c) surface of the hole with clearly visible delamination and extracted fibres

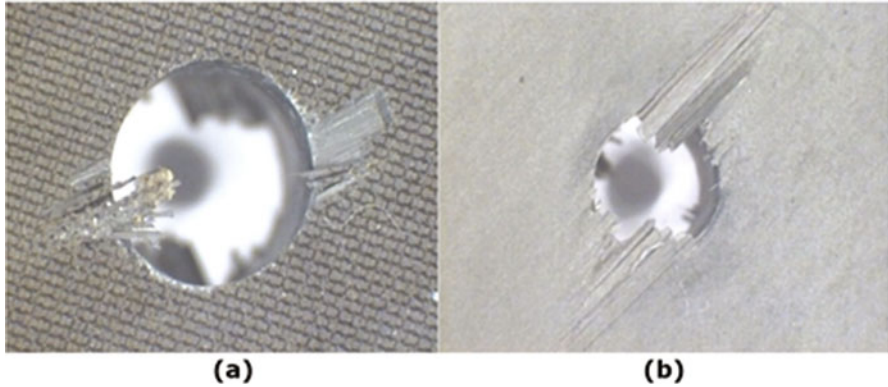


Fig. 3.32 Delamination in a carbon composite CFRP: (a) multidirectional (b) unidirectional

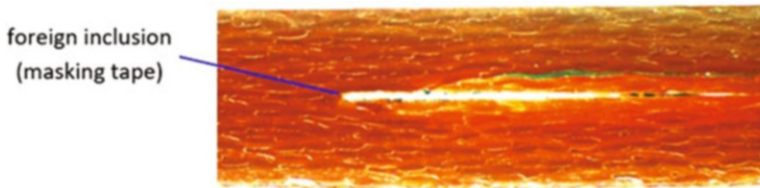


Fig. 3.33 Stereoscopic microscopic view of foreign inclusion (masking tape remaining) within GFRP laminate

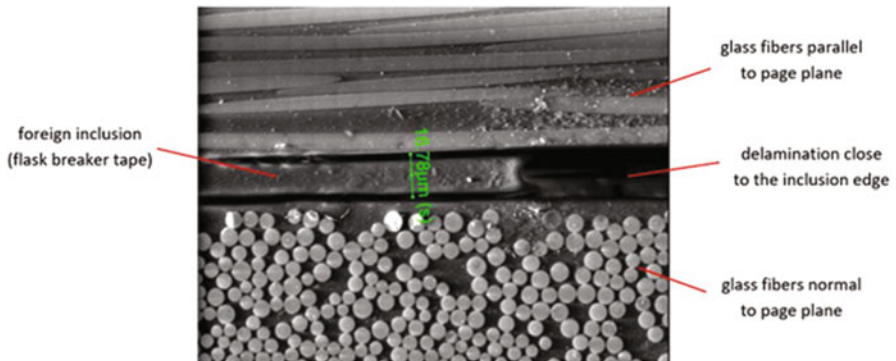


Fig. 3.34 SEM of foreign inclusion (flask breaker tape remaining) within a GFRP laminate; The upper ply has glass fibres oriented in the plane of the picture, whereas the lower glass ply has fibres normal to the picture plane. The average fibre diameter is 5–7 μ m

(b) masking tape, (c) flash breaker tap and (d) peel ply that is an extra layer of synthetic material (glass, nylon or other) which is laid upon the outer surface of the composite during fabrication. This layer is intended to be peeled off in a subsequent bonding step before bonding. Several foreign inclusion examples are shown in Figs. 3.33 and 3.34.

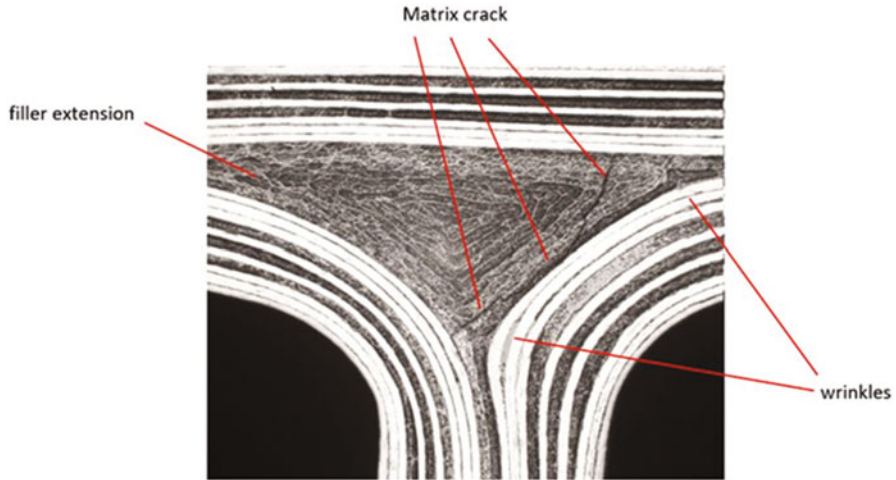


Fig. 3.35 Interfiber matrix cracking in CFRP T-shape radius filler made of unidirectional graphite fibres embedded within resin; The part that experienced a misprocess during fabrication is geometrically distorted and shows besides the crack two wrinkles on the right side and filler extension on the left side

3.2.4 Matrix Cracking

Matrix cracking is both a manufacturing and in-service defect (Fig. 3.35). It is characterized by cracks within the resin cementing the fibres of a laminate structure. It is often caused by mechanical stress lateral to the direction of the fibres, either during manufacturing or in-service. It is usually the first damage to occur when a composite laminate is subjected to mechanical stress such as quasi-static/cyclic tensile loading (Gayathri et al. 2010). Matrix cracking is characterized by damage in one or more layers without reaching the opposite surfaces. It turns into ‘fracture’ when the damage extends through the entire layers of the laminate.

During manufacturing, matrix cracking is often a consequence of thermal and/or residual stresses. It occurs in the through-thickness and transverse directions and can run perpendicular and parallel to the fibres, respectively. The through-thickness cracks occur because of the significantly lower matrix strength/stiffness as compared with the reinforcement and the strain magnification within the matrix pockets. Similarly, transverse cracks appear due to a mismatch between the in-plane Poisson’s ratio of the plies in the loaded and off-axis directions (Abrate 1991). This type of damage usually occurs during service as a result of tensile, fatigue and impact loading and is affected by the polymer matrix (Hu 2007).

Improper curing is a matrix-dominated defect because during the cure cycle the resin changes its physical state from liquid to rubbery to glassy. Incomplete/non-uniform curing creates parts with thickness variation causing residual stress to build up, thus affecting the stiffness and toughness of the composites, whereas over-curing

can lead to matrix cracking or burning. Improper cure can also entrap volatiles, which can lead to void formation (Antonucci et al. 2006).

Mechanical processing steps such as drilling, trimming and machining can introduce inter-laminar matrix cracking. Matrix cracking can affect moisture absorption by providing more space for the moisture to penetrate the laminate. It can also act as a stress concentration point that causes the part to fail.

3.2.5 Porosity

Porosity in composites is a manufacturing defect caused by incomplete gas microbubbles outflow from the part during the process. A part of the microbubbles that should leave the part remains stuck to the layers and/or bonding interfaces and often combine to form discrete bubbles (Fig. 3.36). The discrete bubbles themselves can also combine and lead to macroscopic delamination or disbond. Porosity is generally defined per volume percentage. High porosity level (several percent) critically affects mechanical properties and thus aviation companies tend to severely limit porosity level to low values on critical parts (1.5% or 2% maximum). When the porosity level is high, the individual gas microbubbles often merge into voids. Actually, porosity and voids affect compressive, shear and bending strengths, which are dominated by the matrix properties. They also act as stress concentration points and possible damage initiation sites (Rubin and Jerina 1995).

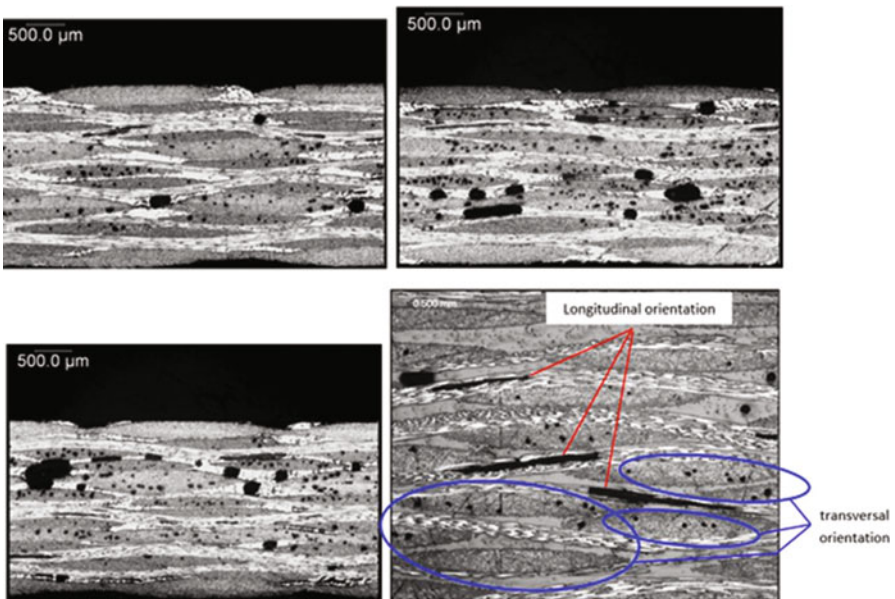


Fig. 3.36 Sections of CFRP laminates with porosity. Porosity bubbles tend to align with fibre orientation and thus often appear either in transversal or longitudinal direction

3.2.6 Fibre Breakage

Fibre breakage occurs when the applied stress is greater than the fracture strength of the fiber. Typically, failure due to fibre breakage occurs in steps. First, the fibre with an existing damage fails, which in turn, increases the load concentration in the surrounding intact fibres. Since the load distribution is now higher for the remaining fibres, the next weakest fibres tend to fail. This process will repeat until the entire structure fractures. Fibre breakage is generally caused in-service due to foreign-object impact, lightning strike, applied load, erosion, scratches and abrasion.

3.2.7 Other Composite Laminate Typical Defects

Apart from the defects mentioned above, composite laminate may have other defects such as non-uniform laminate thickness and wrinkles or waviness. Non-uniform laminate thickness is a typical manufacturing defect generally related to non-uniform pressure or moulding tool misplacement during fabrication. An example of non-uniform laminate thickness in radius is shown in Fig. 3.37. Wrinkles (waviness) is also a typical manufacturing defect generally related to uncontrolled layer displacement during processing. Wrinkles can significantly affect the mechanical properties of composite laminates. A typical laminate wrinkle in a radius is shown in Fig. 3.38. Waviness can be formed during the cool-down phase of composite

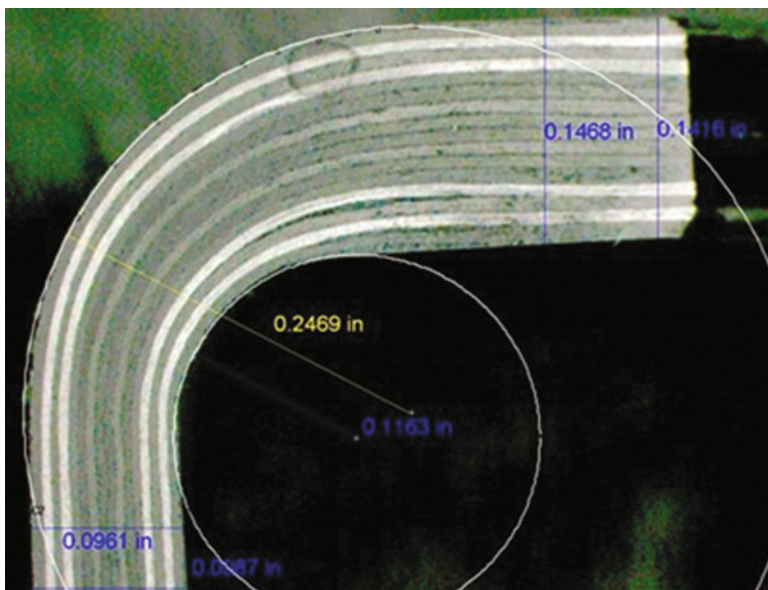


Fig. 3.37 Laminate non-uniform thickness in composite CFRP radius



Fig. 3.38 Laminate wrinkles in composite radius

manufacturing due to a mismatch in the thermal expansion between fibres and matrix and/or composite part and the tool plate (Kugler and Moon 2002). Also, during the fabrication stage, the lamina oriented in different directions attempts to slip with respect to one another. If this slippage is restricted by the neighbouring plies, waviness can form (Vanclooster et al. 2009). Because of waviness, shear stresses can be induced because of the offset angle between the fibres and the applied load. This shear stress produces shear strains, which leads to greater misalignment of fibres. Therefore, waviness reduces the compressive strength of a composite (Wisnom 1993).

3.2.8 Typical Honeycomb Core Defects

Apart from honeycomb to laminate disbond mentioned above, honeycomb cores may also suffer additional defects (see Figs. 3.39, 3.40, 3.41, and 3.42) that may occur both at manufacturing or in-service steps as defined: (a) honeycomb to honeycomb disbond in multicore structures, (b) condensed core that is a lateral distortion of the size of the cells relative to their axis, (c) buckled core that is a general lateral shift of the cells relative to their axis, (d) crushed core that is a collapse of the core parallel to the cell axis and (e) torn core that is characterized by cell breaking in a perpendicular direction to the cell axis, and this defect is often related to excessive core crushing.

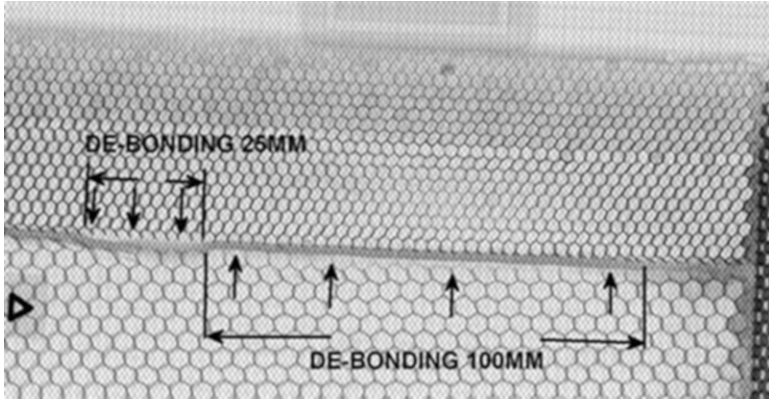


Fig. 3.39 X-ray radiography of honeycomb core to core disbond

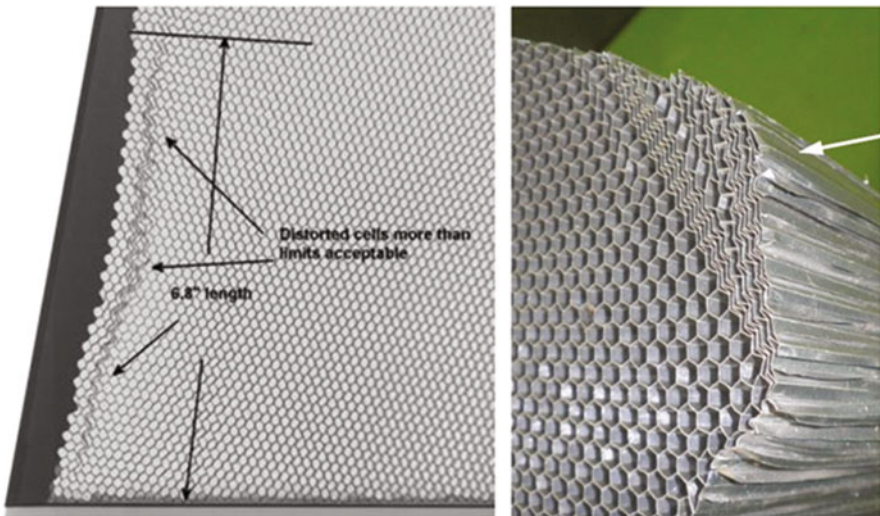


Fig. 3.40 X-ray radiography and visual examples of condensed honeycomb cores

3.2.9 Typical Foam Core Defects

Apart from foam to adhesive disbond defects mentioned above, foam cores may also experience other types of defects that may occur (see Fig. 3.43) both at manufacturing and in-service steps as defined: (a) core cracking that is generally related to excessive stress applied to the core and (b) core subsurface cracking that can be considered as a typical foam disbond defect. Since at bonding surface involving foam cores, an adhesive is always showing some slight penetration within the foam (less than 1 mm in thickness), the disbond appears within the foam just below the adhesive penetration line rather than at the foam limit line.

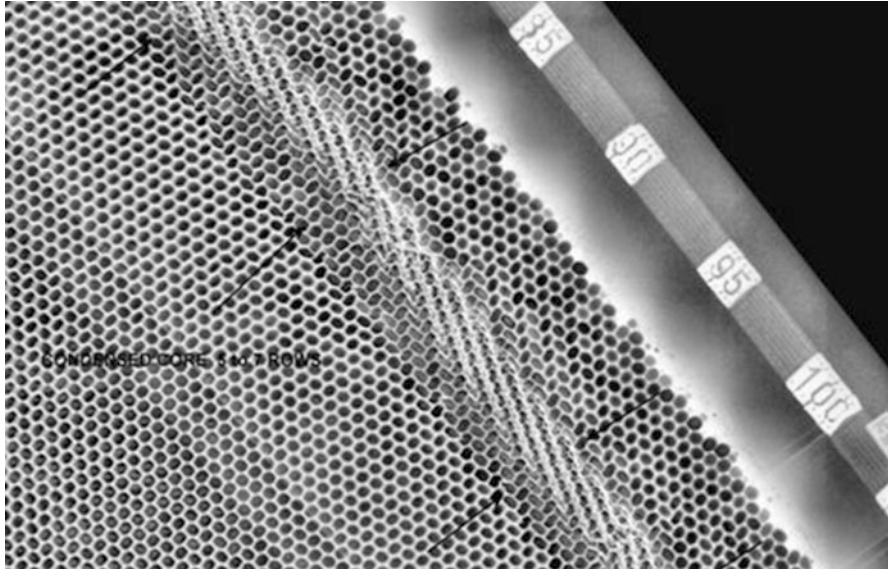
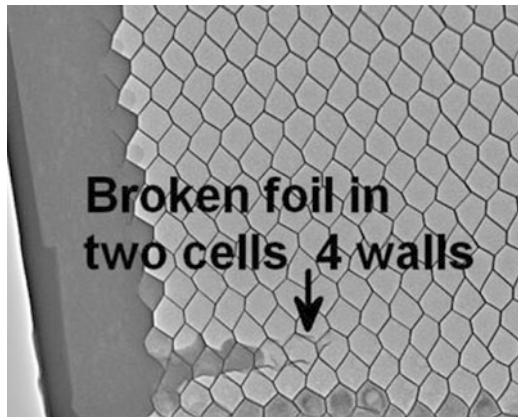


Fig. 3.41 X-ray radiography and buckled honeycomb core

Fig. 3.42 X-ray radiography and torn honeycomb core



3.2.10 Ingress of Moisture and Temperature

The material properties of fibre composites are also influenced by moisture and temperature. The effect is notably large at higher temperatures and moisture. Figure 3.44 shows the effect on the material properties obtained on small specimens (T300, fiber volume fraction = 0.6, 914C). The matrix 914C is one of the first generation used in aerospace. However, the general behaviour for different resin systems is similar.

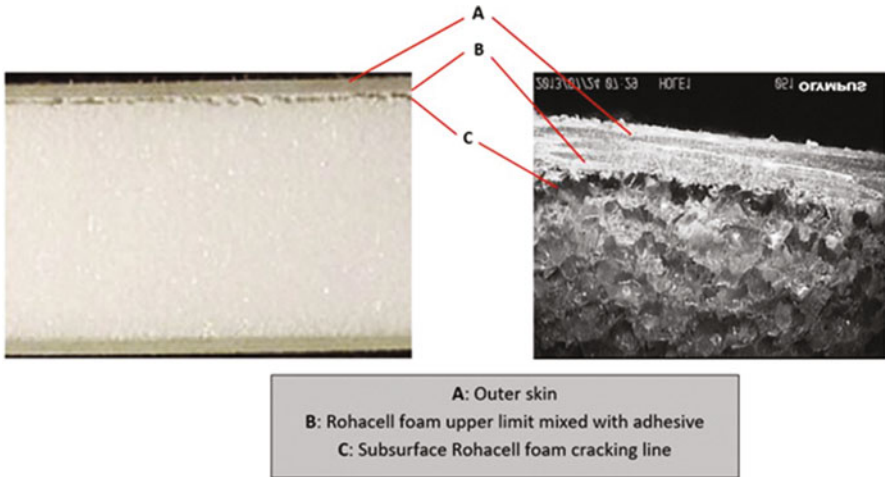


Fig. 3.43 Rohacell foam core subsurface cracking; This is a typical foam core disbond. Disbond appears below the actual Rohacell foam to skin interface as subsurface cracking rather than at the rohacell foam outer limit that is mixed with an adhesive

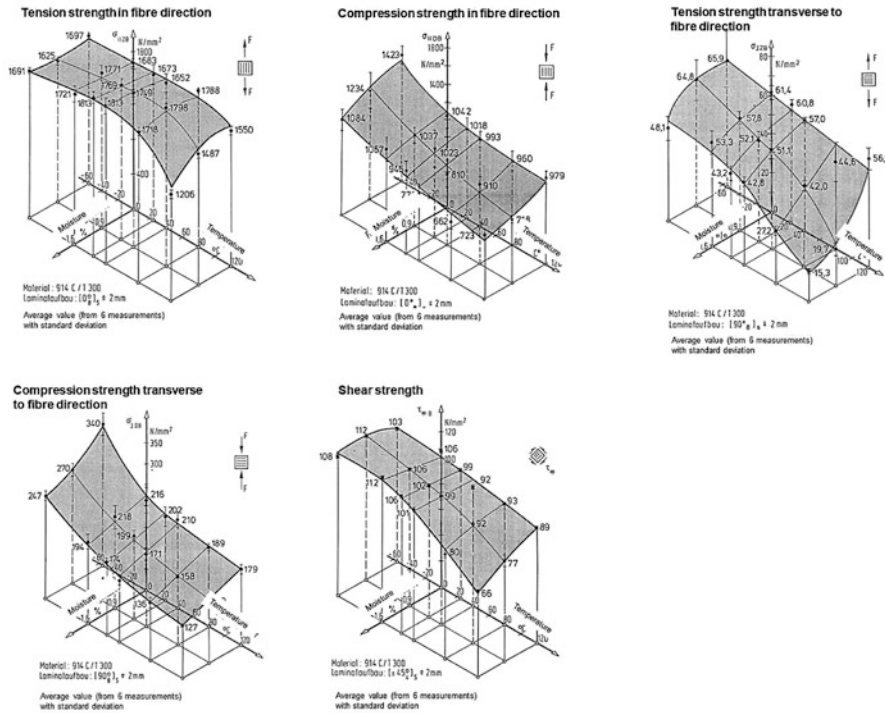


Fig. 3.44 Influence of moisture and temperature on the material properties (T300, phi = 0.6, 914C) (Gädke 1988)

3.2.11 Fatigue

Fatigue is the weakening of a material caused by cyclic loading that results in progressive and localized structural damage and growth. In metallics, the growth of cracks is considered. Fibre reinforced composites shows three phases of damage growth: (a) onset of first matrix cracks. With the growing number of cycles, the crack density increases and gets more compact. Crack density reaches its saturation level when the characteristic crack pattern is reached, (b) formation and growing of delamination and (c) buckling of delaminated areas and degradation until collapse. Different examples of fatigue loaded structures are as follows.

Figure 3.45 illustrates the characteristic crack pattern of a $[(0, +45, -45, 90)_2]_S$ laminate under $R = -1$ fatigue loading. Although the panel looks quite damaged the residual strength is still 85%. Figure 3.46 shows the influence of small impact damage on damage tolerance. For the static case, the influence of strength is reduced significantly to about 30-40%. However, under fatigue loading, these values are almost constant and only very slightly reduced to 25% strength, which is very damage tolerant. This behaviour is different from metallics where the influence of cracks is smaller for the static case and much larger for the fatigue loading. Figure 3.47 shows the fatigue behaviour of a $[0_2, +45, 0_2, -45, 0, 90]_S$ laminate with an artificial delamination of $\phi 10$ mm in the middle of the plate. The stress amplitude is ± 400 MPa and the stress ratio $R = -1$. The number of cycles until collapse is reached at 14.2×10^4 . It can be seen that the artificial delamination is almost no growing until collapse. However, there are more delaminations at the edges due to the free edge effects. Figure 3.48 shows the results of a stiffened CFRP panel cyclically loaded by axial compression. The panel was partly artificial pre-damaged by separation of the second stringer by a Teflon layer. In each cycle,

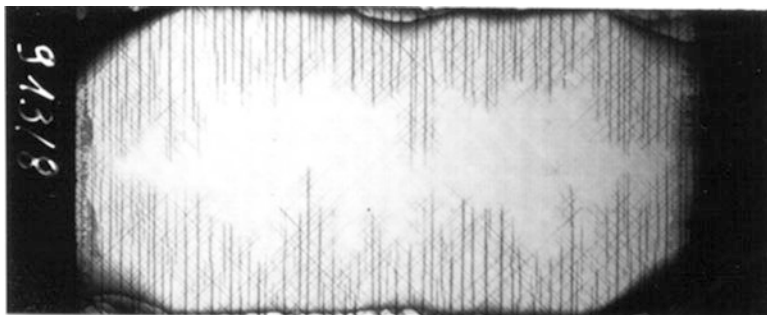


Fig. 3.45 Characteristic crack muster of a $[(0,+45,-45,90)_2]_S$ laminate under $R = -1$ fatigue loading which still has 85% of residual strength

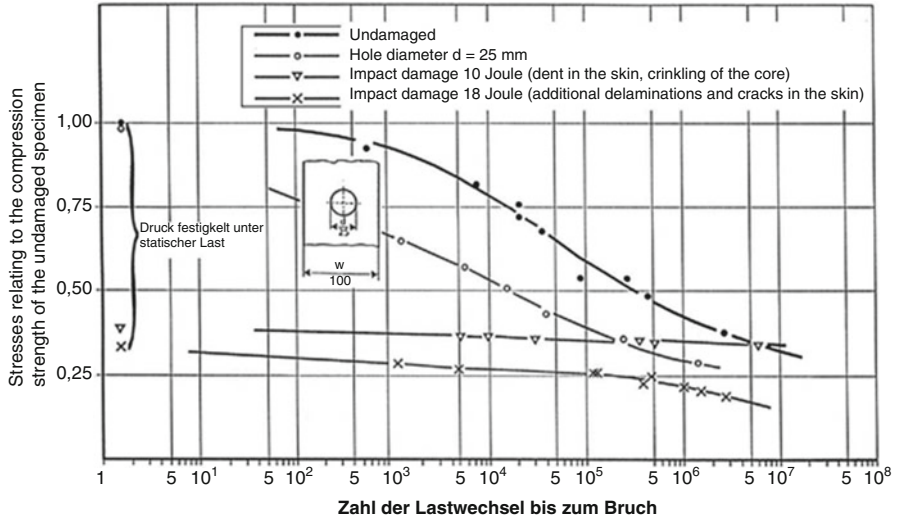


Fig. 3.46 Fatigue behaviour of a sandwich structure, $R = -1$, $f = 5$ Hz, Skin: GFRP fabrics [$\pm 45, 0/90$], Core: Nomex honeycomb 8 mm, Width $w = 100$ mm, Length [350(180) mm]

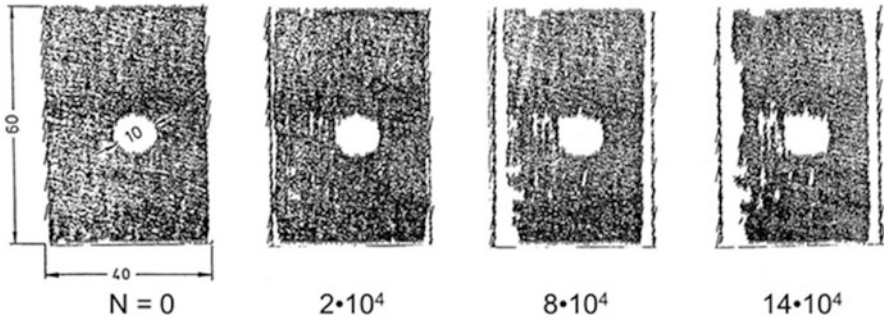


Fig. 3.47 Delamination growth under fatigue loading of a $[0_2, +45, 0_2, -45, 0, 90]_S$ laminate with an artificial delamination $\phi 10$ mm in the middle, stress amplitude ± 400 MPa, $R = -1$, the number of cycles until collapse $N = 14,2 \cdot 10^4$

the panel was loaded almost by collapse load. One cycle took 7 s. The figure shows thermography images at different cycles until collapse. In the first figure, the artificial separation of the second stringer is visible. In the next steps, other stringers start to separate from the skin. But the artificial separation does not grow until collapse (Degenhardt et al. 2008).

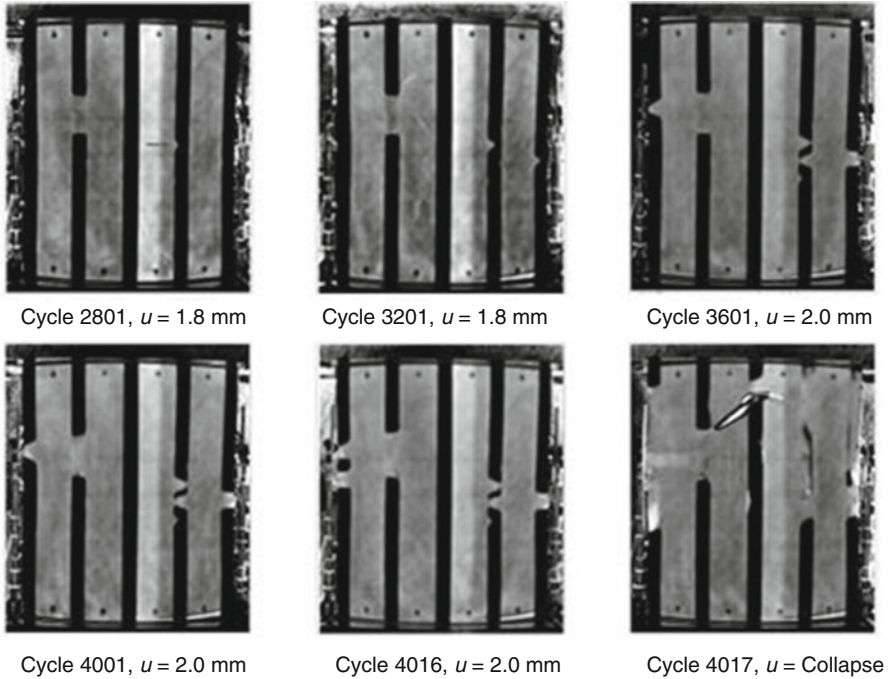


Fig. 3.48 Thermo-graphy images of a stiffened CFRP panel cyclically loaded by axial compression

3.3 Defects in Coatings

The main aim of the use of coatings (thin or thick films) in aircraft structures is to reduce or delay the effect of corrosion and wear in the component's structural integrity. These are important as corrosion and wear can cause serious safety and economic effects in the aerospace sector. Coatings of aircraft structures are expected to have a prolonged life in a very demanding or extreme environment, which includes thermo-mechanical loading cycles and ultraviolet radiation (Tiong and Clark 2010). The intrinsic resistance of the underlying substrate (alloys) alone is not sufficient to protect aircraft structural surface from demanding or extreme environments (Tiong and Clark 2010). Combination of corrosion and wear remain some of the considerable risks to aircraft structures and their integrity; both can decrease substrate section thicknesses, initiate micro-cracks, create stress concentrations zones and potentially inducing fatigue cracking leading to catastrophic failure. High quality coating material requirements for aeronautical applications makes the defect detection and inspection techniques of prime importance, both in manufacturing and in-service operation. The following subsections describe the major defects encountered in coating materials.

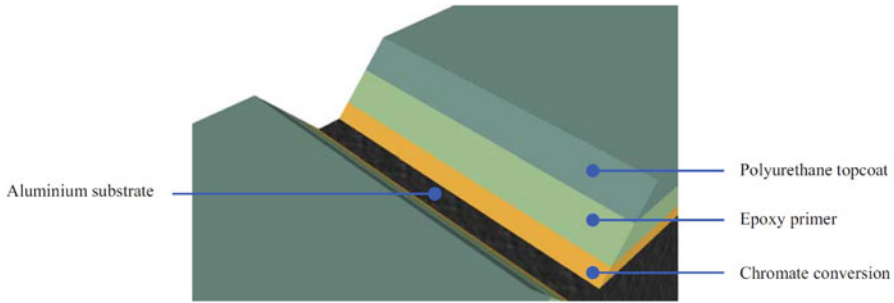


Fig. 3.49 Aircraft structural coating that consists of polyurethane topcoat, epoxy primer, chromatic conversion on the aluminium substrate (Tiong and Clark 2010)

3.3.1 Defects During the Manufacturing Process

One of the main aspects of applying surface coatings to the substrate is to improve the overall performance of the coated components. This can be achieved through the proper application of coatings technology, their characterization, testing and evaluation. As an example (Fig. 3.49), for corrosion-resistant applications, most aircraft surfaces are painted with a shielding layer consisting of chromatic conversion on the substrate, an epoxy primer and a polyurethane topcoat (typical total thickness of about 50–125 μm). The role of epoxy primers is to inhibit corrosion of underlying substrates, whereas the topcoat (polyurethane) is a layer that is resistant to a range of chemicals and weather, largely flexible layer and provides the desired surface appearance. A layer of sealant coat is useful at faying surfaces (surfaces that are in contact at a joint) to help provide the flexibility of the layer and prevent cracking (Tiong and Clark 2010).

Some of the manufacturing defects in paint layer during the application, drying and curing stages may include bleeding (leeching out of the painted layer), sagging (dripping of paint from top to bottom forming wavy appearance), wrinkling (formation of undulating wrinkling film), crawling (inability to form a film), crating (formation of small bowl-shaped depressions), lifting (by layers of coating on existing paint), prolonged drying time (inability to dry) and loss of gloss (caused by severe absorption of undercoat).

Beyond corrosion-resistant applications where paints are most suitable, over the last few decades, the number of coating of film deposition methods for wear protection in high-temperature applications such as chemical vapour deposition, physical vapour deposition, electrodepositing, radio frequency ion source implantation, electron beam implantation, thermally sprayed coating (air plasma, flame spray, high-velocity oxy-fuel), chemical catalytic reduction deposition, vacuum-diffused deposition and plasma arc deposition has evolved (Awang et al. 2020). There are many but some of the materials as a thin protective coating for aircraft applications are polymer, ceramic, diamond-like carbon (DLC), TiN, NiTi, (TiB+TiC)/Ti64, TiAlN, AlCrN, Al₂O₃, WS₂ and stellite.

Considering thermal spray coating technology in the aerospace and defence sector, it is used in a range of applications which includes landing gear parts (bearings, axles, pins), jet engine parts (blades, vanes, combustion liners, compressor casings, nozzles), actuation parts (pistons, pumps, flaps), engine cowling and wing span structures. Thermal spray coatings (e.g. using thermal barrier materials) protect engine turbine blades from high temperatures and ensures high reliability for a long period of time. In landing gear parts, thermally sprayed coatings are replacing hard chromium plating as the preferred coating method to provide improved mechanical performance. Some of the coating materials manufactured using thermal spray coating techniques are metals (e.g. MCrAlY), ceramics (e.g. zirconia, alumina), cermets (e.g. WC-Co) and composites (Gansert 2013).

Taking an example of alumina (Al_2O_3) coatings sprayed onto steel substrates using thermally sprayed techniques, have been used in aircraft parts because of their wear resistance properties (Thirumalaikumarasamy et al. 2014). Figures 3.50 and 3.51 shows some of the manufacturing features and defect in thermally sprayed coatings (air plasma spray-APS and high-velocity oxy-fuel-HVOF). The sprayed surfaces (Fig. 3.50a, b) show that the Al_2O_3 particles have spread and non-melted or semi-molten particles not distinguishable. Polished cross-sections of the sample (Fig. 3.50c, d) show a qualitatively higher porosity for the APS alumina

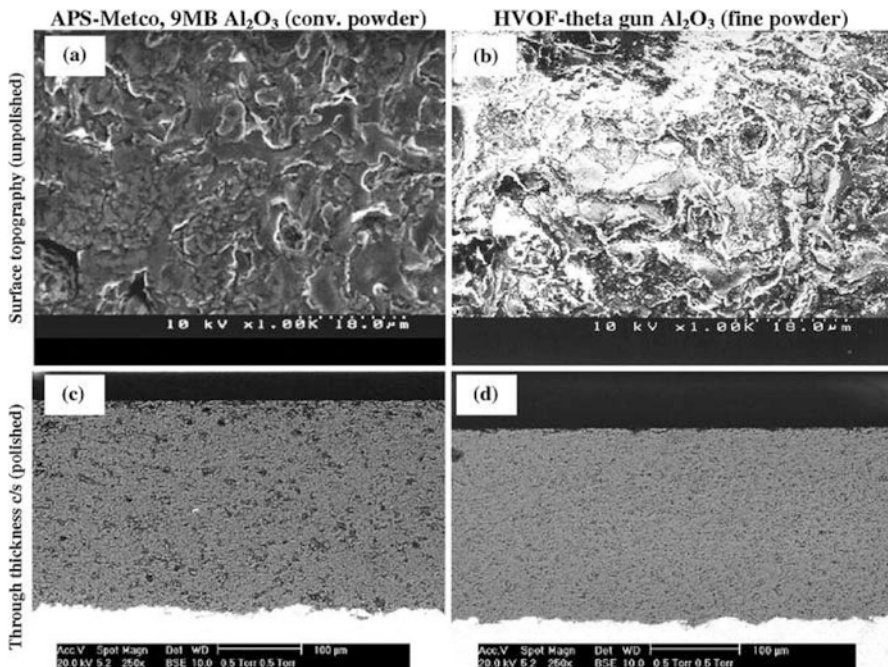


Fig. 3.50 Thermally sprayed alumina coatings on steel substrates: (a) and (b) showing surface topographies with definite splat morphologies, (c) and (d) through-thickness coating cross-sections (polished surface) (Ahmed et al. 2012)

(conventional powder) than HVOF alumina (fine powder). Average coating porosity was measured as 2.8% and 8.8% for the HVOF and APS coatings, respectively (Ahmed et al. 2012). The microscopic investigation revealed pores, voids, un-molten particle, non-bonded inter-splat areas and vertical cracks in splats, including columnar grain structure in lamellae (Fig. 3.51).

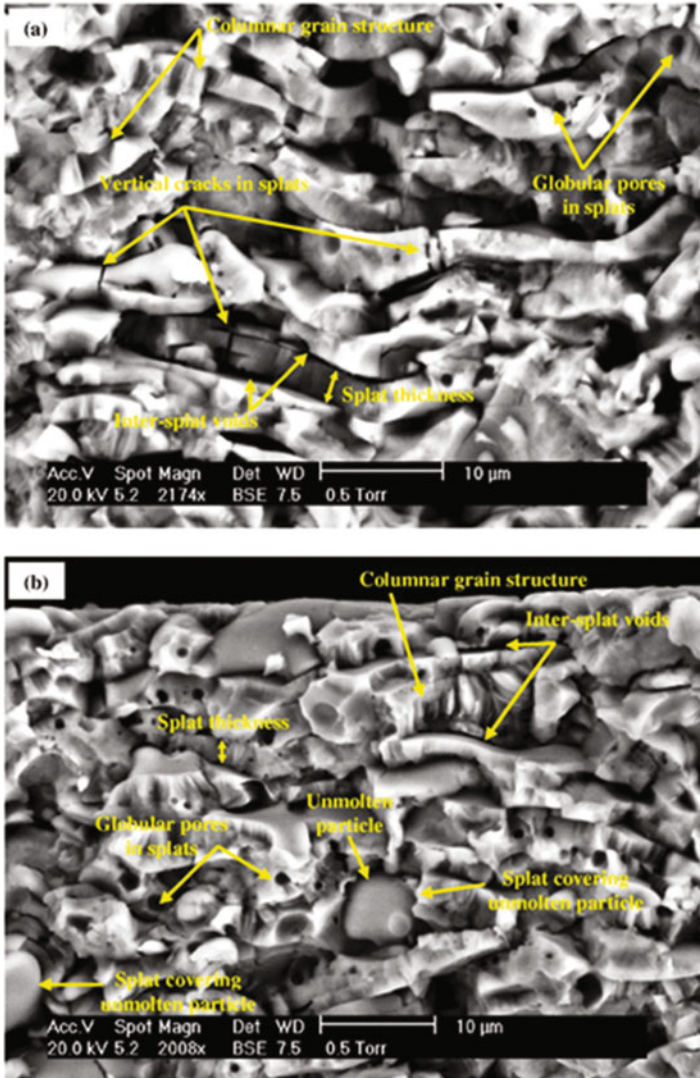


Fig. 3.51 SEM images of Al_2O_3 coatings (cryogenically fractured coating flakes) showing splat morphologies with columnar grain structure, pores, voids, vertical cracks in splats and unmolten particles: (a) APS Al_2O_3 and (b) HVOF Al_2O_3 (Ahmed et al. 2012)

All such coatings with underlying substrates require an optimized process parameter for coatings to adhere for a long period of time under service conditions. However, each of the coating deposition methods could induce some manufacturing defects if the process parameters are not appropriately managed. This can include poor adherence of coating to the substrate, high porosity, micro-cracks, non-uniform mechanical properties, through-thickness tensile residual stresses, poor wear resistance (sliding/erosive/abrasive), poor thermo-mechanical behaviour, etc. However, with the advancement in the coating deposition technologies and process optimization and control, it has been anticipated that the coating materials deposition quality measured during manufacturing is critical for enhancing our understanding of future generation applications (e.g. high-speed aircraft). Post-manufacturing coating characterization can include various microstructural characterizations and understanding the role of structure-property relationship through advanced characterisation tools (e.g. nanomechanical testing (Faisal et al. 2014; Faisal et al. 2017), acoustic emission sensor based in-situ mechanical testing (Faisal et al. 2011a), neutron diffraction residual strain testing (Ahmed et al. 2012), tribomechanical testing (Ali et al. 2017)). Overall, the coating tests can include mechanical, physical, chemical and weathering, whereas, the coating evaluation can include evaluation under various environmental conditions (e.g. under normal operation and/or in corrosive and wear conditions). All these testing including testing with sensors have the potential to improve our understanding of the structure-property relationships and failure characteristics of current and future generation coatings or thin films.

3.3.2 Defects During In-service Conditions

In-service defects in coatings can be classified according to the nature of environmental damage (corrosion, wear) and physical damage (thermo-mechanical loading) in aircraft structure. Overall, the testing of the integrity of coatings onto the substrate is extremely important for the evaluation of the coating-substrate system. Considering the extreme loading conditions in which the aircraft operates (more for the military than civilian aircraft), the obligation of very high mechanical strength of coating-substrate system deviates other gradual concerns (e.g. corrosion, wear) (Korb and Olson 1997). However, in all cases, it is important that coating is resistant to corrosion, has high adhesion strength with the substrate or between various layers and minimize creep in high-temperature conditions (Pokluda 2010).

Several coatings have been applied to aircraft engine parts (e.g. compressor blades) to develop multifunctional erosion and corrosion mitigations in harsh in-service conditions (Sun et al. 2020). In this work, the multi-arc ion plating technique was applied for TiN/Ti coating fabrication on the TC4 (Ti-5.60Al-3.07V, wt%) substrate. Note that such nitride coating depends not only on high mechanical strength but also on the complex mix of environmental conditions such as erosion and corrosion. Figure 3.52 shows the morphology and mechanism of pitting corrosion of TiN/Ti coating onto TC4 after 576 h salt spray corrosion). From

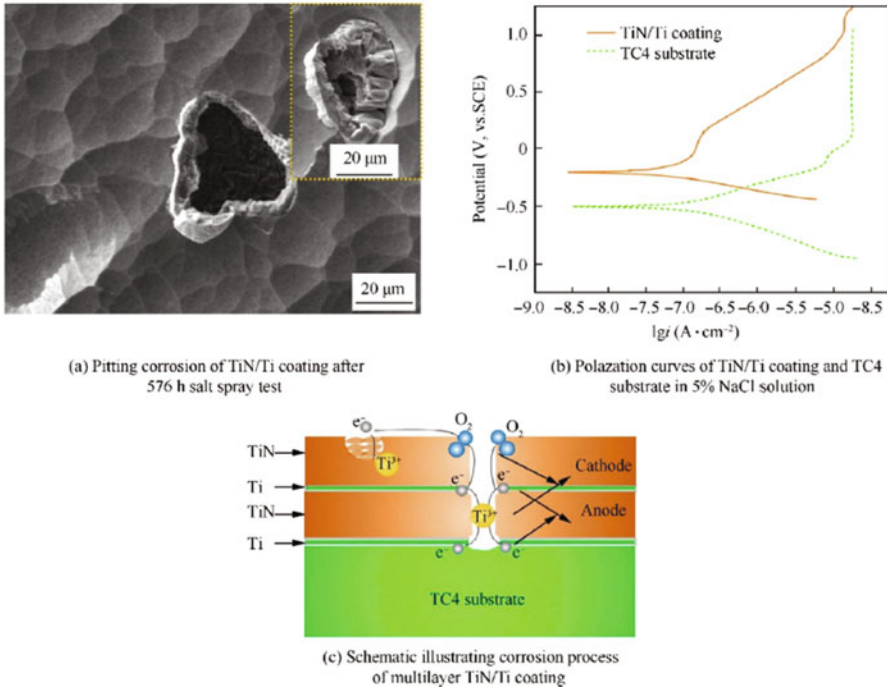


Fig. 3.52 Morphology and mechanism of pitting corrosion of TiN/Ti coating (Sun et al. 2020)

the Tafel polarization plots in Fig. 3.52b, it was observed that the corrosion potential difference promoted the corrosion cells between TiN and Ti, which were the cathode and anode for electrochemical corrosion (Sun et al. 2020), respectively, with corrosion process schematic shown in Fig. 3.52c. It was concluded that the structural design of multilayer dense coatings can be an improved way to prevent the medium of corrosion solutions.

Common defects in paint coatings during service life could be peeling or flaking, chalking, blistering, rust staining, algae or fungi growth, etc. For each of these defects, it requires a range of preventive and remedial methods that are necessary to rectify any unexpected defect.

Wear or damage of the coated surface due to the impact of small sand particles or large objects (such as bird strike), including indentation of the structure during handling process is what is thought to be the most common reason of inducing surface defects. If the coating layer is brittle, then potentially failure such as peeling or flaking can occur (e.g. Fig. 3.53). Physical damage to the coated surface can include thermal shock and fatigue while operating at various altitudes.

In most cases, the coating and substrate materials have different thermal expansion properties, therefore, a combination of thermal shock and fatigue loading can induce coating failure. During in-service conditions, as an example, the engine does not run constantly; therefore, during every flight, a change in thermo-mechanical

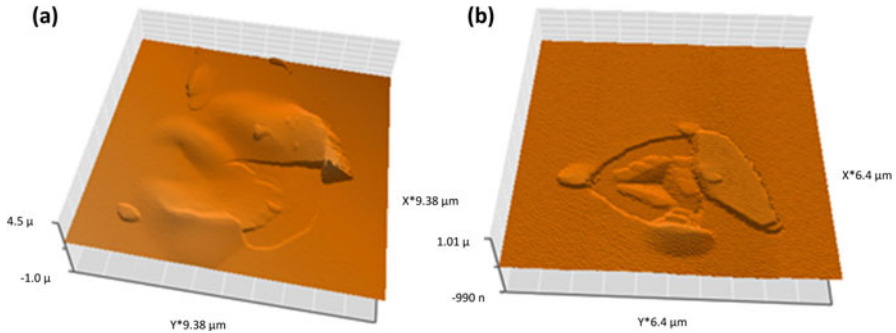


Fig. 3.53 Failure in brittle coating (100 nm thick DLC on silicon substrate) during 20-cycles nanoindentation: (a) under conical indenter at 200 mN and (b) Berkovich indenter at 10 mN

loading will cause significant strain mismatch at the interface of the coating-substrate system, leading to thermal fatigue damage to the coatings mainly.

The ductile-to-brittle transition (DBT) is important for the understanding of fracture or failure processes (Milne et al. 2003). In aircraft engine parts with coatings, if the ductile-to-brittle transition temperature of coatings is within the temperature range of the engine start phase, then the thermo-mechanical loading stress can cause failure in coatings. As the aircraft flies in airspace with various moisture contents and potentially a corrosive environment with excessive temperature would have an add on effect (oxidation and reduction of materials) to those effects mentioned above, leading to coating failure.

Coated components in aircraft structures when properly tested and in-situ monitored using sensors during in-service operations, can ensure a satisfactory lifespan before being further used. It is understood that regular maintenance may reduce the occurrence of in-service failures in coatings and associated parts by replacing suspect parts. However with the nature of some of the aircraft parts (e.g. turbine engine, landing gear), it is difficult all the time to inspect thoroughly each element of a given assembly. As such the structural health monitoring (SHM) using advanced sensing tools may be a way forward.

3.4 Defects in Joints

3.4.1 Adhesively Bonded Joints

Adhesive bonding of primary aircraft structures has been in use for more than 60 years. The qualification process of new adhesive technology is a protracted process involving fluid immersion testing, high, low and cyclic thermal performance testing followed by static buckling and fatigue testing. Adhesive bonding is for

example used in bonding stringers to the fuselage and to the skin to stiffen the structures against buckling. It is also used to manufacture the honeycomb structures used in the flight control structures such as elevators, ailerons, spoilers etc. Defects can be introduced both in manufacturing and during service. Thus, the characterization of defects both at the manufacturing and during service conditions is important. The qualification of an adhesive system is carried out not to assess the static performance but to evaluate the long-term durability. The evaluation is usually in comparison with an existing proven technology.

The aim of defect identification and characterization in adhesive bonds is to understand the mechanisms that lead to the creation of the defect, the effect of the defect on the performance of the adhesive joint and ultimately the damage tolerance of the joint. As with fastener-based joints, where the repair can be performed and the joint performance reinstated to 100% post-repair through a simple replacement of the fastener, a 100% regain of the adhesive joint strength is impossible unless a complete reapplication of the adhesive is performed. Hence, the defect type (e.g. Fig. 3.54) and severity must be identified accurately to assess the residual strength of the adhesive bond.

The adhesive bonding of two substrates is a complex phenomenon involving various fields of study. Several theories have been proposed to explain the bond formation, some of them being, mechanical interlocking, interface layer formation, weak boundary layer formation etc. The defects observed in adhesive bonds can be broadly classified into two categories namely those created during the manufacture and in-service defects. Manufacturing defects are created due to improper fabrication

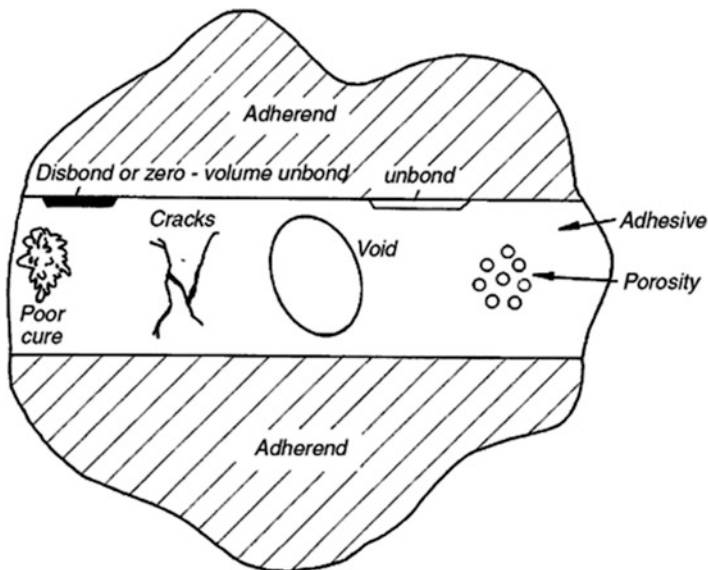


Fig. 3.54 Defects in an adhesive bond (da Silva et al. 2018)



Fig. 3.55 Void in the adhesive caused by premature handling of the joint before the adhesive cured (da Silva et al. 2018)

techniques related to substrate preparation and adhesive application. Conversely, service defects can be created due to environmental and operational loading factors.

Manufacturing defects in adhesive bonds are classified into three main types: (a) complete voids, disbonds, porosity. This type of defect occurs because of air trapped within the adhesive during the fabrication stage (e.g. Fig. 3.55), the presence of volatiles, defects in the application of the adhesive or insufficient quantity of adhesive. The mixing of the adhesive and hardener during fabrication can sometimes introduce air trapped within the mixture (b) poor adhesion, the improper bond between the adherends and the adhesives. This kind of defects occurs due to improper surface preparation and impurities being present on the surfaces of the adherends before fabrication and (c) kissing defects caused by the local disbonding of the adhesives and adherends. These are also called zero volume disbonds due to the very small dimensions along with the thickness. The wider category of surface disbonds into which kissing bonds fall into that created by the application of adhesive only on one of the adherends in the fabrication stage. Kissing bonds are the worst case of this.

The definition of kissing bonds varies, and several conflicting statements have been made in the literature. For example, Nagy (1991) defined kissing bonds as contact between two compressed but otherwise unbonded surfaces. Jiao and Rose (1991) defined them as two surfaces in perfect contact with each other, however without any ability to transmit shear stresses. However, this definition is not valid in the case of real adhesive bonds as no two surfaces can be in perfect contact and so can be applied in modelling studies only. They also proposed another method of modelling the joint with a thin layer of liquid present between the two disbonded

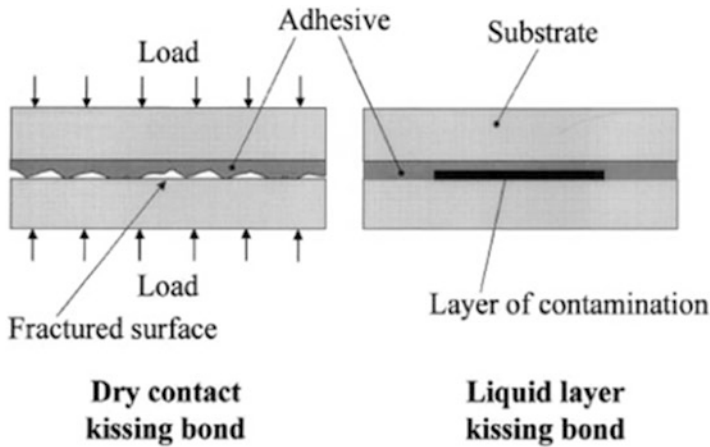


Fig. 3.56 Schematics of dry contact and liquid layer kissing bonds (Brotherhood et al. 2002)

surfaces. Due to the intimate contact of the surfaces in a kissing bond (e.g. Fig. 3.56), where some or all of the surface asperities on both the surfaces are in contact, despite the complete lack of adhesive strength, they are very difficult to detect with many of the conventional non-destructive evaluation techniques. With this combination of undetectability and severity, the presence and detection of kissing bonds present a significant practical problem in the application of adhesive bonds in primary load-carrying structures.

Problems with curing in terms of temperature, cure time or the improper mixing of the different parts of the adhesive mixture also cause porosity and adhesive cracks within the adhesive layer. Poor cure sometimes adjusts itself as the adhesive cures, though slowly. Voids are sometimes also caused because of the relative motion of the adherends with respect to each other during the cure (Fig. 3.55). The presence of voids has been shown to not have a significant effect on the failure initiation in lap joints (Karachalios et al. 2013). This was because, in most of the joints, the failure strain of the adhesive is quite low compared to the yield strength of the adherend materials used. However, if a rubber toughened epoxy were to be used along with high strength alloys for the adherends, the joint strength is almost proportional to the bonded area (Karachalios et al. 2013).

A brief discussion on the effect of the external contaminants introduced in the fabrication stage is given in the following paragraphs. Surface contaminants can be broadly categorized into two groups, namely organic and inorganic. The surface preparation required before bonding is different in each case, organic contaminants being the easier to remove through a simple degreasing process. Inorganic contaminants, conversely, need to be removed by degreasing, de-smutting and in some cases, deoxidization. Surface contamination tends to reduce the surface free energy. The effect of surface contaminants is studied by Smith and Crane (1980) using different levels of the controlled introduction of contaminants on the adherend surfaces. Contaminants like silicone grease, oils, fingerprints, cigarette smoke

residues, mucous, drink residues, lubricating oil were introduced on aluminium adherends which were chromium acid and phosphoric acid anodized. In joints with lubricating oil introduced, no significant reduction in the lap shear strength has been observed at contaminant thicknesses of 10 nm. However, in the case of silicone grease, a significant reduction in strength was observed in the contaminant thickness range of 3.5–20 nm. This is accompanied by a tendency towards a dominant interfacial failure. In the automotive industry, tolerance of adhesive bond strength to surface contamination of adherends has been tested. For example, Minford (1981) evaluated the effect of adherend immersion in lubricant solution on the joint strength. He reported that the presence of the oil did not make any difference till the surface concentration reached 0.95mg/cm^2 . The strength of the bond dropped by around 50% and the failure transitioned from 90% cohesive to more than 40% interfacial adhesive failure. Similarly, the bonds retained their original strength till an oil concentration of 0.62 gm/cm^2 when exposed to a humid or salt spray environment for 180 days. The effect of the presence of oil has been found to reduce the glass transition temperature (T_G) during the cross-linking process while curing. This has been noticed with an adhesive containing 6% dicyandiamide and with the same adhesive containing CaCO_3 filler. The reduction in TG was not noticed in the case of fully cross-linked adhesive. Similarly, Anderson (1993) studied the effects of HD-2 grease contamination on one of the adherends on the double tapered cantilever beam and butt joint tensile test performance. Hysol EA913 and EA946 were tested and the former exhibited a 50% reduction in the tensile strength at an oil contamination of 400 mg/m^2 , whereas the latter did not exhibit any reduction in strength.

Interfacial degradation appears in adhesive bonds when exposed to environmental factors such as high temperature and humidity. The bond formation across the interface is due to secondary and dispersive forces across. The interface work of adhesion is found to be a function of the interfacial free energies of the adherend and adhesive and the surface free energy. Metals tend to form oxide layers on the surface which are polar. This polar nature attracts water molecules which themselves are polar because of the hydrogen bonds. This leads to a disruption in the interfacial bonding between the adhesives and adherends. The work of adhesion in an inert environment tends to be positive leading to a strong bond, whereas in the presence of moisture, the work of adhesion could be negative leading to a disbond along the interface. In addition, certain metal oxides, such as aluminium oxide, react with water to form hydroxides which exhibit loose adhesion to the metal surface leading to a weak interfacial layer.

The general effect of hot and humid environments on the adhesive bond strength is summarised in Fig. 3.57. It shows the aluminium alloy lap joint strength degradation with respect to time of exposure to humidity. As shown, lower levels of humidity have significantly less effect on the bond strength compared to higher levels. This leads to the argument that there exists a critical concentration of moisture in the adhesive below, in which there will be no joint strength degradation. The dotted line in the plot indicated the strength recovery in a joint exposed to high humidity levels after exposure to lower humidity levels. This was attributed to the

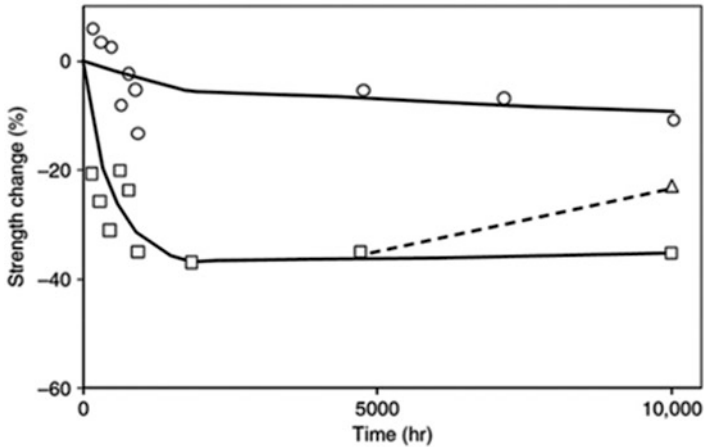


Fig. 3.57 Nitrile-phenolic adhesive-bonded aluminium alloy joints exposed to wet air at 50°C and circle legend—50%RH, square legend—100%RH, triangle legend—joint exposed to 100%RH for 5000 h and stored at 50% RH for 5000 h (Comyn et al. 1987)

failure in the primer close to the oxide layer rather than directly at the interface. The effect of moisture diffusion into the adhesive cannot be reversed and the joint strength degradation is irreversible. Moisture ingress in adhesive bonds can either be through direct absorption and diffusion through the adherends and the adhesive. In some cases, where the adherend diffusion is not possible, the cracks and voids present within the bond line promote the moisture uptake. Moisture usually leads to plasticization of the adhesive and/or changes in the glass transition (T_G) temperature in some cases. The rate at which the moisture diffuses into the bond line depends on the diffusion coefficient which in turn depends on the environmental temperature. Hence, hot and wet environments pose the most aggressive form of accelerated ageing to adhesive bonds.

Moisture diffusion in adhesives is dictated by Fick's law where the rate of diffusion of water is directly proportional to the square root of the exposure time. Where case II diffusion dynamics are in play, the diffusion rate is directly proportional to the exposure time. This is characterized by a saturated and swollen diffusion front travelling through the pristine polymer. Though Fick diffusion is seen in most adhesives, environmental conditions such as high temperature and high humidity tend to promote case II diffusion. Evidence has also been recorded of bulk adhesives that exhibit Fickian diffusion behaviour exhibit case II diffusion when bonded in a joint (Liljedahl et al. 2009). Once diffusion occurs, the moisture either occupies the free spaces or voids within the bond line as free water or exists as bound water. Bound water is responsible for the volumetric changes within the bond line, leading to residual stresses and undesirable stress concentrations which further promotes case II diffusion (Adamson 1980). The bound water can further be classified into Type I and Type II, in which Type I is responsible for single hydrogen bonds that

result in plasticization of the adhesive and reduction in the TG value of the adhesive (Zhou and Lucas 1995; Zhou and Lucas 1999a). Type II is where the water molecules form multiple hydrogen bonds lead to a promotion in secondary cross-linking and thus do not have a significant effect on T_G as that of Type I (Zhou and Lucas 1995). Typically, Type I water can be removed by low-temperature heating, Type II might need heating to a higher temperature (Zhou and Lucas 1999b). Kinloch et al. (2000) have reported that relatively viscous adhesives have difficulty penetrating the asperities and pores within the adherend and so promote the diffusion of moisture along the interface leading to premature rupture of the joint. However, when a low viscosity primer was applied to the adherend before adhesive application, the strength reduction has decreased drastically as the primer fills in the gaps which could be occupied by water. Similarly, moisture absorption in composite pre-pregs before curing is known to cause significant problems in bonding. The absorbed moisture diffuses to the surface of the substrate upon curing thus completely preventing any adhesion along the interface.

3.4.2 Friction Stir-Welded Joints

Metallic materials can be joined by a variety of methods including welding, brazing, adhesive bonding and mechanical fastening. For aerospace applications, friction stir welding (FSW) is very attractive because of ability to weld butt, lap- and T-joints, the ability to join difficult to weld classical alloys, ability to join dissimilar alloys, possible elimination of cracking in the fusion and heat-affected zone (HAZ), lack of weld porosity, etc. (Campbell 2006; Myśliwiec and Śliwa 2018; Śliwa et al. 2019; Myśliwiec et al. 2019).

Friction stir welding (FSW) is a solid-state joining process. It involves rotating a cylindrical tool with a short protrusion or ‘pin’, which is plunged between two metal plates (Fig. 3.58).

High pressure and shear strain plastically deform and consolidate the workpieces using material extrusion from the front to the back of the tool. The plates are clamped with a sturdy fixture to the backing plate with an anvil piece of hardened steel

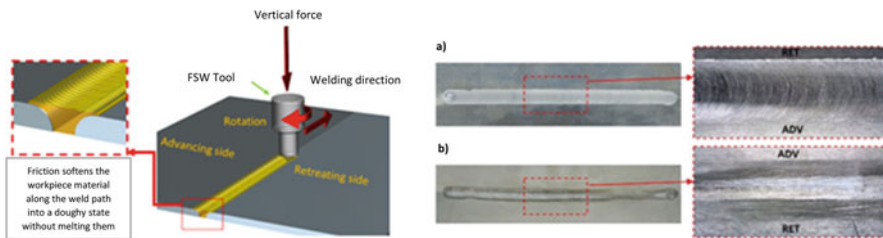


Fig. 3.58 Scheme of the FSW process—a lap joint and example joint without any defect (advancing side-a, retreating side-b) (Myśliwiec et al. 2019)

underneath the path of the FSW tool, counteracting the vertical and horizontal forces arising during welding. The combination of frictional and deformation heating around the immersed rotating pin and at the interface between the shoulder of the tool and the plates leads to the consolidation of the two metal plates as the tool traverses along the joint line. FSW process was invented in the Welding Institute (TWI) in the UK in 1991 and has been researched extensively since then and applied in various fields such as the automotive, marine and aerospace industries, where aluminium alloys are heavily used (Thomas et al. 1991; Huang et al. 2018).

Global trends in CO₂ emission and gas price have attracted extensive attention from the automotive manufacturing industry to produce lighter, safer and environmentally friendly vehicles (Guo et al. 2019). In conventional FSW, a tool consisting of a probe and a shoulder was commonly used. Generally, the diameter of the shoulder is about three times bigger than that of the probe. However, this type of tool is associated with several issues. One is the significant through-thickness temperature gradient because the heat generated by the shoulder is much higher than that by the probe, with the peak temperature developing at the top surface, which affects joint microstructure and properties. Another issue is the generation of the flash and arc corrugation because some plastic material moves out of the weld (Zhang et al. 2012).

To receive good welds of metals using friction stir welding (FSW) and avoid defects of such joints it is necessary to know characteristics of the material flow of alloys in FSW (e.g. Colligan 1999) by using a tracer material. Xu et al. (2001) developed two finite element models to predict the material flow during the FSW of Al alloys. Mishra and Ma (2005) described the current state of understanding and development of FSW. Fujii et al. (2006) demonstrated the influence of tool geometry, welding parameters and joint configurations on material flow and temperature distribution in FSW. Vijayan and Raju (2008) outlined the detailed parameters governing the joining process, including the rotation rate, welding speed, axial force and tool geometry. Kulkarni et al. (2018) investigated the influence of the type of the backing plate material on weld quality. Hook defects on AS (advancing side) and on RS (retreating side) of SSFSLW (stationary shoulder friction stir lap welding) joints at different welding speeds have been identified by Wen et al. (2019).

The FSW weld does not demonstrate many of the defect encountered in normal fusion welding and distortion is significantly less. But to consider the influence of all conditions and the process parameters on the final result of joining, it could be shown that the main possible defects (e.g. Fig. 3.59) occur when there is an inappropriate choice of parameters for a given case, especially for welding very thin sheets, and when plastic flow and stir materials in the welding zone are difficult to realize. The welds are created by the combined action of frictional heating and plastic deformation of the joined materials due to the rotating tool. To avoid defects, all important parameters, mainly the speeds and feeds influencing the heat input during welding, must be carefully chosen.

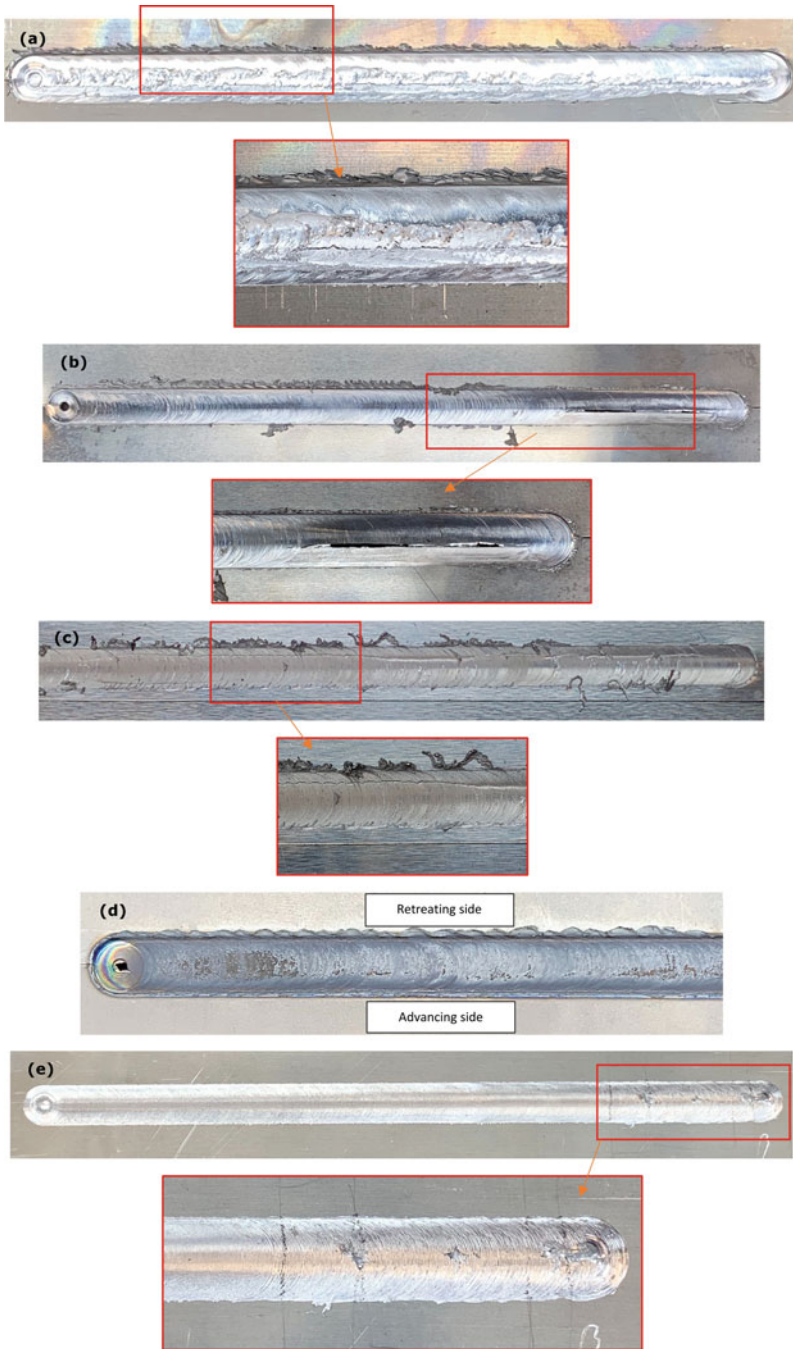


Fig. 3.59 Friction stir weld (FSW) joints with defects; (a) butt joints of AA2024-T3 of 2 mm in thickness defect types: exceeds flash, cracking of the joints, the unnormal stirring of the material, (b) butt joints of AA7075-T6 of 0.5 mm in thickness, defect types: exceeds flash, wormhole, (c) lap joints of AA2024-T3 1 mm in thickness, defect types: exceeds flash, cracking of the joints, (d) butt joints of titanium grade 5 of 0.5 mm in thickness, defect types: excessive oxidation of the joints and (e) butt joints of AA2024-T3 of 0.5 mm in thickness, defect type: cavities

3.5 Concluding Remarks

Understanding the fundamental nature of material defects or imperfections during manufacturing and in-service condition has been very important in materials and structural design of aircrafts over the last decades. Apart from testing and characterization of materials and structures using standard procedures, the application of sensors to carryout destructive, semi-destructive or non-destructive testing techniques are useful tools for investigating the condition of the materials or structural parts.

In the following chapters, the state-of-the-art methods of SHM and damage detection systems have been clearly laid out. Over the last years, the advancement in sensors, instrumentation, signal and image processing, including statistical analysis techniques, has led to a rapid change towards digitization (i.e. conversion to digital format) and digitalization (i.e. the use of digital technologies) of various sectors, including those in materials and manufacturing. Application of principles of artificial intelligence (AI) and machine learning (ML) approaches for digitalization is likely to bring substantial improvements in operational efficiency, defect detection, decision making and materials cost efficiency of aircraft structures.

If the structure of an aircraft is monitored, a tremendous amount of data can be generated by everyday operations. While there are existing methods of SHM and damage detection systems, but not clear how much is of current interest. Therefore, it is necessary to develop new improved models based on data-driven as well as theory-driven methodologies in real operation of aircraft and check the validity of existing models by synthesizing prior knowledge along with multimodal data in machine learning approaches.

Potentially, the systematic creation of digital twin (DT) to understand the fundamental nature of material defects or imperfections during manufacturing and defect during the in-service condition in aircraft structures can be a way forward. Through this, the utilization of large sets of Internet of Things (IoT) sensors data and combining it with historical findings in physical modelling along with artificial intelligence and advanced statistical algorithms can help in providing a near-real-time representation of aircraft structural defect analysis. With such a method, a continuous SHM monitoring and defect inspection can be done to save the efforts by physically inspecting the real aircraft asset. Also, it can be used for the pattern of aircraft structure manufacturing analysis, structural parts life estimation, failure diagnostics and prognostics, structural integrity monitoring and long-term production estimation. All such advancement can help in developing an intelligent decision support system for the type of defect in the various structural materials or parts.

References

- Abrate S (1991) Matrix cracking in laminated composites: a review. *Compos Eng* 1:337–353. [https://doi.org/10.1016/0961-9526\(91\)90039-U](https://doi.org/10.1016/0961-9526(91)90039-U)

- Adamson MJ (1980) Thermal-expansion and swelling of cured epoxy-resin used in graphite-epoxy composite- materials. *J Mater Sci* 15:1736-1745. <https://doi.org/10.1007/BF00550593>
- Aeronautics Guide, Forms of Corrosion (2019) Aircraft corrosion control, <https://www.aircraftsystemstech.com/2019/04/forms-of-corrosion-aircraft-corrosion.html>
- Ahmed R, Faisal NH, Paradowska AM et al (2012) Residual strain and fracture response of Al₂O₃ coatings deposited via APS and HVOF techniques. *J Therm Spray Technol* 21:23–40. <https://doi.org/10.1007/s11666-011-9680-7>
- Aircraft Owners and Pilots Association (n.d.) Aircraft Corrosion, Aircraft Owners and Pilots Association Website, <https://www.aopa.org/go-fly/aircraft-and-ownership/maintenance-and-inspections/aircraft-corrosion>
- Alemour B, Badran O, Hassan MR (2019) A review of using conductive composite materials in solving lightning strike and ice accumulation problems in aviation. *JAerosp Technol Manag* 11:e1919. <https://doi.org/10.5028/jatm.v11.1022>
- Ali O, Ahmed R, Faisal NH et al. (2017) Influence of post-treatment on the microstructural and tribomechanical properties of suspension thermally sprayed WC–12 wt%Co nanocomposite coatings. *Tribol Lett* 65:33. doi:<https://doi.org/10.1007/s11249-017-0815-y>
- Al-Jabbouli H, Koç E, Akça Y (2015) Classification of main faults in the production process of extruded aluminium profiles. *Int J Eng Technol* 7:84–90
- Anderson GL (1993) Continuum and fracture mechanical studies of contaminated bonding surfaces. *J Adhes* 41:129–137. <https://doi.org/10.1080/00218469308026558>
- Antonucci V, Cusano A, Giordano M et al. (2006) Cure-induced residual strain build-up in a thermoset resin. *Compos A* 37:592-601. doi:<https://doi.org/10.1016/j.compositesa.2005.05.016>
- Archer E, McIlhagger A (2015) Ch. 14 repair of damaged aerospace composite structures. In: Soutis C (ed) *Polymer composites in the aerospace industry*. Woodhead Publishing, Irving PE, pp 393–412
- Arrieta AJ, Striz AG (2005) Optimal design of aircraft structures with damage tolerance requirements. *Struct Multidisc Optim* 30:155–163
- Awang M, Khalili AA, Pedapati SR (2020) A review: thin protective coating for wear protection in high-temperature application. *Metals* 10:42. <https://doi.org/10.3390/met10010042>
- Banis D, Marceau JA, Mohaghegh M (1999) Design for corrosion. *Aero Magazine*, Issue 7, July 1999, Boeing. Available also, http://www.boeing.com/commercial/aeromagazine/aero_07/corrosn.html
- Bhadshia HKDH (2006) Aircraft undercarriage: martensitic steel. <https://www.phase-trans.msm.cam.ac.uk/2006/Undercarriage/Undercarriage.html>
- Black S (2013) Lightning strike protection strategies for composite aircraft. *Composite World*. <https://www.compositesworld.com/articles/lightning-strike-protection-strategies-for-composite-aircraft>
- Blaha J, Kremaszky C, Werner EA (2002) Carbide distribution effects in cold work tool steel. Proceedings of the 6th international tooling conference. Karlstad University, Karlstad, pp 289–298
- Bolotin VV (1996) Delaminations in composite structures: its origin, buckling, growth and stability. *Compos Part B* 27:129–145
- Brand C, Boller C (1999) Identification of life cycle cost reduction in structures with self-diagnostic devices. NATO RTO symposium on design for low cost operation and support. Ottawa, Canada, 21–22 October 1999.
- Brooks CR, Choudhury A (2002) Failure analysis of engineering materials. The McGraw-Hill Education, New York, NY. <http://www.ncbi.nlm.nih.gov/pubmed/101221>
- Brotherhood C, Drinkwater B, Guild F (2002) The effect of compressive loading on the ultrasonic detectability of kissing bonds in adhesive joints. *J Nondestruct Eval* 21(3):95–104
- Campbell FC (2006) Manufacturing technology for aerospace structural materials. Elsevier, Amsterdam
- Civil Aeronautics Board, Accident Investigation (1949) Available report, SA-178, File No. 1, <https://www.baaa-acro.com/sites/default/files/import/uploads/2016/04/NC93044.pdf>. Released 0117
- Colligan BK (1999) Supplement to the Weld J 6:229–237

- Comyn J, Brewis DM, Tredwell ST (1987) Bonding of aluminium alloy with some phenolic adhesives and a modified epoxide adhesive, and strength changes on exposure to moist air at 50°C. *J Adhes* 21(59-78):59–78. <https://doi.org/10.1080/00218468708074959>
- Criou O (2007) A350 XWB family & technologies. Presentation at Hamburg University of Applied Sciences 20 September 2007. https://www.fzt.haw-hamburg.de/pers/Scholz/dgIrh/hh/text_2007_09_20_A350XWB.pdf
- da Silva LFM, Öchsner A, Adams RD (2018) De/Anti-icing process coordination handbook of adhesion technology, 2nd edn. Springer International Publishing. <https://deicing.net/>
- Degenhardt R, Wilckens D, Klein H et al (2008) Experiments to detect the damage progress of axially compressed CFRP panels under cyclic loading. *Key Eng Mater* 383:1–24
- Dolbeer RA, Wright SE (2008). Wildlife strikes to civil aircraft in the United States 1990–2007. US Department of Transportation, Federal Aviation Administration, Office of Airport Safety and Standards, Serial Report 14. Washington D.C., USA
- Dolbeer RA, Begier MJ, Miller PR et al (2019) Wildlife strikes to civil aircraft in the United States 1990–2018. US Department of Transportation, Federal Aviation Administration, Office of Airport Safety and Standards, serial report. Washington, DC, p 25
- Ejaz N, Qureshi IN, Rizvi SA (2011) Creep failure of low pressure turbine blade of an aircraft engine. *Eng Fail Anal* 18:1407–1414. <https://doi.org/10.1016/j.engfailanal.2011.03.010>
- Faisal NH, Ahmed R, Reuben RL (2011a) Indentation testing and its acoustic emission response: applications and emerging trends. *Int Mater Rev* 56:98–142. <https://doi.org/10.1179/1743280410Y.0000000004>
- Faisal NH, Reuben RL, Ahmed R (2011b) An improved measurement of Vickers indentation behaviour through enhanced instrumentation. *Meas Sci Technol* 22:18 pp. art no. 015703. <https://doi.org/10.1088/0957-0233/22/1/015703>
- Faisal NH, Ahmed R, Goel S et al (2014) Influence of test methodology and probe geometry on nanoscale fatigue mechanisms of diamond-like carbon thin film. *Surf Coat Technol* 242:42–53
- Faisal NH, Prathuru AK, Goel S et al. (2017) Cyclic nanoindentation and nano-impact fatigue mechanisms of functionally graded TiN/TiNi film (Special edition on Functional Performance of Shape Memory Alloys). *Shape Memory Superelasticity* 3(2):149–167. <https://doi.org/10.1007/s40830-017-0099-y>
- Fang T-T (2018) Point defects in crystalline materials. Elements of structures and defects of crystalline materials. pp 83–127
- Findlay SJ, Harrison ND (2002) Why aircraft fail. *Mat Today* 5:18–25. [https://doi.org/10.1016/S1369-7021\(02\)01138-0](https://doi.org/10.1016/S1369-7021(02)01138-0)
- Freitas M, Infante V, Baptista R (2019) Failure analysis of the nose landing gear axle of an aircraft. *Eng Fail Anal* 101:113–120. <https://doi.org/10.1016/j.engfailanal.2019.03.010>
- Fujii H, Cui L, Maeda M et al (2006) Effect of tool shape on mechanical properties and micro-structure of friction stir welded aluminum alloys. *Mater Sci Eng A* 419:25–31. <https://doi.org/10.1016/j.msea.2005.11.045>
- Gädke M (1988) Hygrothermomechanisches Verhalten kohlenstofffaserverstärkter Epoxidharze. VDI-Bericht, Reihe 5, Nr. 136, VDI-Verlag, Düsseldorf
- Gansert R (2013) Thermal spray coatings in the aerospace and defense industries. *Int Thermal Spray Surface Eng* 8
- Gayathri P, Umesh K, Ganguli R (2010) Effect of matrix cracking and material uncertainty of composite plates. *Reliab Eng Syst Saf* 95:716–728. <https://doi.org/10.1016/j.res.2010.02.004>
- Gilbert JL (2020) *Metals: basic principles, biomaterials science*, 4th edn. pp 205–228.e1
- Girodin G, Manes L, Moraux J-Y et al. (2002) Characterisation of the XD15N high nitrogen martensitic stainless steel for aerospace bearings. 4th International conference on launcher technology ‘Space Launcher Liquid Propulsion’, 3–6 2002. Liege, Belgium
- Guo S, Shah L, Ranjan R et al (2019) Effect of quality control parameter variations on the fatigue performance of aluminum friction stir welded joints. *Int J Fatigue* 118:150–161. <https://doi.org/10.1016/j.ijfatigue.2018.09.004>

- Hartman N (2008) Deicing an aircraft during a snow event. https://www.wikiwand.com/en/Deicing_fluid
- Heimbs S (2012) Energy absorption in aircraft structures, In: International workshop on hydraulic equipment and support systems for mining, Huludao, China, pp 17-18
- Hiroshi N (2014) Defects in metals, physical metallurgy, 5th edn. pp 561-637
- Hu HW (2007) Physical aging in long term creep of polymeric composite laminates. *J Mech* 23:245-252. <https://doi.org/10.1017/S1727719100001283>
- Huang Y, Wan L, Meng X et al (2018) Probe shape design for eliminating the defects of friction stir lap welded dissimilar materials. *J Manuf Process* 35:420-427. <https://doi.org/10.1016/j.jmapro.2018.08.026>
- Jiao D, Rose JL (1991) An ultrasonic interface layer model for bond evaluation. *J Adhes Sci Technol* 5:631-646. <https://doi.org/10.1163/156856191X00530>
- Karachalios EF, Adams RD, da Silva LFM (2013) Strength of single lap joints with artificial defects. *Int J Adhes Adhes* 45:69-76. <https://doi.org/10.1016/j.ijadhadh.2013.04.009>
- Kinloch AJ, Little MSG, Watts JF (2000) The role of the interphase in the environmental failure of adhesive joints. *Acta Mater* 48:4543-4553. [https://doi.org/10.1016/S1359-6454\(00\)00240-8](https://doi.org/10.1016/S1359-6454(00)00240-8)
- Korb LJ, Olson DL (eds.) (1997) ASM handbook – corrosion, 9th edn. ASM International 13
- Kugler D, Moon TJ (2002) Identification of the most significant processing parameters on the development of fibre waviness in thin laminates. *J Compos Mater* 36:1451-1479. <https://doi.org/10.1177/0021998302036012575>
- Kulkarni BS, Pankade SB, Andhale SR et al (2018) Effect of backing plate material diffusivity on microstructure, mechanical properties of friction stir welded joints: a review. *Procedia Manuf* 20:59-64. <https://doi.org/10.1016/j.promfg.2018.02.008>
- Kutyinov VF, Ionov AA (1996) Ch. 1 specific features of composite-material structural design. In: Zagainov GI, Lozinolozinsky GE (eds) *Composite materials in aerospace design*. Chapman and Hall, ISBN 0412584700. pp 1-117
- Lee BW, Suh J, Lee H et al (2011) Investigations on fretting fatigue in aircraft engine compressor blade. *Eng Fail Anal* 18:1900-1908. <https://doi.org/10.1016/j.engfailanal.2011.07.021>
- Liljedahl CDM, Crocombe AD, Gauntlett FE et al (2009) Characterising moisture ingress in adhesively bonded joints using nuclear reaction analysis. *Int J Adhes Adhes* 29:356-360. <https://doi.org/10.1016/j.ijadhadh.2008.07.005>
- McBrearty JF (1956) Fatigue and fail-safe airframe design. *SAE Trans* 64:426-436
- Mills T, Prost-Domasky S, Honeycutt K, Brooks C (2009) Chapter 3: corrosion and threat to aircraft structural integrity. In: *Corrosion control in aerospace industry*. Woodhead publishing series in metals and surface engineering. 35-66. <https://doi.org/10.1533/9781845695538.1.35>
- Milne I, Ritchie RO, Karihaloo B (2003) Interfacial and nanoscale failure, comprehensive structural integrity – section 8. Elsevier Science Ltd, Amsterdam. isbn:978-0-08-043749-1
- Minford J (1981) *Aluminium*. 57(10):657
- Mishra RS, Ma ZY (2005) Friction stir welding and processing. *Mater Sci Eng R* 50:1-78. <https://doi.org/10.1016/j.mser.2005.07.001>
- Mittelstedt C, Becker W (2007) Free-edge effects in composite laminates. *Appl Mech Rev* 60:217-245. <https://doi.org/10.1115/1.2777169>
- Mouritz A (2012a) Chapter 3, Materials and material requirements for aerospace structures and engines. In: Mouritz A (ed) *Introduction to aerospace materials*. Woodhead Publishing Limited, pp 39-56. ISBN: 978-1-85573-946-8
- Mouritz A (2012b), Chapter 21, Corrosion of aerospace metals. In: Mouritz A (ed) *Introduction to aerospace materials*. Woodhead Publishing Limited, pp 498-520. ISBN: 978-1-85573-946-8
- Mouritz A (2012c), Chapter 22, Creep of aerospace materials. In: Mouritz A (ed) *Introduction to aerospace materials*. Woodhead Publishing Limited, pp 521-530. ISBN: 978-1-85573-946-8
- Myśliwiec P, Śliwa RE (2018) Friction stir welding of thin sheets of magnesium alloy AZ31B. *Arch Metall Mater* 63(1):45
- Myśliwiec P, Śliwa RE, Ostrowski R (2019) Friction stir welding of ultra thin AA2024-T3 aluminium sheets using ceramic tool. *Arch Metall Mater* 64(4):1385-1394

- Nagy PB (1991) Ultrasonic classification of imperfect interfaces. *J Adhes Sci Technol* 5:619–630. <https://doi.org/10.1163/156856191X00521>
- Pawłowska P, Sliwa RE (2015) Backward extrusion of aluminum alloy sections used in aircraft structural components. *Arch Metall Mater* 60:2805–2811
- Peel CJ, Gregson PJ (1995) Design requirements for aerospace structural materials, high performance materials in aerospace. Chapman & Hall, London
- Pokluda J (2010) Damage and performance assessment of protective coatings on turbine blades. *Intech Eur* 2010:283–304
- Rebhi L, Krstic B, Boutemedjet A et al (2018) Fatigue fracture analysis of an ADF antenna in a military aircraft. *Eng Fail Anal* 90:476–488. <https://doi.org/10.1016/j.engfailanal.2018.04.013>
- Rosato D (2013) Designing with plastics and composites: a handbook. Springer Science & Business Media, Boston
- Rossmann A (2020), Damage due to Stress Corrosion Cracking (SCC) in Aeroengine Safety, Institute of Thermal Turbomachinery and Machine Dynamics, Graz University of Technology. <https://aeroenginesafety.tugraz.at/doku.php?id=5:54:542:5422>
- Rubin AM, Jerina KL (1995) Evaluation of porosity in composite aircraft structures. *Mech Compos Mater* 30:587–600. <https://doi.org/10.1007/BF00821276>
- Rupke JE (2006) What happens when lightning strikes an airplane? *Scientific American*, <https://www.scientificamerican.com/article/what-happens-when-lightning/#:~:text=Although%20passengers%20and%20crew%20may,the%20nose%20or%20wing%20tip>
- Ruth AS (1973) Own work, CC by 3.0. <https://commons.wikimedia.org/w/index.php?curid=25218657>
- Śliwa RE, Pawłowska B, Balawender T (2016) Metallic lightweight composite profiles for aviation obtained in extrusion process, AVT-264 Specialist,s Meeting on Design, Manufacturing and Application of Metallic Lightweight Material Components for Military Vehicles (NATO – unclassified + Sweden+Australia and New Zealand, NATO Conference, 2016, Tallin, Estonia
- Śliwa RE, Balawender T, Hadasik E et al (2017) Metal forming of lightweight magnesium alloys for aviation applications. *Arch Metall Mater* 62:1559–1566. <https://doi.org/10.1515/amm-2017-0239>
- Śliwa RE, Myśliwiec P, Ostrowski PR et al. (2019) Possibilities of joining different metallic parts of structure using friction stir welding methods. *Procedia Manuf* 27:158–165. <https://doi.org/10.1016/j.promfg.2018.12.059>
- Smith T, Crane R (1980) Proceedings of the national SAMPE symposium, p 2
- Sun Z, He G, Meng Q et al (2020) Corrosion mechanism investigation of TiN/Ti coating and TC4 alloy for aircraft compressor application. *Chin J Aeronaut* 33:1824–1835. <https://doi.org/10.1016/j.cja.2019.08.015>
- Sweers G, Birch B, Gokcen J (2014) Lightning strikes: protection, inspection, and repair. *AERO Magazine by Boeing* 4:19–28
- Snyder D (2014) Computational design of high-strength, SCC-resistant aluminum alloys for aerospace applications. Presented in Materials Technology Laboratory / Steel Research Group, 30th Annual Meeting, Northwestern University, 24–25 March 2014, Evanston, IL, USA. https://chimid.northwestern.edu/docs/SRG2014/SRG2014_Snyder.pdf
- Thirumalaikumarasamy D, Shanmugam K, Balasubramanian V (2014) Corrosion performance of atmospheric plasma sprayed alumina coatings on AZ31B magnesium alloy under immersion environment. *J Asian Ceramic Soc* 2:403–415. <https://doi.org/10.1016/j.jascer.2014.08.006>
- Thomas WM, Nicholas ED, Needham JC et al. (1991) Friction stir butt welding. International Patent Application PCT/GB92/02203 GB patent Application 9125978.8.
- Tiffany CF, Gallagher JP, Babish C et al. (2010) Threats to structural safety, including a compendium of selected structural accidents/incidents, USAF Technical Report ASC-TR- 2010-5002, Aeronautical Systems Center Engineering Directorate. Wright-Patterson Air Force Base, OH 45433–7101
- Tiong UH, Clark G (2010) The structural environment as a factor affecting coating failure in aircraft joints. *Procedia Eng* 2:1393–1401. <https://doi.org/10.1016/j.proeng.2010.03.151>

- Tomblin J, Seneviratne W, Pillai GR (2009) Effect of disbonds, lightning strikes, and low-velocity impact damage on adhesively bonded composite joints, FAA-AR-09-4, Final Report. <http://www.tc.faa.gov/its/worldpac/techrpt/ar094.pdf>
- Trifkovic D, Stupar S, Bosnjak S et al. (2011) Failure analysis of the combat jet aircraft rudder shaft. *Eng Fail Anal* 18:1998–2007. <https://doi.org/10.1016/j.engfailanal.2011.05.017>
- Tyczyński P, Śliwa RE, Ostrowski R (2015) Analysis of possibilities for modification of drill bit geometrical parameters used to drill holes in composite materials of various composition. *Aircraft Engineering and Aerospace Technology* 87(2):120–130. <https://doi.org/10.1108/AEAT-06-2014-0094>
- US National Oceanic and Atmospheric Administration (n.d.) Icing Tutorial, National Weather Service ZHU training page, https://www.weather.gov/source/zhu/ZHU_Training_Page/ZHU_Training_Page.html
- Vanclooster K, Lomov SV, Verpoest I (2009) On the formability of multi-layered fabric composites. in ICCM—17th International Conference on Composite Materials. Edinburgh, United Kingdom
- Vijayan S, Raju R (2008) Process parameter optimization and characterization of friction stir welding of aluminum alloys, *International Journal of Applied Engineering Research*, 3:1303–1316
- Vorontsov AN, Murzakhanov GK, Shchugorev VN (1990) Delamination failure of composite structures. *Mech Compos Mater* 25:723–737. <https://doi.org/10.1007/BF00613361>
- Wanhill RJH, Amsterdam E (2010) Aircraft Stress Corrosion in the Netherlands: 1965–2010, National Aerospace Laboratory (NRL) Report.
- Wen Q, Li WY, Wang WB et al (2019) Experimental and numerical investigations of bonding interface behavior in stationary shoulder friction stir lap welding. *J Mater Sci Technol* 35:192–200. <https://doi.org/10.1016/j.jmst.2018.09.028>
- Wisnom MR (1993) Analysis of shear instability in compression due to fibre waviness. *J Reinf Plast Compos* 12:1171–1189. <https://doi.org/10.1177/073168449301201103>
- Xu S, Deng X, Reynolds AP et al. (2001) Finite element simulation of material flow in friction stir welding. *Sci Technol Weld Joining* 6:191–193. <https://doi.org/10.1179/136217101101538640>
- Zhang YN, Cao X, Larose S et al (2012) Review of tools for friction stir welding and processing. *Can Metall Q* 51:250–261. <https://doi.org/10.1179/1879139512Y.0000000015>
- Zhou JM, Lucas JP (1995) The effects of a water environment on anomalous absorption behaviour in graphite-epoxy composites. *Compos Sci Technol* 53:57–64. [https://doi.org/10.1016/0266-3538\(94\)00078-6](https://doi.org/10.1016/0266-3538(94)00078-6)
- Zhou JM, Lucas JP (1999a) Hygrothermal effects of epoxy resin. Part I: the nature of water in epoxy. *Polymer* 40:5505–5512. [https://doi.org/10.1016/S0032-3861\(98\)00790-3](https://doi.org/10.1016/S0032-3861(98)00790-3)
- Zhou JM, Lucas JP (1999b) Hygrothermal effects of epoxy resin. Part II: variations of glass transition temperature. *Polymer* 40:5513–5522. [https://doi.org/10.1016/S0032-3861\(98\)00791-5](https://doi.org/10.1016/S0032-3861(98)00791-5)

Open Access This chapter is distributed under the terms of the Creative Commons Attribution 4.0 International License (<http://creativecommons.org/licenses/by/4.0/>), which permits use, duplication, adaptation, distribution and reproduction in any medium or format, as long as you give appropriate credit to the original author(s) and the source, a link is provided to the Creative Commons license and any changes made are indicated.

The images or other third party material in this chapter are included in the work's Creative Commons license, unless indicated otherwise in the credit line; if such material is not included in the work's Creative Commons license and the respective action is not permitted by statutory regulation, users will need to obtain permission from the license holder to duplicate, adapt or reproduce the material.



Chapter 4

Aerospace Requirements



Zahra Sharif Khodaei and Stephen Grigg

Abstract This chapter covers the overview of requirements arising in the aerospace industry for operating a structural health monitoring (SHM) system. The requirements are based on existing standards and guidelines and include both requirements on the physical components of the system (such as sensors, data acquisition systems and connectors) and their functional requirements (such as reliability, confidence measure and probability of detection). Emphasis has been given to on-board and ground-based components because they have different functionality requirements. An important factor in the reliability of the system is the effect of the environment and operational loads on the reliability of the diagnosis and, consequently, prognosis. The recommended guidelines for testing the reliability of the system under varying operational conditions are presented. This chapter is then finalized by reporting on methodologies for optimal sensor number and placement, based on different sensor technologies and different optimization algorithms.

Presently, there are various international committees comprising industry, government and academia with a mission to develop guidelines, procedures, processes and standards for the implementation and certification of structural health monitoring (SHM) technologies for a variety of application to commercial and military aircraft. This is only achievable through close collaboration between regulators, operators, aircraft manufacturers, system developers and research institutes.

An effective SHM system should not result in any significant negative effects on the performance of the host structure after the integration of its components. The SHM system architecture can be divided into two significant attributes as shown in Fig. 4.1 (SAE International 2013):

Z. Sharif Khodaei (✉)
Imperial College London, London, UK
e-mail: z.sharif-khodaei@imperial.ac.uk

S. Grigg
Cardiff University, Cardiff, UK

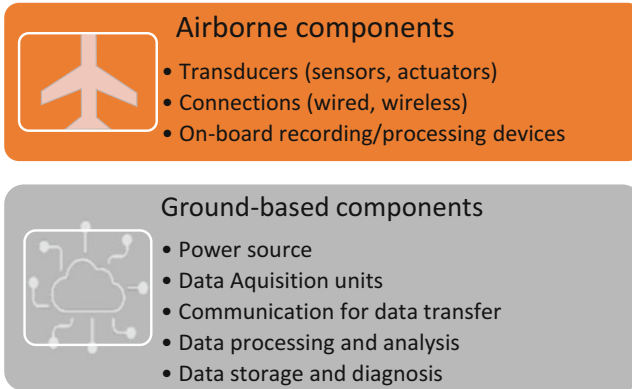


Fig. 4.1 Physical components of SHM systems

- Physical architecture: components and subsystems such as sensors, transducers, data acquisition (DAQ) systems, amplifier, wires, connectors and their interconnections
- Functional architecture: performance requirements such as reliability, probability of detection (POD), intended function (level of diagnosis) and damage size (BVID).

For an SHM system to apply to an aircraft under operational condition, a maintenance strategy should be dependent on factors such as the additional weight, additional cost and the reliability of both diagnosis and prognosis. The benefits of SHM that come from the early damage detection, reduced grounding times and reduced human error need to be evaluated against the additional cost that the system introduces. This can be introduced by evaluating the value of information (VOI) (Straub 2014), which should be integrated with the reliability analysis to compute the probability of failure of the system. The first step in designing and developing the SHM system is for the engineer to define what is the purpose of the diagnostic system, or what is the intended function for the system that defined the level of detailed information the diagnosis will be providing about the integrity of the structure (Sharif Khodaei and Aliabadi 2016). SHM intended that elementary functions can be divided into four levels (SAE International 2013):

- Level 1 (Detecting the presence of damage): This is the most elementary function of the system where it indicates whether damage exists or not with a pre-defined quality and to an acceptable probability (false positive and missed detection).
- Level 2 (Detection of damage location): Damage is not only detected but also localized with a prescribed accuracy (either zonal or exact coordinates depending on the required level of accuracy).
- Level 3 (Detection of damage size): This level of functionality is in addition to detection and localizing results in detecting the damage size to a set POD.

- Level 4 (Detection of damage characteristics and the influence on residual strength): The SHM system may be targeted towards characterizing the type of damage such as debonding, delamination, severity and single and multiple damages.

The level of accuracy of the decision making (intended functions mentioned above) will require a different combination of transducers in terms of number and location. This means that the VOI of the system will increase with the increase of complexity of the decision making. For example, to size damage (Level 4) with an acceptable probability, a lot more transducers are required than just detecting damage (Level 1). Therefore, each different level will require different system requirements. Based on the intended function selected, the system requirements will then be defined. There will be a different set of requirements for airborne SHM and ground-based SHM equipment, and it should cover the following specifications (SAE International 2013).

Functional requirements included the type of features to be monitored, details of the DAQ, handling and storage. By contrast, the operational requirements specify the interfaces between the operator and maintenance crew and between the airborne and on-ground SHM components. This means that the operational requirements will influence the type of actions and decision that will result from the diagnosis (e.g. ground or continuous operation and repair or replace), the type and form of information requirements (e.g. go/no-go) and timing (how often to acquire data, time interval and how long to store the data).

Performance requirements define the attributes of the system that makes it useful for application to a space vehicle. It includes function specifics such as accuracy (flaw size), reliability, reusability, range, resolution, speed and response time.

The system requirement shall include the following specification for both airborne and ground-based equipment:

- *Physical requirements* include system/item attributes such as system weight (mass, size), cooling and power consumption.
- *Environmental requirements* depict the condition in which the SHM system is required to perform and/or survive (temperature, vibration, vacuum, shock and radiation). These requirements will strongly depend on the specific location of the SHM system within the aircraft.
- *Structural requirements* are correlated to specified application scenarios and include the sensor and equipment integration.
- *Installation requirements* consider the permanently integrated SHM equipment such as sensors, wires, connectors and DAQ units. Their protection, calibration and baseline measurement, manufacturing and assembly will be addressed.
- *Re-usability requirements* are self-diagnostic capabilities to define faulty parts during installation and operation, reparability and maintainability of permanent parts.
- *Interface requirements* include the physical system and item interconnections such as data integrity, data availability and communication.

- *Safety and reliability requirements* are related to the redundancy requirements of the system, risk, false alarm and miss-detection rates and functional hazard assessment.

The requirement for ground-based equipment should be the same as those of existing non-destructive inspection (NDI). The standards already used for NDI equipment may include the following:

- MIL-STD-810: Test Method Standard for Environmental Engineering Considerations and Laboratory Tests;
- MIL-STD-461: Requirements for the Control of Electromagnetic Interference Characteristics of Subsystems and Equipment;
- RTCA DO-278: Guidelines for Communication, Navigation, Surveillance and Air Traffic Management (CNS/STM) Systems Software Integrity Assurance.
- ATA MSG-3: SHM working group recommendations to facilitate the incorporation of SHM in maintenance programme of aircraft.

The requirements for airborne equipment should be met through environmental qualification tests as required by RTCA/DO160C.

4.1 Power Consumption

Power consumption is part of the physical requirements of the SHM system. Traditionally power is supplied to the system through wires; this however does have some significant disadvantages such as the cost associated with installing the wiring. This wiring also adds significant weight to an aircraft, reducing efficiency and increasing the cost of operation. That is the reason why there is a great interest in implementing wireless SHM system (Noel et al. 2017; Lee et al. 2016; Dutta et al. 2005; Rusci et al. 2017; Sutton et al. 2017; Li et al. 2010; Champaigne and Sumners 2007); in fact, it is estimated that in the lifetime of an aircraft, cost savings of 14–70 million dollars could be achieved (Gao et al. 2018). The removal of wires although have weight saving benefits, creates a clear problem: how to power the device in a manageable way? This has led to developments in terms of energy efficiency of the electronic units (DAQs and sensors) (Fu et al. 2018, 2019). In terms of passive SHM system monitoring (e.g. impact events), advancements have been carried out to develop energy efficient event-triggered systems (Fu et al. 2018 Yuan et al. 2016; Qiu et al. 2013; Yuan et al. 2014). Similarly, for active sensing (guided wave excitation and sensing), several wireless monitoring systems have been developed, each with advantages and shortcomings in terms of size and weight of the units, power consumption and the response time (Fu et al. 2019; Aranguren et al. 2013; Zhang 2013; Zhong et al. 2015). Most of the proposed wireless DAQ units are battery operated, with some recent research in terms of energy harvesting capabilities. A unique development which overcomes the wiring and energy challenges of a passive unit was proposed through inductively coupled transducer system (Zhong

et al. 2014) where its ideal for ground maintenance but will require access to the embedded sensors. Therefore, not ideal for areas with limited accessibility.

Batteries are common within wireless sensors; however, concerns over their safety and their limited battery life mean that application within aerospace structures is restricted. To remove the need for batteries, or to extend their lives, energy harvesting is being utilized. Available sources of power vary depending on the application and location, typically when available solar power has been used, as it can produce the highest power for its size. Within aviation, however, this is not a reliable single source of power and its integration will interfere with the aerodynamics of the structure, so alternative sources must be considered; for aircraft applications, the most applicable are vibration and thermal (Le et al. 2015).

Vibration harvesters are very effective in areas where consistent vibration exists, such as near engines, or helicopter gearboxes, as available energy is abundant at a known frequency. Elsewhere, vibration may also be high because of airflow; however, this is highly dependent on operating conditions, making it random and difficult to harvest. Although values are very dependent on the aircraft type and operating conditions, studies have shown that the typical frequency is between 100 and 500 Hz, up to 5 g (Thomas 1962). Within helicopters, rotor speeds will also lead to lower frequency vibration (Le et al. 2015). Although advancements had been made into less resonant sensors (Townsend et al. 2019), most vibrational energy harvesters only operate efficiently at resonance, making it possible near consistent sources. Stated values for vibration based-energy harvesters in research vary, as the acceleration that they are exposed to is not uniform. The size of the harvesters is also variable, some being micro-electromechanical systems and others not; this makes direct comparison difficult. It however can be concluded that a vibrational energy harvester suitable for a wireless system is likely to produce at most milliwatts of power (Wei and Jing 2017).

Another option that has the potential to produce higher power values is the thermoelectric generator (TEG), which harvests energy between two faces where a temperature gradient exists. This includes areas near the engine outlets or the outer shell of the aircraft during take-off and landing, where over 50 °C of temperature difference can be temporarily produced. Most TEG utilize the phenomenon called the Seebeck effect, and when operating in the conditions found on-board an aircraft can generate hundreds of milliwatts (Hamid Elsheikh et al. 2014), be it for a limited time period.

Power availability on-board an aircraft is limited, meaning the power consumption of any wireless device must be kept to a minimum, whether it is powered by battery or energy harvesting.

4.2 System Reliability/Durability

A key feature for the certification of the SHM is its reliability compared to existing NDE techniques. It should follow MIL-HDBK-1823 which is the handbook for Nondestructive Evaluation System Reliability Assessment. The reliability requirements should cover the minimum performance constraints. The reliability of the SHM system includes both on-board and on-ground equipment. This means that the SHM installation, wiring, connectors and sensors must survive the harsh environmental and operational conditions of flight and their service life should be comparable to the life of the structure. If their service life does not comply with the service life of the host structure, there should be reliable ways of detecting, repairing or replacing faulty parts (Yue et al. 2018).

Moreover, fault-tolerant design of equipment and installations should be considered in reliability analysis for the chosen intended function, e.g. tolerance in sensor placement, baseline measurements. These requirements can be linked with the design, development and optimization of the SHM system to increase its reliability and redundancy.

The APR 4671 guidelines can be followed for the safety requirements of an SHM system which is acceptable by industry. These include the following:

- The SHM system must follow the airworthiness regulation for systems and equipment which are to be installed on-board of aircraft. These requirements ensure that the integration of the on-board SHM system should not reduce the safety of the structure and hence have any adverse effects on the safety of the passengers, operators and maintenance technicians.
- The installation and operation of the SHM system should not have any noticeable effects on the performance and the reliability of the structure. In addition, the maintenance of the SHM should also be possible.
- The SHM system should not use any chemicals which can harm the environment during its manufacturing process, an application that includes integration and operation or during the repair and replacement stage which could result in the disposal of material.
- Potential conditions that can fail SHM items (hardware) and diagnosis algorithm, (software) should be identified and solutions to solve, repair and replace them should be in place. Each failure should be classified based on its criticality, and the introduction of safety requirements should be carried out to meet the safety requirements of integrated systems and maintenance.

The SHM should remain effective for the expected life duration of the host structure and survive its surrounding environmental and operational conditions of flight.

4.3 Effect of Operational Conditions

The SHM system should function reliably under all foreseeable operation conditions of flight. The operational requirements for an SHM enabled aircraft will specify interfaces between the maintenance crew and on-aircraft and ground SHM components

The on-board requirement of the SHM system should follow RTCA/DO-160C certification guidelines for environmental conditions and test procedures of airborne equipment to ensure the reliability, durability and long life of the installation of on-board equipment as well as their operation.

The on-ground requirements are primarily directed towards condition-based monitoring (CBM).

The ground operational requirements should report on the following:

- Damage detection should be decomposed into its elementary functions i.e. detection of damage presence, localization of damage, detecting the size and severity of the damage. For each of these levels, the reliability and POD under the operational conditions of the flight should be demonstrated.
- A development assurance level (DAL) for each of the elementary functions listed above is based on the negative effects that their failure will have on the airworthiness of the structure as well as on the reliability of the operation.
- The quality characteristic of SHM measurements and functions e.g. accuracy, reliability, precision and durability.
- The operation of the SHM system should not result in any reduced performance of the structure not it should reduce the reliability or the remaining useful life of the host structure.
- The requirement for ground-based equipment should be the same as those of existing or known equivalent from non-destructive testing (NDT).

As part of the reliability assessment of the SHM system, the accuracy of the measured parameter (e.g. strain, guided wave) under operational conditions must be compared with the real value that the structure experiences and the error of the measurement evaluated. The Table 4.1 describes the different test methods and procedures that should be followed for on-board electronics (sensors, connectors, wires) (Salmanpour et al. 2017).

For example for a regional aircraft operating within Europe the operational and environmental test following MIL-STD 180G guidelines requires the on-board SHM equipment to be tested in 'Basic cold C1' category, with daily air temperature ranging between -32 and -21 °C, (-33 to -25 °C induced) in the low range with the extremely low temperature in Europe set as -55 °C in Russia.

Depending on the location of the equipment on board of an aircraft, the RTCA DO-160 specifies a specific vibration profile. The functionality and longevity of the SHM components as well as the reliability of the diagnosis should be tested in the presence of the vibration load.

Table 4.1 Integrity test: environmental load cases and references

Test category	Reference test method
Pressure (altitude)	MIL-STD-810G-Method-500.5
Temperature and altitude	RTCA/DO-160F Section 4
Temperature	RTCA/DO-160F Section 5 MIL-STD-810G-501.5 to 503.5
Humidity	RTCA/DO-160F Section 6 MIL-STD-810G-Method-507.5
Acceleration	MIL-STD-810G-Method-513.6
Vibration	RTCA/DO-160F Section 8 MIL-STD-810G-Method-514.6
Fluid susceptibility	RTCA/DO-160F Section 11
Combined loading: temperature and altitude and humidity	MIL-STD-810G-Method-520.3
Combined loading: temperature and vibration	MIL-STD-810G-Method-520.3
Sensor—Fatigue	Defined based on the frequency of acquisition and the life expectancy of each structural part
Mechanical and fatigue for sensor integrity and installation integrity	Following ASTM standards as provided for mechanical tests
Impact tests	The output from calibration tests on each representative coupon

4.4 Size/Weight Restrictions

For aeronautical applications, the decision to have a permanently installed SHM system for structural prognosis will be driven by its reliability, cost and the added weight of the system. The additional weight of the on-board SHM system might be outweighed by the reduction of structure thickness and hence weight which be one of the benefits of the application of SHM. Therefore, the restriction of size and weight of the SHM components is closely related to sensor optimization which is presented in the next section. Some recent innovations have resulted in reducing the weight of the wires and connectors significantly which is specifically beneficial to guided wave-based SHM systems. Considering that each sensor has to be connected from both positive and negative terminals with a wire to the DAQ unit, for a sparse network of sensors, this results in a substantial additional weight. In addition, handling of the wires is an added challenge to have them fixed to the structure. During the operation, they could become projectile and they can break the sensor terminals as well as cause safety concerns. This challenge is not so significant for fibre optic sensors or embedded sensors. However, for piezoceramic sensors, the proposed solutions are in the form of a ready-made layer that can be installed onto the structure either during manufacture or assembly and will include sensors, wires, connectors and the protective layer. Examples of these solutions are the smart layer by Stanford (Qing et al. 2009), Diagnostic film by Imperial College shown in

Fig. 4.2 Example of Diagnostic film by ICL (Bekas et al. 2018)



Fig. 4.2 (Bekas et al. 2018) and the integrated SHM layer (Schmidt et al. 2016), just to name a few.

4.5 Optimal Sensor Placement

As it was emphasized in the previous sections, the performance and reliability of the SHM system is a critical factor in its uptake as a maintenance strategy. The performance of the diagnosis based on the sensor data is directly related to the number and position of the sensors. There is a balance between the cost and the benefit of how many sensors should be added to the host structure without affecting its functionality but still diagnose the structure with high reliability. Therefore, specialized optimization algorithms should be developed which takes into account the specific outcome of the SHM system for composite structures as well as the limitations in terms of placement of sensors and their numbers.

Depending on the application of the SHM, different SHM techniques have been developed which include: vibration-based methods, strain monitoring and ultrasonic guided wave-based techniques. Each class of techniques will have different inputs and outputs, different types of sensors and different operational parameters and hence a different objective function to optimize. There have been many approaches proposed for the optimal sensor placement (OSP) for SHM systems mostly based on an objective function which is the POD of the damage detection algorithm. These techniques include data-driven methods such as an artificial neural network (ANN) in (Staszewski and Worden 2001), genetic algorithm (GA) (Guo et al. 2004) and Bayesian approach (Flynn and Todd 2010a, 2010b), which the objective function for all of them is based on the POD of the damage detection algorithm. The disadvantage of such an approach is that first, it requires a lot of data to be able to build the POD function. Secondly, the POD function for damage detection in composite

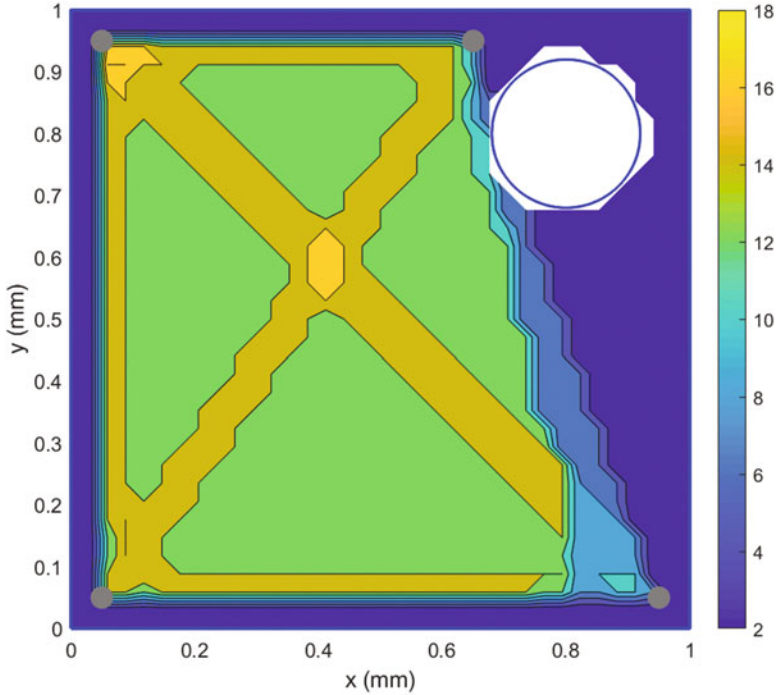


Fig. 4.3 Optimal 4 sensor location for a plate with a corner hole

structures is not well defined because of the complex nature of the damage. Last but not least, if any changes will be made to the damage detection algorithm, the optimum sensor number and location will then no longer be valid. In a different work, Fendzi et al. (2014) proposed an optimization strategy based on GA but one which does not depend on the damage detection algorithm, but it depends on a POD function constructed from scattered energy of guided wave interacting with a damage. This scattering is a theoretical model and does not represent the scatter profile in a complex composite structure. Most of the reported techniques are application-specific and consequently cannot be evaluated in a comparative study. Moreover, their performance depends on tuning factors which makes it impossible to compare for two different techniques. A different approach was proposed in (Thiene et al. 2016) where the optimization is based on maximum area coverage (MAC) within a sensor network and applies to any structure of complex geometry and any damage detection algorithm which is based on guided waves in the pitch-catch configuration. In addition, complex geometries such as plates with openings can also be considered. The objective function (which is to maximize the guided wave coverage) is then optimized using a genetic algorithm (GA) optimization framework. An example of optimal locations for 4 sensors on a rectangular plate with a hole is shown in Fig. 4.3, where the objective was set to maximize the area inside the sensor network (to avoid edge reflected waves).

A comprehensive review is presented in (Ostachowicz et al. 2019) where different OPS algorithms for different SHM techniques are thoroughly investigated. This area of research still requires a lot of attention to propose an optimum method with could be adapted to any structure and any SHM method.

4.6 Summary

In summary, this chapter presented an overview of the requirements that need to be addressed, for any SHM system to be considered for CBM of a real aeronautical structure under real operational and environmental conditions. The most important factor for an SHM to be used in diagnosis and prognosis is for the designer and the maintenance engineer to show that the SHM system can survive the life cycle of the structure, and if not, each component can be identified when malfunctioning, repaired or replaced. The second important factor is to demonstrate that the SHM methodology is capable of diagnosis with the same level of accuracy and reliability (often called 90/95%) of non-destructive techniques that are currently being used by manufacturers and aircraft operators. To this end, the SHM system needs to be considered from the design stage to manufacturing, assembly and finally operational life of the structure.

References

- Aranguren G, Monje P, Cokonaj V, Barrera E, Ruiz M (2013) Ultrasonic wave-based structural health monitoring embedded instrument. *Rev Sci Instrum* 84(12):Art. no. 125106
- Bekas DG, Sharif-Khodaei Z, Aliabadi MHF (2018) An innovative diagnostic film for structural health monitoring of metallic and composite structures. *Sensors* 18:2084. <https://doi.org/10.3390/s18072084>
- Champaigne KD, Summers J (2007) Low-power electronics for distributed impact detection and piezoelectric sensor applications. In: *Proc. Aerosp. Conf*, pp 1–8
- Dutta P, Grimmer M, Arora A, Bibyk S, Culler D (2005) Design of a wireless sensor network platform for detecting rare, random, and ephemeral events. In: *Proc. 4th Int. Symp. Inf. Process. Sensor Netw*, pp 497–502
- Fendzi C, Morel J, Rebillat M et al (2014) Optimal sensors placement to enhance damage detection in composite plates. In: *7th European workshop on structural health monitoring*
- Flynn EB, Todd MD (2010a) Optimal placement of piezoelectric actuators and sensors for detecting damage in plate structures. *J Intell Mater Syst Struct* 21:265–274. <https://doi.org/10.1177/1045389X09338080>
- Flynn EB, Todd MD (2010b) A Bayesian approach to optimal sensor placement for structural health monitoring with application to active sensing. *Mech Syst Signal Process* 24:891–903. <https://doi.org/10.1016/j.ymssp.2009.09.003>
- Fu H, Sharif Khodaei Z, Aliabadi MHF (2018) An event-triggered energy-efficient wireless structural health monitoring system for impact detection in composite airframes. *IEEE Internet Things J* 6(1):1183–1192

- Fu H, Sharif Khodaei Z, Aliabadi MHF (2019) An energy-efficient cyber-physical system for wireless on-board aircraft structural health monitoring. *Mech Syst Signal Processing* 128:352–368
- Gao S, Dai X, Hang Y et al (2018) Airborne wireless sensor networks for airplane monitoring system. *Wirel Commun Mob Comput* 2018:1–18. <https://doi.org/10.1155/2018/6025825>
- Guo HY, Zhang L, Zhang LL et al (2004) Optimal placement of sensors for structural health monitoring using improved genetic algorithms. *Smart Mater Struct* 13:528–534. <https://doi.org/10.1088/0964-1726/13/3/011>
- Hamid Elsheikh M, Shnawah DA, Sabri MFM et al (2014) A review on thermoelectric renewable energy: principle parameters that affect their performance. *Renew Sust Energ Rev* 30:337–355. <https://doi.org/10.1016/j.rser.2013.10.027>.
- Le MQ, Capsal JF, Lallart M et al (2015) Review on energy harvesting for structural health monitoring in aeronautical applications. *Prog Aerosp Sci* 79:147–157. <https://doi.org/10.1016/j.paerosci.2015.10.001>
- Lee Y, Blaauw D, Sylvester D (2016) Ultralow power circuit design for wireless sensor nodes for structural health monitoring. *Proc IEEE* 104(8):1529–1546
- Li P, Olmi C, Song G (2010) Energy efficient wireless sensor network for structural health monitoring using distributed embedded piezoelectric transducers. *Proc SPIE* 7647:7647–7647-11
- Noel AB et al (2017) Structural health monitoring using wireless sensor networks: a comprehensive survey. *IEEE Commun Surveys Tuts* 19(3):1403–1423
- Ostachowicz W, Soman R, Malinowski P (2019) Optimization of sensor placement for structural health monitoring: a review. *Struct Health Monit* 18:963–988. <https://doi.org/10.1177/1475921719825601>.
- Qing XP, Beard SJ, Kumar A, Li I et al (2009) Stanford multiactuator–receiver transduction (SMART) layer technology and its applications. *Encyclopedia of Structural Health Monitoring*. <https://doi.org/10.1002/9780470061626.shm098>
- Qiu L, Yuan S, Liu P, Qian W (2013) Design of an all-digital impact monitoring system for large-scale composite structures. *IEEE Trans Instrum Meas* 62(7):1990–2002
- Rusci M, Rossi D, Farella E, Benini L (2017) A sub-mW IoT-endnode for always-on visual monitoring and smart triggering. *IEEE Internet Things J* 4(5):1284–1295
- SAE International (2013) Aerospace recommended practice. In: *Guidelines for implementation of structural health monitoring on fixed wing aircrafts*. SAE International, p 95
- Salmanpour MS, Sharif Khodaei ZS, Aliabadi MHF (2017) Impact damage localisation with piezoelectric sensors under operational and environmental conditions. *Sensors* 17:1178. <https://doi.org/10.3390/s17051178>.
- Schmidt D, Kolbe A, Kaps R et al (2016) Development of a door surround structure with integrated structural health monitoring system. In: *Smart intelligent aircraft structures (SARISTU)*. Springer, Cham, pp 935–945
- Sharif Khodaei Z, Aliabadi MH (2016) A multi-level decision fusion strategy for condition based maintenance of composite structures. *Materials* 9:790. <https://doi.org/10.3390/ma9090790>
- Staszewski WJ, Worden K (2001) Overview of optimal sensor location methods for damage detection. In: *SPIE's 8th annual international symposium on smart structures and materials*. International Society for Optics and Photonics
- Straub D (2014) Value of information analysis with structural reliability methods. *Struct Saf* 49:75–85. <https://doi.org/10.1016/j.strusafe.2013.08.006>
- Sutton F et al (2017) The design of a responsive and energy-efficient event-triggered wireless sensing system. In: *Proc. ACM EWSN*, pp 144–155
- Thiene M, Khodaei ZS, Aliabadi MH (2016) Optimal sensor placement for maximum area coverage (MAC) for damage localization in composite structures. *Smart Mater Struct* 25:095037. <https://doi.org/10.1088/0964-1726/25/9/095037>.
- Thomas CE (1962) Flight vibration survey of C-130A aircraft Aeronautical systems. DIV Wright-Patterson AFB OH

- Townsend S, Grigg S, Picelli R et al (2019) Topology optimization of vibrational piezoelectric energy harvesters for structural health monitoring applications. *J Intell Mater Syst Struct* 30:2894–2907. <https://doi.org/10.1177/1045389X19873392>.
- Wei C, Jing X (2017) A comprehensive review on vibration energy harvesting: modelling and realization. *Renew Sust Energ Rev* 74:1–18. <https://doi.org/10.1016/j.rser.2017.01.073>
- Yuan S, Mei H, Qiu L, Ren Y (2014) On a digital wireless impact monitoring network for large-scale composite structures. *Smart Mater Struct* 23(8):Art. no. 085007
- Yuan S, Ren Y, Qiu L, Mei H (2016) A multi-response-based wireless impact monitoring network for aircraft composite structures. *IEEE Trans Ind Electron* 63(12):7712–7722
- Yue N, Khodaei ZS, Aliabadi M A (2018) Repairable installation procedure for SHM sensors onto composite structures. 9th European workshop on structural health monitoring, July 10-13, 2018, Manchester, United Kingdom
- Zhang C (2013) Trigger circuit for low-power structural health monitoring system. U.S. Patent 8 401 804, Mar. 19
- Zhong CH, Croxford AJ, Wilcox PD (2014) Passive wireless ultrasonic transducer systems. *AIP Conference Proceedings* 1581:1896. <https://doi.org/10.1063/1.4865055>
- Zhong CH, Croxford AJ, Wilcox PD (2015) Portable wireless ultrasonic systems for remote inspection. *AIP Conf Proc* 1650:883. <https://doi.org/10.1063/1.4914693>

Open Access This chapter is distributed under the terms of the Creative Commons Attribution 4.0 International License (<http://creativecommons.org/licenses/by/4.0/>), which permits use, duplication, adaptation, distribution and reproduction in any medium or format, as long as you give appropriate credit to the original author(s) and the source, a link is provided to the Creative Commons license and any changes made are indicated.

The images or other third party material in this chapter are included in the work's Creative Commons license, unless indicated otherwise in the credit line; if such material is not included in the work's Creative Commons license and the respective action is not permitted by statutory regulation, users will need to obtain permission from the license holder to duplicate, adapt or reproduce the material.



Chapter 5

Ultrasonic Methods



Vykintas Samaitis, Elena Jasiūnienė, Pawel Packo, and Damira Smagulova

Abstract Ultrasonic inspection is a well recognized technique for non-destructive testing of aircraft components. It provides both local highly sensitive inspection in the vicinity of the sensor and long-range structural assessment by means of guided waves. In general, the properties of ultrasonic waves like velocity, attenuation and propagation characteristics such as reflection, transmission and scattering depend on composition and structural integrity of the material. Hence, ultrasonic inspection is commonly used as a primary tool for active inspection of aircraft components such as engine covers, wing skins and fuselages with the aim to detect, localise and describe delaminations, voids, fibre breakage and ply waviness. This chapter mainly focuses on long range guided wave structural health monitoring, as aircraft components require rapid evaluation of large components preferably in real time without the necessity for grouting of an aircraft. In few upcoming chapters advantages and shortcomings of bulk wave and guided wave ultrasonic inspection is presented, fundamentals of guided wave propagation and damage detection are reviewed, the reliability of guided wave SHM is discussed and some recent examples of guided wave applications to SHM of aerospace components are given.

5.1 Introduction to Ultrasonic Inspection

Ultrasonic inspection is based on interaction (transmission, reflection and absorption) of the mechanical acoustical waves with the analysed structure at frequencies of 20 kHz or above. Conventional bulk wave ultrasonic techniques have been

V. Samaitis (✉) · D. Smagulova
Kaunas University of Technology, Kaunas, Lithuania
e-mail: vykintas.samaitis@ktu.lt

E. Jasiūnienė
Prof. K. Baršauskas Ultrasound Research Institute, Kaunas University of Technology,
Kaunas, Lithuania

P. Packo
AGH University of Science and Technology, Krakow, Poland

extensively used both for material property evaluation and for flaw detection. Material property evaluation is often based either on elastic modulus evaluation by measuring shear and longitudinal wave velocities, or estimation of frequency-dependent attenuation (Sol et al. 2018; Ito et al. 2015; Lin et al. 2011). Both parameters are very commonly used for evaluation of the characteristics and volume of the localized porosity in composites (Duong et al. 2015; Kim et al. 2013; Podymova et al. 2019). Meanwhile, the flaw detection relies on the analysis of surface, back-wall and intermediate echoes within the investigated structure, presuming that any inclusion, delamination or other defect will introduce a reflection that can be captured by the ultrasonic sensor (Zhang et al. 2020a; Hauffe et al. 2020). Because of their relative simplicity, the conventional bulk wave ultrasonic techniques are often used as a primary tool for evaluation of the structural integrity. Ultrasonic C-scan measurement is a common method to assess the structural integrity of composites using bulk ultrasonic waves. Using such technique, the structural response is collected at different spatial positions across the surface of the sample. The output image is usually a colour coded representation of the amplitude level (transmission losses) of the backwall signal. The success of such measurement depends on the type and origin of defects. For example, delamination and debonding defects can produce discrete reflection which can be detected at certain depths before arrival of the backwall signal. Porosity and ply waviness introduce scattering of ultrasonic signal and increased transmission losses (Zhang et al. 2020b; Towsyfyhan et al. 2020; Pain and Drinkwater 2013). The multi-layered structure of the composite itself generates structural noise, which complicates the inspection, while the resin layers between the fibres can cause inter-ply reflections and interference of ultrasonic signal. Such interference is known to be stronger when the wavelength of ultrasonic signal is equal to odd number of layer thickness (Zhang et al. 2020a). In case of multiple defects present, a shadowing effect and structural noise generated by layers of composite can limit detectability of some defects, especially in the case of normal incidence inspection.

Aircraft structures may have defects of different type and origin. Some of the defects develop during the manufacturing, while others within the life-cycle of the structure. The most common defects found in aircraft structures are described in Chap. 3 of this book. As the bulk wave measurements are mostly localized, based on point-by-point acquisitions using encoded scanners it's not an ideal choice for large and curved aircraft structures. Classical bulk wave inspection methods are currently used in scheduled maintenance of an aircraft. These methods are able to detect defects in limited area only. Furthermore, they usually require disassembly (to have access to parts, hidden defects) and submersion, are slightly operator-dependent and require to repeat the inspection procedure in different areas of the structure (Hellier 2012; Rocha et al. 2013). As a result, bulk wave inspections are reliable but despite advancements in non-contact measurement methods, yet slow and costly, especially for large engineering structures. The scheduled maintenance requires an aircraft to be grounded so it's usually preferred to perform it as quickly and as rarely as possible. This puts some pressure for fleet operators and increases the risk of

human errors. In the case of large structure inspection, additional challenges arise due to the unreliable contact between the structure and ultrasonic sensor which may appear during the scanning. Conventional bulk wave measurement methods require either the submersion or continuous water feed which limits their applicability on site (Towsyfyhan et al. 2020; Ramzi et al. 2015). Special bubblers and water columns are being used then, to provide consistent coupling (Hsu 2013). Air coupled or laser methods enable to partially solve this issue, providing the flexibility to adapt to the complex geometries (Kazys et al. 2017; Pelivanov et al. 2014). However, the impedance mismatch induced losses of air-coupled transducers and expensive equipment of the laser-generated-ultrasound reduces the extent of such approaches.

Current aircraft engineering is trying to implement a “Fail safe” design in which the structure is engineered to maintain the residual strength even in the failure of some structural elements. The scheduled inspection intervals are calculated according to the predicted crack growth rate and loads during the flight (Rocha et al. 2013). In such way it’s ensured that an aircraft will be safe to use before another inspection. Such engineering approach suggests that the inspection intervals could be prolonged with the real-time monitoring techniques, that provide defect state information. Hence, in the case of aircraft inspection, an important aspect is to be able to recognize and continuously monitor the development of defects, since it determines the safety of the passengers and would allow to perform condition based maintenance rather than scheduled. This goal can partly be achieved through Structural Health Monitoring (SHM) systems, which aim to inspect large structures in real-time using a distributed network of embedded sensors. The SHM systems usually are not the standalone ones, since they cannot achieve such high measurement accuracy and sensitivity as bulk wave techniques. On the other hand, such approach in contrast to bulk wave inspection does not require prior knowledge about the locations of defects, as it provides global inspection of the structure. As a result, SHM is frequently used to record the response of the structure under the operational loads and to identify and preferably localise the critical regions where the defects may occur. Meanwhile the bulk wave methods usually follow-up the SHM inspection for more precise defect assessment, size evaluation and etc. In most structures, defects are allowed to exist as long as they are considered as safe (Alokita et al. 2019). For a such already known defects, aircraft inspection can benefit from SHM which continuously monitors their development with the aim to capture the moment when they become critical. Typically a successful SHM system should address the challenges and requirements for inspection of aircrafts. These are usually large and thin structures possessing variable geometry which have to be inspected with one-side access. In most cases, inaccessible parts, hidden reinforcement elements and interfaces exist, while the monitoring system should be capable of detecting both defects like delaminations and structural changes i.e. ply waviness, fibre structure etc. This brings a lot of challenges for implementation of successful SHM system.

5.2 Ultrasonic Guided Wave (GW) Inspection

As an alternative to conventional bulk wave ultrasonic inspection, ultrasonic guided waves (GW) emerged as a technique, which enables the implementation of large scale and on-demand SHM systems, through embedded sensor networks (Croxford et al. 2007). As a result, a periodic pointwise inspection can be replaced with real-time long-range condition monitoring, thus minimizing the downtime, human involvement and disassembly of components. Guided waves itself can be defined as a kind of ultrasonic waves that propagate along the boundaries of the structure, or along thin, plate like structural components. It's a result of interference between the longitudinal and shear waves, that propagate back and forth in the analysed structure and conform to the distinct modes (Rose 2002). Guided waves interrogate with the entire bulk of the structure, are sensitive to the changes in elastic modulus or density of the material and are relatively weakly attenuated; hence, defects of different types and positions inside the component can be detected in large structures employing only a few sensors (Cawley 2007). As the velocity and attenuation of guided waves depend on the properties of the material, various sudden changes in the internal structure such as defects can be detected (Kralovec and Schagerl 2020).

Guided waves arise in bounded media as a result of the superposition of bulk waves that are partially transmitted, reflected and refracted at a structure's boundaries and/or internal interfaces. As the focus of this work is on aerospace applications, we are mainly concerned with light thin-walled structures, i.e. plates. In the case of plates, the medium is bounded by two parallel stress-free surfaces, which convert and reflect elastic waves. After multiple reflections, a steady-state pattern is established giving rise to the so-called Lamb waves (Lamb 1917). Lamb waves possess an infinite number of modes of two possible thickness-symmetry types of the displacement field: symmetric (S_i) and anti-symmetric (A_i). There exist additional family of shear horizontal (SH_i) modes, which decouple from S_i and A_i modes for isotropic structures. The subscript ($i = 0, 1 \dots \infty$) denotes the order of each mode.

Various analysis methods can be employed for calculation of the relationship between wave speed and excitation frequency, i.e. dispersion relationships. For instance, for isotropic, homogeneous, linearly-elastic materials, the dispersion curves can be found using the method of potentials (Viktorov 1967; Rose 2004). Despite its simplicity and mathematical elegance, the method of potentials gives little insight into the physics of the problem. A substantially different approach relies on the partial wave technique (Solie and Auld 1973). Following the latter technique, the first step in formulating the dispersion relationships is the calculation of possible bulk waves for the infinite medium, followed by finding partial waves satisfying stress-free boundary conditions. In addition to dispersion, i.e. phase-frequency relations, the amplitude-frequency characteristics and mode-specific displacement patterns can be found by employing the abovementioned techniques.

Each GW Lamb wave mode has specific dominant displacements; hence, different modes are applied for the detection of particular defects. The anti-symmetric modes possess dominant out-of-plane displacements at low frequencies, therefore

they are commonly used for the detection of delaminations, surface and sub-surface defects (Ramadas et al. 2010; Teramoto et al. 2015). In contrast, symmetrical modes are dominated by in-plane displacements and are widely used for crack and notch assessment (Benmeddour et al. 2009). Such displacement distributions are usually non-uniform across the thickness of the structure and tend to rearrange while frequency-thickness product increases (Rose 2014). The fundamental anti-symmetric modes have a shorter wavelength, leading to a better sensitivity to the defects of small size. Fundamental shear horizontal mode (SH_0) in isotropic media is non-dispersive, so it's frequently employed in various fields intending to avoid complicated signal analysis (Nazeer et al. 2017). The shear horizontal mode has in-plane displacements that are perpendicular to the direction of wave propagation (Rose 2004). Most of the modes of Lamb waves unlike SH_0 are dispersive and display frequency-dependent phase and group velocities. Fundamental 0th order modes usually are fairly non-dispersive at low frequencies and possess quite uniform mode shapes (in-plane and out-of-plane displacements) across the thickness of the sample. Such modes are easily generated and may be a good starting point for any guided wave inspection (Khalili and Cawley 2018; Senyurek 2015). Higher order modes possess relatively short propagation distances due to dispersion, but on the other hand are quite sensitive to small defects due to short wavelength and strong velocity dependence on sample thickness (Masserey et al. 2014; Masserey and Fromme 2015). Hence, the guided wave inspection can be categorized into short to medium and medium to long range.

A typical example of short range inspection can be inspection of aircraft repair patches (Puthillath and Rose 2010; Caminero et al. 2013) and assessment of adhesive bonds (Fromme et al. 2017; Wojtczak and Rucka 2021). Adhesive bonding is frequently used in many aircraft structures to attach wing skins, fuselage stingers and metallic honeycomb to skins for elevators, ailerons, tabs and spoilers (Higgins 2000). Short range guided wave inspection possess relatively minor dispersion, hence the selection of the suitable mode is mostly determined by it's sensitivity. Long range inspection is typically applied for inspection of wing skins, engine coverings and fuselages. In case of long range inspection the dispersion plays a vital role. Due to dispersion various frequency components of the signal travel at different velocities. This leads to a spread of the wave in time domain as it propagates in the structure. Typically for the S_0 mode, the low-frequency components travel faster in comparison to high signal frequencies. In contrast, for A_0 mode high frequencies tend to move more rapidly. As a result, the trail of S_0 mode becomes contracted, while A_0 mode becomes stretched-out (Mitra and Gopalakrishnan 2016). In the presence of dispersion, the velocity of different components of the signal depends on frequency and thickness product. Dispersion is undersirable effect as spreading of wave in time domain reduces the resolution while reduction of the amplitude due to wave spread limits the sensitivity of inspection system (Wilcox et al. 2001a). One of the simplest way to achieve mode control is to select an appropriate frequency-thickness range where only a few fundamental modes exist. For example, if dispersion diagram shows that only a fundamental modes exist below 1 MHz·mm (see Fig. 5.1), it means that for 10 mm

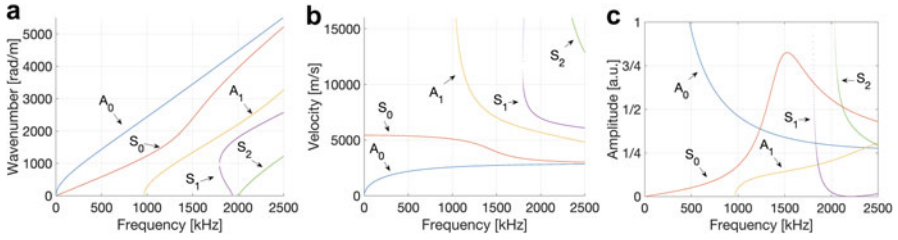


Fig. 5.1 Dispersion ((a)—wavenumber-frequency, and (b)—velocity-frequency) and out-of-plane excitability (c) curves for guided Lamb waves in a 2 mm-thick aluminum plate ($\lambda = 60,500$ MPa, $\mu = 25,900$ MPa and $\rho = 2700$ kg/m³)

plate the fundamental modes will propagate at frequencies below 100 kHz. The frequency-thickness product plays vital role in guided wave inspection of aircraft components. These usually possess different complexity of the geometry—from simple plate-like skin elements, to bends and co-cured stiffeners. In such structures the existence of multiple modes becomes unavoidable, while each structural element introduces its own complexities. For example, stiffeners cause damping of A_0 mode, due to energy leakage into the stiffener and mode conversion which leads to trailing waves. Meanwhile the disbond between skin and stiffener results in a wave propagating in the skin only (Panda et al. 2018). The velocity variation of guided wave modes indicates the thickness change of the structure, which may be caused by different defects, like delamination or disbond or corrosion. To mitigate the effect of dispersion, the bandwidth of the signal for a given plate thickness must be selected carefully, especially for the long-range guided wave applications. Other methods include sparse array excitation which will be discussed in next subchapter. Subsequent sections outline the theoretical background for unbounded and guided wave propagation. As for a linear elastic isotropic medium, guided wave propagation may be considered in a 2-D space, therefore the following discussion is restricted to that simplified case only.

5.2.1 Governing Equations of GW Wave Propagation

5.2.1.1 Waves in Unbounded Media

The momentum equation for a two-dimensional unbounded linear elastic isotropic space is written as

$$\rho \frac{\partial^2 \mathbf{X}}{\partial t^2} = \nabla \cdot \boldsymbol{\sigma} \tag{5.1}$$

where ρ denotes the density, $\mathbf{X} = [u, v]^T$ the particle displacement vector in 2-D space, $\boldsymbol{\sigma}$ the Cauchy stress tensor and t the time. Equation (5.1), together with constitutive and geometric relationships, fully describes wave motion via particle displacements. For small-amplitude waves, the infinitesimal strain definition is given as

$$\varepsilon_{ij} = \frac{1}{2} \left(\frac{\partial X_i}{\partial D_j} + \frac{\partial X_j}{\partial D_i} \right) \quad (5.2)$$

where X_i denote i^{th} component of the particle displacement vector and D_i represents i^{th} spatial direction. Alternative strain measures may be assumed for small but finite or large strains, e.g. the Green-Lagrange strain tensor (Packo et al. 2016).

For a linear elastic isotropic solid in 2-D, the constitutive relation—linking stresses and strains—yields

$$\sigma_{11} = (\lambda + 2\mu)\varepsilon_{11} + \lambda\varepsilon_{22} \quad (5.3)$$

$$\sigma_{22} = (\lambda + 2\mu)\varepsilon_{22} + \lambda\varepsilon_{11} \quad (5.4)$$

$$\sigma_{12} = 2\mu\varepsilon_{12} \quad (5.5)$$

Combining Eqs. (5.1), (5.2) and (5.3)–(5.5) and assuming the time-harmonic factor $e^{i\omega t}$, the elastodynamic equation yields

$$\rho\omega^2 \mathbf{X} - \mathbf{a}_1 \frac{\partial^2 \mathbf{X}}{\partial x^2} - \mathbf{a}_2 \frac{\partial^2 \mathbf{X}}{\partial y^2} - \mathbf{a}_3 \frac{\partial^2 \mathbf{X}}{\partial x \partial y} = 0 \quad (5.6)$$

where the matrices \mathbf{a}_1 , \mathbf{a}_2 and \mathbf{a}_3 are given by

$$\mathbf{a}_1 = \begin{bmatrix} \lambda + 2\mu & 0 \\ 0 & \mu \end{bmatrix}, \quad \mathbf{a}_2 = \begin{bmatrix} \mu & 0 \\ 0 & \lambda + 2\mu \end{bmatrix}, \quad \mathbf{a}_3 = \begin{bmatrix} 0 & \lambda + \mu \\ \lambda + \mu & 0 \end{bmatrix}. \quad (5.7)$$

Equation (5.6) defines the wave motion for an unbounded, linear elastic medium using the Lamé constants λ and μ . To complete the Lamb wave problem, Eq. (5.6) is supplemented by boundary conditions in the following section.

5.2.1.2 Boundary Conditions

Stress-free boundary conditions for Lamb wave propagation in 2-D space require that

$$\sigma_{ij}n_j = 0 \quad \text{at } y = \pm h, \quad i = \{1, 2\}, \quad (5.8)$$

where $\mathbf{n} = \pm [0 \ 1]^T$ is the surface outward-pointing normal vector and $2h$ is the plate thickness. Equation (5.8) results in two sets of equations for the top, $y = +h$, and bottom, $y = -h$, surface

$$\pm \mathbf{b}_1 \frac{\partial \mathbf{X}}{\partial x} \pm \mathbf{b}_2 \frac{\partial \mathbf{X}}{\partial y} = 0, \quad \text{for } y = \pm h, \quad (5.9)$$

where \mathbf{b}_1 and \mathbf{b}_2 are

$$\mathbf{b}_1 = \begin{bmatrix} 0 & \mu \\ \lambda & 0 \end{bmatrix}, \quad \mathbf{b}_2 = \begin{bmatrix} \mu & 0 \\ 0 & \lambda + 2\mu \end{bmatrix}. \quad (5.10)$$

Equations (5.6) and (5.9) define the Lamb wave propagation problem for a plate in 2-D space.

5.2.1.3 Dispersion Relation

The Rayleigh-Lamb problem, given by Eqs. (5.6) and (5.9), assumes the solution of the form $e^{+i(kx + \omega t)}$ and results in (k, ω) pairs that define guided Lamb wave modes, i.e. the dispersion curves. Relating wavenumbers and frequencies—or, equivalently, wave velocities and frequencies—dispersion curves pertain to phase-frequency characteristics of elastic waves as both k and ω appear in the exponential phase factor. It needs to be pointed out that for the full picture of wave propagation characteristics, Eqs. (5.6) and (5.9) may be used to determine the amplitude-frequency, (α, ω) , characteristics usually referred to as excitability curves (Kijanka et al. 2018).

The solution to the Rayleigh–Lamb problem cannot be carried out analytically and requires a numerical procedure. Most widely used are the method of potentials and the partial wave technique (Solie and Auld 1973). While the latter offers clear insight into the physics of the problem, it is most frequently used for practical analyses. Following this procedure (see (Packo et al. 2016) Appendix A), the solutions are given by

$$\mathbf{X} = \frac{1}{2} \alpha \left[\begin{matrix} u^{(S,A)} & v^{(S,A)} \end{matrix} \right]^T e^{+i(kx + \omega t)} + c.c., \quad (5.11)$$

where *c.c.* stands for the complex conjugate of all preceding terms and α denotes the wave amplitude. It clearly follows from the analysis that the modes display even or odd symmetry with respect to the plate's midplane, and are therefore called symmetric— $u^{(S)}$, $v^{(S)}$ —and anti-symmetric— $u^{(A)}$, $v^{(A)}$ —Lamb wave modes. Respective components $u^{(S,A)}$ and $v^{(S,A)}$ are given by

$$u^{(S)} : \frac{k}{\gamma_L} \cos(y\gamma_L) + \frac{2k\gamma_S}{k^2 - \gamma_S^2} \frac{\sin(h\gamma_L)}{\sin(h\gamma_S)} \cos(y\gamma_S), \quad (5.12)$$

$$v^{(S)} : i \sin(y\gamma_L) + i \frac{2k^2}{k^2 - \gamma_S^2} \frac{\sin(h\gamma_L)}{\sin(h\gamma_S)} \sin(y\gamma_S) \quad (5.13)$$

and

$$u^{(A)} : i \frac{k}{\gamma_L} \sin(y\gamma_L) + i \frac{2k\gamma_S}{k^2 - \gamma_S^2} \frac{\cos(h\gamma_L)}{\cos(h\gamma_S)} \sin(y\gamma_S), \quad (5.14)$$

$$v^{(A)} : \cos(y\gamma_L) + \frac{2k^2}{k^2 - \gamma_S^2} \frac{\cos(h\gamma_L)}{\cos(h\gamma_S)} \cos(y\gamma_S) \quad (5.15)$$

for symmetric and antisymmetric modes, respectively.

By employing the partial wave technique, the solution pairs, (k, ω) , are found in two steps. First, partial waves (i.e. waves in infinite medium) are obtained from an eigenvalue problem obtained by combining (5.11) and (5.6). Second, combinations of partial waves that satisfy the boundary conditions, Eq. (5.9), are retained.

Figure 5.1 shows example solutions for a Rayleigh-Lamb problem for an aluminium plate ($\lambda = 60,500$ MPa, $\mu = 25,900$ MPa and $\rho = 2700$ kg/m³), namely multi-modal dispersion curves in (k, ω) (Fig. 5.1a) and (V, ω) (Fig. 5.1b) spaces, and the corresponding excitability curves (Fig. 5.1c). Respective modes are labeled by a letter (S—for symmetric and A—for antisymmetric) and a subscript denoting the mode order. The fundamental antisymmetric and symmetric modes, A₀ and S₀ respectively, are most frequently employed for damage detection. Clear dispersive behaviour—i.e. frequency-dependent velocity—can be observed for all modes.

While interacting with defects, guided waves may undergo partial reflection, refraction, scattering and mode conversion. It means that the energy of the signal can be partially reflected back to the transmitter and convert to a different type of mode. Moreover, in the base of composite inspection, anisotropy plays a significant role, leading to directional dependence of wave velocity for each mode. Those characteristic features of guided waves are usually exploited in the detection of various defects such as cracks (Masserey and Fromme 2015; Chen et al. 2019; Mardanshahi et al. 2020; Barski and Stawiarski 2018), delaminations (Zhao et al. 2019; Munian et al. 2020; Raišutis et al. 2010) and bonding integrity (Yu et al. 2017; Ochôa et al. 2019; Vanniamparambil et al. 2015; Fan et al. 2013).

Despite that guided waves offer significant advantages over the conventional bulk wave testing, many limitations of their use in the majority of engineering structures are still present to overcome. Since many guided wave modes co-exist simultaneously, each having frequency and direction-dependent velocity, after several reflections and mode conversions the receivers usually capture overlapped and distorted time-domain signals that are difficult to interpret. The responses that are captured from defects are usually weak and may be concealed anywhere in the

received signal. Such a response captured from the structure varies from one geometry to another and depends on the type of excitation and environmental conditions, such as temperature, loads and movement-induced vibrations (Su and Ye 2006). In order to obtain useful measurement data it's necessary to excite and receive single guided wave mode minimising the coherent noise from other propagating modes. The variety of structures present in the aerospace sector, ranging from wing panels, to stiffened joints each time requires new developments in sensing, measurement and data analysis technologies. Hence, a deep understanding of the mechanism of guided wave propagation, spatial coverage, interaction with medium and the defects of interest is required for successful in-situ guided wave application.

5.2.2 Active and Passive Guided Wave Inspection

In general, guided wave inspection can be categorized into either active or passive. Passive techniques aim to record structural response induced by natural loads of the structure which happen during the flight of an aircraft. A comprehensive review of passive acoustic NDT techniques is presented in Chap. 7 of this book. One other good example of the passive technique is an embedded optical fibre Bragg grating sensor which has a series of parallel engraved lines (index points of refraction) that provide different reflection and transmission of light under varying strains in the structure. In case of fibre breakage, loss of transmitted light is observed, while the strain changes leads to altered refraction coefficient (Papantoniou et al. 2011). Optical fibre sensors have been extensively used to measure the temperature and strain of aircraft structures and even to detect the delamination type defects by analysing the wavelength shifts and reflection spectra of light (Ecke 2000; Takeda et al. 2002). Such inspection techniques are covered in Chap. 8. Active SHM utilizes both actuators and sensors to measure a response of the structure to a known input. Both bulk wave and guided wave techniques can be categorized as active, however in aerospace SHM applications the guided waves inspections are more commonly used. Guided wave excitation is usually determined by the design of the structural health monitoring system. It essentially depends on the type of defects which has to be detected and the structure under analysis. In the ideal case, the best guided wave mode for inspection should feature low dispersion and attenuation, high sensitivity to damage, easy excitability and detectability (Su and Ye 2006). The dispersion and attenuation depend on the excitation frequency and material properties, while the sensitivity to the defect is determined by the displacement profile of each mode.

5.2.3 Dispersion and Attenuation

High dispersion usually limits the sensitivity to the defect and the inspection length, as the wave-packet of the mode becomes distorted with the distance. To reduce the

effect of dispersion, narrowband excitation is usually applied by increasing the number of cycles of the excitation signal. As a result, the bandwidth of the signal decreases, limiting the extent of dispersion (Wilcox et al. 2001b). On the other hand, it means that the signal itself becomes longer in duration which reduces the temporal resolution. Wilcox et al. introduced a concept of minimum resolvable distance (MRD), which shows the sweet spot on the dispersion curve, where the best compromise between propagation distance, number of excitation signal cycles, wavelength and resolution can be estimated (Wilcox et al. 2001a):

$$\text{MRD} = \frac{c_0}{d} \left[l \left(\frac{1}{c_{\min}} - \frac{1}{c_{\max}} \right) + T_{\text{in}} \right]_{\min}, \quad (5.16)$$

where l and d are the wave propagation distance and the plate thickness; c_{\min} , c_{\max} are the minimum and maximum velocities through the distance l ; c_0 is the velocity at the central frequency; T_{in} is the initial time duration of the wave-packet. Typically, fundamental modes of guided waves such as A_0 and S_0 possess low MRD values and therefore require less cycles for adequate resolution.

Different post-processing strategies exist that can be used to reduce the effect of dispersion after the signal arrives to the sensor. For example, Wilcox presented a technique that uses a priori knowledge of dispersive characteristics of guided wave mode to compress the signals by mapping the time to distance domains (Wilcox 2003). De Marchi et al. introduced the warped frequency transform method to reduce the effect of dispersion. The authors used chirped pulse excitation with the proposed dispersion compensation technique to improve arrival time estimation in the detection of simulated defects on aluminium plate (De Marchi et al. 2013). However, in most cases the reconstructed signals are either still deformed due to non-linearity of the transformation function or the compensation methods are usually efficient for the reconstruction of one targeted mode (Luo et al. 2016). Recently, the sparse decomposition methods, that use a dictionary of non-dispersive signals to decompose guided wave responses obtained from the structures were proposed (Xu et al. 2018). The dictionaries are built exploiting the dispersion curves of the signal, which requires precise knowledge of the material properties. Each atom in the dictionary represents a dispersive signal at a certain distance. By comparing each atom to the measured signal, the non-dispersive analogue can be found.

Attenuation is another limiting factor that can influence the design of the monitoring system. Considering that the reflection from damage is usually weak, the attenuation of guided waves has to be sufficiently low in order to capture such reflections at some distance. The main factors that determine the level of attenuation are dispersion, beam divergence, material damping and leakage of the acoustic energy into the surrounding media (Long et al. 2003; Mustapha and Ye 2014). The leakage depends on the difference between the phase velocity of guided waves in the structure and the velocity of bulk waves in the surrounding medium. Significant leakage is observed in those cases when the phase velocity of guided waves is above the bulk wave velocity in the embedded media. The leaky behaviour of guided

waves are usually exploited while investigating flow and defects in gas or fluid loaded pipes (Djili et al. 2013; Zichuan et al. 2018; Mazzotti et al. 2014).

5.2.4 Guided Wave Excitation and Mode Selection

Ultrasonic guided waves can be excited using different strategies, depending on the application of the monitoring system. Direct contact methods can be either surface mounted or embedded into the structure. Surface-mounted sensors, like piezoelectric wafers are cheap, lightweight, can be arranged in different configurations and easily replaced if necessary (Giurgiutiu 2015). Simple instrumentation is required for such sensors as they operate on the direct and inverse piezoelectric effect. However, surface mounted solutions are not very attractive for in-situ applications as they change the aerodynamics of the structure. Thus for in-service aerospace monitoring systems, integrated sensors are preferred. These have high requirements for durability, as the monitoring system has to be reliable for the whole life-time of an aircraft. Different studies are available that analyse the durability of integrated sensors under varying environmental and cyclic conditions (Giurgiutiu et al. 2004; Melnykowycz et al. 2006; Tsoi and Rajic 2008). Different type of integrated sensors exists, while most commonly piezoelectric and fibre Bragg grating are used. Sensor integration can introduce additional resin-rich regions in the laminate or the sources of crack initiation around the corners of the piezoelectric sensor, therefore the shape and integration design has to be considered carefully taking into account overall strength of the host structure (Veidt and Liew 2012). Fibre Bragg grating sensors are lightweight and designed to be integrated into the composite structures. Such sensors do not require wiring, are cheap, durable and do not change the strength of the host structure (Veidt and Liew 2012; Majumder et al. 2008). Non-contact inspection methods like air-coupled or laser ultrasonics provide an ability to adjust to the complex surface of the structure. Such methods can be adjusted to excite different guided wave modes as the angle between the transducer and the sample can be easily adjusted (Panda et al. 2018; Römmeler et al. 2020). Laser and conventional air-coupled monitoring are usually combined, using conventional piezoelectric transducers for transmission and laser vibrometer for the reception (Jurek et al. 2018). Other researchers combined air-coupled ultrasonic testing with thermal imaging (Rheinfurth et al. 2011). Despite the advantages of air-coupled ultrasonic inspection, it requires some expensive equipment, such as scanners, laser heads etc. and also access to inspected parts; hence, it can be performed only during the maintenance break of an aircraft.

In real-world situations, using many abovementioned guided wave excitation methods multiple modes are being generated simultaneously, unless some specific excitation strategies are applied. Many studies are available that seek to excite specific mode of guided waves (Lee et al. 2008; Li et al. 2016). The simplest solution is to select specific operating points of guided wave dispersion curves, where only a desired modes exist. For example, at low frequency-thickness products, fundamental

zone with zeroth order modes exist. Such modes possess relatively simple mode shapes, are less dispersive and may be easily generated. Limiting the excitation bandwidth and operating at low frequencies can effectively control number of modes present in the structure and the amount of their dispersion. At very high frequency-thickness products (20 MHz · mm and above), higher order guided wave modes have similar group velocities, hence they form a non-dispersive cluster which is called Higher Order Mode Cluster (HOMC) (Jayaraman et al. 2009). Such cluster of modes possess reduced surface sensitivity, thus it's a good choice for localised flaw detection, like pitting corrosion. In the medium frequency-thickness range, many modes exist which are usually dispersive and possess much more complex mode shapes. Inspection at such operating point provides better sensitivity to small defects and thickness variations which is achieved at a cost of mode purity. In order to suppress unwanted modes, some of the following techniques could be mentioned. For instance, in case of air-coupled or laser beam excitation, the ultrasonic signal can be introduced at some incidence angle, which allows to excite specific modes and reduce coherent noise. Such incidence angle is frequency-dependent and may be calculated analytically. This selective mode excitation approach is usually valid for fundamental modes only, as the incident angles of different modes tend to overlap at higher frequencies.

In case of direct sensor placement on the surface of component, different selective mode excitation strategies must be applied. Giurgiutiu et al. used piezoelectric wafer active sensors to excite single guided wave mode (Giurgiutiu 2005; Xu and Giurgiutiu 2007). For a particular mode, the maximum of the strain and displacement functions is achieved when the width of the transducer is equal to odd multiple half wavelengths of the desired mode. In contrast, the minimum occurs in case the width of the sensor is equal to an even number of half wavelengths. In such a way, the size of the transducer introduces spatial filtering phenomena, which allow to enhance or suppress the vibrations of the particular guided wave mode (Giurgiutiu 2011; Samaitis and Mažeika 2017). Another approach for excitation of single guided wave mode is based on the use of interdigital or comb transducers, which consist of two-finger type electrodes that are interchanged and driven by an opposite phase electrical field (Monkhouse et al. 2000; Bellan et al. 2005). The type of mode which is introduced to the structure is determined by the pitch between finger electrodes which has to be equal to half the wavelength of the desired mode. Several design extensions of the classical interdigital transducers can be found, which were proposed by Salas et al. (Salas and Cesnik 2009) and Jin et al. (Jin et al. 2005). Glushkov et al. used a co-axial ring-type transducer for selective omnidirectional mode excitation (Glushkov et al. 2010). The major drawback of piezoelectric wafers and interdigital transducers is that the mode selectivity is related to the size of the transducer. It means that the set of sensors is required to excite different modes. At low frequencies, the physical dimensions of such transducers become large and not convenient for many applications.

Other approaches to generate a single mode are based on the positioning of two or more piezoelectric elements in a sequence on the surface of the sample at the interelement distance equal to the wavelength of the desired mode (Grondel et al. 2002).

Similarly, elements can be positioned on the opposite surfaces and in-phase or out-of-phase excitation is then used to drive the mode of interest (Seung and Hoon 2007). The use of the phased-arrays is another field that contributes to the selective guided wave excitation. Fromme used 32-element circular array and phase addition algorithm to excite A_0 mode on aluminium plate (Fromme et al. 2006). The abovementioned approaches are most suitable for excitation of fundamental guided wave modes such as A_0 or S_0 . It has to be considered that all modes of the wavelength determined by the pitch of array elements will be excited, which is especially important working with higher-order guided wave modes, thus reducing the mode selectivity. To overcome such a problem, recently Veit et al. proposed an approach for selective guided wave excitation using conventional phased array probe having small pitch relative to wavelength of targeted mode. By controlling the input signal bandwidth and the angle of generated beam even higher order modes can be excited both on metallic and composite structures (Veit and Bélanger 2020).

Different researches show, that the mode purity is an important issue for selective guided wave excitation. Usually, the approaches described above can produce some dominant modes; however, other modes might exist with significantly lower displacements and contribute to an overall noise of the signal. Other transducers, especially phased arrays, possess low dynamic range, thus they are limited to detection of relatively large defects.

5.3 Defect Detection

Guided wave defect detection methods can be categorized into baseline and baseline-free. The baseline methods require a baseline dataset, which describes defect-free state of the structure. Then each further collected signal is compared to a baseline to detect the presence of damage. If there are any structural changes present, the guided waves will be reflected or scattered by them. Subtracting such signal from baseline will give the residual, which may indicate the presence of damage. This technique allows to eliminate permanent reflections from object boundaries. Despite its simplicity, such technique is extremely sensitive to changes of surrounding temperature, loads, transducer bonding, aging etc. For instance, some investigations show, that if magnitude of the reflection from the defect is at least -30 dB compared to the direct arrival, the temperature change of 10 °C can conceal the defect even though temperature compensation techniques are used (Croxford et al. 2010; Dai and He 2014). In order to make baseline subtraction work, non-damage related patterns have to be eliminated. The strategies to rule out the temperature influence on guided wave signals are discussed in more details in the POD section of this chapter.

The baseline free methods do not require a set of baseline signals, thus are less susceptible to environmental changes, transducer bonding, etc. Time reversal techniques can be presented as an example of baseline free damage detection (Sohn et al. 2007). Such approach uses at least two transducers where one of them

is dedicated for time reversal of the signal received from the first sensor and reemits it back. The whole procedure can be described as follows:

1. the wave is introduced into the structure by applying the voltage $V_A(t)$ to transmitter A;
2. the propagated wave is captured by sensor B and recorded as voltage $V_B(t)$;
3. signal $V_B(t)$ is reversed in time and reemitted back to transducer A;
4. finally, transducer A receives the signal $V_{BA}(t)$ and compares it with the original input $V_A(t)$.

For a defect-free structures, the input signal $V_A(t)$ should correlate to the reconstructed signal $V_{BA}(t)$, while any mismatch indicates structural changes (Park et al. 2009; Mustapha and Ye 2015). Some studies show that such a technique is not suitable for notch detection in metallic structures, as such defect does not break the time reversibility and only changes the amplitude of the received signals (Gangadharan et al. 2009). It should be also noted during analysis that the reciprocity of the system is only limited to the directly arriving waves. Boundary reflections and non-uniform distribution of attenuation properties may cause asymmetry in wave fields and differences between the original and the re-sent time-reversed signals, especially for multi-modal wavefields.

5.3.1 Defect Localisation and Imaging: Sparse, Phased Arrays and Guided Wave Tomography

Both abovementioned methods are dedicated to detecting structural changes. Unfortunately, these are not suitable to localize and characterize damage. In general, two defect detection approaches based on sensor type and placement can be identified—sensor networks or sparsely arrays and phased arrays (Rocha et al. 2013; Michaels 2016). Sparse arrays use a distributed network of discrete omnidirectional transducers which are positioned at specific regions of interest. Meanwhile phased arrays use closely spaced elements and are based on steering of the wavefront at different directions by applying different lag to each array element. Despite different sensor architectures, all damage detection and localisation methods are based on the assumption that any present discontinuity will produce an unexpected echo, which can be received by sensor.

Defect localization methods are mostly based on time-of-flight (ToF) measurement of defect scattered guided wave signals. In the simplest 1D case damage can be localized as shown in Fig. 5.2a. In such arrangement, the distance l_0 and signal arrival time T_0 between sensors A and B are known. In case of the defect, an additional reflection will be received by sensor B at time instant T_1 . The distance x to the defect can be calculated according to the equation (Dai and He 2014):

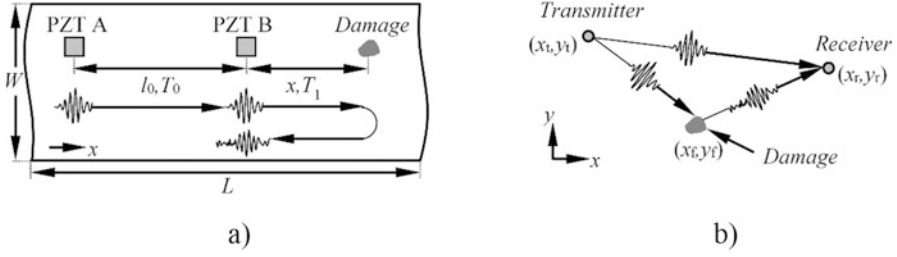


Fig. 5.2 The concept of damage localization in 1D (a) and 2-D (b) case (Dai and He 2014; Michaels and Michaels 2006)

$$\frac{l_0}{T_0} = \frac{2x}{T_1}. \quad (5.17)$$

This works well in presence of single mode only, however the corrections are necessary in case of mode-conversion. In 2-D case (Fig. 5.2b), the spatial defect position can be estimated by calculating the ToF of the signal going from the transmitter through the flaw (Michaels and Michaels 2007):

$$t_{tr}^f = \frac{\sqrt{(x_t - x_f)^2 + (y_t - y_f)^2} + \sqrt{(x_r - x_f)^2 + (y_r - y_f)^2}}{c_g}. \quad (5.18)$$

where subscripts t , r , and f denote the 2-D coordinates of the transmitter, receiver and flaw. To detect damage location with sparsed array, at least three sensors are required. By using triangulation method it's possible to find an intersection of three regions produced by the sensors, where the possible damage is likely to occur. The shape of regions of the likely defect position will depend on transmission and reception approach. If the measurements are taken recording an echo received by each transducer and the wave propagates spherically, the region of the sensor will be in the shape of circle. On the other hand if each transducer acts as transmitter once, while all the transducers act as receivers, the region of the sensor will be in the shape of ellipse (Rocha et al. 2013). Such approach works well if wave velocity is the same in every direction. Otherwise the corrections have to be made and the actual location of the damage will be different. By using at least three sensors the image over the region of interest can be generated. In case of N sensors, the defect scattered signals will arrive at different time instances for each transmitter-receiver pair, depending on actual defect position leading to $N(N-1)/2$ different signals paths. To create an image, the evenly spaced grid points over the inspection area are defined. Then the pixel value at the reconstruction point (x,y) according to the delay and sum (DAS) algorithm can be estimated as (Michaels 2008):

$$P(x, y) = \frac{1}{N} \sum_{n=1}^N |\omega_{nxy} r_n(t - t_{nxy})|^2 \quad (5.19)$$

where ω_{nxy} —is reconstruction weight at specific point (x, y) , t_{nxy} —is the time delay which can be calculated as d_{nxy}/c_g where d_{nxy} —distance from transmitter through point (x, y) to receiver, c_g is the group velocity. Then the 2-D defect map can be created, by repeating this procedure at spatially distributed reconstruction points. At the actual defect locations, such addition will lead to constructive interference of received signals. The major drawback of the DAS method is a large point spread function and artefacts which may be caused by wave reflections from the boundaries and mode-conversion (Michaels 2016).

Reconstruction algorithm for probabilistic inspection of defects (RAPID) method can be shown as another example of sparse array imaging (Zhao et al. 2007). RAPID method uses a circular arrangement of the sensors and assumes that most significant signal changes appear in the direct wave path. Hence, between each transmitter receiver pair a linearly decreasing elliptical spatial distribution of signal change effects due to defects is presumed. In case of N PZT elements, the defect probability at imaging position (x, y) can be expressed as (Zhao et al. 2007):

$$P(x, y) = \sum_{i=1}^{N-1} \sum_{j=i+1}^N P_{ij}(x, y) = \sum_{i=1}^{N-1} \sum_{j=i+1}^N A_{ij} \left(\frac{\beta - R_{ij}(x, y)}{\beta - 1} \right), \quad (5.20)$$

where $P_{ij}(x, y)$ is defect distribution probability estimate for i^{th} transmitter and j^{th} receiver, A_{ij} is signal difference coefficient of the same sensor pair, $(\beta - R_{ij}(x, y))/(\beta - 1)$ is the linearly decreasing elliptical spatial distribution. Different indicators can be used for 2-D reconstruction of the defect position and definition of the pixel value in the reconstruction grid using sparse arrays. For example, Kudela et al. (Kudela et al. 2008) used a concept of damage influence map, which measures the match between the excitation signal and reflection from defect. The idea is based on the arbitrary positioning of the excitation signal on the response from the structure employing different time delays. The delay applied to the signal is then equal to the ToF from the transmitter to the likely damage position. The match between two signals at location (x, y) here is expressed by (Kudela et al. 2008):

$$e_k(x, y) = \int_{t_0}^{t_0 + \Delta t^*} \widehat{S}_T(t) \left[F(t) G(x, y) \widehat{S}_{R,k}(t) \right] dt, \quad (5.21)$$

where t_0 and Δt^* are the start and the width of the time window; $\widehat{S}_T(t) = S_T(t_0, t_0 + \Delta t^*)$ is the windowed excitation signal; $\widehat{S}_{R,k}(t) = S_{R,k}(t_0 + \Delta t, t_0 + \Delta t^*)$ is the signal registered with the k^{th} receiver, $F(t)$ is the window function (Gauss, Hann, etc.); $G(x, y) = e^{\alpha(d_{OP} + d_{PK})}$ is the function dependent on the attenuation; α is the attenuation coefficient; d_{OP} and d_{PK} represent the distances

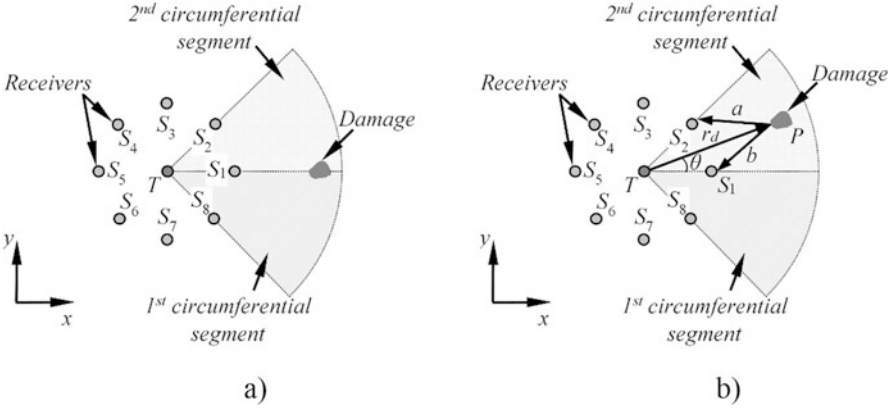


Fig. 5.3 The concept to determine the radial segment of the damage location (a) and the idea of exact damage positioning using the triangulation method (b) (Giridhara et al. 2010)

between the transmitter-imaging point and imaging point-receiver; Δt is the signal time shift, which depends on the x, y coordinates of the imaging point and the group velocities c_{OP} and c_{PK} . The total match at location (x, y) for all transmitter-receiver pairs can be expressed as (Kudela et al. 2008):

$$E = \sum_k \int_S e_k(x, y) dS \approx \sum_k \sum_{i,j} e_k(x_i, y_j), \quad (5.22)$$

Modifications of the proposed technique exist, which were introduced by Wandowski et al. (Wandowski et al. 2011; Wandowski et al. 2016). A slightly different approach was used by Michaels (Michaels and Michaels 2007), where authors used band pass filters with various central frequencies to obtain a set of bandlimited signals for each transmitter-receiver pair. Then the defect map is being created for each central frequency of the applied filter. Eventually, all individual images are combined taking minimum pixel value from all corresponding images, which minimizes phasing and other artefacts.

A modification of sparse array architecture was proposed by Giridhara et al. (Giridhara et al. 2010) who implemented the radial segmentation technique. It consists of a single transmitter and radially distributed receivers, which divide the object into circumferential segments. The signals from neighbouring transducers are compared to determine the location of the defect. If the flaw is somewhere along x axis (Fig. 5.3a), the sensor signals (S_2 and S_8 ; S_2 and S_1 ; S_1 and S_8) will indicate some changes in the structure. If two signals from sensors S_2 and S_8 match, then the damage is in the segment S_1 and S_2 or in the segment S_1 and S_8 . The radial segment of the defect is determined by measuring the ToF of the reflection from the flaw with sensors S_2 and S_8 . The exact defect angular, θ , and radial, r_d , position estimates are found by using triangulation as shown in Fig. 5.3b (Giridhara et al. 2010):

$$\theta = \phi + \cos^{-1}K; \phi = \tan^{-1}\left(\frac{py_{i+1} - qy_i}{px_{i+1} - qx_i}\right); K = \cos(\theta - \phi). \quad (5.23)$$

$$r_d = \frac{p}{2(x_i \cos \theta + y_i \sin \theta - d_i)} = \frac{q}{2(x_{i+1} \cos \theta + y_{i+1} \sin \theta - d_{i+1})}, \quad (5.24)$$

where $p = x_i^2 + y_i^2 + d_i^2$, $q = x_{i+1}^2 + y_{i+1}^2 + d_{i+1}^2$, d_i and d_{i+1} are the total travel path from the transmitter through the flaw to the sensors S_i and S_{i+1} respectively ($d_i = r_d + a$, $d_{i+1} = r_d + b$, $r_d = x^2 + y^2$); a and b are the distances of the sensors $S_i(x_i, y_i)$, $S_{i+1}(x_{i+1}, y_{i+1})$ to the damage $P(a^2 = (x-x_i)^2 + (y-y_i)^2, b^2 = (x-x_{i+1})^2 + (y-y_{i+1})^2)$.

The sparse array approach interrogates the damage from multiple angles, hence the forward scattered and backscattered signals can be recorded if the damage is present within the area of array. Moreover, the reflection energy from the defect is more uniform within the region of sparse array in contrast to phased array inspections. On the other hand, as the phased array elements are located in close proximity to each other, it's much easier to leverage the phase difference which is mainly caused by errors in phase velocity, transducer locations and variation of transducer characteristics (Michaels 2016). Using the phased array imaging, the array elements are delayed so that the azimuth of the wave φ is equal to the azimuth of target reflector φ_0 . To obtain the target direction most of phased array methods sweep the beam at different directions and estimate the maximum of received signal energy. Once the target direction φ_0 is obtained, the distance to the reflector can be estimated using cross correlation or other time delay measurement method. An example of phased array imaging can be embedded ultrasonic structural radar (EUSR) method (Giurgiutiu and Bao 2004; Purekar et al. 2004). The use of phased arrays offers some advantages over single transmitter-receiver measurements, such as steering and focusing, hence large area of the sample can be examined and direction of reflector can be determined almost instantly. However, in practice due to multiple reflections and structural noise it becomes difficult both to distinguish reflector and to measure the time-of-flight precisely, which leads to defect positioning errors. Aircraft components made from composite materials introduce additional complexity for damage detection and localisation. The mechanical properties of composites are direction dependent, hence the circular or elliptical damage regions are no longer valid. Phased array beam steering becomes more complex, as radial velocity distributions must be known. As the velocity of guided waves varies with the propagation direction, wavelength and operating point on the dispersion curve (and dispersion itself) change as well. It means that the sensitivity to the defect and resolution are changing, especially if operating point is located on the dispersive region of the selected mode. This shows that each unique structure requires adaptation of the monitoring system—determination of radial velocity distributions, evaluation of boundary reflections (taking into the account velocity information), identification of present modes. Guided wave tomography is one of the most common imaging methods used to detect and localize structural changes. The tomography aims to reconstruct the spatial distribution of the material properties, which can be based on the projection of wave velocity, attenuation, frequency shift or other features

(Belanger and Cawley 2009). To get the desired resolution, a large number of projections are required which can be collected either using transmission or reflection approach. Among the sensor arrangement topologies, the crosshole, double-crosshole and fan-beam are the most popular ones (Park et al. 2020). Several different tomographic reconstruction techniques exist, namely straight-ray, bent ray and diffraction tomography (Belanger and Cawley 2009; Willey et al. 2014; Belanger et al. 2010). The straight-ray methods neglect refraction and diffraction assuming that projection data corresponds to a line integral of given parameter. Bent ray methods take into account wave field of reflected from the defect, while diffraction tomography is based on Born's approximation.

5.3.2 Guided Wave Interaction with Actual Structural Defect

The damage detection and localisation principles described above exploit many assumptions that simplify the reconstruction. In realistic structures, the response of the defect is much more complex. For example, delamination is one of the most common defects found in multi-layered structures, which develop internally between neighbouring layers of the laminate. After the interaction with delamination, guided waves are scattered and convert to other modes (Feng et al. 2018). Various researches show that fundamental modes of guided waves propagate separately in two sub-laminates created by defect and then interact with each other after exiting the damaged area. A detailed guided wave interaction with delamination type defects was presented by Ramadas et al. who found that in case of delaminations positioned symmetrically across the thickness of the laminate, incident A_0 mode converts to S_0 within the defect and then back to A_0 after exiting. For asymmetrical defects, the mechanism is slightly different as an additional S_0 mode is present upon interaction with defect (Ramadas et al. 2009; Ramadas et al. 2010). It was also observed by various research groups that Lamb wave scattering at the beginning and tip of defect is determined by its position. Schaal et al. estimated frequency-dependent scattering coefficients for fundamental Lamb wave modes at both ends of the defect (Schaal et al. 2017). Based on this approach, Hu proposed a technique to locate delamination defects based on reflection and transmission coefficients of A_0 and S_0 modes (Hu et al. 2008). Shkerdin and Glorieux (Shkerdin and Glorieux 2004) related the transmission coefficients of Lamb waves with the depth and length of delamination, while Birt et al. (Birt 1998) analyzed the magnitude of reflected S_0 mode and its relation to the width of delamination. This shows that different indicators can be developed to detect defects and to assess their parameters. A complex guided wave scattering and mode conversion upon interaction with defects allows to develop various tools to identify and characterize the damage. In most simple cases, ToF measurements of reflected and transmitted guided wave modes can be used to detect the existence and location of the damage. Furthermore, by analysing the magnitude patterns and velocities of guided wave modes, other features like defect size and depth can be extracted.

5.4 Reliability of SHM Systems

SHM is a technique used for monitoring the integrity of in-service structures of aircraft, bridges, pipelines and other components which are continuously exposed to operational load and environmental influence. The goal of SHM technology is to complement NDE techniques to improve reliability of the structure and reduce inspection and repair costs (Meeker et al. 2019; Etebu and Shafiee 2018). Thus, performance of the SHM system is characterized by the quality of sensors, their mounting and reliability of measurements. Reliability of SHM system depends on the quality of received data (Li et al. 2019; Datteo et al. 2018). SHM systems and NDE techniques use the same physical principle for damage detection. However, there are notable differences between the two systems. SHM measurements are carried out by the same array of sensors fixed in the same locations and provide continuous monitoring of the structure. Hence, in contrast to traditional NDE, each new result obtained from sequentially repeated inspections depends on the previous one in SHM system. Assessment of structural integrity is characterized by a large period of time between the first and last inspection in sequence of NDE technique. Conversely, when short time period passed the process is called monitoring. Therefore, SHM is able to control structural integrity in real-time and detect damage before the scheduled maintenance. Another essential distinction of SHM and traditional NDE are the different causes which affect the measurements (Kabban et al. 2015). In the case of SHM application the sources of variability are not the same as for NDE. For instance, NDE variables as sensors, instrumentation and operator are fixed parameters in SHM. Sources of variability in SHM are mostly relate to in-situ effects, such as temperature, aging and load variation. Additionally, key point of SHM system is a fixed nature of sensing probes which leads to a lack of variation in sensor response caused by human factor. If the variability of in-situ effects is low or it can be filtered, the SHM registers variability of the system to defect geometry, inconsistencies of sensors mounting and structural differences (Fisher and Michaels 2009; Cobb et al. 2009).

In order to ensure reliability of SHM system the following activities have to be performed (Etebu and Shafiee 2018; Kabban et al. 2015):

1. Perfect communication between specialists who install sensors and specialists who carry out structural analysis;
2. Careful planning of areas to monitor;
3. Sensor system design;
4. Component replacement design;
5. Data storage design;
6. Testing of sensors system;
7. Aging compensation of sensors.

Reliability of SHM is the evaluation of probability of repeated and successful outcomes of the system under prescribed environmental conditions. Reliability

indicates the quality of fault detection by assessment of four probabilities (Stolz and Meisner 2020; Gallina et al. 2013):

1. Probability of detection (POD)—the system detects faults when they exist in the structure;
2. Probability of false alarms (PFA)—the system detects faults when they do not exist in the structure;
3. Positive predictive probability (PPP)—the system detects no faults when they exist in the structure;
4. Negative predictive probability (NPP)—the system detects no faults when they do not exist in the structure.

Since PPP and NPP are the inverse probabilities of POD and PFA, only first two probabilities have to be assessed. Great attention has to be paid to false calls because they occur often in SHM. POD and PFA are also interdependent through the threshold which defines the level of the system response indicating the presence of damage in the structure (Gallina et al. 2013).

5.4.1 Basic Concepts of POD and PFA

POD is the probability of specified NDE inspection to detect defects in the structure at the time of inspection. MIL-HDBK-1823A provides all statistical tools and procedures to assess POD for reliability validation of NDE techniques. Usually, POD is a function of defect characteristics, i.e. length of the defect. Log Odds and Log Probit probabilistic models are commonly used for POD assessment (Gallina et al. 2013; Aldrin et al. 2016). POD can be assessed by Hit/Miss and signal response analysis. The objective of both configurations is to produce a POD curve vs characteristic parameter of the defect (usually size). Typical POD curve is presented in Fig. 5.4.

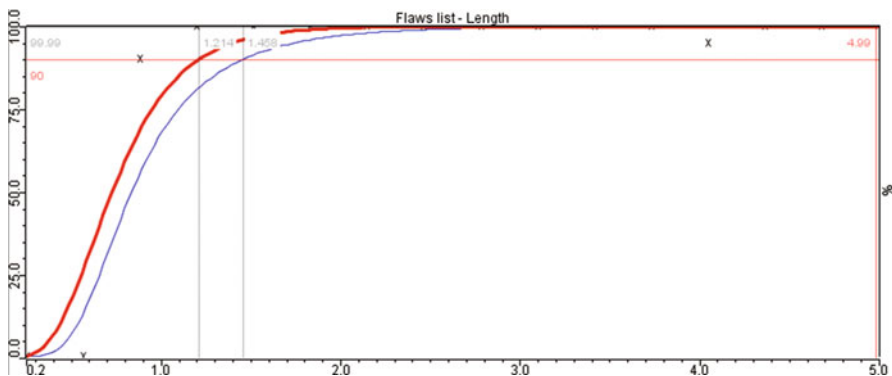


Fig. 5.4 Typical POD curve received by Hit/Miss analysis in red and POD with 95% confidence level in blue

Small size of the defect is characterized by 0 POD (0%) meaning that the system could not detect defect of the specified size. The POD is 1 (100%) in the case of large defects meaning that the system detects defect of specified size reliably. Transition zone where POD curve is increasing between 0 and 1 is under most interest. Additionally, the confidence interval is associated with POD and indicates the content of true value in the interval (Chapuis et al. 2018a; Chapuis et al. 2018b). Hence, confidence bounds characterize the ability of the system to detect particular characteristic parameter (defect size) with defined probability and confidence (Gallina et al. 2013). The usual requirement, especially for aerospace applications, is to determine the minimum size of defect which is detectable in 90% of the inspections at 95 % confidence level, $a_{90/95}$ (Gallina et al. 2013).

Hit/Miss approach is characterized by measurement of qualitative information and determines the presence or absence of the damage. The response of the inspection is binary value of 1 (defect is detected) and 0 (fail to detect the defect). The model of POD in Log-Odds functional is expressed (Chapuis et al. 2018b):

$$\text{POD}(a) = \left[1 + \exp \left(- \left(\frac{g(a) - \mu}{\sigma} \right) \right) \right]^{-1}, \quad (5.25)$$

where a is a characteristic parameter (defect size), $g(a) = a$ or $g(a) = \log(a)$, μ is a defect size detected with a probability of 50% and σ is the steepeness of the function.

Also, POD can be evaluated by signal response approach (\hat{a} vs a) or quantitative measure of defect size. POD curve is based on methodology when there is a relationship between the defect size, a (physical dimension of a defect size), and sensor response \hat{a} (measured response of the system to a target size). In the case of ultrasonic inspection the system provides a response from the defect whose amplitude is dependent on it's size. Signal response approach is able to estimate and build POD curve using greatly smaller amount of data comparing to Hit/Miss analysis (Meeker et al. 2019; Chapuis et al. 2018b). Generally, this approach has a linear model and is expressed as following (Chapuis et al. 2018b):

$$y = \beta_0 + \beta_1 g(a) + \varepsilon, \quad (5.26)$$

where β_0 and β_1 are the coefficients of linear function, $g(a) = a$ or $g(a) = \log(a)$, ε is a random error.

Since the noise exists in any inspection data the boundary which determines damage or no damage output has to be established. For this task the the detection threshold a_{thres} is fixed. Further, the POD curve can be expressed as a function of density of scattered data which is above the detection threshold y_{thres} (Gallina et al. 2013; Chapuis et al. 2018b):

$$\begin{aligned}
 \text{POD}(a) &= P(y > y_{\text{thres}}) = 1 - \Phi_{\text{norm}}\left(\frac{y_{\text{thres}} - (\beta_0 + \beta_1 g(a))}{\sigma_\varepsilon}\right) \\
 &= \Phi_{\text{norm}}\left(\frac{g(a) - \mu}{\sigma}\right),
 \end{aligned} \tag{5.27}$$

where $\Phi_{\text{norm}}(z)$ is the normal density function and $\mu = \frac{y_{\text{thres}} - \beta_0}{\beta_1}$, $\sigma = \frac{\sigma_\varepsilon}{\beta_1}$. The parameters μ and σ are determined according to the methodology of maximum likelihood estimation (Chapuis et al. 2018b).

As it was mentioned in Sect. 5.4, the probability of false alarms or Relative Operating Characteristics (ROC) curve has a significant importance to estimate the performance of SHM and NDE systems (Gallina et al. 2013). Selection of adequate detection threshold is an essential part in PFA assessment. It is a high possibility to classify undamaged regions of the component as damaged due to high number of observations in SHM system. For instance, the detection threshold can be exceeded by the impact of strong background noise when no defect is present. However, the POD and PFA are spatially dependent. Therefore, in order to determine appropriate detection threshold it is useful to plot POD and PFA in the same diagram to establish the overlap between two metrics of system performance (Fig. 5.5) (Gallina et al. 2013; Chapuis et al. 2018b; Schoefs et al. 2012).

In the case of NDE inspections a_{thres} is determined from the measurement when no flaw in the structure is present and the value is set above the background noise level. Since the threshold is set quite high in NDT applications the PFA has usually a low value (Fisher and Michaels 2009). Consequently, the threshold value in NDE for signal response approach is the highest level of noise in the defect free region (Fisher and Michaels 2009). However, it is a challenging task to determine detection threshold for SHM application. In the case of SHM system, a number of measurements of not defective structure will be available before damage occurs. Since the sensors are fixed in SHM system, in-situ effects will affect the signal response—temperature, operational load or sensor degradation. As a result, detection threshold can be determined as a variance in signal response over time from the undamaged structure. Another complexity to define a_{thres} is a dependent measurement of SHM. Due to a large degree of variability the measurement response can be classified as damage even if there is none in accordance with prior measurements (Meeker et al. 2019; Fisher and Michaels 2009; Cobb et al. 2009).

5.4.2 Sources of Variability of SHM System

Before POD assessment, NDE and SHM systems should be completely evaluated in terms of the limits of operational parameters and application in order to list factors that significantly affect the variability of the system (Department of Defense 2009). It is essential to capture all sources of variability. Otherwise, the results of system performance evaluation will be invalid due to missed significant variables. After

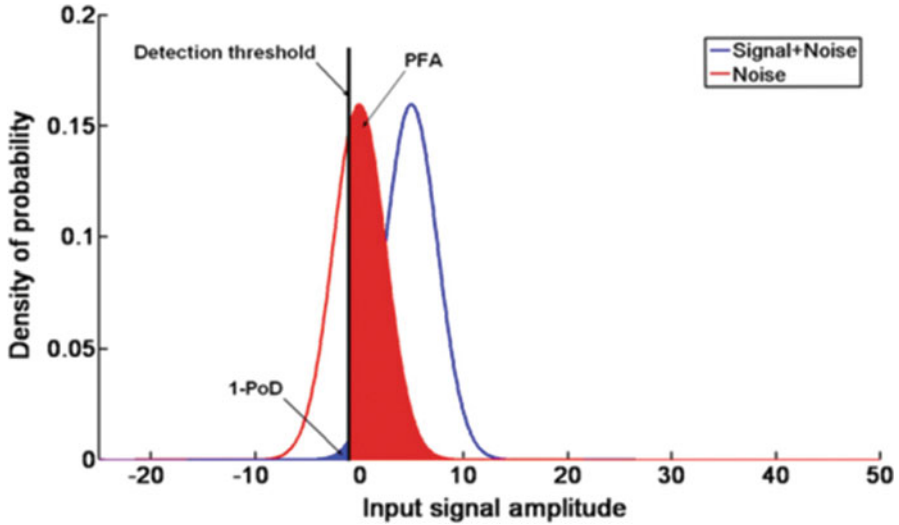


Fig. 5.5 Plot of POD and PFA (Schoefs et al. 2012)

analysis, variables which have negligible impact on the detection can be eliminated (Mandache et al. 2011). There is a risk to overestimate the POD of smaller size defects and underestimate the PFA in the case of missing important influential sources. Factors of SHM system which could affect the signal are as follows (Meeker et al. 2019; Mandache et al. 2011):

1. Shape, size and orientation of the defect as well as the change of these characteristics over time;
2. Defect and sensor location;
3. Environmental conditions (temperature, humidity);
4. Mechanical variables;
5. Change of structural configuration over time;
6. Change of sensor performance over time;
7. Quality of sensor bonding;
8. Sensor degradation and aging;
9. Ambient noise;
10. Dirt;
11. Electromagnetic radiation;
12. Mechanical loads;
13. Data communication.

One of the advantages of SHM system is a reduction of human intervention as an important factor affecting the results due to automatization. However, there is still human involvement in the case of instrumentation installation and interpretation of the recorded data if required, but manual coordination is avoided (Mandache et al. 2011).

To ensure reliable work of SHM system backup power provision has to be implemented, since, power line is often at the risk to fail during emergency cases. Furthermore, SHM sensors durability depends on the power requirements. In the case of battery power supply, low weight and charging capabilities has to be feasible. More appropriate solution is to use self-powered sensors through energy harvesting. Additionally, to reduce the problem of sensors failure within years of exploitation they have to be self-diagnosed or redundant. Redundant SHM system involves sensors, which are not expensive and easy to install. The approach essence is to install multiple number of sensors with overlapping range to provide redundant sensing. Consequently, if one of the sensors fails, the others take over and perform the task. This redundant configuration can create more defect-tolerant and robust system (Mandache et al. 2011; Aldrin et al. 2013). However, redundant elements increase the weight of the system, which, especially in aerospace, should be kept as low as possible.

The sensors have to be optimally placed to assure the sensitivity to the damage as well as condition of structure surface. The guided waves have the ability to confine in thin-wall structures, so they are able to propagate over large distance of the structure with minimal loss of energy and attenuation. In addition, the guided waves are suitable for the inspection of various shapes and geometries of the long structures. Therefore, it is possible to monitor the condition of surface of the structure of different shape. Generally, the more sensors are placed on structure the more detailed information about structure health is received. The coverage of the sensors should be performed in specific way in order to provide adequate information from collected data. Performance requirement and sensor network robustness have to be fulfilled (Mandache et al. 2011; Yi and Li 2012; Abbas and Shafiee 2018).

In the case of monitoring high risk zones the sensors should be placed in close proximity in order to have higher sensitivity in the case of damage occurrence but not placed in potential risk of impact damage place since this can affect the sensor itself (Mandache et al. 2011).

A good quality of coupling between sensor and structure has to be provided. Usually, adhesive is used as a coupling medium. However, degradation of adhesive properties can also affect on the response of the sensor. In aerospace industry during aircraft exploitation, sensors which are placed on the surface of the structure are not applicable due to aerodynamic conditions. This method is possible on the measuring stands in laboratory conditions (Mandache et al. 2011).

Traditional wired SHM system consists of sensor system, data communication and storage system as well as the information analysis system to assess the integrity of the structure. The main disadvantages of wired system is a high cost of long cables, low productivity, time consumption, low flexibility, impact on the weight of the structure and heavy traffic of monitoring channels (Wang et al. 2020). Wired system is exposed to cable and wire breakage during the exploitation and leading to system malfunction. Wireless sensor networks have advantages of low cost, high efficiency, high flexibility. There are various protocols of communication technology widely described in (Alonso et al. 2018). Selection of the communication technology is dependent on the characteristics of infrastructure and monitoring

requirements. However, if the data is transmitted and stored wirelessly there is still issues on the effect of SHM system interaction with other aircraft systems and avionics, electromagnetic and radio frequency interferences, what data has to be collected and at what frequency and etc. (Mandache et al. 2011).

5.4.3 *Analysis of Environmental and Operational Conditions*

In order to define methodology for verifying reliability of SHM it is necessary to understand how sensors and other factors respond to the damage. In the case of guided waves, environmental and operational conditions can change the phase and the amplitude of the signal. The challenge in SHM system is to identify signal changes due to the damage presence from the false calls caused by the environmental and operational parameters influence. Guided wave technique is a suitable tool for damage detection and characterization, however, it has a high sensitivity to these factors. According to the work performed in this field, the impact of these parameters is compensated by development of appropriate modelling process, variation of sensor technologies, processing of the acquired signals, extraction of features as well as statistical methods and machine learning (Mandache et al. 2011; Gorgin et al. 2020). Environmental and operational conditions are huge source of variability in aerospace industry, civil and mechanical engineering. In this section, temperature and mechanical loading are discussed more widely due to their significant influence on SHM systems.

Temperature is the important condition, variation of which is limiting the guided wave SHM systems. Temperature change is dominant influential property of environment condition that affects robustness of guided wave SHM (GWSHM) system (Fendzi et al. 2016). Temperature affects the component under monitoring and the sensing system. Propagation characteristics of Lamb waves significantly depends on temperature variation. Volume and density of the component changes with the temperature variation. This leads to a modification in the elastic properties, change of ultrasound velocity in the material that influence the response of the sensor at damage free place in the component (Mandache et al. 2011).

In order to mitigate this problem many investigations on the change in guided waves properties caused by temperature were conducted experimentally, numerically and analytically. Different configurations of the technique as well as temperature range was studied. Generally, by changing the temperature signal amplitude, time of flight and velocity can change. For instance, Abbas et al. (Abbas and Shafiee 2018) generated wave velocity function for guided wave group velocity evaluation considering frequency and temperature effect. It was found that the function can be used at the temperature which is not higher than 130 °C, since, further temperature increase influences on the bonding characteristics of the sensors. However, the relation between temperature and the output of GWSHM is not linear, since, many factors caused by temperature variation influence on the guided waves. Changed stiffness of the materials has the impact on group and phase velocity; change of

elastic and shear moduli leads to longitudinal and transverse velocities change resulting the decrease of phase velocity of the waves. As a result, in the case of temperature increase the propagating signals arrive later compared to temperature decrease. Expansion and contraction effect can lead to a change of distance between sensors and actuators, additionally, temperature variation has an impact on sensor properties and bonding layer properties (thickness and shear modulus) (Gorgin et al. 2020). Some numerical investigations presented a high impact of the temperature on the propagation of guided waves due to the change of physical properties.

If baseline subtraction technique described in previous section is used to detect structural changes, temperature compensation strategies is a must in order to minimise the residuals caused by environmental factors and to be able to detect smaller defects. Compensation techniques like optimal baseline subtraction (OBS), cointegration or baseline signal stretch (BSS) exist to reduce the influence of temperature to guided wave signals (Croxford et al. 2010; Gorgin et al. 2020; Konstantinidis et al. 2007). A comprehensive study on the influence of temperature to reflection, transmission and velocity of guided waves was recently presented by Abbas et al. (Abbas et al. 2020). In the case of OBS temperature compensation technique the baseline signals are measured over the temperature range whereupon the best matched baseline signal is selected according to subtract from any further reading from the structure. This technique requires large number of baseline signals each at different environmental condition and high temperature resolution. BSS temperature compensation technique is based on model building of the effects on wave signals due to temperature change. The shape change of the signals over the time is calculated (stretch factor) in order to perform time-stretch estimation (dilation or compression of the signal). This method works well for small temperature differences between baseline and current signal, however it's performance deteriorates at sufficiently large temperature differences (Croxford et al. 2007). Clarke et al. proposed to use a combination of OBS and BSS methods to reduce amount of baseline signals describing different temperature regimes (Clarke et al. 2010). In most cases, it's considered, that wave velocity is most important factor that changes with variation of temperature. However, recent studies show, that phase and amplitude of the signal are temperature sensitive as well. Changes in the temperature may cause variation of bonding stiffness between the sensor and the structure. This may alter the frequency response of transducer and lead to phase delay in the signal. Fendzi et al. proposed temperature compensation method that estimates linear dependencies of amplitude and phase delay versus temperature for each transducer pair mounted on the structure (Fendzi et al. 2016). Based on derived amplitude and phase factors, the regression model is then estimated and signal can be reconstructed at selected temperature. Recently Herdovics et al. proposed temperature compensation method which uses two sensors in close proximity only, hence the phase changes are compensated according to the incident wave, while the wave velocity changes are suppressed from echoes. (Herdovics and Cegla 2019). The authors concluded that proposed compensation technique is able to reduce effect of environmental conditions from 7 dB to 20 dB in comparison to conventional single stretch BSS method at temperature difference of 41.5 °C between signals. Mariani

et al. presented a method for temperature compensation that takes into the account both velocity and phase information (Mariani et al. 2020). The main difference is that the later method provides estimate solely based on baseline and subsequent signals. The method demonstrated 97% POD for 0.1% probability of false alarm when the temperature difference ranges were between 7 °C to 28 °C and 35 °C to 55 °C. Meanwhile at the same conditions, standard BSS yielded up to 23% POD only.

Propagation of guided waves, also, can be affected by operational conditions which include vibration, loads and sensor bonding. Vibration can lead to interpretation complexity of structural behavior. The load applied on the structure can change a isotropic medium into an anisotropic medium, effective elastic constants lose symmetry, cause time-shift and phase velocity changes. To compensate the effect of load, the changes of phase shift and signal amplitude have to be taken into account. Additionally, sensor degradation occurs due to mechanical loading leading to piezoceramic transducer deterioration. In order to identify degradation mode as transducer disbonding the electromechanical impedance spectrum is determined by the electrical and the mechanical properties of the transducer and host structure which includes the adhesive line (Rajic et al. 2011). In order to ensure reliable performance of SHM system the influence of mechanical loading on the sensors, which cause its degradation, has to be reduced. The compensation strategy implies the use of specific element as a structural augmentation which is placed between transducer and the structure. As a result, the stresses in transducers caused by loading are reduced (Rajic et al. 2011).

5.4.4 *POD Assessment Solutions*

Comparing to NDE techniques which produce independent observation the data received from SHM system is dependent due to continuous data collection. Despite the fact that uncertainty factors of NDE and SHM differ, the same mathematical framework is applied for both systems (Giannelo et al. 2016). Guided waves provide fast and cost-effective evaluation of different damage types compared to other approaches of SHM system. GWSHM has several indicators allowing to detect defects in the structure: changes in natural frequencies, in time of flight, in strain, in time domain signal and other characteristics. In order to evaluate POD of SHM system it is necessary to cover all sources of variability. As it was mentioned above, there are two configurations to assess POD—signal response and Hit/Miss. PFA has to be evaluated for SHM system due to high possibility of false calls (De Luca et al. 2020).

Mandache et al. (Mandache et al. 2011) described time-based POD assessment of SHM system. In comparison to NDE, SHM detects time evolution of the defect with respect to baseline signal. Therefore, POD can be defined not as a function of the defect size, but as a function of time it takes until the damage of certain size is firstly detected or a damage growth on pre-defined percentage. This approach was

proposed by Pollock who investigated the probability of detection of growing crack using acoustic emission. The crack of 4mm was growing to 4.05 mm and detected with a probability of 90% within 6 weeks of monitoring. Shorter period of monitoring time gives lower probability in the case of same crack (Mandache et al. 2011). Another approach to estimate POD of SHM system is to transfer POD from NDT to SHM. Firstly, POD assessment for NDT technique is performed. Then using transfer function where all influencing parameters are taken into account the POD is converted to POD curve equivalent to SHM system. One more alternative is to analyse two parallel structures under similar conditions periodically with NDT and continuously with SHM. The relationship of signal responses to damage between two systems is transferred to the POD curves, assuming that POD of NDT is known (Mandache et al. 2011).

Giannelis et al. (Giannelis et al. 2016) investigated Multi Parameter POD approach for guided waves of SHM. This approach implies the combination of Finite Element numerical simulations and experimental data to receive required POD curve. The combination of numerical and experimental data establishes “Measured vs. Modelled” data diagram considering influencing factors and uncertain parameters. As a result, non-linear responses of the GWSHM system is being linearized by the diagram allowing the use of Berens’ statistical model. Then a POD curve is estimated as a function of modelling data. Multi-Dimensional POD implies the analysis of SHM system responses as a function of damage size with the influence of factors and isolate the recorded signals that are sensitive only to a single influencing factor, including damage. After POD curves of damage size for each independent influencing factor are found then POD fusion of these curves can be performed. Therefore, SHM reliability in the presence of combined influencing factors can be determined (Mandache et al. 2011).

5.4.5 Model-Assisted POD for SHM System

Large scale of experiments are required in order to evaluate POD of the system. A number of repetitive tests has to be performed for the same crack size to take in consideration the uncertainty of influencing factors. This approach of POD evaluation is time-consuming and expensive. Thus, Model Assisted POD (MAPOD) was developed as a solution of the problem (Gallina et al. 2013).

Alfredo et al. states that the support of numerical simulations is required for POD assessment. Verification and validation method of the SHM system has to evaluate all aspects which can influence on detection capability, localization and characterization of the defect as well as an effect of environment and exploitation over time. Since sensors of SHM system are fixed at the same position the main difficulty is that the flaw may occur anywhere what will cause the change in response due to distance between sensors and defect. As a result, model for guided waves SHM system POD assessment is proposed and shown in Fig. 5.6 (Güemes et al. 2020).

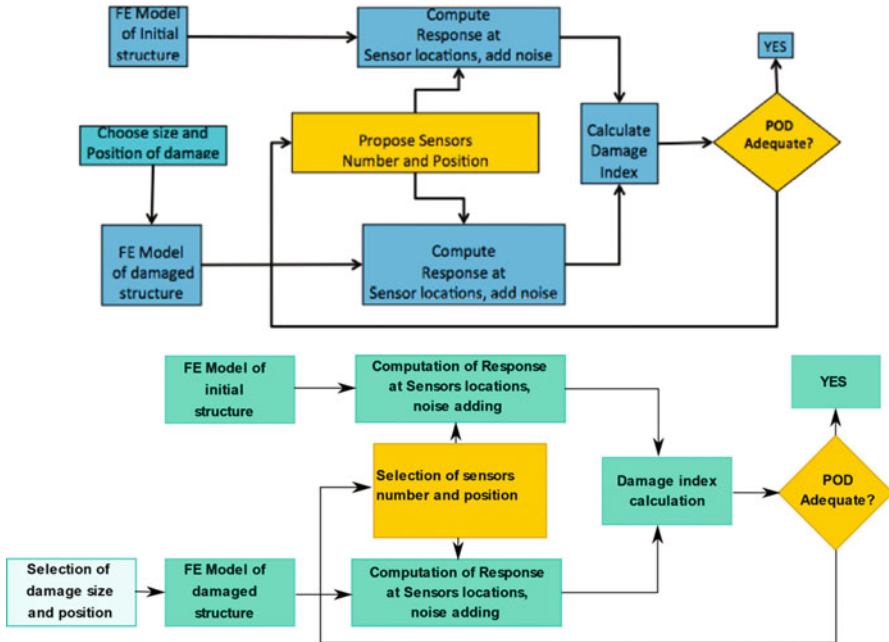


Fig. 5.6 Algorithm used to calculate POD of SHM system (Güemes et al. 2020)

Mainly, there are two MAPOD approaches of high interest: transfer function and full model assisted. Transfer function approach is physics based and used to transfer POD of specific inspection to another with different parameters of inspection. Full model assisted approach is based on the models of uncertainty propagation of specified inspection parameters. Numerical signal of the approach is combined with experimental noise. Nowadays, the use of computer models to evaluate the reliability of SHM system is the most suitable approach. MAPOD reduces experimental inspections of the samples by modelling responses of inspection of the defected material. In the case of effective MAPOD calculations enhance statistical models have to be created. These statistical models characterize system dependency on various influencing factors including defect. Additionally, the polynomial chaos methods reduce the number of samples required for assessment and speed up the MAPOD as well as parallel computing techniques greatly cut down the time of simulations (Gallina et al. 2013; Mandache et al. 2011).

Gallina et al. (Gallina et al. 2013) proposed the MAPOD approach to analyze the Lamb wave SHM system. Propagation signals received by the sensors were collected. Then the effect of dispersion was eliminated by the linear mapping algorithm. All signals were delayed and summed. Location and detection of the damage was performed using imaging technique. Numerical experiments were modelled and empirical white Gaussian noise was added to the recorded signals of sensors for consideration of in-situ factors. The data of simulated experiments was used in statistical analysis for POD curve and PFA evaluation.

Additional example of MAPOD evaluation of SHM systems is described. Cobb et al. (Cobb et al. 2009) proposes hit/miss configuration and model assisted approach for POD estimation of SHM system. Proposed model assisted approach comprises a creation of a series of models:

- Measurement response model which approximates the sensor response;
- Defect propagation model in order to generate sensor responses using a crack growth equation;
- Detection strategy to determine when damage is detected.

After, Hit/Miss analysis of resulting data was performed. Logistics regression was used for modelling binomial response data. POD curve was evaluated and indicates the percentage of all defects of specific size which will be detected (Cobb et al. 2009).

5.5 Guided Wave Applications to SHM of Aerospace Components

The purpose of structural health monitoring is to increase operational safety of aircrafts (Diamanti and Soutis 2010). Ultrasonic guided waves can be exploited for the structural health monitoring of large-scale plate-like aircraft structures (Staszewski et al. 2009). Although there have been investigations for application of the guided waves for metallic and composite aircraft components and structures, guided waves were mostly used up to now for the investigation of the simpler structures, such as pipes (Cawley 2018). In case of most aircraft components, the structures to be inspected have much more complex geometry, including stiffeners and bolt holes, what complicates the propagation of guided waves and thus the inspection. Below, some possible applications of guided waves for the inspection of the most frequently found defect types in the metallic and composite aerospace components as well as adhesive joints are reviewed.

Bae et al. (Bae and Lee 2016) and Choi et al. (Choi et al. 2018) have used serially connected PZT sensor net in combination with laser ultrasonic propagation imaging system for fatigue crack detection in metallic fuselage of Cessna 150 (Bae and Lee 2016). Using finite element modelling Ewald et al. investigated transducer placement for detections of cracks in aluminum aircraft structures using the Lamb wave SHM system (Ewald et al. 2018). Masserey et al. (Masserey and Fromme 2015) have used high frequency 2.25MHz Lamb waves for the monitoring of fatigue crack growth in aluminum specimens. Ihn et al. (Ihn and Chang 2008) have proposed to use an imaging method for quantification of damage in aluminum structures using multiple pitch-catch information. Dalton et al. (Dalton et al. 2001) concluded that guided waves could be used for localized monitoring of metallic airframe structures up to 1 m, however they are not feasible for the monitoring of complete fuselages.

Chang et al. investigated corrosion monitoring using Lamb wave tomography in aluminum plate (Chang et al. 2020). 15 pairs of PZT sensors were used for the excitation and reception of Lamb waves. As A_0 mode is more sensitive to variations in the thickness, it was used for the corrosion monitoring (Chang et al. 2020).

Fakih et al. have used piezoelectric wafers for the excitation of S_0 mode Lamb waves for assessment of flaws in frictions stir welded joints (Fakih et al. 2018). The proposed approach was verified by computed tomography as in the research of Jasiuniene et al. investigating the quality of dissimilar metal joints made by friction stir welding (Jasiūnienė et al. 2017).

Huan et al. suggest using a shear horizontal SH guided wave based SHM system with total focusing method imaging for monitoring of metallic structures (Huan et al. 2019). The suitability of the shear horizontal waves for the defect detection in metallic structures was investigated as well by Petcher et al. (Petcher and Dixon 2015).

The composite materials are used in different aircraft primary structures more and more (Diamanti and Soutis 2010). The most common type of damage is caused by impact, which can cause delaminations, disbonds, matrix cracking, fiber breakage leading to the reduction of structure's life (Diamanti and Soutis 2010).

Impact type of damage was investigated using Lamb waves by different authors: Diamanti et al. have used lamb waves (A_0 mode) for detection and localization of impact damage in composite beams (Diamanti and Soutis 2010); Their investigations have proved that Lamb waves can be used to monitor impact damage evolution in composite laminated structures (Diamanti and Soutis 2010). However, it was concluded, that for application in situ there are still some issues to be solved: durability of bonding layer between the transducer and structure, influence of environmental conditions, etc. (Diamanti and Soutis 2010). Memmolo et al. (2018a, 2018b) have used permanently installed sensors and developed an algorithm using multi-parameter approach to identify hidden flaws due to impact type of damage in composite structure. They have obtained promising results even in the areas with stiffeners and holes (Memmolo et al. 2018a). Katunin et al. have used embedded PZT sensors for detection of barely visible impact damage in GFRP and hybrid Al-GFRP-Al structures (Katunin et al. 2015). They have concluded, that low number of PZT sensors gives only rough image of inspected composite structure and could be used only as initial step of inspection (Katunin et al. 2015). Khodaei et al. (Sharif Khodaei and Aliabadi 2016) have proposed a multi-level approach for barely visible impact damage detection, identification and localization. Their results show that the number and location of the transducers influence the reliability of the detection. Capriotti et al. (2017) have used non-contact air coupled transducers for the generation of guided waves and detection of impact damage (causing cracked skin/stringer and disbonded stringer) in composite aircraft panels.

Lamb waves can also be used for finding of delamination type of defects in composites: Ramadas et al. (Ramzi et al. 2015) have studied the interaction of guided Lamb waves with an asymmetrically located delamination in laminated composite plate. Staszewski et al. (2009) used Lamb waves to detect delamination in the composite plate. One piezo ceramic actuator was used for Lamb wave generation,

and 3D laser vibrometer for reception (Staszewski et al. 2009). Ihn et al. (Ihn and Chang 2008) have used diagnostic imaging method using multiple pitch-catch pairs to quantify the delamination type damage in stiffened composite panels. Qiu et al. (2013) have used PZTs bonded to the structure with advanced two step signal processing for the localization of damage in composite wing panels with stiffeners and bolt holes. Kazys et al. (Kažys et al. 2006; Kazys et al. 2006) have detected delamination and impact type defects using air-coupled excitation of Lamb waves in aerospace honeycomb structures. A study on delamination size and depth extraction on composite plate using A_0 mode was presented by Samaitis et al. (2020, Tiwari et al. (2017).

Panda et al. for excitation and receiving of Lamb waves in composite aileron used air-coupled transducers in pitch catch mode (Panda et al. 2016) and have determined, that fundamental A_0 mode was effective for disbond detection (Panda et al. 2016). In another experiment by Panda et al. (2018) again air coupled transducers were used in pitch-catch configuration for generation and reception of A_0 Lamb wave mode in composite panel with stiffeners for disbond detection. Memmolo et al. (2018c) and Monaco et al. (2016) have investigated the possibilities to detect disbond of stringers in stiffened composites typically used for wing boxes using scattered guided waves and tomographic approach.

Adhesively bonded joints are attractive in aircraft structures as alternative to rivets. However, the degradation of the quality of adhesive joints is still an issue. Yilmaz et al. (Yilmaz and Jasiūnienė 2020) have suggested the techniques for detection of weak composite-adhesive joints using advanced NDT. Castaings (2014) have used the SH guided waves for the evaluation of the adhesion in adhesively bonded aluminum lap joints.

Especially challenging for the inspection are adhesive hybrid metal to composite joints. Advanced ultrasonic testing with novel signal post processing technique was suggested by Jasiūnienė et al. (2019) for detection of defect in the complex joints. Puthillath et al. (Puthillath and Rose 2010) have used ultrasonic guided wave modes with large in-plane displacement at the interface for the inspection of adhesively bonded aircraft repair patch (titanium repair patch bonded to an aluminum aircraft skin). Ren et al. (Ren and Lissenden 2013) also have used ultrasonic guided wave mode with large in-plane displacement at interface for the inspection of adhesive bonds between composite laminates.

Even though there has been a lot of different research of possible SHM application for different aircraft structures in the laboratory conditions, there haven't been a lot applications on real aircrafts due to several unsolved issues (Cawley 2018; Qing et al. 2019) like sensitivity of the SHM systems to environmental changes (Kralovec and Schagerl 2020; Gorgin et al. 2020; Abbas et al. 2020; Fang et al. 2019; Nokhbatolfoghahai et al. 2021), leading to reduced reliability (Memmolo et al. 2018a; Fang et al. 2019) and thus probability of the detection (Meeker et al. 2019; Wu et al. 2015), legal issues and other. Quantification of the extent of the damage as well remains a challenge (Ihn and Chang 2008). Another issue, which still haven't got enough attention is the huge amount of data to be analyzed (Qing et al. 2019). Effect of damaged/inoperative sensors also should be solved introducing self

diagnostic approach (Memmolo et al. 2018a; Qing et al. 2019). On the other hand, weight of the SHM system should be also not forgotten (Memmolo et al. 2018a)—additional weight introduced due to SHM system should be as low as possible.

5.6 Summary

The production of the modern aircraft clearly seeks faster, cheaper production, increased automation, reduced weight and fuel consumption. Modern aircraft manufacturing technologies use resin transfer molding (RTM), high pressure HP-RTM, thermoplastic composites, hybrid metal-composite structures and 3D printed parts (Composites World 2019). For example, HP-RTM are already implemented in some parts of an aircraft, allowing to achieve approx. 30% cost reduction and increase of the production efficiency by 10–20% (Composites World 2019). Thermoplastic composite technology will reduce the amount of assembly steps, eliminate some rivets and fasteners, resulting in reduced overall manufacturing cost. AM technologies, like the ones used in GE9X engine, allow to reduce weight of the engine and to combine multiple parts into single one overcoming the shape restrictions that come from conventional methods such as stamping and casting (Kellner 2020; Bachmann et al. 2017). Boeing is in production of 777X aircraft and in the design stage of New Midsize Aircraft (NMA or 797). Airbus is aiming to replace its most successful single aisle jet A320 with a new A321XLR. New and modern jet's will increasingly use advanced manufacturing technologies, like the ones mentioned above. As these drastically change the design process, the NDT technologies will have to adapt. New knowledge of guided wave interaction with thermoplastic composite joints (Ochôa et al. 2019; Ochôa et al. 2018), HP-RTM components, detection of porosity or lack of fusion between layers of AM parts (Honarvar and Varvani-Farahani 2020) will be a key factor determining the inspection quality. The new NDT technologies will be required to overcome current limitations and provide full characterization of the damage including size, location and depth. This is crucial for successful damage progression models, which are responsible for remaining life predictions of the structure. For example, it has been reported that the depth of delamination is directly related to the damage progression mechanisms (Canturri et al. 2013; Elliott Cramer 2018), so it has to be fully defined by the monitoring system. Different manufacturing processes and novel materials will require different characterization data and assessment of all defects that are present in the structure. The defects of different kinds will have to be described differently depending on their nature and progression mechanisms. Hence, the SHM system will have to be versatile and adaptive enough. Both in-service and production line inspection technologies will become crucial as they will determine the manufacturing rates and safety of new structural designs, while guided waves demonstrate a serious potential to become one of the key SHM technologies of the future aircraft.

References

- Abbas M, Shafiee M (2018) Structural health monitoring (SHM) and determination of surface defects in large metallic structures using ultrasonic guided waves. *Sensors* 18:3958
- Abbas S et al (2020) Experimental investigation of impact of environmental temperature and optimal baseline for thermal attenuation in structural health monitoring based on ultrasonic guided waves. *Wave Mot* 93:102474
- Aldrin JC, Knopp JS, Sabbagh HA (2013) Bayesian methods in probability of detection estimation and model-assisted probability of detection evaluation. *AIP Conf Proc* 1511(1):1733–1740
- Aldrin JC, et al. (2016) Best practices for evaluating the capability of nondestructive evaluation (NDE) and structural health monitoring (SHM) techniques for damage characterization. Available from <<https://ui.adsabs.harvard.edu/abs/2016AIPC.1706f0002A>>. ISBN 0094-243X
- Alokita S et al (2019) Structural health monitoring of biocomposites, fibre-reinforced composites and hybrid composites. In: Jawaid, Mohammad; Thariq, Mohamed and Saba, Naheed (eds) 4 – Recent advances and trends in structural health monitoring, Woodhead Publishing, Cambridge, pp 53-73. Available from <<http://www.sciencedirect.com/science/article/pii/B9780081022917000046>>. Isbn 9780081022917
- Alonso L, et al. (2018) Middleware and communication technologies for structural health monitoring of critical infrastructures: A survey. *Comp Stand Interfaces* 56:83-100.
- Bachmann J, Hidalgo C, Bricout S (2017) Environmental analysis of innovative sustainable composites with potential use in aviation sector—a life cycle assessment review. *Sci China Technol Sci* 60:1301–1317
- Bae DY, Lee JR (2016) A health management technology for multisite cracks in an in-service aircraft fuselage based on multi-time-frame laser ultrasonic energy mapping and serially connected PZTs. *Aerospace Sci Technol* 54:114–121. <https://doi.org/10.1016/j.ast.2016.04.014>
- Barski M, Stawiarski A (2018) The crack detection and evaluation by elastic wave propagation in open hole structures for aerospace application. Available from <<http://www.sciencedirect.com/science/article/pii/S1270963818302190>>. ISBN 1270-9638
- Belanger P, Cawley P (2009) Feasibility of low frequency straight-ray guided wave tomography. Available from <<http://www.sciencedirect.com/science/article/pii/S0963869508001205>>. ISBN 0963-8695
- Belanger P, Cawley P, Simonetti F (2010) Guided wave diffraction tomography within the born approximation. ISBN 1525-8955
- Bellan F, et al. (2005) A new design and manufacturing process for embedded lamb waves interdigital transducers based on piezopolymer film. Available from <<http://www.sciencedirect.com/science/article/pii/S0924424705003468>>. ISBN 0924-4247
- Benmeddour F et al (2009) Experimental study of the A0 and S0 lamb waves interaction with symmetrical notches. Available from <<http://www.sciencedirect.com/science/article/pii/S0041624X08001480>>. ISBN 0041-624X
- Birt EA (1998) Damage detection in carbon-fibre composites using ultrasonic Lamb waves. *Insight* 40(5):335
- Caminero MA et al (2013) Analysis of adhesively bonded repairs in composites: damage detection and prognosis. *Compos Struct* 95:500–517
- Canturri C et al (2013) Delamination growth directionality and the subsequent migration processes – the key to damage tolerant design. *Compos Part A Appl Sci Manufact* 54:79–87
- Capriotti M et al (2017) Non-destructive inspection of impact damage in composite aircraft panels by ultrasonic guided waves and statistical processing. *Materials* 10(6):616
- Castangs M (2014) SH ultrasonic guided waves for the evaluation of interfacial adhesion. *Ultrasonics* 54(7):1760–1775
- Cawley P (2007) Practical guided wave inspection and applications to structural health monitoring. In: Proceedings of the 5th australasian congress on applied mechanics (ACAM 2007), Brisbane, Australia. ISBN 0858-258625

- Cawley P (2018) Structural health monitoring: closing the gap between research and industrial deployment. *Struct Health Monit* 17(5):1225–1244. <https://doi.org/10.1177/1475921717750047>
- Chang M, Yuan S, Guo F (2020) Corrosion monitoring using a new compressed sensing-based tomographic method. *Ultrasonics* 101:105988. <https://doi.org/10.1016/j.ultras.2019.105988>
- Chapuis B, Calmon P, Jenson F (2018a) Best practices for the use of simulation in POD curves estimation: application to UT weld inspection. In: Chapuis B, Calmon P, Jenson F (eds) *Basics of statistics for POD*. Springer International Publishing, Cham, pp 25–32. https://doi.org/10.1007/978-3-319-62659-8_8. isbn:978-3-319-62659-8
- Chapuis B, Calmon P, Jenson F (2018b) Best practices for the use of simulation in POD curves estimation. Springer International Publishing, Cham. isbn:978-3-319-62658-1
- Chen J, Yuan S, Jin X (2019) On-line prognosis of fatigue cracking via a regularized particle filter and guided wave monitoring. Available from <<http://www.sciencedirect.com/science/article/pii/S0888327019303309>>. ISBN 0888-3270
- Choi Y, Abbas SHL, Jung R (2018) Aircraft integrated structural health monitoring using lasers, piezoelectricity, and fiber optics. *Meas J Int Meas Conf* 125:294–302. <https://doi.org/10.1016/j.measurement.2018.04.067>
- Clarke T, Simonetti F, Cawley P (2010) Guided wave health monitoring of complex structures by sparse Array systems: influence of temperature changes on performance. *J Sound Vib* 329(12):2306–2322
- Cobb A, Michaels J, Michaels T (2009) *Ultrasonic structural health monitoring: a probability of detection case study*, vol 1096
- Composites World (2019) Next-gen aerospace: advanced materials and processes. Available from <<https://gbmsupplements.mydigitalpublication.com/publication/?i=587161&p=&pn=>>
- Croxford AJ et al (2007) Strategies for guided-wave structural health monitoring. *Proc R Soc Lond A Math Phys Eng Sci* 463(2087):2961–2981
- Croxford AJ et al (2010) Efficient temperature compensation strategies for guided wave structural health monitoring. *Ultrasonics* 50(4–5):517–528
- Dai D, He Q (2014) Structure damage localization with ultrasonic guided waves based on a time-frequency method. *Sig Process* 96:21–28
- Dalton RP, Cawley P, Lowe MJS (2001) The potential of guided waves for monitoring large areas of metallic aircraft fuselage structure. *J Nondestruct Eval* 20(1):29–46. <https://doi.org/10.1023/A:1010601829968>
- Datteo A et al (2018) On the use of AR models for SHM: a global sensitivity and uncertainty analysis framework. *Reliab Eng Syst Saf* 170:99–115
- De Luca A et al (2020) Guided wave SHM system for damage detection in complex composite structure. *Theor Appl Fract Mec* 105:102408
- De Marchi L, Perelli A, Marzani A (2013) A signal processing approach to exploit chirp excitation in lamb wave defect detection and localization procedures. Available from <<http://www.sciencedirect.com/science/article/pii/S0888327012003913>>. ISBN 0888-3270
- Department of Defense (2009) *Nondestructive evaluation system reliability assessment*. Department of Defense, United States of America
- Diamanti K, Soutis C (2010) Structural health monitoring techniques for aircraft composite structures. Available from <https://ac.els-cdn.com/S0376042110000369/1-s2.0-S0376042110000369-main.pdf?_tid=5b5f4ba4-51f1-4802-a081-b6bcf08f71ee&acdnat=1521634767_e5a756eb7a134a9013ab38b619702f>. ISBN 0376-0421
- Djili S, et al. (2013) Notch detection in copper tubes immersed in water by leaky compressional guided waves. Available from <<http://www.sciencedirect.com/science/article/pii/S0963869512001417>>. ISBN 0963-8695
- Duong NT, et al. (2015) Relation between the ultrasonic attenuation and the porosity of a RTM composite plate. Available from <<http://www.sciencedirect.com/science/article/pii/S1875389215007567>>. ISBN 1875-3892

- Ecke W (2000) Optical fibre grating strain sensor network for x-38 spacecraft health monitoring. Available from <https://doi.org/10.1117/12.2302163>
- Elliott Cramer K (2018) Current and future needs and research for composite materials NDE. Available from doi:<https://doi.org/10.1117/12.2291921>
- Etebu E, Shafiee M (2018) Reliability analysis of structural health monitoring systems, pp 2243–2247. ISBN 9781351174664
- Ewald V, Groves R, Benedictus R (2018) Transducer placement option of Lamb wave SHM system for hotspot damage monitoring. *Aerospace* 5(2):39
- Fakih MA et al (2018) Detection and assessment of flaws in friction stir welded joints using ultrasonic guided waves: experimental and finite element analysis. *Mech Syst Sig Proces* 101:516–534. <https://doi.org/10.1016/j.ymsp.2017.09.003>
- Fan Z et al. (2013) Feature-guided waves for monitoring adhesive shear modulus in bonded stiffeners. Available from <http://www.sciencedirect.com/science/article/pii/S0963869512001673>. ISBN 0963-8695
- Fang F et al (2019) Dynamic probability modeling-based aircraft structural health monitoring framework under time-varying conditions: validation in an in-flight test simulated on ground. *Aerospace Sci Technol* 95:105467
- Fendzi C et al (2016) A data-driven temperature compensation approach for structural health monitoring using Lamb waves. *Struct Health Monit* 15(5):525–540. <https://doi.org/10.1177/1475921716650997>
- Feng B, Ribeiro AL, Ramos HG (2018) Interaction of lamb waves with the edges of a delamination in CFRP composites and a reference-free localization method for delamination. Available from <http://www.sciencedirect.com/science/article/pii/S0263224117306425>. ISBN 0263-2241
- Fisher J, Michaels J (2009) Model-assisted probability of detection for ultrasonic structural health monitoring. In: 4th European American workshop on reliability of NDE, 2009
- Fromme P et al (2006) On the development and testing of a guided ultrasonic wave array for structural integrity monitoring. *IEEE Trans Ultrason Ferroelectr Freq Control* 53(4):777–785
- Fromme P, Reymondin J-P, Masserey B (2017) High frequency guided waves for disbond detection in multi-layered structures. *Acta Acustica United Acustica* 103:932–940
- Gallina A, Pačko P, Ambroziński Ł (2013) Model assisted probability of detection in structural health monitoring.. Available from <https://doi.org/10.1002/9781118536148.ch3>. ISBN 9781-118536148
- Gangadharan R et al (2009) Time reversal technique for health monitoring of metallic structure using Lamb waves. *Ultrasonics* 49(8):696–705
- Gianneo A, Carboni M, Giglio M (2016) Reliability aspects and multi-parameter POD formulation for guided wave based SHM techniques
- Giridhara G et al (2010) Rapid localization of damage using a circular sensor array and Lamb wave based triangulation. *Mech Syst Signal Process* 24(8):2929–2946
- Giurgiutiu V (2005) Tuned lamb wave excitation and detection with piezoelectric wafer active sensors for structural health monitoring. *J Intell Mater Syst Struct* 16(4):291–305
- Giurgiutiu V (2011) Structural damage detection with piezoelectric wafer active sensors. *J Phys Conf Ser* 305(1):012123
- Giurgiutiu V (2015) 16 – Structural health monitoring (SHM) of aerospace composites. In: Irving PE, Soutis C (eds) Woodhead Publishing. Available from <http://www.sciencedirect.com/science/article/pii/B9780857095237000165>. ISBN 9780-857095237
- Giurgiutiu V, Bao JJ (2004) Embedded-ultrasonics structural radar for in situ structural health monitoring of thin-wall structures. *Struct Health Monit* 3(2):121–140
- Giurgiutiu V, Zagrai AB, Jingjing B (2004) Damage identification in aging aircraft structures with piezoelectric wafer active sensors. *J Intell Mater Syst Struct* 15(9–10):673–687
- Glushkov EV et al (2010) Selective lamb mode excitation by piezoelectric coaxial ring actuators. *Smart Mater Struct* 19(3):035018

- Gorgin R, Luo Y, Wu Z (2020) Environmental and operational conditions effects on Lamb wave based structural health monitoring systems: a review. *Ultrasonics* 105:106114. <https://doi.org/10.1016/j.ultras.2020.106114>
- Grondel S et al (2002) Design of optimal configuration for generating A0 Lamb mode in a composite plate using Piezoceramic transducers. *J Acoust Soc Am* 112(1):84
- Güemes A, et al. (2020) Structural health monitoring for advanced composite structures: a review. ISBN 2504-477X
- Hauffe A, Hähnel F, Wolf K (2020) Comparison of algorithms to quantify the damaged area in CFRP ultrasonic scans. Available from <<http://www.sciencedirect.com/science/article/pii/S0263822319336153>>. ISBN 0263-8223
- Hellier C (2012) Handbook of nondestructive evaluation, 2nd edn. McGraw-Hill Professional, New York
- Herdovics B, Cegla F (2019) Compensation of phase response changes in ultrasonic transducers caused by temperature variations. *Struct Health Monit* 18(2):508–523. <https://doi.org/10.1177/1475921718759272>
- Higgins A (2000) Adhesive bonding of aircraft structures. *Int J Adhes Adhes* 20(5):367–376
- Honarvar F, Varvani-Farahani A (2020) A review of ultrasonic testing applications in additive manufacturing: defect evaluation, material characterization, and process control. *Ultrasonics* 108:106227
- Hsu, D. K. (2013) 15 – Non-destructive evaluation (NDE) of aerospace composites: ultrasonic techniques. In: Karbhari, Vistasp M (ed) Non-destructive evaluation (NDE) of polymer matrix composites. Woodhead Publishing, Cambridge. Available from <<http://www.sciencedirect.com/science/article/pii/B9780857093448500154>>. ISBN 9780-857093448
- Hu N, et al. (2008) Identification of delamination position in cross-ply laminated composite beams using S0 Lamb mode. Available from <<http://www.sciencedirect.com/science/article/pii/S0266353807004113>>. ISBN 0266-3538
- Huan Q et al (2019) A high-resolution structural health monitoring system based on SH wave piezoelectric transducers phased array. *Ultrasonics* 97:29–37
- Ihn J-B, Chang F-K (2008) Pitch-catch active sensing methods in structural health monitoring for aircraft structures. *Struct Health Monit* 7(1):5–19. <https://doi.org/10.1177/1475921707081979>
- Ito J, et al. (2015) Ultrasonic wave propagation in the corner section of composite laminate structure: numerical simulations and experiments. Available from <<http://www.sciencedirect.com/science/article/pii/S0263822314006825>>. ISBN 0263-8223
- Jasiūnienė E et al (2017) Investigation of dissimilar metal joints with nanoparticle fillers. *NDT E Int* 92:122–129
- Jasiūnienė E et al (2019) Ultrasonic non-destructive testing of complex titanium/carbon fibre composite joints. *Ultrasonics* 95:13–21
- Jayaraman C, Chitti Venkata K, Balasubramaniam K (2009) Higher order modes cluster (Homc) guided waves-a new technique for ndt inspection. In: AIP conference proceedings, vol 1096
- Jin J, Quek ST, Wang Q (2005) Design of interdigital transducers for crack detection in plates. *Ultrasonics* 43(6):481–493
- Jurek M, et al. (2018) Non-contact excitation and focusing of guided waves in CFRP composite plate by air-coupled transducers for application in damage detection. Available from <<http://www.sciencedirect.com/science/article/pii/S2452321618304384>>. ISBN 2452-3216
- Kabban S, Christine M et al (2015) The probability of detection for structural health monitoring systems: repeated measures data. *Struct Health Monitor* 14(3):252–264
- Katunin A, Dragan K, Dziendzikowski M (2015) Damage identification in aircraft composite structures: a case study using various non-destructive testing techniques. *Compos Struct* 127:1–9. <https://doi.org/10.1016/j.compstruct.2015.02.080>
- Każyński R et al (2006) Air-coupled ultrasonic investigation of multi-layered composite materials. *Ultrasonics* 44:e819–e822

- Kazys R, et al. (2006) Ultrasonic air-coupled non-destructive testing of aerospace components. pp 1–8. Available from <<https://www.ndt.net/article/ecndt2006/doc/We.1.1.5.pdf>>
- Kazys JR, Slieteris R, Sestoke J (2017) Air-coupled ultrasonic receivers with high electromechanical coupling PMN-32%PT strip-like piezoelectric elements. *Sensors* 17(10):2365
- Kellner T (2020) The next generation: a team of young engineers helped bring 3D printing inside the World's largest jet engine. Available from <<https://www.ge.com/news/reports/the-next-generation-this-team-of-young-engineers-helped-bring-3d-printing-inside-the-worlds-largest-jet-engine>>
- Khalili P, Cawley P (2018) The choice of ultrasonic inspection method for the detection of corrosion at inaccessible locations. *NDT & E Int* 99:80–92
- Kijanka P, Staszewski WJ, Packo P (2018) Generalised semi-analytical method for excitability curves calculation and numerical modal amplitude analysis for lamb waves. *Struct Contr Health Monit* 25(7):e2172
- Kim K-B, Hsu DK, Barnard DJ (2013) Estimation of porosity content of composite materials by applying discrete wavelet transform to ultrasonic backscattered signal. Available from <<http://www.sciencedirect.com/science/article/pii/S0963869513000212>>. ISBN 0963-8695
- Konstantinidis G, Wilcox PD, Drinkwater BW (2007) An investigation into the temperature stability of a guided wave structural health monitoring system using permanently attached sensors. *IEEE Sens J* 7(5):905–912
- Kralovec C, Schagerl M (2020) Review of structural health monitoring methods regarding a multi-sensor approach for damage assessment of metal and composite structures. ISBN 1424-8220
- Kudela P, Ostachowicz W, Żak A (2008) Damage detection in composite plates with embedded PZT transducers. *Mech Syst Signal Process* 22(6):1327–1335
- Lamb H (1917) On waves in an elastic plate. *Proc R Soc Lond Ser A Containing Papers Math Phys Character* 93(648):114–128
- Lee TH, Choi IH, Jhang KY (2008) Single-mode guided wave technique using ring-arrayed laser beam for thin-tube inspection. Available from <<http://www.sciencedirect.com/science/article/pii/S0963869508000340>>. ISBN 0963-8695
- Li S, et al. (2016) Leak detection and location in gas pipelines by extraction of cross spectrum of single non-dispersive guided wave modes. Available from <<http://www.sciencedirect.com/science/article/pii/S0950423016302650>>. ISBN 0950-4230
- Li L et al (2019) Sensor fault detection with generalized likelihood ratio and correlation coefficient for bridge SHM. *J Sound Vib* 442:445–458
- Lin L et al (2011) A novel random void model and its application in predicting void content of composites based on ultrasonic attenuation coefficient. *Appl Phys A* 103(4):1153–1157
- Long R, Lowe M, Cawley P (2003) Attenuation characteristics of the fundamental modes that propagate in buried iron water pipes. *Ultrasonics* 41(7):509–519
- Luo Z et al (2016) A reshaped excitation regenerating and mapping method for waveform correction in lamb waves dispersion compensation. *Smart Mater Struct* 26(2):025016
- Majumder M, et al. (2008) Fibre bragg gratings in structural health monitoring—present status and applications. Available from <<http://www.sciencedirect.com/science/article/pii/S0924424708002380>>. ISBN 0924-4247
- Mandache C, et al. (2011) Considerations on structural health monitoring reliability. [cited 5 Aug 2020]
- Mardanshahi A et al (2020) Detection and classification of matrix cracking in laminated composites using guided wave propagation and artificial neural networks. Available from <<http://www.sciencedirect.com/science/article/pii/S0263822319345684>>. ISBN 0263-8223
- Mariani S, Heinlein S, Cawley P (2020) Compensation for temperature-dependent phase and velocity of guided wave signals in baseline subtraction for structural health monitoring. *Struct Health Monit* 19(1):26–47. <https://doi.org/10.1177/1475921719835155>
- Masserey B, Fromme P (2015) In-situ monitoring of fatigue crack growth using high frequency guided waves. *NDT & E Int* 71:1–7

- Masserey B, Raemy C, Fromme P (2014) High-frequency guided ultrasonic waves for hidden defect detection in multi-layered aircraft structures. *Ultrasonics* 54(7):1720–1728
- Mazzotti M, Marzani A, Bartoli I (2014) Dispersion analysis of leaky guided waves in fluid-loaded waveguides of generic shape. Available from <<http://www.sciencedirect.com/science/article/pii/S0041624X13001832>>. ISBN 0041-624X
- Meeker W, Roach D, Kessler S (2019) Statistical methods for probability of detection in structural health monitoring.
- Melnykowycz M et al (2006) Performance of integrated active fiber composites in fiber reinforced epoxy laminates. *Smart Mater Struct* 15(1):204–212
- Memmo V, et al. (2018a) Damage localization in composite structures using a guided waves based multi-parameter approach. ISBN 2226-4310
- Memmo V, Pasquino N, Ricci F (2018b) Experimental characterization of a damage detection and localization system for composite structures. *Measurement* 129:381–388
- Memmo V et al (2018c) Guided wave propagation and scattering for structural health monitoring of stiffened composites. *Compos Struct* 184:568–580
- Michaels JE (2008) Detection, localization and characterization of damage in plates with an array of spatially distributed ultrasonic sensors. *Smart Mater Struct* 17(3):035035. <https://doi.org/10.1088/0964-1726/17/3/035035>
- Michaels JE 2016 Structural health monitoring (SHM) in aerospace structures. In: Yuan F-G (ed) 9 – Sparse array imaging with guided waves under variable environmental conditions, Woodhead Publishing, pp. 255-284. Available from <<http://www.sciencedirect.com/science/article/pii/B978008100148600093>>. ISBN 9780081001486
- Michaels JE, Michaels TE (2006) Enhanced differential methods for guided wave phased array imaging using spatially distributed piezoelectric transducers. *AIP Conf Proc* 820(1):837–844
- Michaels JE, Michaels TE (2007) Guided wave signal processing and image fusion for in situ damage localization in plates. *Wave Motion* 44(6):482–492
- Mitra M, Gopalakrishnan S (2016) Guided wave based structural health monitoring: a review. *Smart Mater Struct* 25(5):053001
- Monaco E, et al. (2016) Methodologies for guided wave-based SHM system implementation on composite wing panels: results and perspectives from SARISTU Scenario, vol 5. pp 495-528. ISBN 978-3-319-22412-1
- Monkhouse RSC et al (2000) The rapid monitoring of structures using interdigital lamb wave transducers. *Smart Mater Struct* 9(3):304
- Munian RK, Roy Mahapatra D, Gopalakrishnan S (2020) Ultrasonic guided wave scattering due to delamination in curved composite structures. Available from <<http://www.sciencedirect.com/science/article/pii/S0263822319339169>>. ISBN 0263-8223
- Mustapha S, Ye L (2014) Leaky and non-leaky behaviours of guided waves in CF/EP Sandwich structures. *Wave Motion* 51(6):905–918
- Mustapha S, Ye L (2015) Propagation behaviour of guided waves in tapered sandwich structures and debonding identification using time reversal. *Wave Motion* 57:154–170
- Nazeer N, Ratassepp M, Fan Z (2017) Damage detection in bent plates using shear horizontal guided waves. *Ultrasonics* 75:155–163
- Nokhbatolfighahai A, Navazi HM, Groves RM (2021) Evaluation of the sparse reconstruction and the delay-and-sum damage imaging methods for structural health monitoring under different environmental and operational conditions. *Measurement* 169:108495
- Ochôa P et al (2018) Experimental assessment of the influence of welding process parameters on Lamb wave transmission across ultrasonically welded thermoplastic composite joints. *Mech Syst Sig Process* 99:197–218
- Ochôa P et al. (2019) Diagnostic of manufacturing defects in ultrasonically welded thermoplastic composite joints using ultrasonic guided waves. Available from <<http://www.sciencedirect.com/science/article/pii/S0963869518306017>>. ISBN 0963-8695

- Packo P et al (2016) Amplitude-dependent lamb wave dispersion in nonlinear plates. *J Acoust Soc Am* 140(2):1319–1331
- Pain D, Drinkwater BW (2013) Detection of fibre waviness using ultrasonic array scattering data. *J Nondestruct Eval* 32(3):215–227
- Panda RS, Rajagopal P, Balasubramaniam K (2016) Rapid ultrasonic inspection of stiffened composite ailerons. Available from <<http://www.ultrargroup.com/>>
- Panda RS, Rajagopal P, Balasubramaniam K (2018) Rapid guided wave inspection of complex stiffened composite structural components using non-contact air-coupled ultrasound. Available from <<http://www.sciencedirect.com/science/article/pii/S0263822318321305>>. ISBN 0263-8223
- Papantoniou A, Rigas GA, Nikolaos D (2011) Assessment of the Strain Monitoring Reliability of Fiber Bragg Grating Sensor (FBGs) in advanced composite structures. *Compos Struct* 93(9):2163–2172
- Park HW, Kim SB, Sohn H (2009) Understanding a time reversal process in Lamb wave propagation. *Wave Motion* 46(7):451–467
- Park J, et al. (2020) High-precision noncontact guided wave tomographic imaging of plate structures using a DHB algorithm. ISBN 2076-3417
- Pelivanov, Ivan, et al. (2014) NDT of fiber-reinforced composites with a new fiber-optic pump-probe laser-ultrasound system. Available from <<http://www.sciencedirect.com/science/article/pii/S2213597914000056>>. ISBN 2213-5979
- Petcher PA, Dixon S (2015) Weld defect detection using PPM EMAT generated shear horizontal ultrasound. *NDT E Int* 74:58–65. <https://doi.org/10.1016/j.ndteint.2015.05.005>
- Podymova NB, et al. (2019) Laser-ultrasonic nondestructive evaluation of porosity in particulate reinforced metal-matrix composites. Available from <<http://www.sciencedirect.com/science/article/pii/S0041624X19302707>>. ISBN 0041-624X
- Purekar AS et al (2004) Directional piezoelectric phased Array filters for detecting damage in isotropic plates. *Smart Mater Struct* 13(4):838
- Puthillath P, Rose JL (2010) Ultrasonic guided wave inspection of a titanium repair patch bonded to an aluminum aircraft skin. *Int J Adhes Adhes* 30(7):566–573
- Qing X, et al. (2019) Piezoelectric transducer-based structural health monitoring for aircraft applications. ISBN 1424-8220
- Qiu L et al (2013) A quantitative multidamage monitoring method for large-scale complex composite. *Struct Health Monit* 12(3):183–196. <https://doi.org/10.1177/1475921713479643>
- Raišutis R et al. (2010) Application of ultrasonic guided waves for non-destructive testing of defective CFRP rods with multiple delaminations. Available from <<http://www.sciencedirect.com/science/article/pii/S0963869510000393>>. ISBN 0963-8695
- Rajic N, Tsoi KA, Rosalie C (2011) Issues on the durability of piezoceramic transducers for in situ SHM using acousto ultrasonics. [cited 5 Aug 2020]
- Ramadas C et al (2009) Interaction of the primary anti-symmetric Lamb mode (Ao) with symmetric delaminations: numerical and experimental studies. *Smart Mater Struct* 18(8):085011
- Ramadas C et al (2010) Interaction of guided Lamb waves with an asymmetrically located delamination in a laminated composite plate. *Smart Mater Struct* 19(6):065009
- Ramzi AR, Mahmud MF, Elmi AB (2015) Immersion ultrasonic inspection system for small scaled composite specimen. *J Eng Appl Sci* 10:17146–17150
- Ren B, Lissenden CJ (2013) Ultrasonic guided wave inspection of adhesive bonds between composite laminates. *Int J Adhes Adhes* 45:59–68
- Rheinfurth, M., et al. (2011) Air-coupled guided waves combined with thermography for monitoring fatigue in biaxially loaded composite tubes. Available from <<http://www.sciencedirect.com/science/article/pii/S026635381000480X>>. ISBN 0266-3538
- Rocha B et al (2013) New trends in structural health monitoring. In: Ostachowicz W, Güemes JA (eds) *Structural health monitoring of aircraft structures*, Vienna, Springer Vienna, pp 81–148. https://doi.org/10.1007/978-3-7091-1390-5_2. isbn:978-3-7091-1390-5

- Römmeler A, et al. (2020) Air coupled ultrasonic inspection with lamb waves in plates showing mode conversion. Available from <<http://www.sciencedirect.com/science/article/pii/S0041624X19303816>>. ISBN 0041-624X
- Rose JL (2002) A baseline and vision of ultrasonic guided wave inspection potential. *J Pressure Vessel Technol* 124(3):273–282
- Rose JL (2004) *Ultrasonic waves in solid media*. Cambridge University Press. ISBN 978-0521548892
- Rose JL (2014) *Ultrasonic guided waves in solid media*. Cambridge University Press. Available from <https://doi.org/10.1017/CBO9781107273610>. ISBN 9781107273610
- Salas KI, Cesnik CES (2009) Guided wave excitation by a CLoVER transducer for structural health monitoring: theory and experiments. *Smart Mater Struct* 18(7):075005
- Samaitis V, Mažeika L (2017) Influence of the spatial dimensions of ultrasonic transducers on the frequency spectrum of guided waves. ISBN 1424-8220
- Samaitis V, Mažeika L, Rekuviėnė R (2020) Assessment of the length and depth of delamination-type defects using ultrasonic guided waves. ISBN 2076-3417
- Schaal C et al (2017) An analytical study of the scattering of ultrasonic guided waves at a delamination-like discontinuity in a plate. *Proc Inst Mech Eng C J Mech Eng Sci* 231(16):2947–2960
- Schoefs F, Abraham O, Popovics JS (2012) Quantitative evaluation of contactless impact echo for non-destructive assessment of void detection within tendon ducts. *Constr Build Mater* 37:885–892
- Senyurek VY (2015) Detection of cuts and impact damage at the aircraft wing slat by using Lamb wave method. *Measurement* 67:10–23
- Seung BK, Hoon S (2007) Instantaneous reference-free crack detection based on polarization characteristics of piezoelectric materials. *Smart Mater Struct* 16(6):2375
- Sharif Khodaei Z, Aliabadi M (2016) A multi-level decision fusion strategy for condition based maintenance of composite structures. *Materials* 9(9):790
- Shkerdin G, Glorieux C (2004) Lamb mode conversion in a plate with a delamination. *J Acoust Soc Am* 116(4):2089–2100
- Sohn H et al (2007) Combination of a time reversal process and a consecutive outlier analysis for baseline-free damage diagnosis. *J Intell Mater Syst Struct* 18(4):335–346
- Sol T et al. (2018) Nondestructive ultrasonic evaluation of additively manufactured. AlSi10Mg samples. Available from <<http://www.sciencedirect.com/science/article/pii/S2214860418300484>>. ISBN 2214-8604
- Solie LP, Auld BA (1973) Elastic waves in free anisotropic plates. *J Acoust Soc Am* 54(1):50–65
- Staszewski WJ, Mahzan S, Traynor R (2009) Health monitoring of aerospace composite structures – active and passive approach. *Compos Sci Technol* 69(11–12):1678–1685
- Stolz C, Meisner C (2020) Challenges for SHM reliability and application in aerospace industry. Available from:<<https://www.sto.nato.int/publications/STO%20Meeting%20Proceedings/STO-MP-AVT-305/SMP-AVT-305-KN2.pdf>>
- Su Z, Ye LLY (2006) Guided Lamb waves for identification of damage in composite structures: a review. *J Sound Vib* 295(3–5):753–780
- Takeda S, Okabe Y, Takeda N (2002) Delamination detection in CFRP laminates with embedded small-diameter fiber bragg grating sensors. *Compos A Appl Sci Manufact* 33(7):971–980
- Teramoto K, Rabbi MS, Khan TI (2015) Detection of sub-surface delamination based on the spatio-temporal gradient analysis over the A0-mode lamb wave fields. Available from <<http://www.sciencedirect.com/science/article/pii/S1875389215008342>>. ISBN 1875-3892
- Tiwari KA, Raisutis R, Samaitis V (2017) Hybrid signal processing technique to improve the defect estimation in ultrasonic non-destructive testing of composite structures. ISBN 1424-8220
- Towsyfyhan H, et al. (2020) Successes and challenges in non-destructive testing of aircraft composite structures. Available from <<http://www.sciencedirect.com/science/article/pii/S1000936119303474>>. ISBN 1000-9361

- Tsoi K, Rajic N (2008) Durability and acoustic performance of integrated piezoceramic transducer elements under cyclic loading. *Mater Forum* 33.
- Vanniamparambil PA et al. (2015) An active–passive acoustics approach for bond-line condition monitoring in aerospace skin stiffener panels. Available from <<http://www.sciencedirect.com/science/article/pii/S1270963815001005>>. ISBN 1270-9638
- Veidt M, Liew CK (2012) 17 – Non-destructive evaluation (NDE) of aerospace composites: structural health monitoring of aerospace structures using guided wave ultrasonics. In: Karbhari VM (ed) Woodhead Publishing. Available from <<http://www.sciencedirect.com/science/article/pii/B9780857093448500178>>. ISBN 9780-857093448
- Veit G, Bélanger P (2020) An ultrasonic guided wave excitation method at constant phase velocity using ultrasonic phased array probes. Available from <<http://www.sciencedirect.com/science/article/pii/S0041624X19303932>>. ISBN 0041-624X
- Viktorov IA (1967) Rayleigh and lamb waves physical theory and applications. Springer US. ISBN 978-1-4899-5683-5
- Wandowski T, Malinowski P, Ostachowicz WM (2011) Damage detection with concentrated configurations of piezoelectric transducers. *Smart Mater Struct* 20(2):025002
- Wandowski T, Malinowski PH, Ostachowicz WM (2016) Circular sensing networks for guided waves based structural health monitoring. *Mech Syst Signal Process* 66–67:248–267
- Wang Y et al (2020) A piezoelectric sensor network with shared signal transmission wires for structural health monitoring of aircraft smart skin. *Mech Syst Sig Process* 141:106730
- Wilcox PD (2003) A rapid signal processing technique to remove the effect of dispersion from guided wave signals. ISBN 1525-8955
- Wilcox P, Lowe M, Cawley P (2001a) The effect of dispersion on long-range inspection using ultrasonic guided waves. *NDT & E Int* 34(1):1–9
- Wilcox PD, Lowe MJS, Cawley P (2001b) Mode and transducer selection for long range lamb wave inspection. *J Intell Mater Syst Struct* 12(8):553–565
- Wiley CL, et al. (2014) Guided wave tomography of pipes with high-order helical modes. Available from <<http://www.sciencedirect.com/science/article/pii/S0963869514000449>>. ISBN 0963-8695
- Wojtczak E, Rucka M (2021) Monitoring the curing process of epoxy adhesive using ultrasound and lamb wave dispersion curves. *Mech Syst Signal Process* 151:107397
- Wu Z et al (2015) Validation and evaluation of damage identification using probability-based diagnostic imaging on a stiffened composite panel. *J Intell Mater Syst Struct* 26(16):2181–2195. <https://doi.org/10.1177/1045389X14549873>
- Xu B, Giurgiutiu V (2007) Single mode tuning effects on Lamb wave time reversal with piezoelectric wafer active sensors for structural health monitoring. *J Nondestruct Eval* 26(2):123
- Xu C-B, et al. (2018) A guided wave dispersion compensation method based on compressed sensing. Available from <<http://www.sciencedirect.com/science/article/pii/S0888327017305265>>. ISBN 0888-3270
- Yi T-H, Li H-N (2012) Methodology developments in sensor placement for health monitoring of civil infrastructures. *Int J Distrib Sens Netw* 8(8):612726. <https://doi.org/10.1155/2012/612726>
- Yilmaz B, Jasiūnienė E (2020) Advanced ultrasonic NDT for weak bond detection in composite-adhesive bonded structures. *Int J Adhes Adhes* 102:102675
- Yu X et al. (2017) Feature guided wave inspection of bond line defects between a stiffener and a composite plate. Available from <<http://www.sciencedirect.com/science/article/pii/S0963869517301883>>. ISBN 0963-8695
- Zhang Z, et al. (2020a) Ultrasonic detection and characterization of delamination and rich resin in thick composites with waviness. Available from <<http://www.sciencedirect.com/science/article/pii/S0266353819328751>>. ISBN 0266-3538

- Zhang Z et al (2020b) Visualized characterization of diversified defects in thick aerospace composites using ultrasonic B-scan. *Compos Commun* 22:100435
- Zhao X et al (2007) Active health monitoring of an aircraft wing with embedded piezoelectric sensor/actuator network: I. Defect detection, localization and growth monitoring. *Smart Mater Struct* 16(4):1208–1217. <https://doi.org/10.1088/0964-1726/16/4/032>
- Zhao G et al. (2019) Detection and monitoring of delamination in composite laminates using ultrasonic guided wave. Available from <<http://www.sciencedirect.com/science/article/pii/S0263822319310827>>. ISBN 0263-8223
- Zichuan F, Jiang WW, William MD (2018) Non-contact ultrasonic gas flow metering using air-coupled leaky lamb waves. Available from <<http://www.sciencedirect.com/science/article/pii/S0041624X17310466>>. ISBN 0041-624X

Open Access This chapter is distributed under the terms of the Creative Commons Attribution 4.0 International License (<http://creativecommons.org/licenses/by/4.0/>), which permits use, duplication, adaptation, distribution and reproduction in any medium or format, as long as you give appropriate credit to the original author(s) and the source, a link is provided to the Creative Commons license and any changes made are indicated.

The images or other third party material in this chapter are included in the work's Creative Commons license, unless indicated otherwise in the credit line; if such material is not included in the work's Creative Commons license and the respective action is not permitted by statutory regulation, users will need to obtain permission from the license holder to duplicate, adapt or reproduce the material.



Chapter 6

Vibration Response-Based Damage Detection



**Maria Pina Limongelli, Emil Manoach, Said Quqa,
Pier Francesco Giordano, Basuraj Bhowmik, Vikram Pakrashi,
and Alfredo Cigada**

Abstract This chapter aimed to present different data driven Vibration-Based Methods (VBM) for Structural Health Monitoring (SHM). This family of methods, widely used for engineering applications, present several advantages for damage identification applications. First, VBMs provide continuous information on the health state of the structure at a global level without the need to access the damaged elements and to know their location. Furthermore, damage can be identified using the dynamic response of the structure measured by sensors non-necessarily located in the proximity of damage and without any prior knowledge about the damage location. By principle, VBMs can identify damage related to changes in the dynamic properties of structures, such as stiffness variations due to modifications in the connections between structural elements, or changes in geometric and material properties. A classification of different VBMs was presented in this chapter. Furthermore, several case studies were presented to demonstrate the potential of these methods.

M. P. Limongelli (✉) · P. F. Giordano · A. Cigada
Politecnico di Milano, Milano, Italy
e-mail: mariagiuseppina.limongelli@polimi.it

E. Manoach
Institute of Mechanics, Bulgarian Academy of Sciences, Sofia, Bulgaria

S. Quqa
University of Bologna, Bologna, Italy

B. Bhowmik · V. Pakrashi
University College Dublin, Dublin, Ireland

© The Author(s) 2021

M. G. R. Sause, E. Jasiūnienė (eds.), *Structural Health Monitoring Damage Detection Systems for Aerospace*, Springer Aerospace Technology, https://doi.org/10.1007/978-3-030-72192-3_6

6.1 Introduction

A broad class of damage detection methods, the so-called vibration-based methods, rely on dynamic data acquired by sensors positioned over the investigated structure. The objective of this review, which is not intended to be comprehensive, is to describe the use and goals of these methods that allow assessing structural damage conditions related to changes in the dynamic behaviour of the structure, e.g., damages that cause losses of stiffness. Furthermore, vibration-based methods are used to detect damage at a global level, using sensors not necessarily located in the proximity of the damage. The flowchart describing a general vibration-based strategy is shown in Fig. 6.1.

The identification of system parameters through vibration analyses and modal techniques has seen an active and ongoing interest for the last three decades (Fritzen et al. 1998; Fritzen 1986). The evolution of this field of research (Kerschen et al. 2005) and the move towards self-diagnosis (Fritzen and Kraemer 2009) has received further attention. The choice, distribution and placement of sensors, inextricable related to the value that can be obtained from them has been looked into in detail as well (Papadimitriou 2004; Papadimitriou et al. 2001; Papadimitriou and Lombaert 2012). Output-only identification (Basseville et al. 1993; Basseville et al. 2001) and sub-space type approach (Basseville et al. 2004; Mevel et al. 1999), damage parameter identification (Pardo De Vera and Güemes 1998; Görl and Link 2001) enabling the connection between models and reality (Alvin et al. 2003), including nonlinear aspects (Farrar et al. 2007) have been proposed. This development had also gone hand in hand with typical evolution of technology (Güemes et al. 2001). Despite this strong interest around the turn of the twenty-first century, there are several gaps, especially around the demonstrative examples of relevant aspects of aerospace monitoring that are yet to be addressed.

Depending on number and location of the recorded responses, different levels of refinement in the identification of damage can be achieved, namely detection, localization and assessment (Rytter 1993). Modal frequencies that can be used to

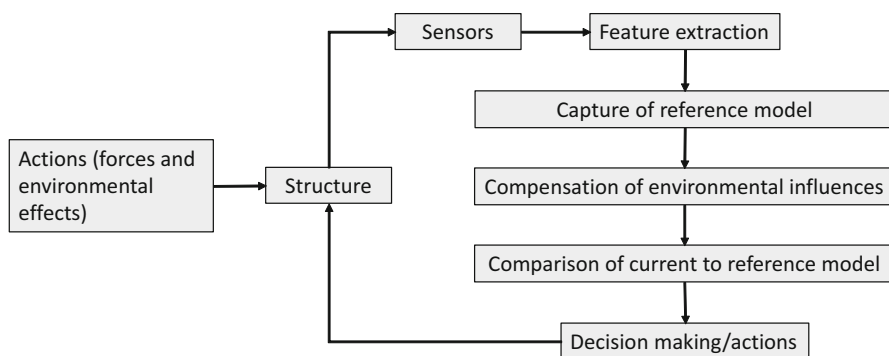


Fig. 6.1 General flowchart for vibration-based SHM methods

detect damage can, in principle, be identified using the response measured at a single location, provided all the modes contribute to that response. Damage detection, i.e., the identification of the existence of damage, might be carried out using a single sensor able to capture significant features of the structural response, e.g., the natural frequencies. The identification of damage location requires more distributed measurements and thereby a higher number of responses. Damage assessment, i.e., the identification of type and severity of damage, requires a numerical model of the structure that maps the dynamic records to different damage types and scenarios. The calibration of a such and the results it can provide depends on the number of responses available for its updating.

In literature, several methods for vibration-based damage identification have been proposed and different ways can be used for their classification. A traditional distinction is between model-based methods that make use of a numerical (e.g., finite element) model of the structure for the identification of damage and response-based methods that only use the experimental measured response to forced or ambient vibrations. In model-based methods, damage is identified through a procedure of model updating aimed at modifying the parameter of the model to achieve a better agreement with the experimental response. The most common model updating techniques include optimal matrix update, sensitivity-based and eigenstructure assignment methods (Doebling et al. 1996; Imregun and Visser 1991; Mottershead and Friswell 1993). The quality of the model updating is strictly related to the uncertainty in the model parameters and depends on the class of mathematical model chosen, on the measurement errors, excitation bandwidth and on the number and location of sensors (Limongelli and Giordano 2020; Papadimitriou et al. 2000).

The choice of the type of sensors is driven by the frequency range of interest. Accelerations are commonly measured and used directly to extract damage features or integrated to obtain velocities and displacements. In the latter case, a proper pre-processing is needed before performing the integration and information about residual displacements may be lost in the integration. Strain measurements are a further choice but provide local rather than global information and require the deployment of a higher number of sensors.

This chapter is limited to response-based methods, i.e., output-only. In fact, measuring the input excitation in aerospace applications may be challenging. Model-based methods have usually a considerable computational cost due to the need to update the parameters of the model which might involve iterative optimization procedures. This makes them less suitable for real-time applications. Conversely, response-based methods are not suitable to provide both the type and the severity of the damage, whereby model-based methods become a useful option.

Several vibration-based methods that rely only on recorded responses have been proposed in the literature. These methods can be classified in several ways, concerning the definition of the Damage Sensitive Features (DSFs).

One of the most common classifications concerns the domain where DSFs are retrieved, namely, frequency, time, and time-frequency domain. The oldest and most popular methods operate in the frequency domain. Among these, Frequency Response Functions (FRFs) and modal parameters are the most employed. Natural

frequencies have been used in the first studies to detect damage (Cawley and Adams 1979; Ostachowicz and Krawczuk 1990). Generally, natural frequencies are not suitable to detect small damage and to localize damage due to their sensitivity to environmental changes (Peeters and De Roeck 2001). More advanced methods based on natural frequencies have been developed (Chang and Chen 2005; Li et al. 2020; Xiang and Liang 2012). Several frequency-domain methods are based on the use of modal or operational parameters (Limongelli 2019), mainly combinations of frequencies, modal shapes, and their derivatives (Abdel Wahab and De Roeck 1999; Pandey et al. 1991; Ratcliffe 1997; Stubbs et al. 1992) or in terms of operational shapes retrieved from frequency response functions (Dutta and Talukdar 2004; Giordano and Limongelli 2020; Limongelli 2010; Pai and Jin 2000; Parloo et al. 2003; Zhang et al. 2013).

Conversely, time-domain methods operate directly on the recorded time series, using separation techniques, filtering, and training time series models. In turn, these methods may be divided into parametric and non-parametric approaches. The first describes the underlying stochastic process using autoregressive and/or moving average parameters. Furthermore, non-parametric approaches involve the direct estimation of features, such as time spectra and covariance, of the collected time series, which are then employed as DSFs.

Recently, time-frequency methods have also been employed for structural and damage identification, relying on two-dimensional (i.e., time-frequency or time-scale) distributions which highlight the presence of features in the collected signal.

Another common classification is based on the applicability of the methods to either time-invariant or variant scenarios. The former concern cases where the structural dynamic features and the external conditions (i.e., loads and environment) do not vary over time, whereas the latter allows the identification of damage during the occurrence of structural modifications, such as change of boundary conditions, or environmental variations.

In this chapter, a survey of common response-based methods (schematized in Fig. 6.2) for damage identification was provided. This non exhaustive survey is intended to give an insight into the most used methods for SHM for aerospace engineering, providing recent trends in research.

6.2 The Rationale of Vibration-Based Methods

Vibration-based methods for damage identification are based on the premise that a change of stiffness induces changes in modal and operational parameters that can be thereby used as damage features. Environmental and operational effects as well may produce variations of these features and must be carefully accounted for as will be illustrated in Sect. 6.3.

The equation of motion of an n degree of freedom structure subjected to an excitation, $F(t)$, can be written as:

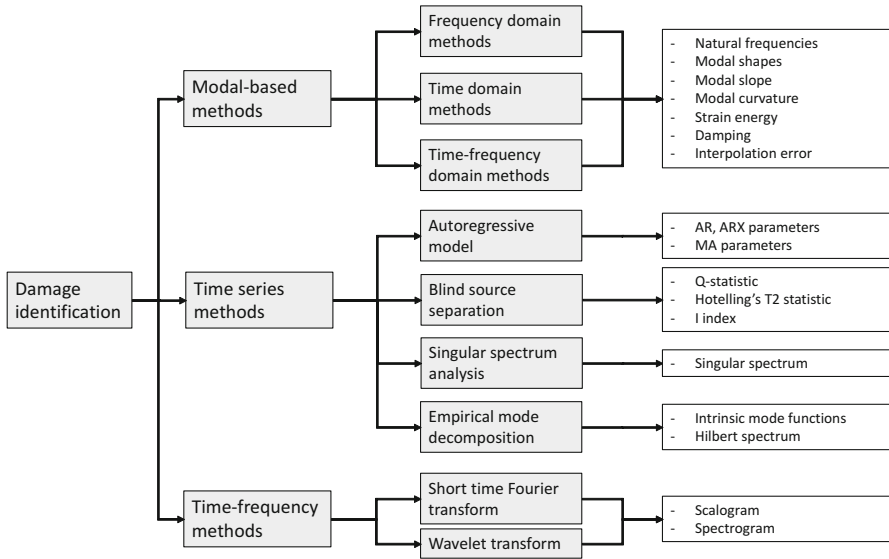


Fig. 6.2 Classification of vibration-based SHM methods

$$M\ddot{X}(t) + C\dot{X}(t) + KX(t) = F(t) \tag{6.1}$$

where $X(t)$ is the $(n \times 1)$ vector of displacement coordinates while M , K and C are the $(n \times n)$ mass, stiffness and viscous damping matrices of the system, $F(t)$ is the $(n \times 1)$ excitation vector. The natural frequencies can be estimated starting from the equation of free vibrations for undamped systems, as follows:

$$M\ddot{X}(t) + KX(t) = 0 \tag{6.2}$$

By introducing the change of coordinates $X(t) = w_i q_i(t)$ and the general solution $q_i(t) = A_i \cos \omega_i t + B_i \sin \omega_i t$, a matrix eigenvalue problem is obtained:

$$Kw_i = \omega_i^2 Mw_i \tag{6.3}$$

The n eigenvalues and eigenvectors of this problem are respectively the squares of the circular frequencies ω_i^2 and the mode shape vectors ϕ_i of the n degrees of freedom system. The natural frequencies f_i are related to the circular frequencies by means of the relation $f_i = \omega_i/2\pi$. The mode shapes are defined in arbitrary scale. It can be shown that for the real, symmetric, positive definite mass and stiffness matrices, the eigenvalues are real and positive.

6.3 Environmental and Operational Influences

The basic objective of vibration based SHM is to ascertain if damage is present or not based on measured dynamic characteristics of the system to be monitored. The damage can alter the stiffness, the mass or the energy dissipation of a structure and in this way change its basic dynamic characteristics. These characteristics (natural frequencies, vibrational modes, damping) could be strongly influenced by the environmental and operational conditions. This fact is noticed by many authors, see (Balmès et al. 2008; Giraldo et al. 2006; Lysgaard et al. 2021; Sohn 2007; Sohn et al. 2001; Wah et al. 2017), and different approaches are proposed to consider this problem. During the operation of a structure, or during the tests of a structure for damage, measurements are stored, and the selected features are extracted from data. These features then have to be compared with the features corresponded to the intact structure. If, however, the environmental conditions (temperature, humidity, wind) of the measured features are different from the reference ones, a false alarm for a damage could arise, or the damage could be masked. In reference (Manoach et al. 2012a), for example, it was shown that if the temperature of the tested beam is different from the reference one, the selected feature (Poincaré map) extracted from the measured forced response of the tested beam cannot locate the existing damage. The temperature changes are the most important environmental condition which has to be taken into account in SHM process. Thermal loads introduce stresses due to thermal expansion, which lead to changes in the modal properties. Additional important environmental and operational conditions could be wind-induced variation effect, boundary conditions, humidity (Sohn 2007).

In this sense, a key factor for SHM is to define a reference state for the expected systems or structures. The reference signals which are used to detect a potential damage in a structure should be recorded considering all possible environmental and operational factors. In many cases, however, these conditions cannot be repeated in the tested structure. That is why, several approaches to overcome the problem with the different conditions have been proposed in the literature. A possible way is to use multivariate statistical tools (so called Principal Component Analysis (PCA)) to extract features that are sensitive to damages but less sensitive to the effects of the changing environmental conditions (Manson 2002; Yan et al. 2005a).

Sohn et al. (2001) proposed an auto-associative neural network to perform NonLinear Principal Component Analysis (NLPCA). The authors have proposed to perform peculiar training of the NLPCA using the auto-associative neural network to extract the dependency of the damage sensitivity features on the unmeasured environmental conditions. Another approach (Reynders et al. 2014) was to use Kernel PCA to create nonlinear output-only model of the undamaged structure to be used as baseline. In Reference (Yan et al. 2005b), a method is proposed which introduces the concept of two maximal and minimal environmental conditions as baseline so as to remove the need to use features from a wide range of environmental conditions as baseline.

Considering all these studies, it could be concluded that the proper definition of the reference state of the intact structure and taking into account the environmental and operational conditions could be crucial for the correct and reliable SHM.

6.4 Modal-Based Methods and Damage Features

Modal parameters, i.e., modal shapes, natural frequencies and modal damping are among the most used DSFs in SHM applications due to their direct physical interpretation. Several studies have been presented in the scientific literature aimed at detecting, localizing or even quantifying damage, using the modal parameters or quantities derived from them.

Different techniques have been proposed to identify modal parameters based on structural vibrations (namely, Operational Modal Analysis (OMA) techniques), which operate in the frequency, time, or joint time-frequency domain.

In the first case, the Fourier transform is applied to the recorded signal and the modal parameters are identified by analysing resonance peaks in the spectrum of the structural response. The most used methods in this context are the basic frequency domain approach and Frequency Domain Decomposition (FDD) (Brincker and Ventura 2015). As concerns time-domain approaches, free decay responses are generally employed upon obtaining them through correlation or random decrement functions. The Ibrahim Time-Domain (ITD), the stochastic subspace identification and the Eigensystem Realization Algorithm (ERA) are well-known methods (Brincker and Ventura 2015). However, both time and frequency approaches are based on strict assumptions about the nature of exciting input and structural behaviour. Firstly, the excitation must be stationary and have a wide frequency band. Furthermore, structural behaviour should be linear and not vary over time. To relax the assumptions on the nature of the input and the non-variability of structural conditions, several methods have been proposed based on time-frequency and Time-Scale Representations (TFRs) generally obtained using the Short-Time Fourier Transform (STFT) and the Wavelet Transform (WT). For modal identification, simple ridge extraction (Delprat et al. 1992; Rankine et al. 2007) or other methods, such as the clustered filter bank approach (CFB) (Quqa et al. 2020) or the Modal Assurance Distribution (MAD) (Quqa et al. 2021), are employed.

6.4.1 *Natural Frequencies*

Natural frequencies are amongst the first DSFs employed in SHM applications due to their ease of evaluation. Nevertheless, several studies confirmed that damage identification methods based solely on natural frequencies may not be reliable if applied to complex structures or if the damaged entity is modest (Güemes et al. 2020). Generally, damage is a local phenomenon, whereas natural frequency is a

global feature not appropriate to identify the damage location except for simple applications. There are however attempts to localize damage only based on the information about the natural frequencies. Such methods can be found in the works of Cawley and Adams (1979) and Ostachowicz and Krawczuk (1990). Herein, the authors used the frequency shifts to detect damage.

A more advanced method to detect and localize damage was developed recently in Li et al. (2020). Particularly, the authors have studied the damage-induced Relative Natural Frequency Change (RNFC) curves:

$$\Delta\omega_{i,j} = \frac{\omega_j - \omega_{i,j}^*}{\omega_j} \quad (6.4)$$

where ω_j is the j -th natural frequency of the intact beam and $\omega_{i,j}^*$ is the j -th natural frequency of the damaged beam with the damage at the i -th sensor location. Lin and Cheng (2008) proposed an index based on the natural frequencies and used it to determine the depths of two cracks in a monodimensional structural element. Chang and Chen (2005) and Xiang and Liang (2012) presented a two-step multiple damage detection method that estimates the natural frequency-based defect severity upon localizing the damage through the mode shapes.

6.4.2 Mode Shapes

The simplest and easiest (after natural frequency method) method which uses the changes in the mode shapes is the so-called modal displacement method (Allemang and Brown 1982; Farrar and James 1997; Farrar et al. 1994). The Modal Displacement (MD) method is based on the difference in the measured modal displacements of damaged and healthy structures. The maximal absolute value of the differences between the modal displacements of a beam could be representative of the damage location. The maximal absolute value of the differences between the modal displacements at location $i = 1, \dots, N_{\text{nodes}}$ is computed as follows:

$$\Delta w_i = \sum_{j=1}^{N_{\text{modes}}} \left| w_{ij}^* - w_{ij} \right| \quad (6.5)$$

where N_{nodes} is the number of nodes used to discretize the beam, N_{modes} is the number of identified modes, w_{ij} is the displacement of the j -th mode at the i -th node of the intact beam and w_{ij}^* is the same for the damaged beam.

Based on the mode shapes, several techniques have been developed over the years to improve the performance of the modal displacement method. An example of such method is the so-called Modal Assurance Criterion (MAC) method suggested by Allemang and Brown (1982), which detects mode shape changes over the entire structure by taking advantage of the orthogonality of the normal modes. Kim et al.

(1992) furthered the MAC in the development of the Coordinate Modal Assurance Criterion (COMAC) method, which uses modal node displacements to detect and locate damage. An example of successful usage of MAC to correlate modes of undamaged space shuttle orbiter body flap with a damaged flap is the work (West 1984).

6.4.3 Modal Slope

Another simple method for damage detection is based on the modal slopes (i.e., the first derivative of modal shapes). The absolute differences between the squared modal slopes of the damaged and healthy structures at location $i = 1, \dots, N_{\text{nodes}}$ is computed as follows:

$$\Delta W_i'^2 = \sum_{j=1}^{N_{\text{modes}}} \left| w_{ij}'^{*2} - w_{ij}'^2 \right| \quad (6.6)$$

where N_{modes} is the number of identified modes. Sign “prime” in the equation denotes derivative with respect to the space variable. Damage is located at the location where the damage index $\Delta W_i'^2$ reaches the maximum value. This method is more often used considering only the first mode, i.e., $N_{\text{modes}} = 1$. The method frequently gives additional, false peaks and it is not widely used for real applications (Manoach et al. 2016a).

6.4.4 Modal Curvature

A popular modal-based approach is the Modal Curvatures method (MC) (Pandey et al. 1991), which shows a better sensitivity to damage than the aforementioned DSFs. In this case, the damage indicator is defined at location $i = 1, \dots, N_{\text{nodes}}$ by the following expression:

$$\Delta W_i'' = \sum_{j=1}^{N_{\text{modes}}} \left| w_{ij}''^* - w_{ij}'' \right| \quad (6.7)$$

MC-based methods are generally more reliable than the MD-based approaches, especially if curvatures are directly measured from the strain mode shape (Deraemaeker et al. 2006). The authors of (Pandey and Biswas 1994) noticed that MC-based damage detection generally leads to a curve which has a prominent peak at the damage location, but may also manifest smaller outliers, generating issues in practical applications. Ciambella and Vestroni (2015) have managed to avoid this disadvantage. By using a perturbative solution, they have proved that the modal

curvatures do not provide information on the damage location, if not properly processed. The authors thus introduced a novel filtering procedure for MCs, which leads to effective damage localization considering only one mode.

A modification of the modal curvature method is the Modal Curvatures Square Method (MCSM) (Deraemaeker et al. 2006), which can be used to enhance the differences in the curvatures of the intact and damaged structures, i.e.

$$\Delta W_i'^2 = \sum_{j=1}^{N_{modes}} \left| w_{ij}'^2 - w_{ij}''^2 \right| \quad (6.8)$$

6.4.5 Strain Energy

The Modal Strain Energy method (MSE) is one of the most effective modal-based methods. It was suggested in Stubbs et al. (1995) and Stubbs and Kim (1996). Primarily developed for addressing strain-based theories for Euler-Bernoulli beams, the method has been extended to portal blocks, sway frames, cables and complex systems as a whole in the later stages. This was pioneered by the exemplary work by Cornwell et al. (1999).

Numerical evaluations and experimental test beds have evidenced the method applicability to deep (Timoshenko) beams where bending and shear deformation contributes to the strain energy. Considering the i -th element of the beam, the j -th mode strain energy for the healthy and damage structure are obtained as:

$$U_{ij} = \frac{1}{2} \int_{a_i}^{a_{i+1}} \left\{ (EI)_i \left(\frac{\partial^2 w_j}{\partial x^2} \right)^2 + k \frac{(Ebh)_i}{2(1+\nu)} \left(\frac{\partial w_j}{\partial x} - \psi_j \right)^2 \right\} dx;$$

$$U_{ij}^* = \frac{1}{2} \int_{a_i}^{a_{i+1}} \left\{ (EI)_i^* \left(\frac{\partial^2 w_j^*}{\partial x^2} \right)^2 + k \frac{(Ebh)_i^*}{2(1+\nu)} \left(\frac{\partial w_j^*}{\partial x} - \psi_j^* \right)^2 \right\} dx, \quad (6.9)$$

and

$$U_j = \sum_{j=1}^n U_{ij}, U_j^* = \sum_{j=1}^n U_{ij}^*$$

where j is the mode index, U_{ij} is the strain energy of j -th mode for the i -th element. The variables for the damaged beam are denoted by ‘*’. Angles ψ_i and ψ_i^* denote the rotation of the cross-section of the i -th elements for the intact and damaged beam, respectively.

In the above-mentioned articles, it was shown that the strain energy ratio

$$\frac{(EI)_i^*}{(EI)_i} = \frac{J_{ij}}{U_j^*} = \frac{\gamma_i^*}{\gamma_i} = f_i$$

$$\gamma_i^* = J_{ij}U_j^*; \gamma_i = J_{ij}^*U_j \quad (6.10)$$

where

$$J_{ij}^* = \int_{a_i}^{a_{i+1}} \left\{ \left(\frac{\partial^2 w_j^*}{\partial x^2} \right)^2 + k \frac{6}{h^2(1+\nu)} \left(\frac{\partial w_j^*}{\partial x} - \psi_j^* \right)^2 \right\} dx$$

$$J_{ij} = \int_{a_i}^{a_{i+1}} \left\{ \left(\frac{\partial^2 w_j}{\partial x^2} \right)^2 + k \frac{6}{h^2(1+\nu)} \left(\frac{\partial w_j}{\partial x} - \psi_j \right)^2 \right\} dx \quad (6.11)$$

can successfully indicate damages.

In addition to the localization, the extent of damage is also indicated by the strain energy ratio. This ratio tends to 1 for the undamaged regions and it becomes higher when damage occurs.

Detection of fault is incentivized by the numerical value of strain energy. Considering the neighborhood of damage, strain energy can prove to be a vital indicator using a damage index. This index f_i is an excitation frequency dependent parameter that can be related to the cumulative strain energy ratio as:

$$f_m = \frac{1}{N} \sum_{j=1}^N f_{j_m} \quad (6.12)$$

An improved version of the method described by Stubbs and Kim (1996) is presented here. Complications might arise when the angular rotation has to be determined directly. In Manoach et al. (2017), the authors have critically investigated the second term that evolves from the expression of strain energy (as a direct resultant of shear stress). Comparisons using both the formulas have also been carried out. In some cases, consideration of the full strain energy could essentially improve fault detection and its extent.

6.4.6 Damping

Modal damping has also been proposed as a possible feature for damage detection since the presence of a crack in a cross-section of a thin-walled structure will increase internal friction, which in turn will increase the value of damping (Manoach et al. 2016b, 2012b; Yamaguchi et al. 2013).

This possibility was firstly highlighted by Williams and Salawu (1997) and Farrar et al. (1994) who both concluded that measuring modal damping from vibration data

produced large deviations that significantly decreases damping as a reliable damage indicator.

Kyriazoglou et al. (2004) explored the use of the specific damping capacity SDC for damage detection and localization in composite laminates:

$$SDC = \frac{\Delta U}{U} \quad (6.13)$$

where ΔU is the energy dissipated in one cycle and U is the total energy stored in that cycle. In this work, the change in natural frequencies or flexural modulus was used as a damage indicator in glass-fiber-reinforced plastic laminates; however, the authors had concluded that SDC is more sensitive to damage.

6.4.7 Interpolation Error

The interpolation method (Limongelli 2010) is based on the use of cubic spline functions to interpolate the deflected shapes estimated from dynamic records. One of the main advantages of this method is that it does not require the estimation of the modal curvatures to obtain the damage indices. The interpolation is carried out at the i -th location considering all the measured components of the deflected shapes $w_1, w_2, \dots, w_{i-1}, w_{i+1}, \dots, w_n$ except w_i . The interpolation error is defined as follows:

$$\begin{aligned} E_{k,i} &= \left| \left(c_{0,k,i} + c_{1,k,i}(z_i - z_{i-1}) + c_{2,k,i}(z_i - z_{i-1})^2 + c_{3,k,i}(z_i - z_{i-1})^3 \right) - w_{k,i} \right| \\ &= |\widehat{w}_{k,i} - w_{k,i}| \end{aligned} \quad (6.14)$$

The coefficients $c_{0,i}$, $c_{1,i}$, $c_{2,i}$, and $c_{3,i}$ of the cubic spline function are computed imposing interpolation and continuity conditions at all the instrumented locations. Due to the so-called ‘Gibbs’ phenomenon for splines functions, a sharp increase of the interpolation error arises at the locations with curvature discontinuities, thus allowing to locate damage. Refer to (Limongelli 2003) for additional information on the interpolation procedure. The interpolation error method can be applied using both modal and operational shapes since the curvature discontinuity affects both types of deformed shapes (Giordano and Limongelli 2020). To increase the sensitivity of the damage feature and increase the difference between its value at the damaged and undamaged locations, the interpolation error is computed combining the contribution of all the n_{shapes} modal or operational shapes as follows:

$$E_i = \sqrt{\sum_{k=1}^{n_{shapes}} |\widehat{w}_{k,i} - w_{k,i}|^2} \quad (6.15)$$

Changes of interpolation error between two different states (reference and potentially damaged) highlight the onset of a curvature discontinuity. Hence, the difference of interpolation error δE_i defined in Eq. (6.16) is assumed as the damage feature at location i .

$$\delta E_i = E_i^D - E_i^U \quad (6.16)$$

The extension of this method to two-dimensional structures has been proposed in Limongelli (2017), and it is referred to as the surface interpolation method (SIM). The SIM is based on the use of a bi-cubic spline interpolating function, which can be thought of as a surface constructed from sets of cubic spline functions. A comprehensive and rigorous description of the SIM can be found in Limongelli (2019).

The readers who are interested to see more references for different modal-based methods for damage detections can turn to these excellent review articles: Doebbling et al. (1996); Maia et al. (2003) and Montalvão et al. (2006).

6.5 Time Series Methods

6.5.1 Autoregressive Parameters

Autoregressive (AR) models are widely used for time series modelling (Gul and Necati Catbas 2009; Nair et al. 2006; Sohn and Farrar 2001; Worden et al. 2002; Yao and Pakzad 2012), due to the simple procedure required for the identification of an underlying model, performed through linear least-squares minimization which involves low computational effort and model uncertainties (Datteo et al. 2018).

AR models were developed in econometrics to describe time-varying processes, representing the output variable as a linear combination of its own previous samples plus an error term. In particular, each sample $x[t]$ of a collected signal is expressed as:

$$x[t] = c + \sum_{i=1}^p \varphi_i x[t-1] + \varepsilon[t] \quad (6.17)$$

where φ_i are the AR parameters, p is the model order, i.e., the number of lags considered in the description of each sample of the output variable, c is a constant and $\varepsilon[t]$ is the error term. The order is generally not known a priori, requiring specific techniques to find the optimal value. To this aim, the Aikake Information Criterion (AIC) and the Bayesian Information Criterion (BIC) are widely employed (Ljung 1998) in research.

In the last decades, several types of autoregressive models have been investigated for SHM. Sohn et al. (2000) studied features based on the analysis of residuals, generating control charts (X-Chart, S-Chart, EWMA) where outliers can be easily

identified. Yao and Pakzad (2012) compared different pattern recognition algorithms using AR models and introduced the Cosh spectral distance as a new damage feature.

Despite the growing use in SHM applications, AR models are only-pole functions and spurious poles are usually introduced to represent the response of complex systems, which also depend on the zeros of the FRF of the physical model (Yao and Pakzad 2012). Moreover, the use of these models in the field of structural dynamics is based on the assumption that the force that excites the system is a random Gaussian process, which is generally acceptable only when analysing long enough time series.

Other advanced models have been used for better describing the dynamic behaviour of complex and time-varying systems. AutoRegressive Moving Average (ARMA) has been successfully employed to describe the response of linear systems subjected to random excitation (Datteo et al. 2018), employing however a nonlinear least-squares approach to identify the moving average coefficients, which involves high computational cost and convergence issues. Sohn and Farrar (2001) proposed a two-stage prediction model, i.e., combining auto-regressive and AutoRegressive with eXogenous inputs (ARX) techniques, consisting of a linearized version of ARMA, to address these problems. The ARX model was also used by Roy et al. (2015), who provided a mathematical formulation relating the variations in ARX coefficients with the stiffness of the structure, which cannot be directly provided in the case of a pure AR model.

Due to the univariate nature of AR, ARX and ARMA models, they are usually employed for damage detection, performing novelty detection on single data channels considered individually. To the aim of damage localization, multivariate extensions of the aforementioned models have been presented, including multivariate autoregressive (MAR) models (Achilli et al. 2020) and vector autoregressive moving average (VARMA) (Entezami and Shariatmadar 2019; Mosavi et al. 2012). In such models, each sample of a given time series (representing the signal collected by a given acquisition channel) is described using also the p past samples of other signals, collected at different locations. Recently, nonlinear extensions of time series methods, such as the nonlinear autoregressive models with exogenous variables (NLARX) have been presented to deal with systems that show strongly nonlinear behavior. Hu and Kaloop used this model combined with wavelet neural networks to identify the thermal response of a bridge (Hu and Kaloop 2015).

Time-dependent extensions of ARMA models were also proposed to deal with time-varying systems and nonstationary excitation (Poulimenos and Fassois 2006; Spiridonakos and Fassois 2009; Spiridonakos and Fassois 2012). The class of functional series time-dependent autoregressive moving average (FS-TARMA) were surveyed in (Spiridonakos and Fassois 2014), where a comparative assessment of the main modelling and identification literature methods is presented.

Similar to the use of ARX is the idea behind the use of Kalman Filtering (Seibold et al. 1996). A reference multi-input multi-output state space model is identified and produces residuals when used on new measurements. The residual is used as a damage feature.

A dynamic input reconfiguration architecture based on the input control redundancy available in the system can be achieved by the use of Nullspace-based Subspace Fault Detection (NSFD) (Varga 2011). Using both ultrasonic and vibration-based studies, methods based on NSFD has shown promise towards SHM of aerospace structures. Narrowband burst signals have shown wide applicability to excite systems in order to reduce the impact of multimodal wave dispersion and propagation. However, with the NSFD method being extremely adaptable, simulated sensor signals are obtained from narrowband, broadband and more specifically, random excitations for fault detection based SHM (Peni et al. 2018; Varga 2011). As multiple applications of NSFD have been researched over the years, notable among them involve the methods based on dynamic nullspace computed from the linear time-varying model of the system. Cases where no uncertainty is considered invoke the possibility of influencing the nominal control loop with the most advanced Fault Tolerant Control (FTC) techniques (Shokravi et al. 2020). However, environmental impact studies necessitate a paradigm shift towards enabling robust active methods such as linear parameter-varying, switching, and gain-scheduled certifiable algorithms.

6.5.2 *Intrinsic Mode Function and Hilbert Spectrum*

Damage detection of structural elements has received considerable attention with the introduction of Empirical Mode Decomposition (EMD) (Huang et al. 1998; Kunwar et al. 2013; Li et al. 2007; Peng et al. 2005; Xu and Chen 2004; Yang et al. 2004). Associated with EMD is the energy Damage Index (DI) that differentiates the damaged state of the system from its pristine state. The EMD method decomposes a signal into Intrinsic Mode Functions (IMFs) that satisfies the following conditions: (i) it is a well-behaved mono-component function and (ii) the average values of the envelopes defined by the local extrema are zero. A stalwart in the signal decomposition genre, EMD decomposes any given signal into its corresponding IMFs, even under nonstationary environments, in an adaptive manner, without pre-selecting any basis (Huang et al. 1998; Xu and Chen 2004). In modal identification theory, for MDOF systems, modes of vibration can be obtained based on the free-vibration responses.

IMFs are extracted through *sifting*, a technique rigorously discussed in supporting literature. Suppose a signal $x(t)$ is to be decomposed. The running mean of the envelope is subtracted which produces the difference $x(t) - m_1 = h_1$ to obtain primary IMF, containing the shortest period component of the signal. The component h_1 is now examined if it satisfies the conditions sufficient for an IMF. In case of discrepancies, sifting continues in successive iterations until the conditions for an IMF are addressed. Sifting decomposes the data into n IMFs, C_i and a residue r_n —a statistical constant or a mean trend. Mathematically, the procedure can be expressed as:

$$X(t) = \sum_{i=1}^n C_i + r_n \quad (6.18)$$

where $X(t)$ represents an acceleration response for any n -DOF system. Localization of damage is carried out by employing the DI based on the energy of the first IMF of the signal. The vibration response extracted from the health system is first acquired and filtered to retain only the first natural frequency within the data. The first IMF is then extracted through EMD to obtain the energy for each sensor as:

$$E = \int_0^{t_0} (IMF)^2 dt \quad (6.19)$$

Finally, the DI for each sensor is given by the following expression:

$$DI = \left| \frac{E_{Healthy} - E_{Damaged}}{E_{Healthy}} \right| \times 100 \quad (6.20)$$

High index values may be associated with proximity to the damage in a monitored system. However, a key drawback of this approach is the requirement of measured responses at all floor levels. To overcome these difficulties, recently developed damage detection algorithms premised on decorrelating the signals using orthogonal transformations are utilized.

6.5.3 Signal Components

The method of separating signal constituents from a mixture without prior information about the sources is known as Blind Source Separation (BSS) (Belouchrani et al. 1997; Sadhu and Hazra 2015; Zang et al. 2004). A signal decomposition tool, BSS has not only been used in acoustics, but also for structural modal identification and damage detection in built infrastructures (Hazra et al. 2012). BSS estimates primary source signals from the vibration output of monitored systems infested with noise. The estimation, mostly carried out on output signals, primarily identifies the mixing system first and then estimates the source signals implicitly by some suitable optimization procedure (Hazra et al. 2012). In addition to its utility as a system identification tool, BSS uses its second-order statistics such as auto-correlation functions (Antoni 2005) or higher-order statistics like non-Gaussianity (Belouchrani et al. 1997) for structural damage detection. Independent Component Analysis (ICA)—a form of BSS-0 has been extensively used for identifying damage patterns of dynamical systems (Hyvärinen and Oja 2000; Sadhu and Hazra 2015). However, it was later observed that ICA suffered from some performance issues such as the presence of higher structural damping and measurement noise. The use of auto-correlation functions prompted the utilization of Second-Order Blind Identification

(SOBI)—pivoted around windowing of the vibration datasets—that proved insensitive towards lower structural damage levels.

Considering an MDOF structure subjected to Gaussian broadband excitation, $F(t)$, the equation of motion can be expressed as:

$$\mathbf{M}\ddot{\mathbf{X}}(t) + \mathbf{C}\dot{\mathbf{X}}(t) + \mathbf{K}\mathbf{X}(t) = F(t) \quad (6.21)$$

where $\mathbf{X}(t)$ is the vector of displacement coordinates while \mathbf{M} , \mathbf{C} and \mathbf{K} are the mass, damping and stiffness matrices of the system, respectively. The solution to Eq. (6.21) can be written according to:

$$\mathbf{X}(n) = \mathbf{A}\mathbf{S}(n) \quad (6.22)$$

In the above equation, \mathbf{X} is the measurement matrix, the matrix of the corresponding modal coordinates is represented by \mathbf{S} and \mathbf{A} is the modal transformation matrix with n number of the total datapoints in the sample space. Furthermore, it has been observed that the columns of the mixing matrix \mathbf{A} are linearly independent that corresponds to the vibratory structural modes. SOBI evaluates two covariance matrices at time lags 0 ($\mathbf{R}_x(0)$) and p ($\mathbf{R}_x(p)$) respectively, and perform joint diagonalization to estimate the unknown mixing matrix, \mathbf{A} . Mathematically, one can write:

$$\left. \begin{aligned} \mathbf{R}_x(0) &= E[\mathbf{X}(n)\mathbf{X}(n)^T] = \mathbf{A}\mathbf{R}_s(0)\mathbf{A}^T \\ \mathbf{R}_x(p) &= E[\mathbf{X}(n)\mathbf{X}(n-p)^T] = \mathbf{A}\mathbf{R}_s(p)\mathbf{A}^T \end{aligned} \right\} \quad (6.23)$$

where $\mathbf{R}_s(p) = E[\mathbf{S}(n)\mathbf{S}(n-p)^T] = \mathbf{I}$. Typically, SOBI encompasses three key steps that are addressed sequentially: whitening orthogonalization and unitary transformation. As the data predominantly evolves from a zero-mean process, the first step towards whitening is carried out by diagonalizing $\mathbf{R}_x(0)$ as: $\mathbf{R}_x(0) = \mathbf{V}_x\boldsymbol{\lambda}_x\mathbf{V}_x^T$, with \mathbf{V}_x and $\boldsymbol{\lambda}_x$ being the principal components of eigenspace. The whitened signals are then obtained from the following equation with \mathbf{Q} idealized as the whitening matrix:

$$\bar{\mathbf{X}}(n) = \boldsymbol{\lambda}_x^{-1/2}\mathbf{V}_x^T\mathbf{X}(n) = \mathbf{Q}\mathbf{X}(n) \quad (6.24)$$

The correlation between the measured responses is removed using whitening, given by the relation: $\mathbf{R}_{\bar{x}}(0) = E[\bar{\mathbf{X}}(n)\bar{\mathbf{X}}(n)^T] = \mathbf{I}$, obtaining the following expressions:

$$\mathbf{R}_{\bar{x}}(p) = \frac{1}{N} \left[\sum_{n=1}^N \bar{\mathbf{X}}(n)\bar{\mathbf{X}}(n-p)^T \right] = \mathbf{Q}\mathbf{A}\mathbf{R}_s(p)\mathbf{A}^T\mathbf{Q}^T \quad (6.25)$$

From the above equation, it can be understood that both the whitened covariance matrix and the matrix product $\mathbf{Q}\mathbf{A}$ (a unitary matrix) can be numerically diagonalized. The EVD of the matrix $\mathbf{R}_{\bar{x}}(p)$ satisfies the relation, $\mathbf{V}_{\bar{x}}\mathbf{R}_{\bar{x}}(p)\mathbf{V}_{\bar{x}}^T = \boldsymbol{\lambda}_{\bar{x}}$. As the

diagonal matrix $\lambda_{\bar{x}}$ has distinct eigenvalues, the mixing matrix can be estimated, according to:

$$\hat{\mathbf{A}} = \mathbf{Q}^{-1} \mathbf{V}_{\bar{x}} = \mathbf{V}_x \lambda_x \mathbf{V}_{\bar{x}}^T \quad (6.26)$$

SOBI carries out an approximate joint diagonalization approach based on Givens rotation technique to find the unitary matrix $\mathbf{Q}\mathbf{A}$ that diagonalizes the whitened covariance matrix $\bar{\mathbf{R}}_x(p)$ at one or several non-zero time lags. The problem then transforms into finding a minimum performance index \mathcal{J} such that the unitary diagonalization satisfies the relation $\mathbf{D} = \mathbf{V}^T \tilde{\mathbf{R}}_{\bar{x}}(p) \mathbf{V}$. Therefore:

$$\mathcal{J}(\mathbf{V}, p) = \sum_p \sum_{1 \leq i \neq j \leq n_s} \left\| \mathbf{D}_{ij}^p \right\|^2 \quad (6.27)$$

where, \mathbf{V} is the unitary matrix and also the joint approximate diagonalizer for all p -shifted covariance matrices $\tilde{\mathbf{R}}_{\bar{x}}(p)$. Once the mixing matrix is obtained, the estimated sources can now be evaluated, which was the primary objective of carrying out SOBI:

$$\hat{\mathbf{S}}(n) = \hat{\mathbf{A}}^{-1} \mathbf{X}(n) \quad (6.28)$$

The matrix $\hat{\mathbf{S}}(n)$ contains the modal responses from which the modal constituents (i.e., natural frequencies and damping ratios) can be obtained. Once the modal responses are obtained from SOBI, the instant and location of damage need to be identified. However, it is a well-understood fact that the computational efficiency of the entire process is significantly escalated due to the simultaneous algebraic operations that take place in windows and permutation ambiguity (Cichocki and Amari 2002). To overcome these impediments, comparatively recent trends in structural damage detection are explored such as singular spectrum analysis incorporated in a recursive first-order perturbative framework.

Structural damage manifests in the form of alteration of inherent system properties that form the implementation of BSS as a damage detection tool. Time series models with pre-selected model orders are used to characterize the sources that are obtained from the past observations and then the future measurement sources are accordingly predicted (Zang et al. 2004). The newer measurements contain the information about the damaged state of the structure and are compared against the baseline data pre-recorded from the pristine state of the system, which enables the estimation of damage adaptively.

6.5.4 Damage Indices Based on Extracted Features

PCA is a methodical dynamic exploratory analysis that yields uncorrelated data on an orthogonal basis derived from the physical dataset (De Boe and Golival 2003;

De Oliveira and Inman 2015; Gharibnezhad et al. 2015; Hot et al. 2012; Jolliffe 1986; Kerschen et al. 2005; Koh et al. 2005; Lee et al. 2005; Li et al. 2000; Lovera et al. 2000; Misra et al. 2002; Mujica et al. 2014; Nguyen and Golinval 2010; Richman 1986; Tipping and Bishop 1999; Yan et al. 2005a). In recent years, PCA has been explored for dimensionality reduction, to account for operational and environmental variability and so on (De Oliveira and Inman 2015; Gharibnezhad et al. 2015; Lee et al. 2005; Li et al. 2000; Nguyen and Golinval 2010; Yan et al. 2005b). PCA detects the presence and location of structural damage along with its extent from vibration-based outputs. PCA, however, requires a baseline model from the healthy structure and compares it with the monitored state to identify the presence of damage through statistical DIs such as T^2 , Q , I^2 , and ϕ ; instances of which, are replete in literature (Jolliffe 1986).

PCA, a method to orthogonally project data onto a lower-dimensional space, ensures that variance of the projected data is maximized. A lower-dimensional uncorrelated dataset reveals relevance which can be obtained using eigenvalue decomposition on the covariance matrix obtained from the physical responses. It is closely related to the method of Proper Orthogonal Decomposition (POD) (Feeny 2002; Feeny and Liang 2003; Han and Feeny 2003; Kappagantu and Feeny 2000a, 2000b; Kerschen and Golinval 2003). Consider a multivariate dataset X obtained from sensor responses. PCA seeks an orthogonal transformation of the form: $T = PX$ where T represents the space of transformed variables that are decorrelated in the orthogonal space. So, PCA can be thought of as a constrained optimization problem where the objective is to diagonalize TT^T subject to the constraint $PP^T = I$. Mathematically, it translates to defining an objective function O as under:

$$O = TT^T - \Lambda(PP^T - I) \quad (6.29)$$

The optimal transformation is obtained by setting the partial derivative of O to zero as follows:

$$\frac{\partial O}{\partial P^T} = 0 \Rightarrow (X^T X)P = \Lambda P \quad (6.30)$$

This decomposition produces the Principal Orthogonal Values (POVs) (the eigen value matrices) and Proper Orthogonal Matrices (POMs) (eigen vector matrices) (Feeny and Liang 2003; Kappagantu and Feeny 2000b; Kerschen et al. 2005). The POVs maps the relative significance of each POM in the response. The uncorrelated new set of variables produced are known as the principal orthogonal components (POCs) (Feeny and Liang 2003). Potentially, the uncorrelated newer set of variables have improved lower dimensional information that aids in faster structural damage detection process. As these projections are sometimes not enough by themselves, it is necessary to use certain statistical parameters that are considered as DIs. In this context, a few DIs and their utility are described next.

Q-statistic (SPE index) represents the variability of the data projection within the residual subspace. Considering the i -th row of the matrix \mathbf{E} , the *Q-statistic* for each experimental observation is defined as:

$$Q_i = e_i e_i^T = x_i (\mathbf{I} - \mathbf{P}\mathbf{P}^T) x_i^T \quad (6.31)$$

Hotelling's T^2 -statistic (D index) checks the variability of the projected data in the new space of the PCs using score matrix \mathbf{T} . The concept of Euclidean distance comes into effect by utilizing the covariance matrix \mathbf{C}_X as the normalization factor. For the i -th sample, the DI is expressed according to:

$$\begin{aligned} T_i^2 &= \sum_{j=1}^r \frac{t_{sij}^2}{\lambda_j} = t_{si} \mathbf{\Lambda}^{-1} t_{si}^T \\ &= x_i \mathbf{P}\mathbf{A}^{-1} \mathbf{P}^T x_i^T \end{aligned} \quad (6.32)$$

In the above equation, t_{si} is the i -th row vector of the matrix \mathbf{T} , defined as the projection of the experiment x_i onto the new space, related by the expression, $t_{si} = x_i \mathbf{P}$.

Combined index (ϕ index) is essentially a blend of the *Q*-index and the T^2 index for merging information into a single value. The mathematical expression defining this DI is given as:

$$\begin{aligned} \phi \text{ index} &= Q \text{ index} + T^2 \text{ index} \\ &= x^T \mathbf{M}_\phi x \\ &= x^T (\mathbf{I} - \mathbf{P}\mathbf{P}^T + \mathbf{P}\mathbf{A}^{-1} \mathbf{P}^T) x \end{aligned} \quad (6.33)$$

I index has its very roots in its utilization for clinical studies and mainly used for meta-analysis, accounting for a percentage of heterogeneity. The *I* index provides variation in study outcomes between experimental trials and can be mathematically defined as:

$$I \text{ index} = x^T \mathbf{M}_I x \quad (6.34)$$

6.5.5 Singular Spectrum Analysis (SSA)

An extension of the application of EigenValue Decomposition (EVD), (which is the crux of PCA) to elicit Principal Components (PCs), using the inputs from a single dataset, arranged in a Hankel structure, referred to as Singular Spectral Analysis

(SSA), is also gaining popularity in recent times (Carniel et al. 2006; Chao and Loh 2014; Elsner and Tsonis 1996; Groth and Ghil 2015; Hassani 2010; Hassani et al. 2011; Kilundu et al. 2011; Lakshmi et al. 2017; Liu et al. 2014; Murotani and Sugihara 2005).

In the strictest sense, prior assumptions regarding stationarity, normality or linearity of a feasible dataset can be alleviated with the use of SSA. As a non parametric method, the projection of time series into a smaller dimensional space ensures lagged signal components by itself. Most of the variance is retained, which explains the key signatures in the series (Carniel et al. 2006; Elsner and Tsonis 1996; Hassani 2010; Hassani et al. 2011). A significant point of difference between conventional PCA and contemporary SSA is that Singular Value Decomposition (SVD) is carried out using PCA (Bhowmik et al. 2019a; Chao and Loh 2014; Groth and Ghil 2015; Kilundu et al. 2011; Lakshmi et al. 2017; Murotani and Sugihara 2005).

The reconstruction process in SSA ensures that the principal components are adopted from the signal subspace. This automatically removes any noise components associated with the signal and acts as a filter for cleaning datasets.

The primary function of SSA is to decompose a time series into simpler components and then reconstructing the acquired principal components onto a new time series. Predominantly, the simpler components arise either from slowly varying trend, harmonic component and/or noise. While the slow trend corresponds to slow varying additive constituents, the harmonic series makes up for the periodic nature of the time series. The effects of noise are removed through an automatic filter. Any aperiodic series can be treated as the noise that does not affect the functioning of the reconstruction process. SSA proceeds by evolving a Hankel covariance matrix from the single set of sensor responses obtained through monitoring. A sliding window is incorporated to resolve the principal components in their order of significance. This window is usually selected to have a lesser size (in terms of samples) as compared to the actual length of time series. This forms the first step in embedding. Subsequent decomposition of the matrix into elementary matrices according to decreasing eigen significance is commonly termed as the SVD step of the method. The automatic noise removal process is attributed to the truncation of matrices to approximate the original matrix—in a method called ‘grouping’—that includes principal components only from the signal subspace. Finally, the reconstruction phase involves a diagonal averaging approach which mimics the original time series in terms of signal constituents, eliminating all the noise components at this stage.

6.5.6 First-Order Eigen Perturbation (FOEP) Technique

With the advent of statistical signal processing techniques aimed at extracting the key features of damage, methods for structural damage prognosis function mostly in batch mode operations. In this context, a class of mathematically consistent

algorithms has been developed that solely address damage detection in *real time*. Succinctly, FOEP is stated as the way of expressing the eigenstructure of the $(k + 1)^{th}$ step in terms of the eigenstructure at the k^{th} step as the $(k + 1)^{th}$ data streams in. This can be accomplished by structuring the EVD of the response covariance matrix in terms of the rank one perturbation of the ensuing eigenspace updates (Bhowmik et al. 2020a, 2020b; Bhowmik et al. 2019a, 2019b). The initial covariance estimate from the streaming data is first obtained. A key advantage to using FOEP lies in its inherent formulation where the eigenspace is updated at each instant of time instead of the covariance matrix, which contributes to the reduction of computational complexities. Tracking these eigenspace updates in real time with the use of certain pre-defined DSFs indicates structural damage in real time.

To explore FOEP, consider the eigenvalues of a perturbed matrix $C + \Delta C$ to be of the form $\Lambda + \alpha\alpha^T$, i.e., the *rank-one update* of the matrix Λ . Using the following definitions:

$$\begin{aligned} CV &= \Lambda V \\ (C + \Delta C)(V + \Delta V) &= (V + \Delta B)(\Lambda + \Delta\Lambda) \end{aligned} \quad (6.35)$$

where, ΔV and $\Delta\Lambda$ are the perturbation matrices. The EVD of the diagonally dominant term can be expanded as follows:

$$C + \Delta C = V\Lambda V^T + V\Delta\Lambda V^T + V\Delta\Lambda V^T + \Delta V^T\Lambda V^T + O(\epsilon^3) \quad (6.36)$$

Recognizing that $C = V\Lambda V^T$ and realizing the fact that $V^T = I$, the EVD of the perturbed matrix ΔC (ignoring second-order perturbation terms) can be written as:

$$\Delta C = \alpha\alpha^T = V\Delta\Lambda V^T + V\Delta\Lambda V^T + \Delta V^T\Lambda V^T + O(\epsilon^3) \quad (6.37)$$

The above expressions provide an insight into the data-driven nature of the FOEP strategy. Recent research has demonstrated the uniqueness of the FOEP technique to be applied for multivariate datasets—ranging from dynamic system monitoring to online surveillance and real-time compressive sensing.

6.6 Time-Frequency Methods

In the aerospace field, most dynamic structures show time-varying behaviour due to modifications in mass and/or geometry (Ni et al. 2016; Senba and Furuya 2008). And conventional identification methods that viably opt for stationarity of signals are sometimes not suitable for robust needs. Both parametric and non-parametric approaches have been considered for modelling and analysis of non-stationary signals in the narrowband domain. Under parameterized techniques, methods such as TARMA are noteworthy (Poulimenos and Fassois 2006; Spiridonakos and

Fassois 2009; Spiridonakos and Fassois 2012). Cases of non-parametric approaches require the time-frequency representations (TFRs) of the signal that not only accommodates information from the time domain but also combines the retrospect from the frequency domain. This provides more intuition of modal parameters such as natural frequencies, mode shapes and damping ratios which can be subsequently—and effectively—be used for damage detection purposes (Fan and Qiao 2011). Recent literature has amalgamated a mix of traditional linear algebra and derivate sub-band coding which essentially forms the opposite sides of the same coin—a complete damage identification framework—using a variety of transforms based on TFRs.

Due to the growing interconnections between the fields of linear algebra and sub-band coding, which are seen as two parts of a single framework (Vetterli and Kovačević 1995), a substantial number of transforms leading to different TFRs have been recently proposed in the literature.

6.6.1 Scalogram and Spectrogram

Predominant linear transforms involving STFT (Gabor 1946) and wavelet (Daubechies 1992) are most effective in identifying the state of structural damage from its inherent parameters. In a first of its kind, the STFT utilizes a complex function in fixed windows whereas, the WT effectively employs a family of more flexible interpretations and algebraic functions. In particular, the Short-Time Fourier Transform (STFT) of the signal $x(t)$ is defined as:

$$STFT_x(\omega, \tau) = \int_{-\infty}^{\infty} w^*(t - \tau)x(t)e^{-j\omega t} dt \quad (6.38)$$

where $w^*(t - \tau)$ indicates the complex conjugate of a window function $w(t - \tau)$, usually selected as a Gaussian window. Shifting this window in time allows the time-frequency description of the energy of a signal. The spectrogram is the energy distribution associated with the STFT, that is:

$$S(f, \tau) = |STFT(\omega, \tau)|^2 \quad (6.39)$$

Conversely, the continuous wavelet transform (CWT) of the signal $x(t)$ is defined as follows:

$$CWT_x(a, b) = \frac{1}{\sqrt{a}} \int_{\mathbb{R}} \psi^* \left(\frac{t-b}{a} \right) x(t) dt \quad (6.40)$$

where the factor $\frac{1}{\sqrt{a}}$ is to conserve the norm and $\psi_{a, b}(t)$ is a function that is scaled and translated to expand the signal in the time-scale domain. The energy distribution associated with the CWT is called a scalogram and its definition is similar to the one

of the spectrogram. Such techniques have been used by Nagarajaiah and Basu (2009) to successfully identify modal parameters in output-only conditions (i.e. using only the structural response). Moreover, Kijewski and Kareem (2003) have shown the ability of time-frequency representations to track accurately time-varying modal parameters.

The Wigner–Ville distribution (WVD) (Boashash 2003; Cohen 1995) has been increasingly adopted based on its inherent TFR fundamentals. Additionally, the approach does not employ any windowing function except for its autocorrelation, as follows:

$$WD_x(\omega, \tau) = \int_{-\infty}^{\infty} x\left(\tau + \frac{t}{2}\right)x^*\left(\tau - \frac{t}{2}\right)e^{-j\omega t} dt \quad (6.41)$$

However, multi-component practical applications are more involved due to their inherent bilinear structure that automatically creates cross-terms. This has the potential to undermine distribution readability and suffer from problems of closely spaced modes (in addition to vanishing and crossing modes of interest). In an attempt to improve these methods, reassignment and synchro squeezing have shown to be quite effective in identifying the underlying features of interest in the TF domain (Auger et al. 2014). Highly localized distributions can be derived using such techniques on spectrograms and scalograms. Of particular interest is SST—based on scalograms obtained through CWT—as an effective substitute to the traditional (yet effective) EMD (Daubechies et al. 2011).

Approach to elicit signal constituents corresponding to various instantaneous frequencies (which are aptly termed as intrinsic mode functions or IMFs). Without imposing a strong reliance on any basis function (Huang et al. 1998), the method is generally clubbed together with the Hilbert transform (HT)—resulting in the Hilbert–Huang Transform (HHT)—to identify patterns in the TF domain called the Hilbert spectrum. Although mode mixing has been identified as a typical cause of concern for EMD, the Ensemble Empirical Mode Decomposition (EEMD) has demonstrated an improvement using a noise-assisted procedure (Wu and Huang 2009).

Recently, multivariate techniques based on the concept of modulated multivariate oscillations were introduced (Lilly and Olhede 2012; Omidvarnia et al. 2012). Multivariate extensions of the WVD (Stanković et al. 2018), SST (Ahrabian et al. 2015) and EMD (Rehman and Mandić 2010) were recently presented.

In general, non-parametric methods require post-processing of some sort for modal parameter extraction in the TF domain. This is converse to the working of the EMD that extracts information from TFRs, which usually involves the decomposition into separate modal responses—mimicking a single degree of freedom system (Avenidaño et al. 2018; Iatsenko et al. 2016). Ridge extraction was typically performed to this aim, finding the local maxima of distributions over time (Delprat et al. 1992; Rankine et al. 2007). The basic structure of the TFR can be used to identify the modal parameters after extraction of the ridges. However, the frequency peaks associated with the information pattern might correspond to issues regarding complete reconstruction of decoupled modal responses.

Moreover, these procedures may suffer from issues related to non-stationary amplitudes, narrowband disturbances and noise (Staszewski 1998). Wang et al. (2013) proposed a dynamic optimization strategy that directs the use of penalty function for noisy signals in contrast to the use of the SVD approached by other authors in the same domain (Le and Paultre 2013; Özkurt and Savaci 2005). Quqa et al. (2020) proposed a decentralized algorithm for near-real-time extraction of modal responses suitable for wireless smart sensing nodes, based on a filter bank that must be updated at the occurrence of particular situations. In a further study, a fully-adaptive procedure called Decomposition Algorithm based on Modal Assurance (DAMA) was presented (Quqa et al. 2021), less sensitive to noise and narrowband disturbances. Also, image processing techniques can be applied to TFRs to extract useful information. De-noising of TFRs was first investigated by Liu et al. (2004) and progressed to attenuating the cross-terms of WVD (Gómez et al. 2011). Recent strategies has incorporated separation of modal components (Zhang et al. 2013) associated with the TF plane of the energy peaks of different vibratory modes. The watershed transform—a morphology inherent segmentation method (Vincent et al. 1991)—uses scalograms to separate narrowband seismic waves (Roueff et al. 2004). A persisting problem of these methods lie in the difficulty of effectively separating closely spaced modes of interest.

6.7 Drawbacks and Limitations

Some of the key limitations associated with the use of vibration-based methods are summarized as under:

1. In many cases of damage detection, the change in natural frequencies to determine the instant of damage is masked by the varying operational and environmental conditions. For this reason, successful damage detection facilities are carried out in a controlled environment and not implemented as field problems. To alleviate this drawback, a statistical damage detection model using a pattern recognition technique is needed to distinguish damage-induced changes from environment-induced changes. Damage markers should correctly describe the embedding of the environmental variables into the algorithm, which remains a field of development of the response-based methods.
2. Most of the vibration-based methods are currently offline in nature, i.e., they require batches of data to compare against a recorded set of data obtained from a pristine state of the structure. To track the changes in the structure as and when the vibration data streams in real time, the aforementioned methods need to be implemented in an adaptive fashion that could identify damage at a particular instant of time, without using pre-recorded data.
3. A limitation in response-based methods is the detection of damage for cases with *progressive damage* because of the time-varying nature of the vibrating system. Damage involving changes of stiffness over a period of time, progressively, is

captured only through a recursive implementation since the data from a particular instant is taken into consideration and compared against the data obtained from the previous timestamp.

4. Almost all the methods discussed in the previous section utilize the data gathered from a large number of sensors. In practical scenarios, the number of sensors instrumented is mostly less than the total number of active DOF due to cost considerations and accessibility issues. This requires an immediate development of algorithms that detect the exact instant of damage for underdetermined cases (where the number of sensors is less than the number of DOF) as well, in a single framework, utilizing the principles of recursion in a perturbation approach.

There are also opportunities. Response-based methods can be improved by benefiting from the more recent development of signal processing techniques, for example, Complete Ensemble Empirical Mode Decomposition (CEEMD) and its improvements (Colominas et al. 2014; Torres et al. 2011), empirical wavelet transform (Gilles 2013) and variational mode decomposition (Dragomiretskiy and Zosso 2014). Instead of extracting features using specific signal processing techniques, an alternative that is receiving more attention recently is through machine learning, in particular deep learning. Deep learning, e.g. using Deep Convolutional Neural Networks, provides a powerful tool to extract features in a data-driven manner, which often outperforms hand-crafted features (Lin et al. 2017). There are however still many open problems, including effective network architectures and interpretability of the results.

6.8 Case Studies

This section contains numerical and laboratory case studies relevant to aerospace applications. Following a brief description of the benchmark models, the main results obtained using some of the aforementioned identification methods are reported, together with the references to the related published works.

6.8.1 *Vibration-Based Damage Detection in a Composite Plate by Means of Acceleration Responses*

The case study presented in References (Limongelli 2017; Limongelli 2019) was reported herein, in which the SIM is applied to detect damage on a lab specimen. The investigated structure is a 500 cm \times 500 cm glass fibre/vinylester composite plate with 1 cm thickness. Free-free boundary conditions were simulated by suspending the plate with a bungee cord. The person holding the plate in the figure is for demonstration purposes only. Damage due to an impact is simulated through the removal of an area of material with dimensions 1.5 \times 1.5 cm and 0.6 cm depth. The

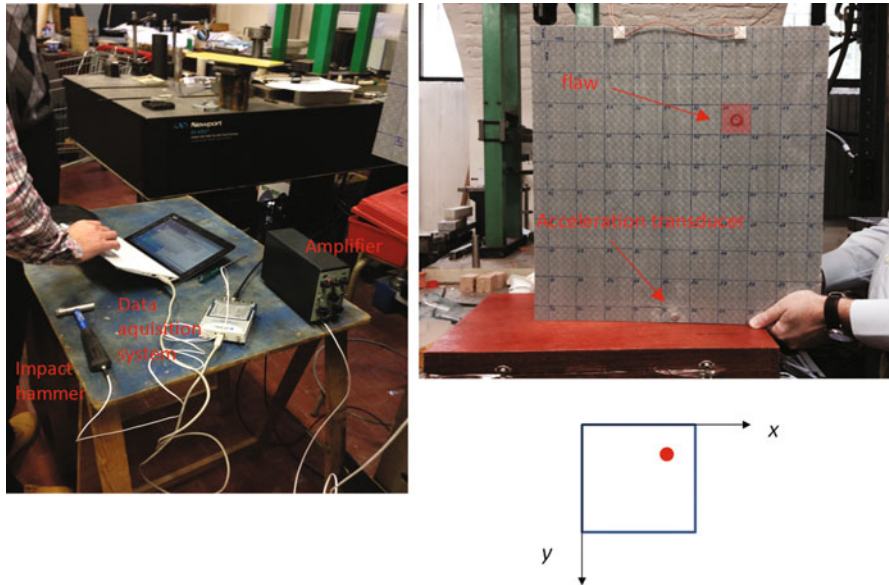


Fig. 6.3 Composite plate and flaw induced (Limongelli 2019)

plate was excited by an impulsive hammer at each point on the grid. The dynamic response of the plate in terms of acceleration is recorded in the reference and damaged configurations in all the nodes of a grid composed of 10×10 nodes. Figure 6.3 shows the location of damage and the layout of the grid. The Operational Deformed Shapes were determined as FRFs between each grid point and a reference one. The frequency range of the fundamental modes of the plate in the reference configuration is considered for the application of the SIM. Additional information on this experiment can be found in Limongelli (2017).

Figure 6.4 displays the results obtained by applying the SIM. The SIM can correctly localize damage since the damage index exhibits the highest values at the four nodes of the damaged elements. Some false alarm can be found at locations close to the flaw because of the interpolation process (Limongelli 2011). However, this phenomenon does not hamper the correct localization of damage since it influences locations close to the flaw only.

6.8.2 Numerical Comparison of Modal-Based Methods for Damage Detection

A numerical study has been carried out to compare the most popular modal-based methods. A laminated composite beam with length $l = 0.4$ m, thickness $h = 0.004$ m, width $b = 0.02$ m was considered. The following effective material properties were

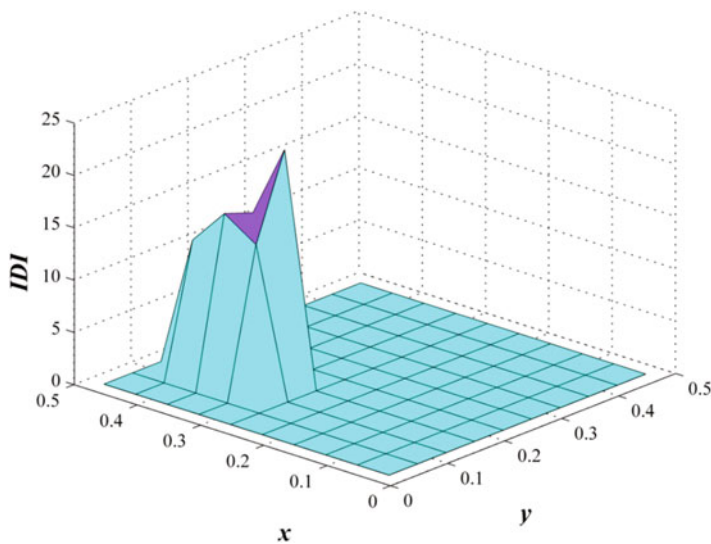


Fig. 6.4 Results for the damage induced in the composite plate (Limongelli 2019)

Table 6.1 Natural frequencies of the beam in the healthy and damaged conditions

Mode number	Frequencies Rad/s		Difference %
	Healthy	Damaged	
1	2.739284E+02	2.738425E+02	0.32
2	7.526039E+02	7.462084E+02	0.85
3	1.286927E+03	1.284473E+03	0.19
4	1.469070E+03	1.444934E+03	1.64
5	2.415473 +03	2.390013E+03	1.05

obtained and used in the calculations: Young modulus $E = 53.3 * 10^9 \text{ N/m}^2$, density $\rho = 1866 \text{ kg/m}^3$, Poisson’s ratio $\nu = 0.4$. It was considered that due to delamination in a small part of the beam the elastic modulus is reduced to $E_d = 37.33 * 10^9 \text{ N/m}^2$. The length of the damage is 3.75% of the total length of the beam.

Table 6.1 shows the computed first five natural frequencies of the beam. The computations were done by MSC NASTRAN software, discretizing the intact and damaged beams with 80 linear beam elements. The beam was modelled by the Timoshenko beam theory. It can be observed that the differences in the natural frequencies of healthy and damaged beams are very small—the first three ones are <1%. Such small damages cannot be identified experimentally on the base of the measured natural frequencies.

Figure 6.5 displays the most popular modal-based damage indices (based on modal displacement, modal slope, modal curvature, and strain energy) constructed for this beam. The location of the damage is highlighted in red (elements 17, 18 and 19). All considered damage indices have a maximum at the damage location. For modal shapes, modal slopes squares and even for the modal curvatures, some

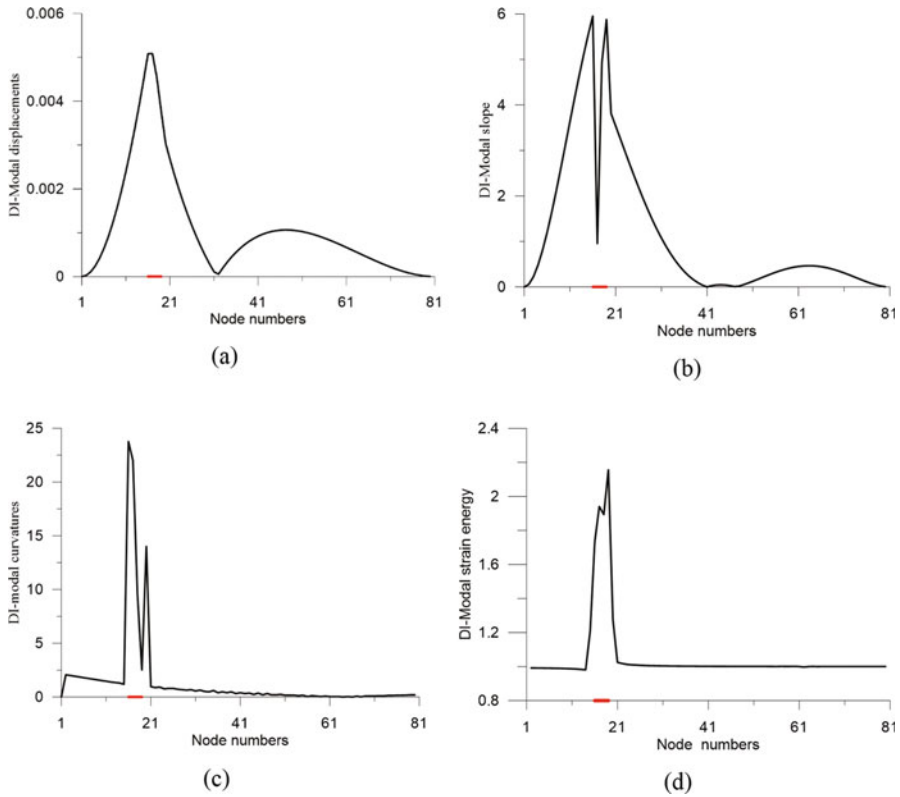


Fig. 6.5 Modal-based damage indexes for the damaged beam. (a) modal displacements DI; (b) modal slopes squares DI; (c) modal curvatures DI; (d) strain energy DI

additional peaks are observed in the curves of the damage indexes. This could confuse the potential user of these indexes, especially in the case of multiple damages. Moreover, the shapes of the peaks in the first two indexes are long-winded and could not be indicative of the extent of the damage. The best possibility to predict the damage are its location and extend of the damage index based on the modal strain energy. The considered indices are constructed on the base of the first normal mode.

6.8.3 Vibration-Based Monitoring of a Scaled Wind Turbine Blade by Means of Acceleration and Strain Responses

This case study reports the analyses presented in Jaksic et al. (2016a) where a 1.4 m-long polypropylene wind turbine blade (1.7 kg) is monitored with strain gauges, accelerometer (Microstrain G-Link) and a laser Doppler vibrometer (Polytec

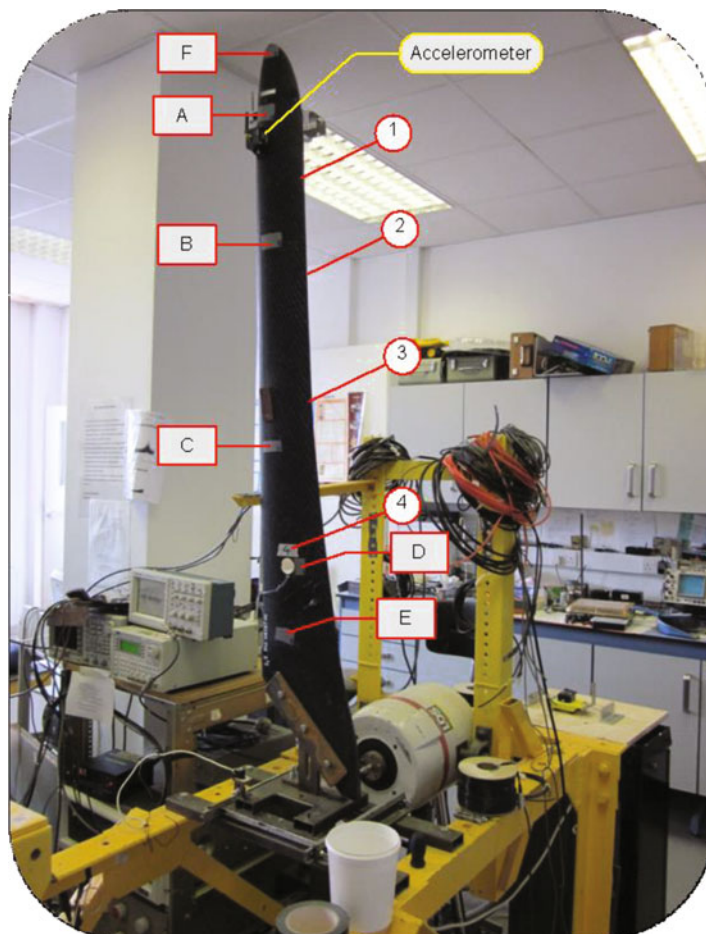


Fig. 6.6 Monitoring of a wind turbine blade in a laboratory setup using strain gauges, accelerometer and laser Doppler vibrometer (adapted from Jaksic et al. 2016b)

RSV-150), as shown in Fig. 6.6. The blade was excited through an electrodynamic shaker, clamped at base, through harmonic resonance (2 Hz–7 Hz), sine sweep (3 Hz–5 Hz) and white noise in keeping with the natural frequency of the blade. Examples of time-domain responses from these sensors are provided in Fig. 6.7a–c.

A delay vector variance analysis (Jaksic et al. 2016a) is employed as a marker for monitoring this blade under various excitations and compare signal nonlinearities of the responses with respect to a Gaussian benchmark with a time lag equal to unity and the embedding parameter set to 3, for computational efficiency, convenience and comparability to other results. Figure 6.8 presents an example of how such

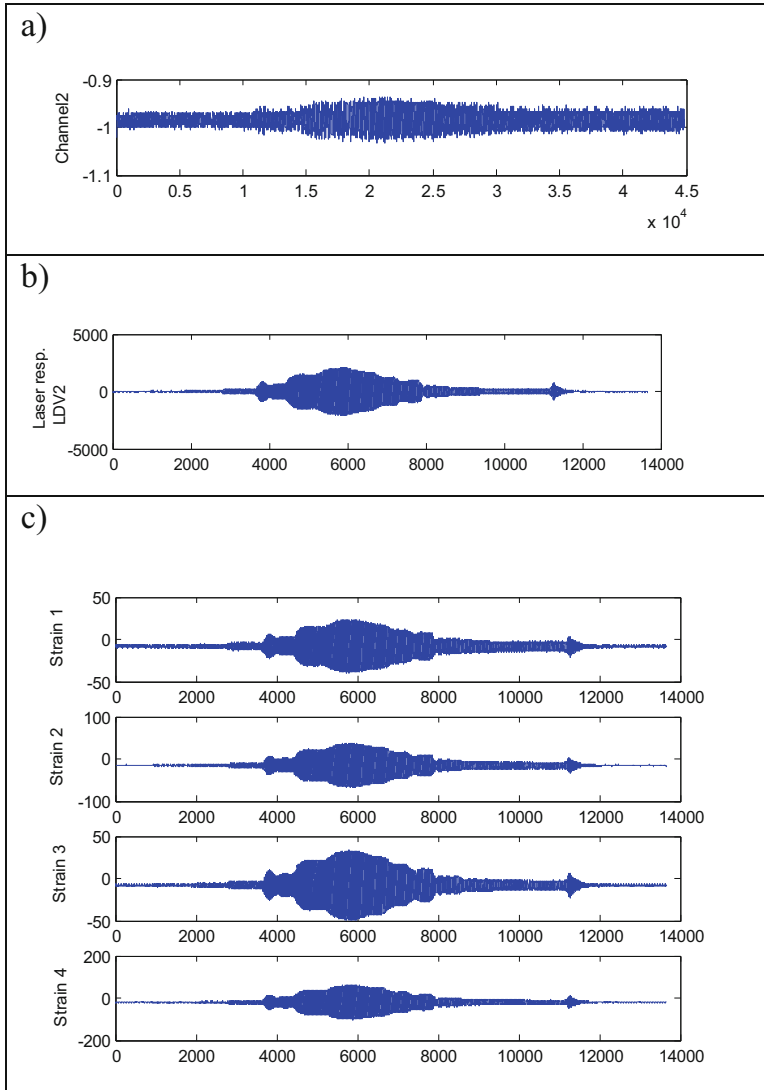


Fig. 6.7 Dynamic responses of a scaled wind turbine blade using from (a) accelerometer, (b) laser Doppler vibrometer and (c) strain gauges.

monitoring can effectively consider several sensors together for various types of excitations. Similar monitoring is also possible for floating wind turbine platforms (Jaksic et al. 2015a), even with control (Jaksic et al. 2015b) and possibly with damage (O'Donnell et al. 2020).

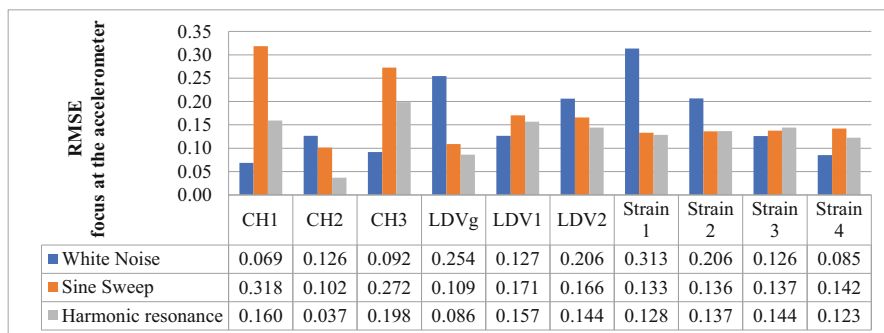


Fig. 6.8 A delay vector variance–based marker driven comparative analysis of a scaled wind turbine blade responses using various sensors and excitation techniques.

6.9 Conclusions

In this chapter, several methods for identification of losses of stiffness using the response to vibrations are presented. The merits, advantages and the drawbacks and limitations of the presented approaches were discussed. These are methods that enable to detect and localize damage using global parameters of the structure and without requiring any prior knowledge about its location. The limitation that descends from the global nature of the damage features is the lower sensitivity to small damages of these approaches with respect to local non destructive damage detection methods. Response-based methods are more feasible for online real-time damage identification purposes with respect to model-based approaches thanks to the lower computational efforts they require. However, the results provided by such methods may prove to be more affected by environmental and operational factors that have to be carefully accounted for in the analysis of the damage features.

When this is done, response-based methods can be reliably applied to detect and localize damage whereas the assessment of type and severity of damage usually requires the development of a calibrated numerical model.

References

- Abdel Wahab MM, De Roeck G (1999) Damage detection in bridges using modal curvatures: application to a real damage scenario. *J Sound Vib.* <https://doi.org/10.1006/jsvi.1999.2295>
- Achilli A, Bernagozzi G, Betti R, Diotallevi PP, Landi L, Quqa S, Tronci EM (2020) On the use of multivariate autoregressive models and outlier analysis for vibration-based damage detection and localization. *Smart Structures and Systems*, Under review
- Ahrabian A, Looney D, Stanković L, Mandić DP (2015) Synchrosqueezing-based time-frequency analysis of multivariate data. *Signal Process* 106:331–341. <https://doi.org/10.1016/j.sigpro.2014.08.010>
- Allemang RJ, Brown DL (1982) Correlation coefficient for modal vector analysis. In: *Proceedings of the international modal analysis conference & exhibit*

- Alvin KF, Robertson AN, Reich GW, Park KC (2003) Structural system identification: from reality to models. *Comput Struct*. [https://doi.org/10.1016/S0045-7949\(03\)00034-8](https://doi.org/10.1016/S0045-7949(03)00034-8)
- Antoni J (2005) Blind separation of vibration components: principles and demonstrations. *Mech Syst Signal Process*. <https://doi.org/10.1016/j.ymsp.2005.08.008>
- Auger F, Flandrin P, Lin Y, McLaughlin S, Oberlin T, Wu H, Auger F, Flandrin P, Lin Y, McLaughlin S, Meignen S (2014) Time-frequency reassignment and synchrosqueezing: an overview. *IEEE Signal Process Mag* 30(6). <https://doi.org/10.1109/MSP.2013.2265316>
- Avendaño LE, Avendaño-Valencia LD, Delgado-Trejos E (2018) Diagonal time dependent state space models for modal decomposition of non-stationary signals. *Signal Process* 147:208–223. <https://doi.org/10.1016/j.sigpro.2018.01.031>
- Balmès É, Basseville M, Bourquin F, Mevel L, Nasser H, Treysède F (2008) Merging sensor data from multiple temperature scenarios for vibration monitoring of civil structures. *Struct Health Monit*. <https://doi.org/10.1177/1475921708089823>
- Basseville M, Benveniste A, Gach-Devauchelle B, Goursat M, Bonnecase D, Dorey P, Prevosto M, Olagnon M (1993) In situ damage monitoring in vibration mechanics: diagnostics and predictive maintenance. *Mech Syst Signal Process*. <https://doi.org/10.1006/mssp.1993.1023>
- Basseville M, Benveniste A, Goursat M, Hermans L, Mevel L, Van der Auweraer H (2001) Output-only subspace-based structural identification: from theory to industrial testing practice. *J Dyn Syst Measurement Control Trans ASME*. <https://doi.org/10.1115/1.1410919>
- Basseville M, Mevel L, Goursat M (2004) Statistical model-based damage detection and localization: subspace-based residuals and damage-to-noise sensitivity ratios. *J Sound Vib*. <https://doi.org/10.1016/j.jsv.2003.07.016>
- Belouchrani A, Abed-Meraim K, Cardoso JF, Moulines E (1997) A blind source separation technique using second-order statistics. *IEEE Trans Signal Process*. <https://doi.org/10.1109/78.554307>
- Bhowmik B, Krishnan M, Hazra B, Pakrashi V (2019a) Real-time unified single- and multi-channel structural damage detection using recursive singular spectrum analysis. *Struct Health Monit*. <https://doi.org/10.1177/1475921718760483>
- Bhowmik B, Tripura T, Hazra B, Pakrashi V (2019b) First-order Eigen-perturbation techniques for real-time damage detection of vibrating. *Theory and Applications. Applied Mechanics Reviews, Systems*. <https://doi.org/10.1115/1.4044287>
- Bhowmik B, Tripura T, Hazra B, Pakrashi V (2020a) Real time structural modal identification using recursive canonical correlation analysis and application towards online structural damage detection. *J Sound Vib*. <https://doi.org/10.1016/j.jsv.2019.115101>
- Bhowmik B, Tripura T, Hazra B, Pakrashi V (2020b) Robust linear and nonlinear structural damage detection using recursive canonical correlation analysis. *Mech Syst Signal Process*. <https://doi.org/10.1016/j.ymsp.2019.106499>
- Boashash B (2003) Theory of quadratic TFDs. *A Comprehensive Reference, Time Frequency Analysis*, pp 59–81. <https://doi.org/10.1016/B978-008044335-5/50024-3>
- Brincker R, Ventura CE (2015) Introduction to operational modal analysis. pp 1–360. <https://doi.org/10.1002/9781118535141>
- Carniel R, Barazza F, Tàrraga M, Ortiz R (2006) On the singular values decoupling in the singular spectrum analysis of volcanic tremor at Stromboli. *Nat Hazards Earth Syst Sci*. <https://doi.org/10.5194/nhess-6-903-2006>
- Cawley P, Adams RD (1979) The location of defects in structures from measurements of natural frequencies. *J Strain Anal Eng Design* 14(2):49–57. <https://doi.org/10.1243/03093247V142049>
- Chang CC, Chen LW (2005) Detection of the location and size of cracks in the multiple cracked beam by spatial wavelet based approach. *Mech Syst Signal Process*. <https://doi.org/10.1016/j.ymsp.2003.11.001>
- Chao SH, Loh CH (2014) Application of singular spectrum analysis to structural monitoring and damage diagnosis of bridges. *Struct Infrastruct Eng*. <https://doi.org/10.1080/15732479.2012.758643>
- Ciambella J, Vestroni F (2015) The use of modal curvatures for damage localization in beam-type structures. *J Sound Vib*. <https://doi.org/10.1016/j.jsv.2014.11.037>

- Cichocki A, Amari S (2002) Adaptive blind signal and image processing. In: Adaptive blind signal and image processing. <https://doi.org/10.1002/0470845899>
- Cohen L (1995) Time frequency analysis: theory and applications. p 299
- Colominas MA, Schlotthauer G, Torres ME (2014) Improved complete ensemble. A suitable tool for biomedical signal processing. Biomedical Signal Processing and Control, EMD. <https://doi.org/10.1016/j.bspc.2014.06.009>
- Cornwell P, Doebling SW, Farrar CR (1999) Application of the strain energy damage detection method to plate-like structures. J Sound Vib. <https://doi.org/10.1006/jsvi.1999.2163>
- Datteo A, Busca G, Quattromani G, Cigada A (2018) On the use of AR models for SHM: a global sensitivity and uncertainty analysis framework. Reliab Eng Syst Saf 170:99–115. <https://doi.org/10.1016/j.res.2017.10.017>
- Daubechies I (1992) Ten lectures on wavelets. In Ten Lectures on Wavelets. <https://doi.org/10.1137/1.9781611970104>
- Daubechies I, Lu J, Wu HT (2011) Synchrosqueezed wavelet transforms: an empirical mode decomposition-like tool. Appl Comput Harmon Anal 30(2):243–261. <https://doi.org/10.1016/j.acha.2010.08.002>
- De Boe P, Golinval JC (2003) Principal component analysis of a piezosensor array for damage localization. Struct Health Monit. <https://doi.org/10.1177/1475921703002002005>
- De Oliveira MA, Inman DJ (2015) PCA-based method for damage detection exploring electromechanical impedance in a composite beam. Structural health monitoring 2015: system reliability for verification and implementation. In: Proceedings of the 10th international workshop on structural health monitoring, IWSHM 2015. <https://doi.org/10.12783/shm2015/94>.
- Delprat N, Guillemain P, Escudie B, Kronland-Martinet R, Tchamitchian P, Torresani B (1992) Asymptotic wavelet and Gabor analysis: extraction of instantaneous frequencies. IEEE Trans Inf Theory 38(2):644–664. <https://doi.org/10.1109/18.119728>
- Deraemaeker A, Reynders E, De Roeck G, Kullaa J (2006) Vibration based SHM: comparison of the performance of modal features vs features extracted from spatial filters under changing environmental conditions. In: Proceedings of ISMA2006: international conference on noise and vibration engineering
- Doebling SWS, Farrar CRC, Prime MBM, Shevitz DWD (1996) Damage identification and health monitoring of structural and mechanical systems from changes in their vibration characteristics: a literature review. Los Alamos National Laboratory. <https://doi.org/10.2172/249299>
- Dragomiretskiy K, Zosso D (2014) Variational mode decomposition. IEEE Trans Signal Process. <https://doi.org/10.1109/TSP.2013.2288675>
- Dutta A, Talukdar S (2004) Damage detection in bridges using accurate modal parameters. Finite Elem Anal Des. [https://doi.org/10.1016/S0168-874X\(02\)00227-5](https://doi.org/10.1016/S0168-874X(02)00227-5)
- Elsner JB, Tsonis A a (1996) Singular Spectrum analysis - a new tool in time series analysis. Springer, Cham
- Entezami A, Shariatmadar H (2019) Damage localization under ambient excitations and non-stationary vibration signals by a new hybrid algorithm for feature extraction and multivariate distance correlation methods. Struct Health Monit 18(2):347–375. <https://doi.org/10.1177/1475921718754372>
- Fan W, Qiao P (2011) Vibration-based damage identification methods: a review and comparative study. Struct Health Monit 10(1):83–111. <https://doi.org/10.1177/1475921710365419>
- Farrar CR, James GH (1997) System identification from ambient vibration measurements on a bridge. J Sound Vib. <https://doi.org/10.1006/jsvi.1997.0977>
- Farrar CR, Baker WE, Dove RC (1994) Dynamic parameter similitude for concrete models. ACI Struct J. 10.14359/4500
- Farrar CR, Worden K, Todd MD, Park G, Nichols J, Adams DE, Bement MT, Farinholt K (2007) Nonlinear system identification for damage detection. LA14353 Los Alamos National Laboratories, Los Alamos NM
- Feeny BF (2002) On the proper orthogonal modes and normal modes of continuous vibration systems. J Vib Acoustics Trans ASME. <https://doi.org/10.1115/1.1421352>

- Feeny BF, Liang Y (2003) Interpreting proper orthogonal modes of randomly excited vibration systems. *J Sound Vib.* [https://doi.org/10.1016/S0022-460X\(02\)01265-8](https://doi.org/10.1016/S0022-460X(02)01265-8)
- Fritzen GP (1986) Identification of mass, damping, and stiffness matrices of mechanical systems. *J Vib Acoustics Trans ASME.* <https://doi.org/10.1115/1.3269310>
- Fritzen CP, Kraemer P (2009) Self-diagnosis of smart structures based on dynamical properties. *Mech Syst Signal Process.* <https://doi.org/10.1016/j.ymsp.2009.01.006>
- Fritzen CP, Jennewein D, Kiefer T (1998) Damage detection based on model updating methods. *Mech Syst Signal Process.* <https://doi.org/10.1006/mssp.1997.0139>
- Gabor D (1946) Theory of communication. Part 1: the analysis of information. *J Inst Electrical Eng Part III Radio Commun Eng* 93(26):429–441. <https://doi.org/10.1049/ji-3-2.1946.0074>
- Gharibnezhad F, Mujica LE, Rodellar J (2015) Applying robust variant of principal component analysis as a damage detector in the presence of outliers. *Mech Syst Signal Process.* <https://doi.org/10.1016/j.ymsp.2014.05.032>
- Gilles J (2013) Empirical wavelet transform. *IEEE Trans Signal Process.* <https://doi.org/10.1109/TSP.2013.2265222>
- Giordano PF, Limongelli MP (2020) Response-based time-invariant methods for damage localization on a concrete bridge. *Struct Concr* 21(4):1254–1271. <https://doi.org/10.1002/suco.202000013>
- Giraldo DF, Dyke SJ, Caicedo JM (2006) Damage detection accommodating varying environmental conditions. *Struct Health Monit Int J* 5(2):155–172. <https://doi.org/10.1177/1475921706057987>
- Gómez S, Naranjo V, Miralles R (2011) Removing interference components in time-frequency representations using morphological operators. *J Vis Commun Image Represent* 22(5):401–410. <https://doi.org/10.1016/j.jvcir.2011.03.007>
- Görl E, Link M (2001) Identification of damage parameters of a full-scale steel structure damaged by seismic loading. *Smart Mater Struct.* <https://doi.org/10.1088/0964-1726/10/3/306>
- Groth A, Ghil M (2015) Monte Carlo singular spectrum analysis (SSA) revisited: detecting oscillator clusters in multivariate datasets. *J Clim.* <https://doi.org/10.1175/JCLI-D-15-0100.1>
- Güemes JA, Menendez JM, Frövel M, Fernandez I, Pintado JM (2001) Experimental analysis of buckling in aircraft skin panels by fibre optic sensors. *Smart Mater Struct.* <https://doi.org/10.1088/0964-1726/10/3/310>
- Güemes A, Fernandez-Lopez A, Pozo AR, Sierra-Pérez J (2020) Structural health monitoring for advanced composite. A review. *J Composites Sci Struct.* <https://doi.org/10.3390/jcs4010013>
- Gul M, Necati Catbas F (2009) Statistical pattern recognition for structural health monitoring using time series modeling: theory and experimental verifications. *Mech Syst Signal Process* 23(7):2192–2204. <https://doi.org/10.1016/j.ymsp.2009.02.013>
- Han S, Feeny B (2003) Application of proper orthogonal decomposition to structural vibration analysis. *Mech Syst Signal Process.* <https://doi.org/10.1006/mssp.2002.1570>
- Hassani H (2010) A brief introduction to singular spectrum analysis. Paper in Pdf Version Available at: www.Ssa.Cf.Ac.uk
- Hassani H, Xu Z, Zhigljavsky A (2011) Singular spectrum analysis based on the perturbation theory. *Real world applications, nonlinear analysis.* <https://doi.org/10.1016/j.nonrwa.2011.03.020>
- Hazra B, Sadhu A, Roffel AJ, Narasimhan S (2012) Hybrid time-frequency blind source separation towards ambient system identification of structures. *Comput Aided Civ Inf Eng.* <https://doi.org/10.1111/j.1467-8667.2011.00732.x>
- Hot A, Kerschen G, Foltête E, Cogan S (2012) Detection and quantification of non-linear structural behavior using principal component analysis. *Mech Syst Signal Process.* <https://doi.org/10.1016/j.ymsp.2011.06.006>
- Hu JW, Kaloop MR (2015) Single input-single output identification thermal response model of bridge using nonlinear ARX with wavelet networks. *J Mech Sci Technol* 29(7):2817–2826. <https://doi.org/10.1007/s12206-015-0610-3>

- Huang NE, Shen Z, Long SR, Wu MC, Snin HH, Zheng Q, Yen NC, Tung CC, Liu HH (1998) The empirical mode decomposition and the Hubert spectrum for nonlinear and non-stationary time series analysis. *Proc R Soc A Math Phys Eng Sci* 454(1971):903–995. <https://doi.org/10.1098/rspa.1998.0193>
- Hyvärinen A, Oja E (2000) Independent component analysis: algorithms and applications. *Neural Netw.* [https://doi.org/10.1016/S0893-6080\(00\)00026-5](https://doi.org/10.1016/S0893-6080(00)00026-5)
- Iatsenko D, McClintock PVE, Stefanovska A (2016) Extraction of instantaneous frequencies from ridges in time-frequency representations of signals. *Signal Process* 125:290–303. <https://doi.org/10.1016/j.sigpro.2016.01.024>
- Imregun M, Visser WJ (1991) A review of model updating techniques *The Shock and Vibration Digest*
- Jaksic V, O’Shea R, Cahill P, Murphy J, Mandic DP, Pakrashi V (2015a) Dynamic response signatures of a scaled model platform for floating wind turbines in an ocean wave basin. *Philos Trans R Soc A Math Phys Eng Sci* 373(2035). <https://doi.org/10.1098/rsta.2014.0078>
- Jaksic V, Wright CS, Murphy J, Afeef C, Ali SF, Mandic DP, Pakrashi V (2015b) Dynamic response mitigation of floating wind turbine platforms using tuned liquid column dampers. *Philos Trans R Soc A Math Phys Eng Sci* 373(2035). <https://doi.org/10.1098/rsta.2014.0079>
- Jaksic V, Mandic DP, Karoumi R, Basu B, Pakrashi V (2016a) Estimation of nonlinearities from pseudodynamic and dynamic responses of bridge structures using the delay vector variance method. *Stat Mech Appl Phys A*. p 441. <https://doi.org/10.1016/j.physa.2015.08.026>
- Jaksic V, Mandic DP, Ryan K, Basu B, Pakrashi V (2016b) A comprehensive study of the delay vector variance method for quantification of nonlinearity in dynamical systems. *R Soc Open Sci* 3(1). <https://doi.org/10.1098/rsos.150493>
- Jolliffe IT (1986) *Principal component analysis and factor analysis.* https://doi.org/10.1007/978-1-4757-1904-8_7
- Kappagantu RV, Feeny BF (2000a) Part 1: dynamical characterization of a frictionally excited beam. *Nonlinear Dyn.* <https://doi.org/10.1023/A:1008344005183>
- Kappagantu RV, Feeny BF (2000b) Part 2: proper orthogonal modal modeling of a frictionally excited beam. *Nonlinear Dyn.* <https://doi.org/10.1023/A:1008303406091>
- Kerschen G, Golinval JC (2003) Physical interpretation of the proper orthogonal modes using the singular value decomposition. *J Sound Vib.* <https://doi.org/10.1006/jsvi.2001.3930>
- Kerschen G, Golinval JC, Vakakis AF, Bergman LA (2005) The method of proper orthogonal decomposition for dynamical characterization and order reduction of mechanical systems: an overview. *Nonlinear Dyn.* <https://doi.org/10.1007/s11071-005-2803-2>
- Kijewski T, Kareem A (2003) Wavelet transforms for system identification in civil engineering. *Comput Aided Civ Inf Eng* 18(5):339–355. <https://doi.org/10.1111/1467-8667.t01-1-00312>
- Kilundu B, Chiementin X, Dehombreux P (2011) Singular spectrum analysis for bearing defect detection. *J Vib Acoustics Trans ASME.* <https://doi.org/10.1115/1.4003938>
- Kim JH, Jeon HS, Lee CW (1992) Application of the modal assurance criteria for detecting and locating structural faults. In: 10th International modal analysis conference, San Diego, CA, USA
- Koh BH, Dharap P, Nagarajaiah S, Phan MQ (2005) Real-time structural damage monitoring by input error function. *AIAA J.* <https://doi.org/10.2514/1.14008>
- Kunwar A, Jha R, Whelan M, Janoyan K (2013) Damage detection in an experimental bridge model using Hilbert-Huang transform of transient vibrations. *Struct Control Health Monit.* <https://doi.org/10.1002/stc.466>
- Kyriazoglou C, Le Page BH, Guild FJ (2004) Vibration damping for crack detection in composite laminates. *Compos A: Appl Sci Manuf.* <https://doi.org/10.1016/j.compositesa.2004.01.003>
- Lakshmi K, Rao ARM, Gopalakrishnan N (2017) Singular spectrum analysis combined with ARMAX model for structural damage detection. *Struct Control Health Monit.* <https://doi.org/10.1002/stc.1960>
- Le TP, Paultre P (2013) Modal identification based on the time-frequency domain decomposition of unknown-input dynamic tests. *Int J Mech Sci* 71:41–50. <https://doi.org/10.1016/j.ijmesci.2013.03.005>

- Lee DS, Park JM, Vanrolleghem PA (2005) Adaptive multiscale principal component analysis for on-line monitoring of a sequencing batch reactor. *J Biotechnol.* <https://doi.org/10.1016/j.jbiotec.2004.10.012>
- Li W, Yue HH, Valle-Cervantes S, Qin SJ (2000) Recursive PCA for adaptive process monitoring. *J Process Control.* [https://doi.org/10.1016/S0959-1524\(00\)00022-6](https://doi.org/10.1016/S0959-1524(00)00022-6)
- Li HL, Deng X, Dai H (2007) Structural damage detection using the combination method of EMD and wavelet analysis. *Mech Syst Signal Process.* <https://doi.org/10.1016/j.ymssp.2006.05.001>
- Li D, Xu Z, Ostachowicz W, Cao M, Liu J (2020) Identification of multiple cracks in noisy conditions using scale-correlation-based multiscale product of SWPT with laser vibration measurement. *Mech Syst Signal Process.* <https://doi.org/10.1016/j.ymssp.2020.106889>
- Lilly JM, Olhede SC (2012) Analysis of modulated multivariate oscillations. *IEEE Trans Signal Process* 60(2):600–612. <https://doi.org/10.1109/TSP.2011.2173681>
- Limongelli MP (2003) Optimal location of sensors for reconstruction of seismic responses through spline function interpolation. *Earthq Eng Struct Dyn.* <https://doi.org/10.1002/eqe.262>
- Limongelli MP (2010) Frequency response function interpolation for damage detection under changing environment. *Mech Syst Signal Process* 24(8):2898–2913. <https://doi.org/10.1016/j.ymssp.2010.03.004>
- Limongelli MP (2011) The interpolation damage detection method for frames under seismic excitation. *J Sound Vib.* <https://doi.org/10.1016/j.jsv.2011.06.012>
- Limongelli MP (2017) The modal surface interpolation method for damage localization. *J Phys Conf Ser.* <https://doi.org/10.1088/1742-6596/842/1/012004>
- Limongelli MP (2019) The surface interpolation method for damage localization in plates. *Mech Syst Signal Process.* <https://doi.org/10.1016/j.ymssp.2018.08.032>
- Limongelli MP, Giordano PF (2020) Vibration-based damage indicators: a comparison based on information entropy. *J Civ Struct Heal Monit* 10(2). <https://doi.org/10.1007/s13349-020-00381-9>
- Lin RJ, Cheng FP (2008) Multiple crack identification of a free-free beam with uniform material property variation and varied noised frequency. *Eng Struct.* <https://doi.org/10.1016/j.engstruct.2007.03.017>
- Lin YZ, Nie ZH, Ma HW (2017) Structural damage detection with automatic feature-extraction through deep learning. *Comput Aided Civ Inf Eng.* <https://doi.org/10.1111/mice.12313>
- Liu WM, Bastante VJR, Rodriguez FR, Evans NWD, Mason JSD (2004) Morphological filtering of spectrograms for automatic speech recognition. In: Proceedings of the fourth IASTED international conference on visualization, imaging, and image processing, pp 546–549
- Liu K, Law SS, Xia Y, Zhu XQ (2014) Singular spectrum analysis for enhancing the sensitivity in structural damage detection. *J Sound Vib.* <https://doi.org/10.1016/j.jsv.2013.09.027>
- Ljung L (1998) System identification: theory for the user, vol 2. Pearson Education
- Lovera M, Gustafsson T, Verhaegen M (2000) Recursive subspace identification of linear and non-linear Wiener state-space models. *Automatica.* [https://doi.org/10.1016/S0005-1098\(00\)00103-5](https://doi.org/10.1016/S0005-1098(00)00103-5)
- Lysgaard P, Amador SDR, Nielsen ST, Katsanos E, Brincker R (2021) Vibration-based damage detection using input-output and output-only environmental models: a comparison. In: Conference proceedings of the society for experimental mechanics series, pp 29–38. https://doi.org/10.1007/978-3-030-47634-2_5
- Maia NMM, Silva JMM, Almas EAM, Sampaio RPC (2003) Damage detection in structures: from mode shape to frequency response function methods. *Mech Syst Signal Process.* <https://doi.org/10.1006/mssp.2002.1506>
- Manoach E, Samborski S, Mitura A, Warminski J (2012a) Vibration based damage detection in composite beams under temperature variations using Poincaré maps. *Int J Mech Sci.* <https://doi.org/10.1016/j.ijmecsci.2012.06.006>
- Manoach E, Warminski J, Mitura A, Samborski S (2012b) Dynamics of a composite Timoshenko beam with delamination. *Mech Res Commun.* <https://doi.org/10.1016/j.mechrescom.2012.08.008>
- Manoach EMIL, Warminski JERZY, Warminska A (2016a) Large amplitude vibrations of heated Timoshenko beams with delamination. *Proc Inst Mech Eng C J Mech Eng Sci.* <https://doi.org/10.1177/0954406215570702>

- Manoach E, Warminski J, Kloda L, Teter A (2016b) Vibration based methods for damage detection in structures. MATEC Web of Conferences. <https://doi.org/10.1051/mateconf/20168305007>
- Manoach E, Warminski J, Kloda L, Teter A (2017) Numerical and experimental studies on vibration based methods for detection of damage in composite beams. Compos Struct. <https://doi.org/10.1016/j.compstruct.2017.03.005>
- Manson G (2002) Identifying damage sensitive, environment insensitive features for damage detection. In: Proceedings of the 3rd international conference on identification in engineering systems, pp 187–197
- Mével L, Hermans L, Van Der Auweraer H (1999) Application of a subspace-based fault detection method to industrial structures. Mech Syst Signal Process. <https://doi.org/10.1006/mssp.1999.1247>
- Misra M, Yue HH, Qin SJ, Ling C (2002) Multivariate process monitoring and fault diagnosis by multi-scale PCA. Comput Chem Eng. [https://doi.org/10.1016/S0098-1354\(02\)00093-5](https://doi.org/10.1016/S0098-1354(02)00093-5)
- Montalvão D, Maia NMM, Ribeiro AMR (2006) A review of vibration-based structural health monitoring with special emphasis on composite materials. Shock Vib Digest. <https://doi.org/10.1177/0583102406065898>
- Mosavi AA, Dickey D, Seracino R, Rizkalla S (2012) Identifying damage locations under ambient vibrations utilizing vector autoregressive models and Mahalanobis distances. Mech Syst Signal Process 26(1):254–267. <https://doi.org/10.1016/j.ymsp.2011.06.009>
- Mottershead JE, Friswell MI (1993) Model updating in structural dynamics: a survey. J Sound Vib. <https://doi.org/10.1006/jsvi.1993.1340>
- Mujica LE, Ruiz M, Pozo F, Rodellar J, Güemes A (2014) A structural damage detection indicator based on principal component analysis and statistical hypothesis testing. Smart Mater Struct. <https://doi.org/10.1088/0964-1726/23/2/025014>
- Murotani K, Sugihara K (2005) New spectral decomposition method for three-dimensional shape models and its applications. J Comput Inf Sci Eng. <https://doi.org/10.1115/1.2052849>
- Nagarajaiah S, Basu B (2009) Output only modal identification and structural damage detection using time frequency & wavelet techniques. Earthq Eng Eng Vib 8(4):583–605. <https://doi.org/10.1007/s11803-009-9120-6>
- Nair KK, Kiremidjian AS, Law KH (2006) Time series-based damage detection and localization algorithm with application to the ASCE benchmark structure. J Sound Vib 291(1–2):349–368. <https://doi.org/10.1016/j.jsv.2005.06.016>
- Nguyen VH, Golinval JC (2010) Fault detection based on kernel principal component analysis. Eng Struct. <https://doi.org/10.1016/j.engstruct.2010.08.012>
- Ni Z, Mu R, Xun G, Wu Z (2016) Time-varying modal parameters identification of a spacecraft with rotating flexible appendage by recursive algorithm. Acta Astronaut 118:49–61. <https://doi.org/10.1016/j.actaastro.2015.10.001>
- O'Donnell D, Murphy J, Pakrashi V (2020) Damage monitoring of a catenary moored spar platform for renewable energy devices. Energies 13(14):3631. <https://doi.org/10.3390/en13143631>
- Omidvarnia A, Boashash B, Azemi G, Colditz P, Vanhatalo S (2012) Generalised phase synchrony within multivariate signals: an emerging concept in time-frequency analysis. In: ICASSP, IEEE international conference on acoustics, speech and signal processing – proceedings, pp 3417–3420. <https://doi.org/10.1109/ICASSP.2012.6288650>
- Ostachowicz WM, Krawczuk M (1990) Vibration analysis of a cracked beam. Comput Struct. [https://doi.org/10.1016/0045-7949\(90\)90123-J](https://doi.org/10.1016/0045-7949(90)90123-J)
- Özkurt N, Savaci FA (2005) Determination of wavelet ridges of nonstationary signals by singular value decomposition. IEEE Trans Circuits Syst II Express Briefs 52(8):480–485. <https://doi.org/10.1109/TCSII.2005.849041>
- Pai PF, Jin S (2000) Locating structural damage by detecting boundary effects. J Sound Vib. <https://doi.org/10.1006/jsvi.1999.2654>
- Pandey AK, Biswas M (1994) Damage detection in structures using changes in flexibility. J Sound Vib. <https://doi.org/10.1006/jsvi.1994.1002>
- Pandey AK, Biswas M, Samman MM (1991) Damage detection from changes in curvature mode shapes. J Sound Vib. [https://doi.org/10.1016/0022-460X\(91\)90595-B](https://doi.org/10.1016/0022-460X(91)90595-B)

- Papadimitriou C (2004) Optimal sensor placement methodology for parametric identification of structural systems. *J Sound Vib.* <https://doi.org/10.1016/j.jsv.2003.10.063>
- Papadimitriou C, Lombaert G (2012) The effect of prediction error correlation on optimal sensor placement in structural dynamics. *Mech Syst Signal Process.* <https://doi.org/10.1016/j.ymsp.2011.05.019>
- Papadimitriou C, Beck JL, Au SK (2000) Entropy-based optimal sensor location for structural model updating. *JVC/J Vib Contr.* <https://doi.org/10.1177/107754630000600508>
- Papadimitriou C, Beck JL, Katafygiotis LS (2001) Updating robust reliability using structural test data. *Probabilistic Eng Mech.* [https://doi.org/10.1016/S0266-8920\(00\)00012-6](https://doi.org/10.1016/S0266-8920(00)00012-6)
- Pardo De Vera C, Güemes JA (1998) Embedded self-sensing piezoelectric for damage detection. *J Intell Mater Syst Struct.* <https://doi.org/10.1177/1045389x9800901102>
- Parloo E, Guillaume P, Van Overmeire M (2003) Damage assessment using mode shape sensitivities. *Mech Syst Signal Process.* <https://doi.org/10.1006/mssp.2001.1429>
- Peeters B, De Roeck G (2001) One-year monitoring of the Z24-bridge: environmental effects versus damage events. *Earthq Eng Struct Dyn.* [https://doi.org/10.1002/1096-9845\(200102\)30:2<149::AID-EQE1>3.0.CO;2-Z](https://doi.org/10.1002/1096-9845(200102)30:2<149::AID-EQE1>3.0.CO;2-Z)
- Peng ZK, Tse PW, Chu FL (2005) An improved Hilbert-Huang transform and its application in vibration signal analysis. *J Sound Vib.* <https://doi.org/10.1016/j.jsv.2004.10.005>
- Peni T, Vanek B, Liptak G, Szabo Z, Bokor J (2018) Nullspace-based input reconfiguration architecture for overactuated aerial vehicles. *IEEE Trans Control Syst Technol.* <https://doi.org/10.1109/TCST.2017.2737622>
- Poulimenos AG, Fassois SD (2006) Parametric time-domain methods for non-stationary random vibration modelling and analysis – a critical survey and comparison. *Mech Syst Signal Process* 20(4):763–816. <https://doi.org/10.1016/j.ymsp.2005.10.003>
- Quqa S, Landi L, Paolo Diotallevi P (2020) Instantaneous modal identification under varying structural characteristics: a decentralized algorithm. *Mech Syst Signal Process* 142:106750. <https://doi.org/10.1016/j.ymsp.2020.106750>
- Quqa S, Landi L, Paolo Diotallevi P (2021) Modal assurance distribution of multivariate signals for modal identification of time-varying dynamic systems. *Mech Syst Signal Process* 148. <https://doi.org/10.1016/j.ymsp.2020.107136>
- Rankine L, Mesbah M, Boashash B (2007) IF estimation for multicomponent signals using image processing techniques in the time-frequency domain. *Signal Process* 87(6):1234–1250. <https://doi.org/10.1016/j.sigpro.2006.10.013>
- Ratcliffe CP (1997) Damage detection using a modified laplacian operator on mode shape data. *J Sound Vib.* <https://doi.org/10.1006/jsvi.1997.0961>
- Rehman N, Mandic DP (2010) Multivariate empirical mode decomposition. *Proc R Soc A Math Phys Eng Sci* 466(2117):1291–1302. <https://doi.org/10.1098/rspa.2009.0502>
- Reynders E, Wursten G, de Roeck G (2014) Output-only structural health monitoring in changing environmental conditions by means of nonlinear system identification. *Struct Health Monit.* <https://doi.org/10.1177/1475921713502836>
- Richman MB (1986) Rotation of principal components. *J Climatol.* <https://doi.org/10.1002/joc.3370060305>
- Roueff A, Chanussot J, Mars JI, Nguyen MQ (2004) Unsupervised separation of seismic waves using the watershed algorithm on time-scale images. *Geophys Prospect* 52(4):287–300. <https://doi.org/10.1111/j.1365-2478.2004.00416.x>
- Roy K, Bhattacharya B, Ray-Chaudhuri S (2015) ARX model-based damage sensitive features for structural damage localization using output-only measurements. *J Sound Vib* 349:99–122. <https://doi.org/10.1016/j.jsv.2015.03.038>
- Rytter A (1993) Vibration based inspection of civil engineering structures [Ph. D. Thesis]. Aalborg University, Denmark, Department of Building Technology and Structural Engineering
- Sadhu A, Hazra B (2015) Structural health monitoring and damage detection, volume 7. In: Conference proceedings of the society for experimental mechanics series. <https://doi.org/10.1007/978-3-319-15230-1>

- Seibold S, Fritzen CP, Wagner D (1996) Employing identification procedures for the detection of cracks in rotors. Modal analysis
- Senba A, Furuya H (2008) Implementation algorithms for self-identification of adaptive structures with variable geometric properties. *Mech Syst Signal Process* 22(1):1–14. <https://doi.org/10.1016/j.ymsp.2007.05.002>
- Shokravi H, Shokravi H, Bakhary N, Rahimian Kolor SS, Petru M (2020) Health monitoring of civil infrastructures by subspace system identification method: an overview. *Appl Sci (Switzerland)*. <https://doi.org/10.3390/APP10082786>
- Sohn H (2007) Effects of environmental and operational variability on structural health monitoring. *Philos Trans R Soc A Math Phys Eng Sci*. <https://doi.org/10.1098/rsta.2006.1935>
- Sohn H, Farrar CR (2001) Damage diagnosis using time series analysis of vibration signals. *Smart Mater Struct* 10(3):446–451. <https://doi.org/10.1088/0964-1726/10/3/304>
- Sohn H, Fugate ML, Farrar CR, Sohn H, Fugate ML, Farrar CR (2000) Damage diagnosis using statistical process control. In: Conference on recent advances in structural dynamics, Southampton, UK
- Sohn H, Worden K, Farrar CR (2001) Novelty detection under changing environmental conditions. In: S.-C. Liu (ed) *Smart structures and materials 2001: smart systems for bridges, structures, and highways*, pp 108–118. <https://doi.org/10.1117/12.434110>
- Spiridonakos MD, Fassois SD (2009) Parametric identification of a time-varying structure based on vector vibration response measurements. *Mech Syst Signal Process* 23(6):2029–2048. <https://doi.org/10.1016/j.ymsp.2008.11.004>
- Spiridonakos MD, Fassois SD (2012) Adaptable functional series TARMA models for non-stationary signal modelling. In: IFAC proceedings volumes (IFAC-PapersOnline) (Vol. 16, Issue PART 1). IFAC. <https://doi.org/10.3182/20120711-3-BE-2027.00200>
- Spiridonakos MD, Fassois SD (2014) Non-stationary random vibration modelling and analysis via functional series time-dependent ARMA (FS-TARMA) models – a critical survey. *Mech Syst Signal Process* 47(1–2):175–224. <https://doi.org/10.1016/j.ymsp.2013.06.024>
- Stanković L, Mandić D, Daković M, Brajović M (2018) Time-frequency decomposition of multivariate multicomponent signals. *Signal Process* 142:468–479. <https://doi.org/10.1016/j.sigpro.2017.08.001>
- Staszewski WJ (1998) Identification of non-linear systems using multi-scale ridges and skeletons of the wavelet transform. *J Sound Vib* 214(4):639–658. <https://doi.org/10.1006/jsvi.1998.1616>
- Stubbs N, Kim JT (1996) Damage localization in structures without baseline modal parameters. *AIAA J*. <https://doi.org/10.2514/3.13284>
- Stubbs N, Kim JT, Topole KG (1992) An efficient and robust algorithm for damage localization in offshore platforms. *ASCE 10th Structures Congress*, 543–546.
- Stubbs N, Kim JT, Farrar CR (1995) Field verification of a non destructive damage localization and sensitivity estimator algorithm. *Imac Xiii*
- Tipping ME, Bishop CM (1999) Probabilistic principal component analysis. *J R Stat Soc Ser B Stat Methodol*. <https://doi.org/10.1111/1467-9868.00196>
- Torres ME, Colominas MA, Schlotthauer G, Flandrin P (2011) A complete ensemble empirical mode decomposition with adaptive noise. In: *ICASSP, IEEE international conference on acoustics, speech and signal processing – proceedings*. <https://doi.org/10.1109/ICASSP.2011.5947265>
- Varga A (2011) On computing minimal proper nullspace bases with applications in fault detection. *Lecture Notes Electrical Eng*. https://doi.org/10.1007/978-94-007-0602-6_20
- Vetterli M, Kovačević J (1995) *Wavelets and subband coding*. Prentice-Hall, Inc.
- Vincent L, Vincent L, Soille P (1991) Watersheds in digital spaces: an efficient algorithm based on immersion simulations. *IEEE Trans Pattern Anal Mach Intell* 13(6):583–598. <https://doi.org/10.1109/34.87344>
- Wah WSL, Chen YT, Roberts GW, Elamin A (2017) Damage detection of structures subject to nonlinear effects of changing environmental conditions. *Procedia Eng*. <https://doi.org/10.1016/j.proeng.2017.04.481>

- Wang C, Ren WX, Wang ZC, Zhu HP (2013) Instantaneous frequency identification of time-varying structures by continuous wavelet transform. *Eng Struct* 52:17–25. <https://doi.org/10.1016/j.engstruct.2013.02.006>
- West WM (1984) Illustration of the use of modal assurance criterion to detect structural changes in an orbiter test specimen. In: Proc. air force conference on aircraft structural integrity
- Williams C, Salawu OS (1997) Damping as a damage indication parameter. In: Proceedings of the international modal analysis conference - IMAC
- Worden K, Sohn H, Farrar CR (2002) Novelty detection in a changing environment: regression and interpolation approaches. *J Sound Vib* 258(4):741–761. <https://doi.org/10.1006/jsvi.2002.5148>
- Wu Z, Huang NE (2009) Ensemble empirical mode decomposition: a noise-assisted data analysis method. *Adv Adapt Data Anal* 1(1):1–41. <https://doi.org/10.1142/S1793536909000047>
- Xiang J, Liang M (2012) Wavelet-based detection of beam cracks using modal shape and frequency measurements. *Comput Aided Civ Inf Eng*. <https://doi.org/10.1111/j.1467-8667.2012.00760.x>
- Xu YL, Chen J (2004) Structural damage detection using empirical mode decomposition: experimental investigation. *J Eng Mech*. [https://doi.org/10.1061/\(ASCE\)0733-9399\(2004\)130:11\(1279](https://doi.org/10.1061/(ASCE)0733-9399(2004)130:11(1279)
- Yamaguchi, H; Matsumoto, Y; Kawarai, K; Dammika, AJ; Shahzad, S; Takanami, R. (2013). Damage detection based on modal damping change in bridges. In: International conference on sustainable built environment, ICSBE'12, Kandy, Sri Lanka.
- Yan A-M, Kerschen G, De Boe P, Golinval J-C (2005a) Structural damage diagnosis under varying environmental conditions—part I: a linear analysis. *Mech Syst Signal Process* 19(4):847–864. <https://doi.org/10.1016/j.ymsp.2004.12.002>
- Yan AM, Kerschen G, De Boe P, Golinval JC (2005b) Structural damage diagnosis under varying environmental conditions - part I: a linear analysis. *Mech Syst Signal Process* 19(4):847–864. <https://doi.org/10.1016/j.ymsp.2004.12.002>
- Yang JN, Lei Y, Lin S, Huang N (2004) Hilbert-Huang based approach for structural damage detection. *J Eng Mech*. [https://doi.org/10.1061/\(ASCE\)0733-9399\(2004\)130:1\(85](https://doi.org/10.1061/(ASCE)0733-9399(2004)130:1(85)
- Yao R, Pakzad SN (2012) Autoregressive statistical pattern recognition algorithms for damage detection in civil structures. *Mech Syst Signal Process* 31:355–368. <https://doi.org/10.1016/j.ymsp.2012.02.014>
- Zang C, Friswell MI, Imregun M (2004) Structural damage detection using independent component analysis. *Struct Health Monit*. <https://doi.org/10.1177/1475921704041876>
- Zhang Z, Xu K, Ta D, Wang W (2013) Joint spectrogram segmentation and ridge-extraction method for separating multimodal guided waves in long bones. *Sci China Phys Mech Astronomy* 56(7):1317–1323. <https://doi.org/10.1007/s11433-013-5110-9>

Open Access This chapter is distributed under the terms of the Creative Commons Attribution 4.0 International License (<http://creativecommons.org/licenses/by/4.0/>), which permits use, duplication, adaptation, distribution and reproduction in any medium or format, as long as you give appropriate credit to the original author(s) and the source, a link is provided to the Creative Commons license and any changes made are indicated.

The images or other third party material in this chapter are included in the work's Creative Commons license, unless indicated otherwise in the credit line; if such material is not included in the work's Creative Commons license and the respective action is not permitted by statutory regulation, users will need to obtain permission from the license holder to duplicate, adapt or reproduce the material.



Chapter 7

Acoustic Emission



Dimitrios G. Aggelis, Markus G. R. Sause, Pawel Packo, Rhys Pullin, Steve Grigg, Tomaž Kek, and Yu-Kun Lai

Abstract Acoustic emission (AE) is one of the most promising methods for structural health monitoring (SHM) of materials and structures. Because of its passive and non-invasive nature, it can be used during the operation of a structure and supply information that cannot be collected in real time through other techniques. It is based on the recording and study of the elastic waves that are excited by irreversible processes, such as crack nucleation and propagation. These signals are sensed by transducers and are transformed into electric waveforms that offer information on the location and the type of the source. This chapter intends to present the basic principles, the equipment, and the recent trends and applications in aeronautics, highlighting the role of AE in modern non-destructive testing and SHM. The literature in the field is vast; therefore, although the included references provide an idea of the basics and the contemporary interest and level of research and practice, they are just a fraction of the total possible list of worthy studies published in the recent years.

D. G. Aggelis (✉)
Vrije Universiteit Brussel, Brussels, Belgium
e-mail: Dimitrios.Aggelis@vub.be

M. G. R. Sause
Institute of Materials Resource Management, University of Augsburg, Augsburg, Germany

P. Packo
AGH University of Science and Technology, Krakow, Poland

R. Pullin · S. Grigg · Y.-K. Lai
Cardiff University, Cardiff, UK

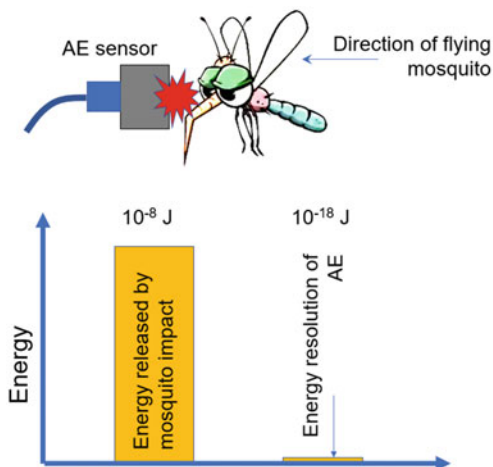
T. Kek
University of Ljubljana, Ljubljana, Slovenia

7.1 Introduction

The safety of structures is of paramount importance. Operational loads, environmental influences and random phenomena such as impacts accumulate damage and compromise the durability of structures. To avoid human casualties as well as loss of capital, structural health monitoring (SHM) procedures are implemented in all fields of engineering, including aeronautics. These procedures involve detection, geometric localization and characterization of damage that allows proper engineering decisions concerning maintenance or replacement of the component. Because of the deterioration of materials and structures, the necessity for suitable inspection and maintenance is crucial. In addition, AE is a valuable tool in any platform for investigation and development of materials in laboratory conditions. It can be applied in intervals or continuously to supply the information in real time as well as a reliable evaluation of the damage condition in materials and structures (Prosser 2002). AE is a monitoring technology that offers certain advantages in the evaluation of materials as well as structures. Some of the basic features include the high sensitivity, which leads to the detection of the actual onset of micro-cracking and the possibility of characterization of the failure mode based on the recorded waveform. In addition, it offers the localization of the sources in one, two or three dimensions.

The sensitivity of AE is demonstrated if we consider that the absolute energy of AE signals is measured with the unit of atto-Joule (or 10^{-18}J !). Therefore, the method allows the detection of the actual initiation of micro-cracking or any other event that would be impossible to detect through other techniques. It is characteristic that a common mosquito of mass 2.5 mg, flying at a speed of 10 cm/s obtains a kinetic energy of approximately 1.25×10^{-8} J, which is already 10 orders of magnitude higher than the limit of the technique (Fig. 7.1).

Fig. 7.1 The amount of energy that can be measured via AE systems is 10 orders of magnitude lower than the kinetic energy of a mosquito



Another advantage is the potential to characterise the fracture mode or generally the source or excitation type. This may seem to some as a ‘detail’, since for many people, the fact that damage exists is important, disregarding the actual mode. However, for composites the mode of the crack in a matrix or the type of failure, such as delamination or fiber pull-out is indicative of the current deterioration stage, and thus, it allows projections on the useful life of the component. This mode characterization is due to the fact that distinct processes involve different motions of the crack tips and emit elastic waveforms with different characteristics. A common example is the fracture of fibrous composite materials. At low load or fatigue cycles, the matrix is expected to crack first. Then, as loading progresses, the density of debonding and pull-out events will increase, whereas eventually, fiber rupture is also possible. The analysis of the waveforms recorded at each loading stage enables the classification of the signals to the different original sources and the evaluation of the current operation stage.

Source localization is an additional strong feature of AE. By applying multiple sensors, the coordinates of the active sources can be defined with good engineering accuracy in one, two or three dimensions, which means that even if a crack is inside the volume of the material and not visible, its location can be evaluated. The localization in most cases is based on the delay of recording of successive signals of the same source event at the different sensors. Considering the material’s wave speed, which can be measured using the same sensors, the location of the source can be determined. Certainly, the different wave modes excited in plate components typical in aeronautics structures, complicate the assessment, but there are strategies to overcome the difficulties, which will be explained in the corresponding section.

Because of the extensive use of AE technology in fracture monitoring studies, some people hesitate to call it a non-destructive testing technique. However, it should be clear that the AE sensors themselves do not inflict any damage (they do not even excite elastic waves as happens in ultrasonics). AE is a ‘passive’ technique. It is similar to filming an impact or a blast by a high-resolution camera. The camera monitors a destructive process, but it is just the monitoring tool, not the cause of damage. Because of the aforementioned advantages, AE is used for fracture monitoring, which is a very demanding and dynamic process, but it is also used for problems of different nature, e.g. the detection of gas leakage from a pipe network or corrosion development in industrial settings.

An interesting correspondence between AE and medical diagnosis is given in Wevers (1997) (see also Fig. 7.2). AE inspection is parallelised to a patient telling a doctor how she/he feels when examined without directly going into surgery to deal with the problem. The advantage of an examination over the surgery is of course that it is non-invasive and can be done for the whole body (global examination). Conversely, the disadvantage is that great skills from the doctor’s side are required to interpret the surface information from the patient (or in engineering the structure) and to relate it to a specific source. In addition, the same medical condition may be manifested by different symptoms in different patients, meaning that a specific way of interpretation AE data in a material using a specific detection system may not be adequate for another material and a different detection system. In any case, AE

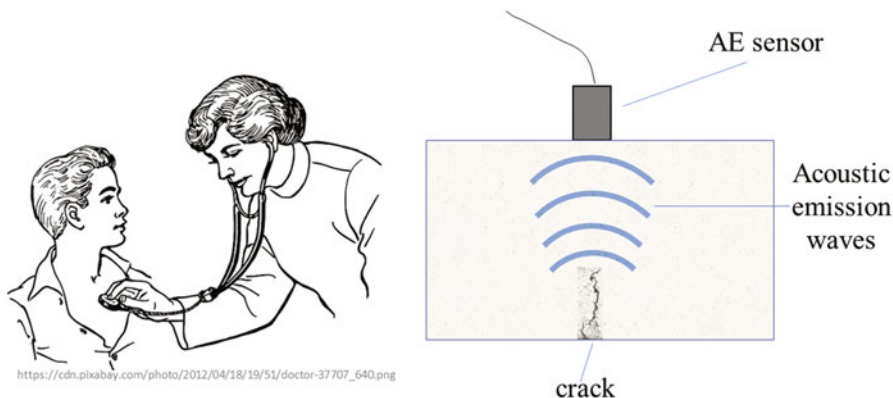


Fig. 7.2 Correspondence between medical stethoscope and AE transducer

allows continuous monitoring from the moment of damage initiation until the failure of the subject.

7.2 Basic Experimental Details and Parameters

The AE technique detects and monitors the transient elastic waves that are emitted after an irreversible phenomenon or process in the material. In most cases, piezoelectric transducers are placed on the surface of the material under test. A layer of ‘couplant’ or viscous liquid is applied between the sensor and the material surface to ensure adequate wave transmission. The couplant may well be petroleum jelly, or roller bearing grease. The sensors transform the pressure on their surface into electric signals. These signals are pre-amplified and are led to the digitization and acquisition board to obtain the signal as a function of time. Apart from recording the full signals, which is always an option in most contemporary systems, the basic parameters of each signal (waveform) are measured and stored as well. Figure 7.3a shows a typical AE system with the main elements, and Fig. 7.3b presents some indicative photographs of measurements.

The total activity of AE (simply how many signals or ‘hits’ were detected) is indicative of the phenomenon under monitoring. In case this is fracture, the number of hits is related to the damage degree and the rate of crack formation and propagation. In addition, the shape of the waveform yields important information relative to the source of the emission. The early AE systems, with no capacity for recording full waveforms, extracted only a set of features indicative of the waveform shape that were also useful for source characterization. Therefore, several parameters are used for the quantification of the waveform. Figure 7.4 shows some of the most basic ones (a, time, and b, frequency domain).

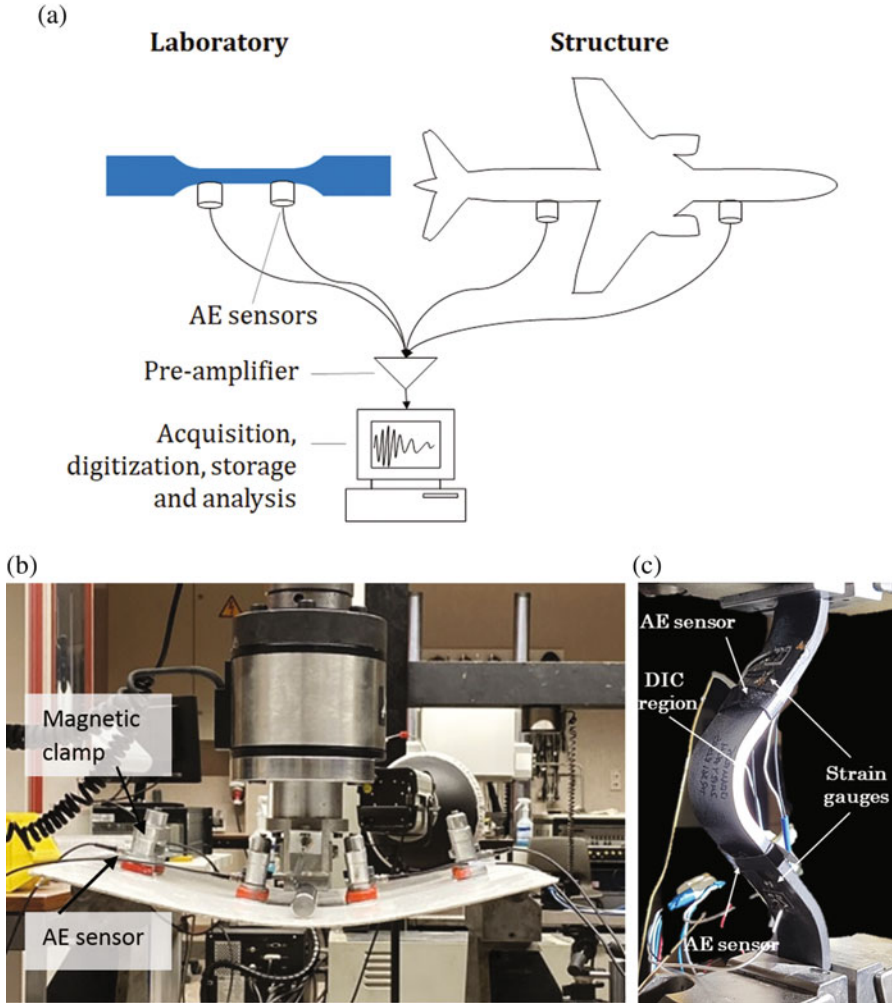


Fig. 7.3 (a) Schematic representation of a typical AE system, (b) photograph during three-point bending testing of glass fiber plate (Ospitia et al. 2020) with four AE sensors, and (c) tensile test of curved carbon fiber composite with AE monitoring by two sensors and digital image correlation (DIC) (Murray et al. 2020)

A basic experimental setting is the ‘threshold’, which is a voltage that should be overpassed to trigger the acquisition. This is an easy way to avoid low amplitude noise (extraneous AE, for example from rubbing) and is relevant to the measurement of most parameters. A parameter that is related to the intensity of the phenomenon is amplitude (A). This is the voltage (V) of the highest peak of the waveform and can also be measured in decibels (dB). dB is defined as:

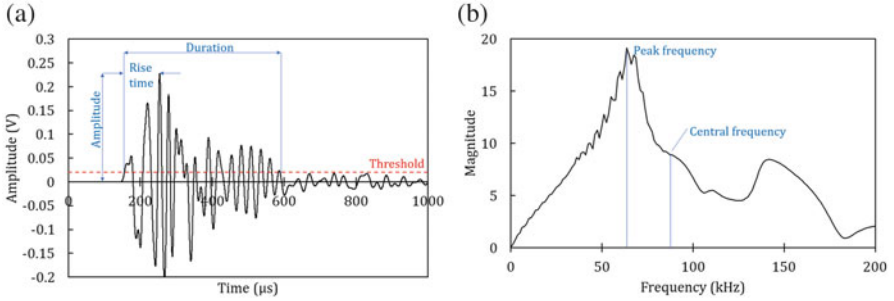


Fig. 7.4 (a) Typical AE waveform with basic AE parameters and (b) fast Fourier transform with basic spectral parameters

$$dB = 20 \cdot \log \left(\frac{A}{A_{ref}} \right) \quad (7.1)$$

where A is the measured voltage and A_{ref} a constant reference value.

Additionally, energy (E) which is defined as the measured area under the rectified signal envelope, considers the content of the whole waveform. Another definition of energy, ‘absolute energy’, comes from the integration of the rectified waveform envelope squared and is measured in ‘attoJoule’. It is considered analogous to the energy released from the source:

$$E_{abs} = \int_0^{t_1} V^2(t) dt \quad (7.2)$$

where the waveform starts at time 0 and ends at t_1 .

The delay between the first threshold crossing and the highest peak is called signal rise time, RT. Duration (Dur) is defined as the delay between the first and the last threshold crossings. Based on the shape of the first part of the waveform, the RA value has been introduced, which is defined by RT over A and is the inverse of the opening slope of the waveform or ‘Grade’ (Philippidis et al. 1998). The frequency content is also important. Different parameters are used for the process of this field of information. The simplest is the average frequency (AF) that is calculated in the time domain as the ratio of the total number of threshold crossings (counts) over the duration of the waveform in kHz. Other parameters such as the peak frequency and the central frequency are calculated in the frequency domain. The former is the frequency with the highest magnitude, and the latter is the centroid of the spectrum (see Fig. 7.4b). To measure these features, the full waveform should be recorded (Grosse and Linzer 2008). Parameters including the energy, RT, Dur, RA and frequency content exhibit sensitivity to fracture sources and are used for fracture mode characterization as will be discussed in more detail below. Practically, the initial part of the waveform contains information more relevant to the source

mechanism, whereas the latter part may contain reflections and generally can be more strongly influenced by the geometry.

There are different approaches as to the analysis of data depending on the application, the setup (sensors, acquisition board) and the preference of the user. Some are based on the AE activity recorded at specific load levels. In other cases, the statistical distribution of the amplitudes is used, whereas in others, the waveform parameters are analyzed (possibly with pattern recognition tools). The treatment of full waveforms (as in ‘signal based’ analysis) is also very widely used; tools such as wavelets and spectral analysis are very useful in revealing hidden information of the sources.

For AE measurement systems with digitization capability, two parameters play a very important role: the ‘sampling rate’ and the ‘dynamic range’. The sampling rate or frequency determines how dense the points within the waveform are or in other words the time lap between two successive points. For example, a sampling rate of 10 MHz means that a waveform that lasts 1 s is represented by 10,000,000 points, and consequently the points are separated by 0.1 μ s. According to Nyquist theorem (Bendat and Piersol 1993), the sampling rate must be at least double than the frequency of the actual signal. In reality, to have a credible representation of the continuous signal to a digitised waveform, the sampling must be 10 times higher or even more. This will improve the credibility of any further analysis in time (localization) or frequency domain. Regarding the dynamic range, this governs the corresponding ‘resolution’ in the voltage scale and expresses how many different voltage readings or levels can be taken between the minimum and maximum voltage. This is given as a power of 2. For example, if the voltage of the acquisition board is 20 V peak to peak, and the number of levels is 2^{16} (16 bits) = 65536, then the resolution in voltage is $20/65536 = 0.000305$ V, meaning that signals with amplitudes differing by less than this value may be measured as equal.

Examples of the application of the aforementioned and other parameters will be discussed in the following sections.

7.3 Fracture Mode Characterization in Plate Structures

Before the detailed description of the fracture mode characterization, a very basic phenomenon in AE should be reported. Its name is derived from Joseph Kaiser who was one of the pioneers of the modern AE testing. Since mechanical load is increasing in a specimen, acoustic activity is normally recorded (moderate load P1 in Fig. 7.5). If the material is unloaded and reloaded to the previous load P1, no AE is observed. This is the ‘Kaiser’ effect (Kaiser 1950), and the lack of recorded AE can be attributed to the fact that the damage related with the specific load level P1 has already occurred during the initial cycle. By increasing the load higher than P1 (up to P2 in Fig. 7.5), AE is again recorded since ‘fresh’ sources are created. Now, assuming that the load P2 caused serious damage, in the event of unloading and reloading, AE will commence at a load lower than the previous maximum

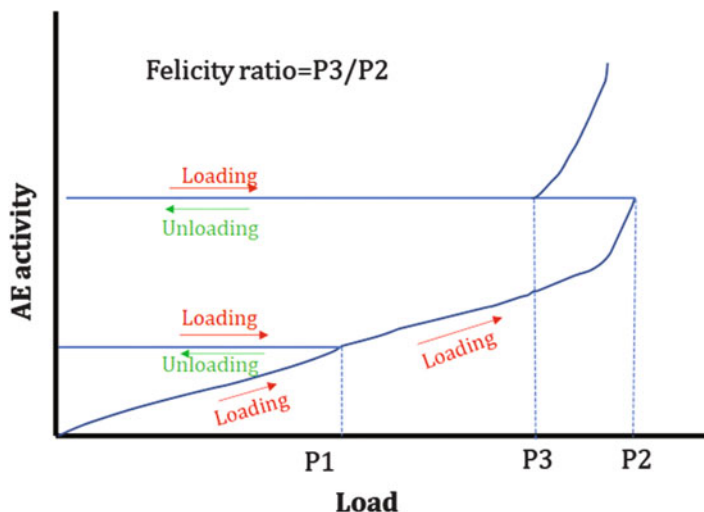


Fig. 7.5 ‘Kaiser effect’ and Felicity ratio

(e.g. $P_3 < P_2$). This can be considered as the result of the cracks and corresponding stress concentrations that locally increase the stress even before the load reaches the previous maximum level. The load at the onset of AE, over the previous maximum load (in this case P_3/P_2), is called the ‘Felicity’ ratio (FR) (Fowler 1977). FR is close to 1 when the material is intact, meaning that the ‘Kaiser effect’ is valid. When the FR decreases, it indicates the accumulation of damage and is commonly used as a powerful parameter in the evaluation of composites (Hamstad 1986; Ono and Gallego 2012; Aggelis et al. 2013; Esola et al. 2018).

The Kaiser effect and FR are quite widespread in the evaluation of structural condition, but they do not directly provide information on the specific manner the material is failing (fracture mode), something that is crucial for composites. Generally, when loading a technical structure made from monolithic materials or mixed materials, the recorded AE signals will likely not originate from the same source type. A basic categorization is the distinction between ‘useful’ signals, such as these originating from any damage formation as outlined in Chap. 3 and ‘useless’ signals, such as, e.g. friction noise from the regular operation of the structure. The successful separation of these two categories is a key item to address for SHM applications and allows to focus on the portion of data that is of interest for the integrity assessment.

To understand and categorise different AE sources in materials, considering their functional principle is helpful. Basic relationships of buried AE source types, their direction of radiation and rise-time with their corresponding AE signal have been discussed in the generalised theory of acoustic emission by Ohtsu and Ono (1984, 1986). In these publications, clear emphasis is made on the importance of the source dynamics for the generation of the acoustic wave. Specifically, for crack growth, Scruby and Wadley have proposed basic relationships between the speed of crack growth, as well as directional radiation effects for metallic materials (Wadley and

Scruby 1981; Scruby 1985). These principles also apply to other materials and are therefore considered as consistent theoretical framework, which forms the baseline for various other analytical descriptions (Wadley and Scruby 1981; Ohtsu and Ono 1984, 1986; Scruby 1985; Green 1995, 1998; Lysak 1996; Giordano et al. 1999; Wilcox et al. 2006).

As a common denominator in these theories, the dynamics of the AE source are inevitably linked to the dynamics of the crack growth. Hence, both the fractured material and the external loading determine the crack speed, which translate into a frequency bandwidth of the source. This results in characteristic frequency range for the AE signals between 10 kHz and 1 MHz observed for most materials, although the experimentally measured bandwidth is additionally compromised by the bandwidth of the type of sensor used.

The amount of energy released by an AE source event and the amplitude of the signal are related to the magnitude and also the velocity of the source event. As result from the basic theories above, the amplitude of the emission is expected to be proportional to the speed of crack propagation and the amount of surface area generated. Thus, large discrete crack jumps generate larger AE signals than those generated by cracks that propagate slowly over the same distance.

Another key characteristic of the AE source is the orientation and movement direction of the crack, which causes a distinct radiation pattern. For the typically thin structures used in aerospace applications, the position of the (microscopic) AE source in the thickness direction will additionally influence the excited frequency range since the originally undisturbed radiation pattern is turned into a guided acoustic wave.

However, material attenuation and guided wave dispersion effects will significantly affect the radiated frequencies and amplitudes as explained in Sect. 7.5. Therefore, numerous attempts have been published that provide analysis strategies for source identification considering the complexity of the situation faced.

7.3.1 AE Source Types

In the following, distinction is made for the established cases of AE source identification procedures for the types of defects categorised in Chap. 2.

For metallic materials, AE can result from the initiation and growth of cracks, particle fracture, sliding and dislocation movements, twinning or phase transformations (Grosse and Ohtsu 2008). Especially for aluminum, several researchers reported that particle fracture is one of the dominant sources for AE (Bianchetti et al. 1976; McBride et al. 1981; Cousland and Scala 1983; Wisner and Kontsos 2018; Wisner et al. 2019). For the fabrication of aircraft parts, typically thin metallic plates are applied, whereas reinforcement and joint elements can be associated with a more complex geometry. For the flat plate structures, substantial research was conducted to understand the relationship between source position, plate thickness and radiation direction. The use of numerical tools such as finite element modeling

provided huge insight in the way guided wave formation occurs in aluminum plates (Prosser et al. 1999; Hamstad et al. 2002a, 2002b; Hamstad 2010). This gave rise to the use of modal AE analysis and time frequency-based interpretation of AE signals as outlined in Sect. 7.3.2.

For composite materials, fracture may refer to the generation and propagation of cracks within the matrix material, along the matrix–fiber interface, or to the fracture of single fiber filaments or as a bundle. Another highly relevant source of AE found in fiber-reinforced polymers is the friction of existing crack surfaces. This occurs often during unloading and re-loading of damaged composites. Since many composites are laminates made from stacked layers with varying fiber orientations, the next scale for categorizing AE sources is the level of individual layers. When such laminates are loaded, cracks occur between the fibers, which grow parallel to the fiber orientation. Their dimensions are limited by the thickness of the layer (or the thickness of several layers when the fibers are oriented together). In addition, the stress concentration caused by such cracks as well as bending loads can induce delamination between the layers. During loading of a composite material or structure, all the mechanisms mentioned above may accumulate and interact until they ultimately cause a complete failure. AE is able to identify all these failure mechanisms, as it is sensitive to the multitude of different damage types spanning from the microscopic to the macroscopic scale (Sause 2016; Sause and Hamstad 2018). Meanwhile, this is not only supported by numerous experimental findings but now also by modelling approaches to predict the AE signal of a given source type, by analytical methods (Wilcox et al. 2006) and by finite element modelling (FEM) (Prosser et al. 1999; Sause and Horn 2010a, 2010b; Sause and Richler 2015). Therefore, considering the expected sequence of occurrence of the different fracture mechanisms, being able to identify the dominant one in real time offers information on the current structural condition and allows projections to the useful life span. As understood, fracture in composites is a fairly complicated and stochastic process because of several mechanisms as well as their possible overlap in time. This complexity is inevitably transferred to the AE signal making the interpretation less than straightforward. Still, some basic indicative principles can be mentioned as the starting point of the effort to understand the connection between AE signals and the original event. As Fig. 7.6 shows, a crack propagation event extending vertical to the axis of the plate results in waveform with different characteristics from a similar crack in the parallel direction. In the case of plates, the reason can be sought in the different amount of energy forming the ‘symmetric’ and ‘antisymmetric’ wave modes (Scholey et al. 2010; Eaton et al. 2011), depending on each case. When a vertical crack is extended (Fig. 7.6a top), this motion excites mostly symmetric components that have higher propagation velocities than antisymmetric, as already discussed in Chap. 5.2. A waveform containing stronger symmetric component is expected to have higher energy in the opening part rather than the later part; see example of Fig. 7.6b. By contrast, when a horizontal crack (delamination in the case of laminated plates) is extended (Fig. 7.6a bottom), the transient motion gives rise to the antisymmetric wave mode. Thus, it is reasonable that for the extreme cases of event orientation, differences are noticed in the waveform shape, practically

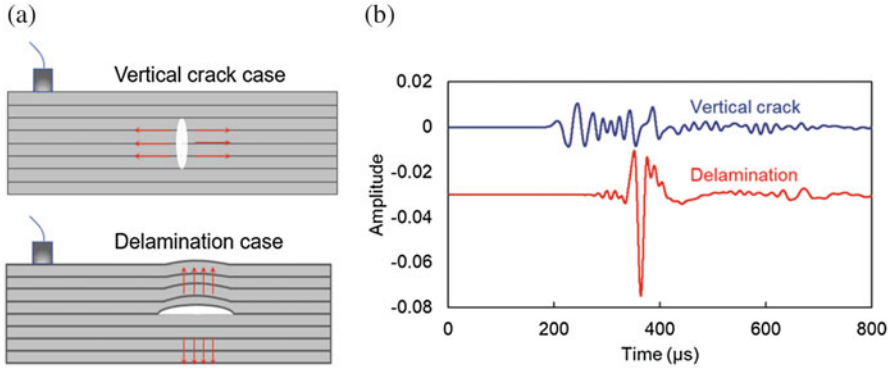


Fig. 7.6 (a) Representation of vertical crack (top) and delamination (bottom) in a laminated composite plate and (b) typical AE waveforms from the two events

resulting in shorter rise time for vertical cracks and longer durations for delaminations. Possible single fiber or fiber bundle rupture is expected to obtain even shorter duration characteristics and higher frequency content, as the fracture incident is usually shorter in time due to the limited fiber cross section to be fractured in one step and the higher speed of crack propagation within the high modulus fiber. The final waveform shape will be influenced by a number of aforementioned factors apart from the orientation, such as the position of the crack in the thickness (non-central sources will yield combination of modes instead of a single one), their displacement increment and speed and the propagation distance to the sensor and sensor characteristics as mentioned below. Despite the strongly stochastic nature of the processes, this visualization can be treated as a starting point of analysis, since it is supported by extended literature in the composites field (Sause and Hamstad 2018; Li et al. 2015; Blom et al. 2014; Kolanu and Raju 2019; Aggelis et al. 2012). Furthermore, recently AE has proven sensitive to the mode of the strain field (shear/tensile) before damage is inflicted in any measurable form (Kalteremidou et al. 2021).

In Fig. 7.7, the wavefields caused by a transverse crack and a delamination type source are contrasted. The source is assumed to happen at the same spot close to the hinge of a landing flap. The color scale is providing the out-of-plane velocity component of the guided waves excited in the airplane wings skin at two discrete time steps after crack growth. Based on the significantly different wavefields, it can readily be understood that the signals picked up by a sensor system will be significantly different as well. In addition, the different AE sources cause different guided wave modes as mentioned above, which will see different propagation behavior as described in Sect. 7.5.

For aircraft structures an additional item is the use of adhesives, coatings or interlayers combined with structural parts made from metals or composites. For the flat plate-like structures, they may be considered as an additional layer of different material that is attached or integrated with the plate. During the lifetime of the component, cracks may form inside the adhesive or coating or at the interface to the

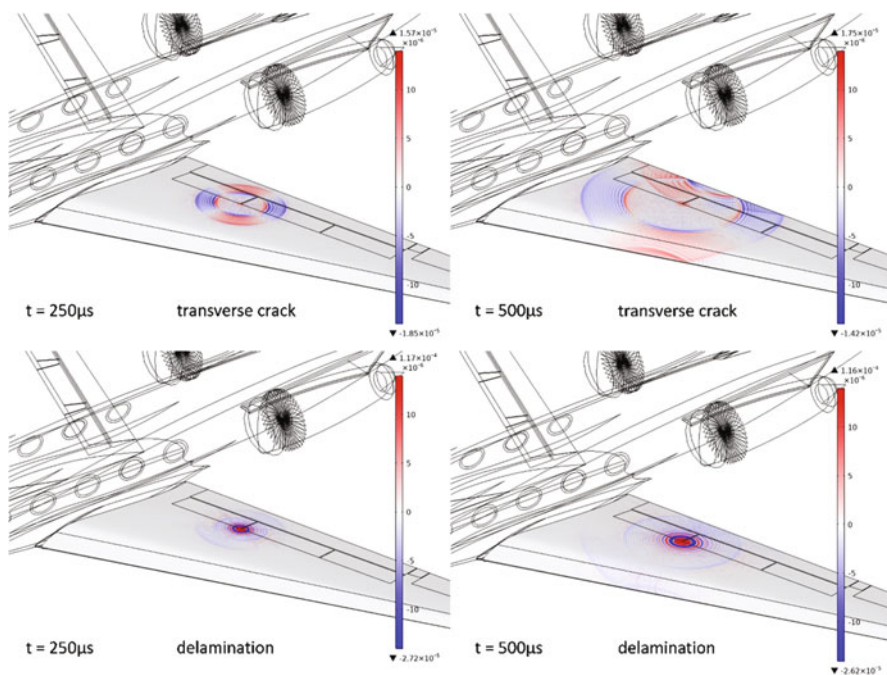


Fig. 7.7 Visualization of the out-of-plane velocity component of the wavefield emitted by a transverse crack (upper row) and delamination (bottom row) at two discrete time steps after the occurrence of the crack in aircraft wing skin.

structural material (Sause 2010). This sort of crack growth is expected to cause AE and was reported in literature several times (Piotrkowski et al. 2005; Sause et al. 2008; Sause et al. 2009; Yao et al. 2012).

7.3.2 Procedures for AE Source Identification

In the last twenty years, many approaches have been proposed that attempt to identify AE sources. These concepts include moment tensor inversion, time inversion approaches, guided wave analysis and pattern recognition techniques. When discussing these techniques, it is useful differentiating between signal classification and source identification. In signal classification, the task is to group signals based on similarity measures. Such clustering is often achieved by data analysis of multiple AE characteristics. The applied methods for AE signal clustering ranges from simple discrete feature value analysis to automated pattern recognition. After clustering of the AE signals, the task of source identification is to assign a specific cluster to a specific source type. Since all source identification procedures are based on the detected signal information it is essential that the AE sensor used does not inhibit the

recording of the required information. Therefore, if frequency information is desired as means of distinction of source types it is mandatory that the sensor covers enough bandwidth and does provide reasonable flatness to ensure proper detection of the propagating wave's frequencies.

Although, in volumetric media, the source type can be derived by moment tension inversion (Aki and Richards 1980; Ohtsu and Ono 1984; Grosse and Ohtsu 2008; Green 1995, 1998), this approach cannot be used in thin structures mainly because most of the information on the orientation of the source is lost in a few millimeters of propagation.

In recent years, the time reversal AE approach has been used to yield the (temporal) source function and the radiation behavior of the source (Ciampa and Meo 2010a; Ozevin and Heidary 2011; Ernst and Dual 2013). This has been demonstrated to measure the orientation of cracks in thin metal plates (Ozevin and Heidary 2011). Consequently, the time reversal approach could be used to obtain further information regarding the origin of the source. However, the approach faces the same challenge as moment tensor inversion, i.e. the precise knowledge of the Green's function of the propagation medium.

Another classification technique that is more suitable for composite materials is the analysis of guided waves. This approach uses the relationship between certain source types and their corresponding guided wave modes as occurring in in plate-like structures (Gorman 1991, 2011; Gorman and Prosser 1991; Gorman and Ziola 1991; Prosser et al. 1995, 1997; Prosser 1996; Morscher 1999; Surgeon and Wevers 1999). The aim is to find specific ratios of certain guided wave modes that are characteristic for a particular type of source. Although such ratios are partly expected, clear assignment of guided wave mode ratios to particular source mechanisms remains challenging. This whole procedure also requires the use of multi-resonant or broadband sensors to cover the frequency range of interest. Ideally, 'flat' sensors are used to avoid that additional resonance artifacts are superimposed on the signatures of the guided wave modes. As an example, it can be mentioned that in certain studies such as Martínez-Jequier et al. (2015), higher energy at low frequency content is associated to delamination events, whereas higher frequency content is associated either with matrix cracks in some cases or with fiber rupture. Practically, the above-mentioned processes are translated to different amplitude and frequency distributions for different failure mechanisms. Despite the general overlap that is stressed in all studies, in some of them, some general separation is suggested based on their amplitude or frequency content (Liu et al. 2012; Mahdavi et al. 2016; Chandarana et al. 2017; Li et al. 2014; Ramirez-Jimenez et al. 2004; De Groot et al. 1995; Li et al. 2014), where fiber breakage shows higher values than those of delaminations and even higher than those of matrix cracking. It is again highlighted, however, that although these processes are reasonably based on the physics of wave propagation in plates after specific source excitation and they are confirmed and used in several cases in literature, they exhibit stochastic character, and their validity for each separate AE event cannot be taken for granted and should be tested by secondary means such as post-mortem studies or validated modeling strategies.

In contrast to classical single AE feature analysis, pattern recognition techniques use a variety of AE features and can therefore be used to group different signal types. This helps to classify signals even when they cannot be distinguished by discrete feature limits, such as a particular peak frequency or particular signal amplitude. In principle, pattern recognition techniques can be divided into two branches, namely supervised pattern recognition and unsupervised pattern recognition. Some of the established pattern recognition approaches can be understood as more general classification routines that follow the idea of mode analysis of guided acoustic waves. Therefore, similar requirements apply to sensor technology (multi-resonant or broadband sensors).

In unsupervised pattern recognition the task is the separation of a set of given objects without prior knowledge into different groups based on their similarity relative to each other. Various approaches have been applied (Anastassopoulos and Philippidis 1995; Anastassopoulos et al. 1999; Baensch et al. 2015a, 2015b; De Oliveira et al. 2004; Doan et al. 2014; Huguet et al. 2002; Kostopoulos et al. 2003; Marec et al. 2008; Philippidis et al. 1998; Ramirez-Jimenez et al. 2004; Richardson et al. 1984; Sause and Horn 2010b; Sause et al. 2009; Sause et al. 2012; Vi-Tong and Gaillard 1987; Yu et al. 1996). As an alternative approach, supervised pattern recognition techniques comprise two successive stages. In the first stage, a set of objects with known assignments (so-called labels) is required. An algorithm is trained to establish a functional relationship between a given set of characteristics and their respective label. In the second stage, the algorithm is applied to objects with the same characteristics, but unknown labels. Based on the established functional relationship the algorithm then provides the object labels based on a measure of similarity to the training data. For this purpose, the distinction of noisy and non-noisy AE signals can be accomplished via unsupervised pattern recognition techniques (Anastassopoulos and Philippidis 1995; Philippidis et al. 1998). Acoustic emission signals resulting from friction and electromagnetic induction can be easily identified in this respect because of their inherent characteristic difference from transient acoustic emission signals (e.g. long constant amplitude signals with broad frequencies or short duration spikes). Through appropriate experimental considerations and finite element simulations, the respective signal types can also be associated with specific failure mechanisms (Bohse and Chen 2001; Haselbach and Lauke 2003; Huguet et al. 2002; Li et al. 2014; Li et al. 2015; Marec et al. 2008; Ramirez-Jimenez et al. 2004; Richardson et al. 1984; Sause and Horn 2010b; Sause et al. 2009; Sause et al. 2012).

Even though pattern recognition techniques are frequently used for AE signals, none of the approaches have yet made it to recognised standards. Meanwhile robust approaches for identification of natural clusters of AE signals have been proposed (Sause et al. 2012) and adopted for composites, wood fracture and study of plant dehydration (Njuhovic et al. 2014; Ritschel et al. 2014; Vergeynst et al. 2014a; Baensch et al. 2015b; Prieß et al. 2015). Influencing factors such as signal propagation, sensor type, pre-damaged material and geometry were identified (Sause and Horn 2010b; Sause 2013; Sause 2016; Sause et al. 2014). However, the main challenge still is the correct assignment of a group of signals to a corresponding

failure type. Therefore, the occurrence of natural clusters is worth considering, but is not sufficient for the correct labelling of the underlying AE source types. In addition, such labelling must be re-validated in each test configuration.

There are several established ways to perform such a task. One choice are phenomenological observations (Prosser et al. 1995), comparative measurements on specimens with known types of AE sources (Huguet et al. 2002; Scholey et al. 2010; Aggelis et al. 2012) or subsequent microscopy (Giordano et al. 1998; Kalteremidou et al. 2018) to verify the existence of damage types reaching to the surface level. X-ray micro computed tomography (μ -CT) has also been used to examine the damage within the volume of the components (Maillet et al. 2019; Zhou et al. 2021). However, these approaches have some drawbacks, as they require in-depth expertise and an understanding of the way signals propagate from the source to the sensor. The use of representative samples with model sources may also be misleading, because multiple microscopic AE sources may be generated at the same time instead of an intended single AE source.

Finally, modelling approaches have been used to allow the assignment of specific groups of signals to specific failure mechanisms, which allows to generate synthetic AE signals that can be subjected to the same feature extraction procedures as the experimental AE signals and then be compared (Sause and Horn 2010b; Burks and Kumosa 2014; Vergeynst et al. 2014b).

However, a general drawback of these AE source identification procedures is the assumption of a singular event happening isolated in time. In reality, damage formation may happen simultaneously and overlap in time. In addition, the time of occurrence of subsequent microscopic sources of damage may begin to overlap with the decay of earlier AE signals. This may lead to a ‘continuous’ stream of AE signals instead of single isolated signals for example when high loading rates are present. In case of such high AE activity, a clear distinction between different failure events is no longer feasible and partly renders source localization or source identification impossible.

Besides the AE sources from damage formation in the material, there are many other possible AE sources that might disturb the interpretation of damage-related AE. During the loading of a structure, there are inevitable physical connections to the surroundings. Oftentimes, the area of load introduction will be subject to stress-concentration effects, which results in preferential AE activity in that area. Since this additional AE activity can easily be detected by the AE sensors, it can easily be misunderstood as result of damage progression in the test section, although the material in the test section is barely damaged. The localization of AE sources can be helpful to reduce the recorded AE signals to those originating only from specific sections of the test structure. Moreover, structural supports are well-known to cause stick slip frictional movement between the support and the loaded structure. Stick-slip-friction is known to be a source that causes high AE activity. To reduce this contribution, a good practice is the use of lubricants at the supports to minimize the friction, or to apply source localization techniques to limit the interpretation on AE signals coming from other parts of the structure. It is also known that electrically driven machines or other powerful electronic devices may cause electromagnetic

induction in the sensor cabling, resulting in spike signals that are not resulting from any damage. In particular, changing the orientation of the cabling relative to the electric devices, as well as adequate grounding, can improve the situation and thus avoid such signals. Generally, the use of sensors with internal preamplifiers can reduce extraneous signals induced in cables, as the signal voltage level is raised directly behind the sensor, therefore resulting in a voltage level much less influenced by the induced noise floor. In addition, actuators or rotating components are subject to internal friction, which can also lead to the generation of artificial AE sources that are detected by the AE equipment. In particular, servo-hydraulic machines usually generate noticeable AE by operating the servo valve, which may interfere with proper detection of AE signals from crack formation. Unlike these artificial AE noise sources, audible noise or vibrations do not necessarily interfere with AE measurements, since these are often predominantly active in the audible range and below. Compared to that, AE measurements start above 10–20 kHz and typically extend to 1 MHz.

Regardless of the type of approach pursued, it is a key requirement to be able to detect the AE signals at all. Based on signal propagation effects (see Sect. 7.5), the signals may easily fall below the detection threshold. Even long before, the reduction of signal-to-noise ratio may lead to severe difficulties for proper source identification as the signal information is affected by digitization effects and coverage by the system electronics noise.

7.4 Localization

From aerospace point-of-view, AE-based inspection strategies are concerned with thin plates and large monitoring areas. This fact reduces the dimensionality of the problem, from 3D to 2D. Although the basic principle of localization is founded on the time difference of arrival (TDOA) measurement for different sensors, physics of wave propagation in plates make the acoustic source localization procedure (ASLP) quite complex. Frequency-dependent wave velocity (i.e. dispersion), multi-modal wavefield, mode-dependent amplitude characteristics make the ASLP difficult (see Chap. 5.2 for guided wave characteristics). Further complexity on the localization procedures may be imposed by direction-dependent properties of fiber-reinforced or woven plastic composites that are common in aerospace structures. Although in many practical cases composite plates are designed as orthotropic or transversally isotropic, non-uniform distribution of fibers or other design-specific features may result in substantial deviations from quasi-omnidirectional wave speed characteristics. Anisotropic elastic properties, resulting in different wave propagation velocities for different directions, bring severe complexity to source localization. Another consequence of anisotropy is difference between the direction of wave propagation, i.e. the wavevector \mathbf{k} , and the energy propagation direction (i.e. the group velocity vector, \mathbf{V}_g) due to non-circular constant-frequency contours of the dispersion relation (Wolfe 2005). Since localization techniques estimate direction of arrival of the

incident wave using different features of the waveform, e.g. local wavenumber, phase or amplitude correlation etc., it needs to be carefully analyzed whether the direction of \mathbf{V}_g or \mathbf{k} is found. For the former, those techniques are approximately valid for materials displaying small directional deviations between \mathbf{k} and \mathbf{V}_g , and/or sources aligned with material symmetry planes—weakly anisotropic composites.

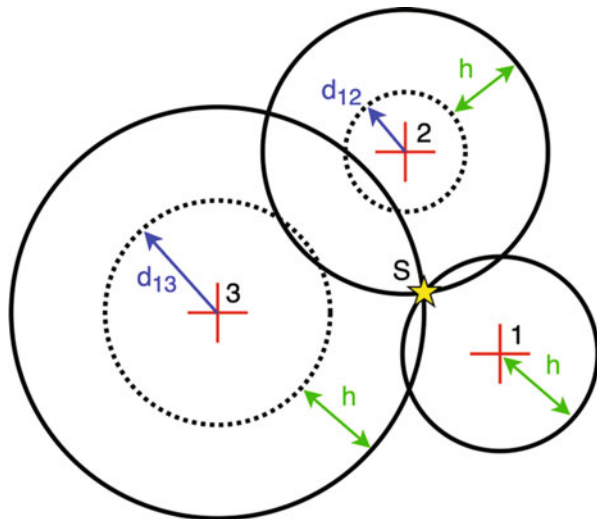
The inspection strategy adopted for ASLP also plays an important role for accuracy. Two main approaches for ASLP rely on periodic or continuous monitoring. In each case, different factors influencing the localization process need to be considered. Some of the factors include mounting and dismounting AE sensors to the structure and their repositioning contrasted to fixed and permanently mounted devices; temperature and time, i.e. aging factors (related to both the structure and the AE system elements), calibration and re-calibration, operator specific issues (e.g. mounting, coupling, calibration) and other. It is therefore of interest to employ ASLP techniques that will be possibly robust to the above factors. This can be (at least partially) achieved by using wave features displaying least possible sensitivity to system's conditions in a particular application, e.g. phase for systems in stable—and energy for unstable—environmental conditions.

This section aims at outlining most widely used ASLP techniques and discussing their capabilities in the context of the above-mentioned requirements. It should be noted that the methods listed in this section are selected from a wide variety of available techniques. Their application typically depends on a number of factors like the type and characteristics of the sensors, acquisition mode, accessibility to the structure hot-spots, time, desired accuracy, availability of material properties of the structure, its geometrical and material complexity, expected type of acoustic source (e.g. impact/crack or leakage) and others. One of important restrictions for a potential ASLP method is the number of sensors applied. A localization method should use minimum possible number of sensors due to: weight and service issues, redundancy and self-check/self-diagnostics and calibration should be possible within the network of sensors, robustness of the system to a single-sensor failure; amount of transferred/processed data etc.

The ASLP methods can be in general classified into two groups: localization with and without knowing material properties of the medium. Knowing material properties substantially simplifies and in general improves accuracy of localization. However, precise information on elastic properties of the medium is most frequently unknown, in particular in the case of anisotropic media. In fact, most of the methods of practical importance are applicable up to moderately anisotropic plates due to fact that for non-coincident \mathbf{k} and \mathbf{V}_g , the direction of energy propagation does not point to the source in general. What is more, for isotropic media, those methods can be frequently applied directly and without the need for solving complex nonlinear equations. Approximate estimates of wave velocities may partially circumvent the problem, but impact localization accuracy. Consequently, methods that do not require material properties for finding the acoustic source location are appealing.

The classical state-of-the-art localization is based on the time difference of arrival (TDOA) measurement for a network of sensors. TDOA is computed from signals acquired by the sensors. During monitoring, all sensors simultaneously register

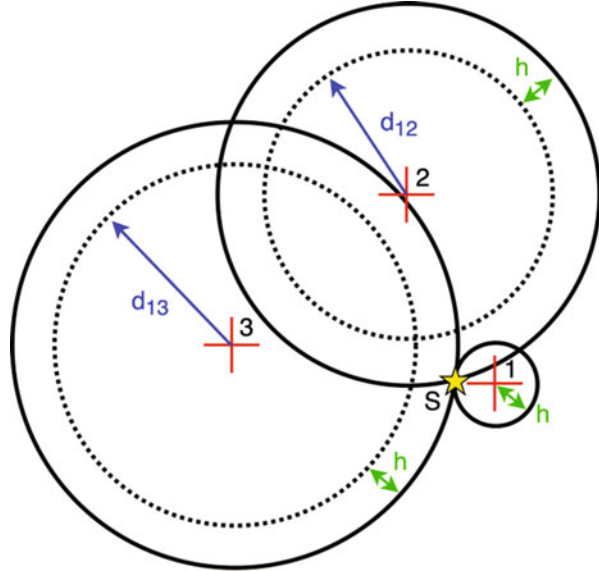
Fig. 7.8 Acoustic source localization via triangulation for known wave speed c (after Kundu 2014)



signals and store them in a circular buffer. The signals are continuously checked and recording starts upon threshold crossing at any of the sensors. After registering an AE event, the signals are analysed and localization estimates are computed by dedicated algorithms, as discussed later. Threshold value depends on application, type of sensor and coupling agent used and is typically adjusted by the operator. Too low threshold value may result in registering invaluable data while too high—missing AE events. Particular localization strategy depends on whether the wave speed in the plate is known at least approximately or unknown—then the TDOA can be combined with a simple iterative triangulation search (Tobias 1976) or a solution of a set of nonlinear equations (frequently solved through an optimization) (Liang et al. 2013). The method has been widely applied in laboratory and industrial conditions, for isotropic and weakly anisotropic plates.

For a triangulation of an acoustic source when the wave speed, c , for an isotropic plate is known, the following simple procedure can be followed (Tobias 1976; Kundu 2014). A set of three sensors—1, 2 and 3, as shown in Figs. 7.8 and 7.9—is placed non-collinearly on the plate. Acoustic source generates an elastic wave that travels from point S (source location, denoted by the yellow star) to the sensors. Although the moment of emission—hence the travel time—from the source is unknown, the TDOA between the sensor that receives the event first (e.g. 1) and the two remaining sensors (e.g. 2 and 3), e.g. T_{12} and T_{13} , are known. Consequently, the distances travelled by the wave in that times are $d_{12,13} = c T_{12,13}$. Next, circles of diameters d_{12} and d_{13} are drawn with sensors 2 and 3 in the centers, respectively (circle at sensor 1 is of radius zero). Finally, to locate the source S , the radii of the three circles are increased uniformly by h until they meet at a common point, as shown in Fig. 7.8. It needs to be noted that the initial estimate of c is important for localization and different values of wave velocity result in different predicted

Fig. 7.9 Acoustic source localization via triangulation for known wave speed $2c$ (after Kundu 2014)



positions of S , as shown in Fig. 7.9. This ambiguity can be (at least partially) resolved by adding redundant sensors to the system.

The above-mentioned triangulation technique for ASLP can be re-formulated in order to avoid the requirement of knowing the wave velocity, c . In that case however, a set of nonlinear trigonometric equations need to be solved in order to locate the source (Liang et al. 2013).

ASLP techniques for plates that require the wave speed as an input parameter suffer additional accuracy problems due to multimodal and dispersive nature of Lamb waves that propagate in these structures. A single value of wave speed does not account for multiple wave modes and the fact that waves at different frequencies propagate at different speeds. Since AE signals are mostly broadband or narrow-, but finite, band, the dispersion effect plays a substantial role in ASLP in guiding media. A method combining the simplicity of the triangulation approach with basic information on wave physics in plates can be found in (Grabowski et al. 2016a). The method employs the time-distance domain transform (TDDT) for mapping the signals acquired by the sensors, transforming them from the time to the distance domain. Subsequently, the localization is performed immediately in the distance domain to find the acoustic source.

In the TDDT-based ASLP (Grabowski et al. 2016a) it is assumed that the source generates a signal whose Fourier transform is denoted by $S_{exc}(\omega)$. The signal travels through the plate and is acquired by the j^{th} sensor as $S_{acq, j}(\omega)$. The propagation medium (i.e. the plate) transforms the excited signal into the acquired signal as follows

$$S_{(acqj)}(\omega) = G(r_j, \omega)S_{exc}(\omega), G(r_j, \omega) = A(r_j, \omega)e^{-ik(\omega)r_j} \quad (7.3)$$

where the signal deformation due to the acquiring sensor characteristics has been neglected (for a full derivation the reader is referred to (Grabowski et al. 2016a)). In Eq. (7.3), G is the transfer function of the plate (assuming the far field propagation conditions), $A(r_j, \omega)$ is the frequency- and distance-dependent amplitude characteristic of the plate, $k(\omega)$ is the dispersion (phase) characteristic and r_j is the unknown distance between the source and the j^{th} sensor. Clearly, the dispersion curves, $k(\omega)$, impose a phase shift for each frequency component of the excited signal.

When material properties and plate thickness are (at least approximately) known, then $k(\omega)$ can be computed and used for mapping the acquired signals from the time to the distance domain. The latter is possible through the sequence of mapping transforms: time-to-frequency ($t \rightarrow \omega$), frequency-to-wavenumber ($\omega \rightarrow k$), wavenumber-to-distance ($k \rightarrow r$). Therefore, the dispersion characteristics work as the TDDT map. Using $k(\omega)$, Eq. (7.3) can be rewritten as

$$S_{exc}(k^{-1}(\omega)) = S_{exc}(k) = A^{-1}(r_j, k^{-1}(\omega))e^{ik(\omega)r_j}S_{acqj}(k^{-1}(\omega)) \quad (7.4)$$

In Eq. (7.4), all characteristics are presented as functions of the wavenumber \mathbf{k} , e.g. $S_{exc}(k^{-1}(\omega)) = S_{exc}(k)$. The distance-domain dispersion-compensated source signal, $S_{exc}(r)$, can be therefore obtained by the inverse Fourier transform of $S_{exc}(k)$ and immediately used for ASLP. For this purpose, three circles of radii r_1 , r_2 and r_3 are drawn around respective sensors, analogously to those presented in Fig. 7.8. The crossing point of the three circles, or the area left between them, is the acoustic source location estimate.

The radii r_1 , r_2 and r_3 are unknowns of equations generated from Eq. (7.4). Therefore, direct inversion of Eq. (7.4) is not possible until r_j are known. Location of the source, given by r_j , is found by realizing that: (a) all acquired signals should be the same after the mapping procedure (namely, there is one source signal that has been deformed differently along different propagation paths r_j) and (b) the amplitude envelope of the compensated signal is at its maximum for the correct r_j values (or, equivalently, the width of the source wave packet is the shortest). By iteratively time shifting the acquired signals and processing by the proposed algorithm, r_j corresponding to the actual source-sensor distances can be found. An example of the shifting procedure used for determining r_j is shown in Fig. 7.10, where the compensated signal amplitude and wave packet width are presented. Clearly, both of these parameters assume their extreme values for the same (or very close) time shift (meaning the same distance). Dispersion-compensated signal after transformation to the distance domain—obtained by applying the procedure outlined above—is shown in Fig. 7.11, along with the waveform before signal processing is applied.

An interesting feature of the TDDT-based method is its ability to differentiate between Lamb wave modes in the signals acquired at the sensors. By selecting different mode-specific branches from the dispersion plot and mapping the same (multi-modal) signal, it may be noted that only parts of the signal corresponding to

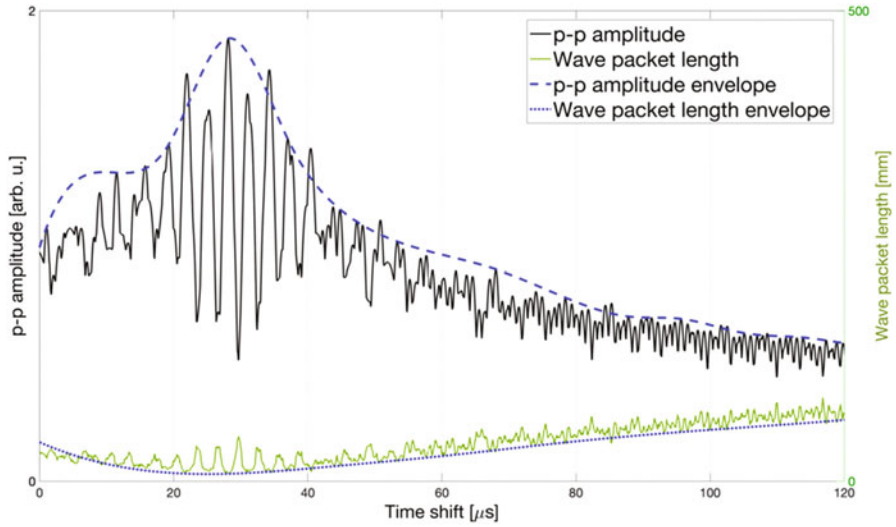


Fig. 7.10 Amplitude and width of a wave packet after dispersion compensation with various time shifts (after Gawronski et al. 2016)

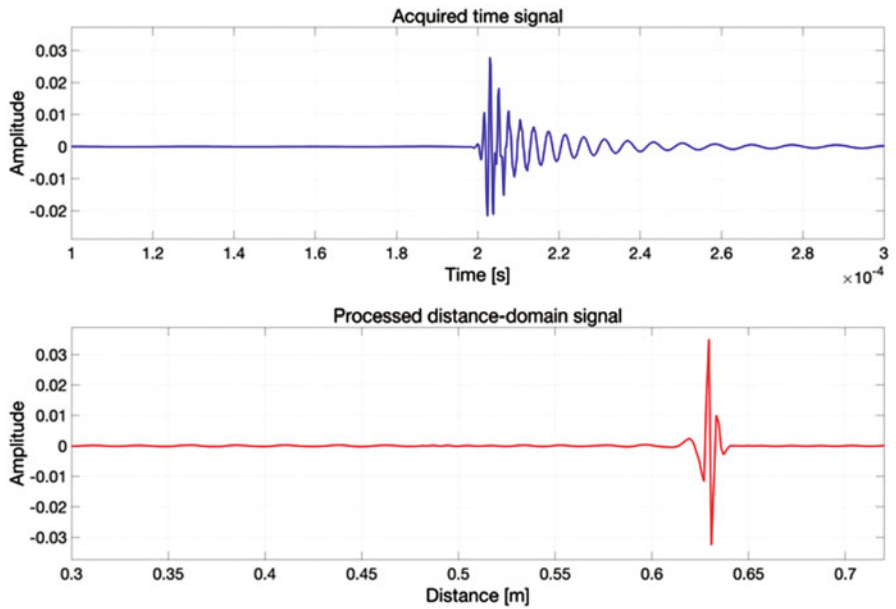
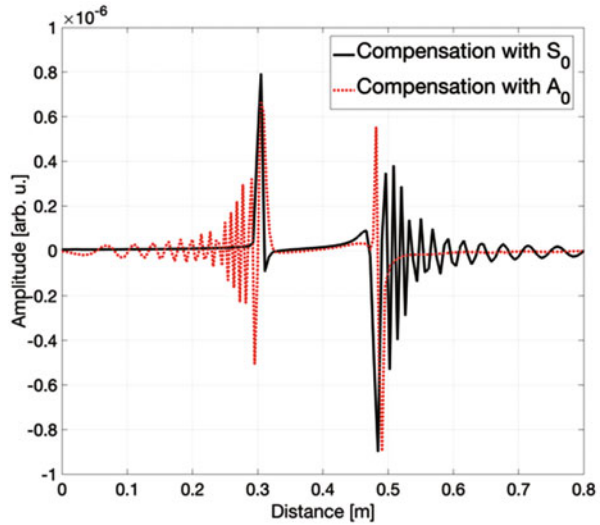


Fig. 7.11 Example signals: time-domain signal acquired at the source (top) and dispersion-compensated and transformed to the distance domain (bottom), after (Grabowski et al. 2016a)

Fig. 7.12 A dispersion-compensated signal mapped through dispersion branches for S_0 and A_0 modes



the mode that match the dispersion branch are properly compensated and placed at a correct distance. An example of such mapping is presented in Fig. 7.12 where the same time signal—containing the S_0 and A_0 wave packets—registered by a sensor was compensated by using the S_0 and (independently) A_0 mode characteristics (black and red lines, respectively). Each time the compensation is carried out only one of the wave packets is properly compressed, proving the ability of the method to distinguish between multiple wave modes.

It needs to be pointed out that the proposed mapping has important consequences and advantages for the localization process. First, the ASLP is performed in a natural, distance, coordinates. Second, no fixed assumption on a single wave velocity is made, but the full spectral characteristics of the medium are used. Therefore, any wave mode of arbitrary frequency band can be transformed. The effect of TDDT is compressive, i.e. the signal is dispersion-compensated and resembles the original signal shape at the source (pertaining to source identification). Finally, various wave modes can be selectively filtered by subsequent processing of the signals with different dispersion branches. As the above brief outline of the TDDT-based ALS neglects the impact of amplitude–frequency characteristics of the plate, the reader is referred to (Grabowski et al. 2016a, 2016b) for details.

In contrast to sparsely distributed sensors, a whole group of cluster-based localization techniques for plate-like structures is based on the concept of a group of three or more AE sensors (Kundu 2012), as shown in Fig. 7.13. The sensors forming a cluster need to be closely-spaced with respect to the distance to the source (D). In (Kundu 2012), a minimum of three sensors are arranged in a right-triangular setup (the so-called L-shaped cluster), however, other arrangements have also been developed, e.g. square (Sen et al. 2020), M-shaped (Grabowski et al. 2015) or Z-shaped (Yin et al. 2018). The concept of the cluster aims at immediately estimating the direction of incident wave knowing the sensors positions not material properties of

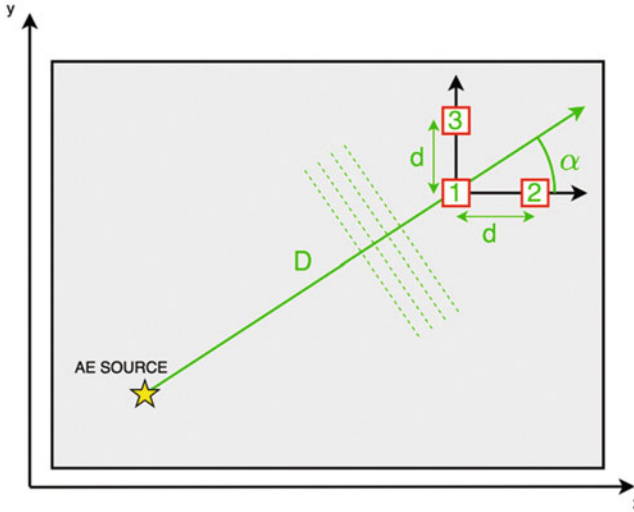


Fig. 7.13 A minimal cluster of three sensors required for estimation of direction of arrival (after Fig. 1 of Kundu 2012)

the medium. As shown in Fig. 7.13 for a single cluster, the incidence angle, α , for the source signal is estimated from two time delays of signals registered by the cluster, namely Δt_{12} and Δt_{13} (12 and 13 being the wave delays between sensors 1 and 2, and 1 and 3, respectively). Then, the angle is given as $\alpha = \tan^{-1}(\Delta t_{13}/\Delta t_{12})$. It may be also noted that the two time delays allow for estimation of the group velocity along α direction, namely $V(\alpha) = d/\sqrt{\Delta t_{12}^2 + \Delta t_{13}^2}$. By using two clusters, two angles are found and the source is localised by solving two linear equations in two unknowns in a 2D space, as shown in Fig. 7.14. This procedure works for isotropic and weakly anisotropic materials, however, for the isotropic case only four sensors, i.e. a three-sensor cluster and a single additional sensor are sufficient for localization (Kundu 2012). In (Ciampa and Meo 2010a) also six sensors were used for ASLP on a composite plate, however, they were grouped in three clusters of two sensors each. This latter approach required the solution of a nonlinear set of equations. A hybrid approach based on the clusters and source location optimization was proposed in (Kundu et al. 2015), where the estimate of the source location is first is given by the technique outlined above (Kundu 2012), and this estimate is further improved by minimizing an error function.

Substantial difficulty with source location using incidence angle prediction may arise for moderately and strongly anisotropic materials. For certain wavefronts and cluster positions with respect to the source, the predicted angles may assume similar values, indicating that the source is very far from the sensing positions (or cannot be found when the predicted angles are equal, e.g. for a plane wave). A cluster-based solution for anisotropic materials, addressing the above issues, can be found in (Park

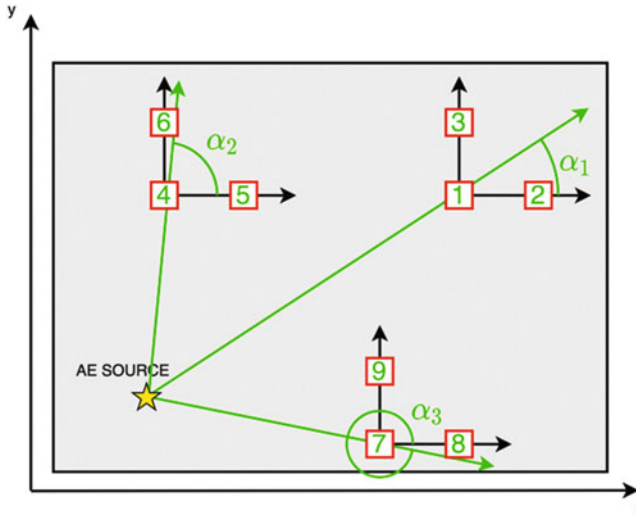


Fig. 7.14 A set of three clusters for (redundant) estimation of source localization (after Fig. 2 of Kundu 2012)

et al. 2017), where a set of three-sensor clusters was combined with an optimization procedure to locate the source. Knowing that for an anisotropic plate the wavefront assumes shapes different than circular, the proposed method assumes a parametric description of the wavefield emitted from the source and performs best fit for the model parameters using the arrival directions estimated by the clusters. In particular, two wavefront shapes—characteristic to weakly and moderately anisotropic plates—were assumed, i.e. elliptic and rhombus, respectively. The corresponding goal functions employ the ellipse and rhombus equations and include angles determined by the clusters. An example of an elliptic wavefront, requiring a minimum of three clusters is shown in Fig. 7.15, while for a rhombus wavefront—for which four clusters are needed—in Fig. 7.16.

Another approach to ASLP that uses collective response of possibly closely-spaced sensors, i.e. clusters, can be achieved by beamforming (McLaskey et al. 2010). Although beamforming (BF) techniques are widely known in active NDT and SHM, their application to acoustic emission is not that common. Acoustic source localization with beamforming employs the same signal processing techniques as in active methods and requires knowledge on material properties of the medium. Both isotropic (McLaskey et al. 2010) and anisotropic (Nakatani et al. 2012) structures can be monitored with beamforming, if the wave speed profile—constant or angle-dependent, respectively—is known.

A method based on two perpendicular clusters of a total of 9 sensors and the beamforming algorithm for AE was proposed in (McLaskey et al. 2010; Xiao et al. 2014). The corresponding setup of ASLP with BF is shown in Fig. 7.17. Each of M sensors, placed at positions r_m , acquires signal $S_m(t)$ in case an AE event is generated. The cluster sweeps the two-dimensional space of possible acoustic source

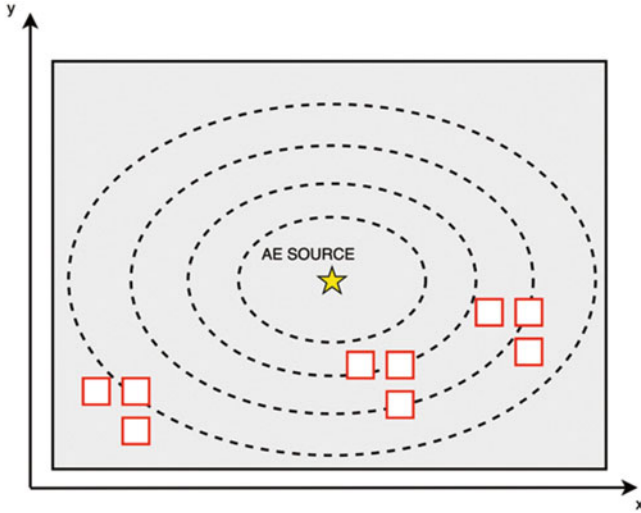


Fig. 7.15 Elliptic wavefront in an anisotropic plate with three clusters required for source localization (after Park et al. 2017)

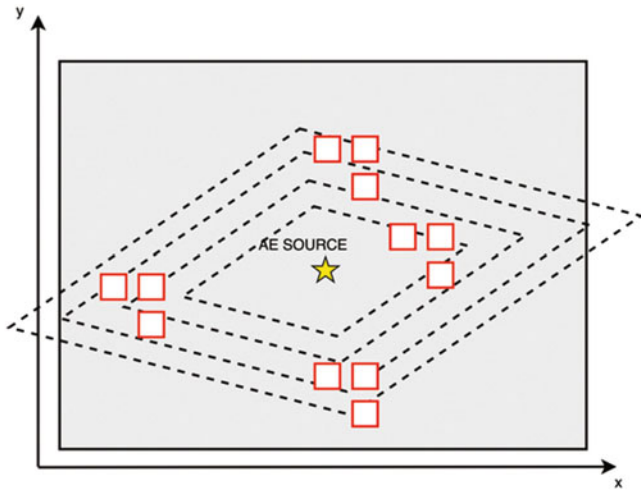


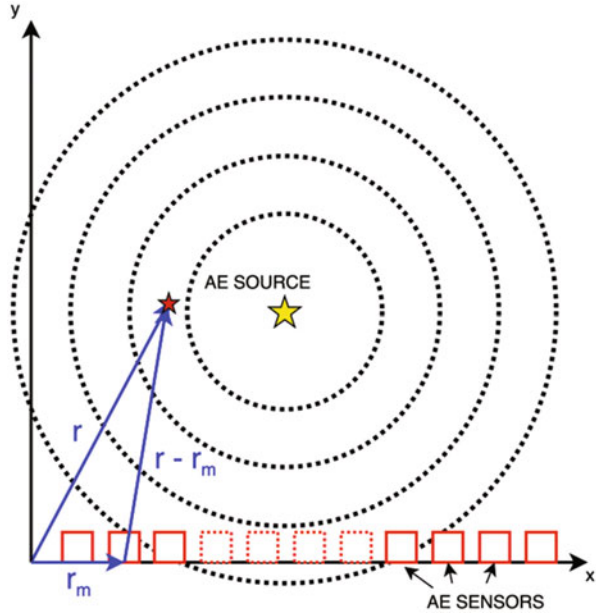
Fig. 7.16 Rhombus wavefront in an anisotropic plate with four clusters required for source localization (after Park et al. 2017)

locations (also known as focal points, red star in Fig. 7.17), r , by applying time delays

$$\Delta_m = \frac{(|r| - |r - r_m|)}{V} \tag{7.5}$$

to each of the S_m time signals and summing them

Fig. 7.17 Acoustic source localization with the beamforming approach (after Xiao et al. 2014)



$$b(r, t) = \frac{1}{M} \sum_{m=1}^M w_m S_m(t - \Delta_m) \tag{7.6}$$

In Eq. (7.6), w_m are weights that can be applied to each individual sensor. $b(r, t)$ assumes maximum value if the focal point r coincides with the source position. In (Nakatani et al. 2012) this concept was further extended to anisotropic media by using direction-dependent wave speed $V(\alpha)$.

Clusters provide highly accurate localization results for isotropic and (weakly) anisotropic media, thus are of wide practical interest. The following factors, however, influence the cluster-based ASLP accuracy. (1) the distance between sensors, d , needs to be small, requiring small sensor footprints; (2) along with small d , the sampling frequency for the signals must be high enough to accurately capture waveform shifts between the sensors (i.e. accurate measurement of Δt); (3) the distance to the source, D , should be large compared to d , allowing for the planar wavefront approximation (and certain assumptions on incidence angles), (4) sensors need to be positioned very accurately within the cluster. Condition (3) implies the ability of monitoring large areas, however, with increasing D , the localization accuracy for anisotropic materials drops. The latter is a result of the non-colinear wave and energy propagation vectors.

To cope with AE localization problems with more sophisticated geometric structure, material/wave propagation characteristics, and flexible sensor configurations, AE localization can be formulated as an optimization problem, seeking a

solution (predicted source location) that leads to TDOA as consistent as possible with the measures. Such methods are mostly formulated as an iterative optimization process, starting from some initial guesses. Existing research proposed to use different optimization techniques. (Ciampa and Meo 2010b) uses Newton's method to optimise a nonlinear formulation to find the source location from an initial guess. Newton's method is known to converge quickly (with quadratic convergence) when the current estimate is close to the true solution. They further incorporate a line search strategy to optimise the step size to ensure improvement during iterations, to improve the robustness of the method. However, such local optimization methods may still converge to local minima. Alternative techniques have considered using more global optimization, such as genetic algorithms (Veloso et al. 2006), particle swarm optimization (Wang et al. 2017), an iterative evolutionary method named Iterative Planar Source method (Mirgal et al. 2020), etc. These methods typically start with a set of initial guesses (e.g. 50). For each estimated source location, they work out the calculated travel time to sensors, and the differences between calculated and measured travel times to sensors are used to calculate fitness values (or equivalent) of the estimated source location. These are then used to update sensor location estimations in the next iteration, with the exact formulae determined by the optimization techniques used. The iterative process tends to converge to a solution close to the true location. By using multiple estimated locations and iteratively optimizing them, such methods have a higher chance of finding the global optimum. More recent methods tend to converge more quickly than previous techniques.

These AE localization techniques still face challenges to cope with potentially complex reflections and reverberations of waveforms, and often ignore the rich signal content. In recent years, with the development of deep learning, techniques based on deep neural networks have been proposed as a way to tackle these challenges (Kalafat and Sause 2015; Ebrahimkhanlou and Salamone 2018a, 2018b). Thanks to the strong learning capabilities, deep neural networks often directly take some representations of the AE waveform as input, such as continuous wavelet transform to retain information in the rich waveform signal. Unlike many conventional techniques, typically based on using a single waveform feature, neural networks may exploit wider frequency bands—therefore richer signals. Different network architectures have been investigated, including an architecture that involves stacked autoencoder layers (which can be trained in an unsupervised manner to learn to extract useful features), followed by supervised layers to predict localization zones as a classification problem (Ebrahimkhanlou and Salamone 2018a) or regress the source location (Ebrahimkhanlou and Salamone 2018b). Alternative architectures such as those based on convolutional neural networks (CNNs) are also considered, where the waveform is analyzed with different times and frequencies to form an image-like input for the CNN to be applied (Ebrahimkhanlou and Salamone 2018a). Deep learning-based methods are able to utilise richer information in the waveform, which rather than being negatively impacted by reflections and reverberations, can effectively exploit such clues to help with localization. Studies

show that this can lead to more accurate localization (Kalafat and Sause 2015) or localization with fewer sensors including one sensor (Ebrahimkhanlou and Salamone 2018b), although sufficient amount of training data is required and more studies are needed for network architectures that reach a better balance of data demands and effectiveness of the learned models.

7.5 Influence of Propagation

A cracking source may be simulated by a near-step function or by half a cycle of short duration in case of impact, as studied in literature (McLaskey and Glaser 2012; Prosser 2002). However, this has no similarity to the much longer waveform recorded by a sensor just a few cm away, due to the complicated physics of wave propagation and transduction, see Fig. 7.18. The initial excitation (crack propagation increment or ‘source’ in our case) propagates through a material with certain characteristics (stiffness, density, attenuation coefficient, heterogeneity, as explained later in the chapter) which strongly influence its shape. Then at reception, the characteristics of the sensor, mainly frequency response will further influence the waveform (not forgetting the coupling conditions), while the acquisition system may also impose further distortion. Therefore, the final digitised waveform has very few similarities to the original source, see Fig. 7.18.

Making certain assumptions, like the point nature of the receiver, the final waveform (W) can be expressed as the convolution ($*$) between the initial excitation

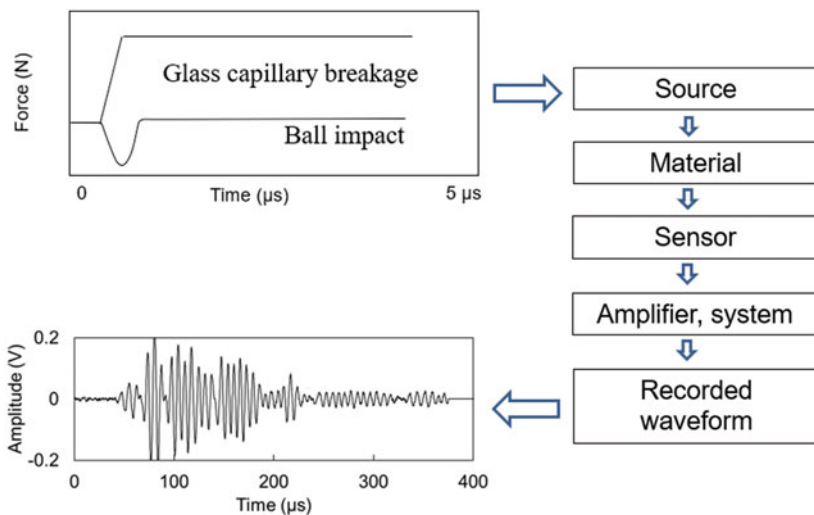


Fig. 7.18 Process chain of AE production and reception (Similar to McLaskey and Glaser 2012)

(E), and the transfer functions of the material (M), the sensor (S) and the amplifier/system (A)

$$W = E * M * S * A \quad (7.7)$$

This is easier handled in frequency domain, where the convolution is expressed by the product of the FFTs of the above functions.

Precise knowledge of the transfer functions of the material and system may allow therefore, to derive the source excitation using the waveform as received at the sensor, assuming that the sensor is not highly resonant. Still this is a tedious process and even slight mistakes in the included process links, may result in significant distortion at the end. Although, tracing back the exact source function may be difficult (though not impossible), still comparisons between sources can be readily conducted, if the experimental conditions remain the same (sensors, material, distance), that is all intermediate transfer functions are constant and therefore, they do not impose differential distortion between different signals.

Below follows a detailed discussion on the exact factors contributing to the above-mentioned material transfer function, which is also related to the Sect. 5.2 that described the formation and propagation mode of guided waves. There are several items that make the occurrence of guided waves unique in the context of AE measurements. Other than for active guided waves, AE sources cannot select a particular frequency or guided wave mode. Instead, based on the duration of crack growth they excite a certain bandwidth and—depending on the position in through-thickness direction—may excite one or more guided wave modes at the same time. Therefore, the interpretation of the AE signals has to deal with this additional complexity.

With the propagation of information in form of guided waves, several items happen. First, the whole wave undergoes attenuation, which can originate from several contributions. Secondly, the guided waves themselves suffer from information distortion due to dispersion. As consequence, after a certain propagation distance, the information contained in the AE signals will be altered, so that information retrieval about the source origin is only feasible up to a limited distance.

As discussed by Pollock (Pollock 1986) and Prosser (Prosser 1996) from the point of view of acoustic emission, there are five key contributions to attenuation:

1. Geometric spreading
2. Thermoelastic and Akhieser dissipation
3. Dispersion
4. Scattering
5. Dissipation into adjacent media

In the near-field range, close to the AE source, the geometrical spreading is the main reason for the attenuation. In volumetric media this is caused by the spherical radiation of energy into the volume, which leads to an energetic decay per dihedral angle with inverse propagation distance. For plate-like structures, the radiation is limited to two dimensions, after the 3D spreading in the very near field over the plate

thickness, causing an energetic decay with square-root of distance to the source. If such guided waves are excited, additional amplitude decay is present since the energy of the elastic waves is split into the distinct modes. In addition, these modes suffer from velocity dispersion, as described below.

In the far field of the AE source, the main contributions to the attenuation are due to thermoelastic and the Akhieser dissipation. The first results from the irreversible heat losses caused by compression during longitudinal wave propagation. The second mechanism results from the disturbance of the equilibrium distribution of the thermal acoustic waves (phonons), which leads to a dissipative energy contribution. In homogeneous isotropic solids, the thermoelastic and the Akhieser dissipation lead to an attenuation for elastic waves as a function of the square of the oscillation frequency.

In the case of guided waves, other effects contribute to the overall AE attenuation. In the case of Lamb waves, contributions to the total damping result from the spatial dispersion and the frequency dispersion (Neau et al. 2001). The attenuation from the spatial dispersion is caused by the relation between phase velocity and wave vector. As discussed by Ward et al. for dispersive media, the phase velocity is directly related to the attenuation by a Kramers-Kronig relationship (Ward 1971). The effect of attenuation due to frequency dispersion occurs during the propagation of non-monochromatic wave packages. Since each frequency component propagates at a certain velocity, an initially short pulse begins to spread in time during propagation. This causes an effective amplitude attenuation with distance of propagation. This is of great importance for the case of guided waves, since the different modes have different attenuation coefficients in addition. These effects are superimposed on the thermoelastic dissipation, since individual guided wave modes are dominated by distinct frequency portions (Prosser 1996). In addition, the propagating waves can be scattered by inhomogeneities depending on the wave frequencies and sizes of the inhomogeneities. Typical examples are the grain structure within metals, fibers in composites or cavities. This can lead to additionally strong attenuation and must be considered when discussing attenuation effects (Aggelis et al. 2004).

In real test settings or in SHM applications, AE signals propagate within the structure under test, which is typically in contact with adjacent items such as nearby structural parts, fittings, fasteners or supply lines. Since a partial transmission of the AE signal into adjacent media leads to a corresponding intensity loss of the reflected wave, such losses can be considerably high and thus even dominate the acoustic attenuation in a given scenario.

As a result of these propagation effects, the information contained in the amplitude and frequency of the AE signal formed during excitation is changed during propagation. Consequently, the detection and identification of a failure mechanism is limited to a certain distance around the position of the acoustic emission excitation. The influence of reflection should be mentioned as they contribute to the recorded signals and influence the obtained waveforms.

For fiber reinforced materials, the attenuation is typically much higher than for metallic materials. This increase of attenuation is due to the pronounced viscoelastic

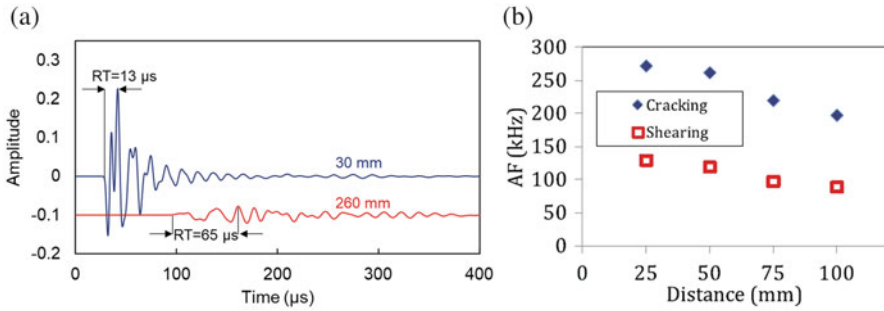


Fig. 7.19 (a) Simulated waveforms received at different distances from the source on a plate of 20 mm thickness, (b) average frequency, AF, for two fracture mechanisms vs. propagation distance in glass fiber composite (Aggelis et al. 2017)

response of the polymeric matrix materials, which are more prone to thermoelastic dissipation. Since higher frequencies are subject to higher attenuation, the relative loss of intensity can make it quite difficult for pattern recognition approaches to properly cluster AE signals of the same source type. Nevertheless, the attenuation effects can be investigated both experimentally and by FEM (Gallego and Ono 2012; Sause 2016) to consider their impact on AE signal interpretation.

In the following figure (Fig. 7.19a), an example of the influence of propagation on the waveform shape is shown. The simulations made through finite difference method concern a vertical crack propagation event in the middle of the thickness of a 20 mm thick plate of material with corresponding longitudinal wave velocity 3000 m/s. Despite the same origin, the two waveforms received at different spots exhibit strong differences in their shape. The amplitude of the second is significantly lower, while the aforementioned ‘spreading’ is obvious. Indicatively, the amplitude drops by 89% while the aforementioned ‘spreading’ is obvious. Indicatively, the amplitude drops by 89% while the RT increases from 13 to 65 μs in just 230 mm of propagation. Fig. 7.19b shows an experimental example of such an effect, where the influence of distance on the average frequency ‘AF’ is shown for two major fracture mechanisms. Vertical cracking is connected to much higher frequency content for any corresponding distance than delaminations (shear), however, the decreasing trend is obvious due to aforementioned attenuation and dispersion mechanisms. It is seen therefore, that consideration of the distance (through localization) is of paramount importance, since signals emitted by high frequency sources but collected far away from the source, tend to obtain similar characteristics to signals coming from low energy sources but recorded close to the source (Aggelis et al. 2017).

7.6 Different Sensor Types

As thoroughly examined above, various physical phenomena in the material can cause elastic waves, which propagate throughout the material. The basic task of sensors is therefore, to detect surface displacements (typically out-of-plane) and to generate an electrical or optical signal. Piezoelectric sensors with an integrated element made of special ceramic, such as $\text{Pb}(\text{Zr}_x\text{Ti}_{1-x})\text{O}_3$ or Lead Zirconate Titanate (PZT) are most often used in practice (Enoki et al. 2000; Moore 2005). PZT sensors need acoustic coupling for the dynamic surface motion of the specimen to result in dynamic strain in the piezoelectric transduction element which is reflected in voltage versus time signal. Piezoelectric transducers are most practical, they offer high sensitivity and are robust. PZT transducers are similar to PZT accelerometers except that the proof mass is replaced by a backing material to control damping. Resonant transducers that have one or more preferred frequencies of oscillation governed by crystal size and shape usually exhibit higher sensitivity and are less costly than broad-band piezoelectric transducers. The proper design of the PZT transducer offers a detection frequency range from 30 kHz to 1 MHz or in the case of resonant sensors, smaller frequency ranges. The transducers can have integrated preamplifier or the preamplifier is connected separately to the sensor. The amplified AE signal is transmitted via signal cables that can be of several hundred meters long to the AE system. Besides the mentioned advantages, they also have disadvantages, namely, the signal does not exactly resemble the actual surface displacements due to limited bandwidth, resonance, and are not always close to the point receiver concept, meaning that their response is the average field acting on their surface. This may cause serious distortion and attenuation when the wavelength is much smaller than the physical size of the transducer, especially for high frequencies (McLaskey and Glaser 2012; Ono 2017; Tsangouri and Aggelis 2018). PZT sensors are electrical sensors and therefore, are susceptible to electromagnetic interference, they also have a limited temperature range of operation (normal PZT cannot be used at temperatures more than 150 °C). In case high temperature application is necessary, the use of waveguides is essential (Godin et al. 2018; Papasalouros et al. 2016).

Recently, optical fiber systems have been gaining more importance for the detection of elastic waves in materials, thus directing research in the field of AE from electro-acoustic sensing technology to photoacoustic sensing technology. In general, optical fiber systems comprise optical sources that can be a laser, laser diode or light emitting diodes (LED), optical fibers, sensing element to transduce the measurement to an optical signal, an optical detector, and processing unit in a form of oscilloscope or optical analyzer. Based on the sensing location, an optical fiber sensor can be classified as extrinsic where the optical fiber is used to carry light to and from an external optical device for sensing or intrinsic where environmental perturbations influence the physical properties of the optical fiber. External perturbations can influence intensity, phase, frequency and polarization. In general, advantages of optical fiber sensors over conventional piezoelectric sensors are their relatively easier integration with little interference into a wide variety of

structures of different materials, immunity to electromagnetic interference, resistance to harsh environments, robustness, lightweight, multifunctional sensing capabilities such as strain, pressure, temperature and acoustic signals (Fidanboyly and Efendioglu 2009). Optical fiber sensors include single fiber and fiber device sensors, optical fiber interferometers, and fiber Bragg grating sensors (Wild and Hinckley 2008). There are many single fiber sensing methods for the detection of AE signals such as evanescent field coupler, fused tapered fiber coupler, frustrated total internal reflection, and fiber microbending. Several interferometer configurations have been proposed i.e. Michelson, Mach-Zehnder, Fabry-Perot, and Sagnac. Interferometric optical fiber sensors have limitation regarding gauge length of the sensor and consequent cross-sensitivity problems with other measurands such as static strain and temperature. Short length Fabry-Perot interferometers offer a significantly reduced gauge length. Shorter gauge lengths can be accomplished with various intensity based single fiber optical methods or with fiber Bragg grating sensors (Wild and Hinckley 2008). FBG sensors are small in size, can be embedded in the structure, and have high sensitivity that is directionally dependent and can affect its performance (Perez et al., 2006; Mabry et al. 2011; Wu and Okabe 2012).

Another type of contact acoustic emission sensor is the capacitive sensor. They constitute two separate electrodes where one electrode is fixed to the substrate. Electrodes are separated by a small gap and form a capacitor under a DC voltage bias. The vibration of the electrode produces a time-varying current. They have been successfully used in laboratory tests. Such transducers can have good fidelity where the electrical signal very closely follows the actual dynamic surface displacement, but typically minimum displacement measured is lower than with PZT sensors (Moore 2005). Capacitive sensors can be in the form of micro-electro-mechanical system (MEMS). MEMS-based transducers for AE can be small, and if produced on a large scale inexpensive. They can integrate several transducers with different resonant frequencies on the chip that covers the frequency range of interest (Ozevin et al. 2006). Ozevin reported almost three times lower signal to noise ratio in the dB scale for MEMS transducers compared to conventional PZT transducer with results in fewer AE events detected.

Contact transducers for AE measurements have disadvantages in monitoring AE behavior in small or thin specimens related with the size of the transducer. Non-contact optical transducers in a form of laser interferometry offer quantitative and highly localized measurements of the surface motion. They do not disturb elastic waves, also they are not limited by frequency response (Kline et al. 1978). Out-of-plane displacement and velocity of the surface movement can be measured. The laser beam can be focused at a very small spot of the order of microns. For higher sensitivity a reflective surface is needed and it is difficult to get an adequate signal to noise ratio (Enoki et al. 2000). The interferometer can be internally calibrated to yield absolute displacement amplitudes.

7.7 Dedicated Aeronautics Applications and Examples

Over the last 30 years AE monitoring has been used to assess damage initiation and growth in aircraft structures, primarily during ground testing (Martin et al. 1995). Within this early testing, problems arose regarding the quantity of data produced, distinguishing noise from damage, and accurate source localization in complex structures. In recent years the increasing use of carbon fibre reinforced polymers (CFRP) has introduced new challenges, in addition to those already faced. Recent developments have enabled more success with the technology in real applications. Although there are only limited cases of AE monitoring being used for in service structures, ground-based testing has been improved greatly by these advances. Haile et al. (2017) used 12 AE sensors to monitor four high risk areas during fatigue testing of a full-scale UH-60 helicopter fuselage. The composite fuselage was manufactured from advanced thermoplastics and thermoset carbon-fibre, with additional stiffeners. Time of arrival (TOA) was used to locate sources, however, complicity made this difficult. The work concluded that further methods were required to enable large-scale monitoring of complex structures in real operating conditions. A technique applied to aircraft structures to improve AE localization is the Delta-T approach. Initially developed by Baxter (Baxter et al. 2007) the technique requires the structure to be mapped with Hsu-Nielsen sources. From this, a map of the difference in arrival times at each pair of sensors can be created. Pearson et al. (2017) trialed the technique on a relatively simple A320 wing rib, where an average 9.3 mm increased accuracy was seen. Fatigue testing of an aluminium panel with a number of large holes was also presented. In this testing the Delta-T technique located AE events generated from a crack with greater accuracy, increased confidence and a greater number of lower energy events which were unsuccessful with the standard TOA technique. The technique was also used for location of damage on an A320 landing gear fatigue test, where a crack was located to 10 mm accuracy (Holford et al. 2017). In the early days of AE monitoring, only the amplitude and other simple features of the event were considered; this enabled noise filtering, however was very reliant on the skill of the engineer (Martin et al. 1995). As aforementioned, recent advances in classification, through approaches such as artificial neural networks ANN, enable automatic classification of waveforms, which enables clear differentiation between damage and noise (Crivelli et al. 2014).

Impact monitoring in aircraft structures is vital, in particular within carbon fibre reinforced polymers (CFRP) where barely visible impact damage (BVID) result in delamination of fibres, causing the strength of the structure to be compromised. Traditional non-destructive testing (NDT), required technicians to manually inspect the structure using ultrasonic probes, a time-consuming process that requires downtime for the aircraft. As existence of damage is inevitable, aircrafts are designed damage tolerant (Talreja and Phan 2019), increasing their weight. AE can be used to detect impact to an aircraft structure, either by detecting the impact itself, or any growth under fatigue. After the loss of space shuttle Columbia due to impact damage Prosser (Prosser et al. 2004) investigated the use of AE monitoring of the leading

edge of space shuttles. It was found that although accelerometers could locate impact events, ultrasonic sensors had lower background noise and so were more suited for impact detection. The detection of impact in a composite aircraft is not only vital during service, but also during manufacturing, where tools drop and knocks during transport cause damage. The earlier damage is detected, the quicker it is resolved, saving money. To detect impact during manufacture, wireless systems have been utilised, as the associated problems with battery life are less vital. Gianni et al. (2020) developed a low power system, capable of accurately determining the time of arrival of an impact wave at a piezoelectric sensor. The distributed array of sensor nodes were time correlated via GPS, and source localization performed at a central hub. Within this work impact sources were located on a simple aluminium plate, however advanced localization algorithms, such as the Delta-T method could be used.

In another application, the integrity of bearings within a helicopters main gearbox is vital, as the large speed reduction causes high forces, which make them prone to pitting, spalling and contact wear. SHM of these has been applied since the 1990s, known as Health and Usage Monitoring Systems (HUMS), which record and analyse vibrations. Although these systems have reduced accidents, they are not completely accurate, and failures still occur. This failure is generally attributed to the noise produced within the system masking the useful signals. In recent years AE has been applied to the problem, since the frequency of interest is higher than that generated by sliding and friction in the bearing. This has been shown to enable AE monitoring to identify the presence of damage significantly earlier than vibration techniques (Elasha et al. 2018).

7.8 General Considerations

While the use of SHM systems is imperative in an aerospace structure, several points should be examined to make sure the system works properly, and it is compatible with in-flight requirements. One is the additional weight the SHM system will bring, something that eventually accounts for higher fuel consumption and air transport cost. The potential weight saving of removing non-essential wiring from an aircraft could save an estimated 14–60 million over a commercial aircrafts life (Gao et al. 2018). Doing so would reduce costly and time-consuming maintenance and installation of wiring (Yedavalli and Belapurkar 2011). Commercially available wireless AE systems with transmission capacity of several hits/s exist (Mistras 2013; Shen 2017). However, while wireless systems are promising, they still require power. Batteries could supply the required energy, but are heavy, expensive and their performance is low in cold conditions typical of a flying aircraft, while their use is restricted in aerospace industry. Therefore, energy harvesting is a requirement combined with an energy storage device, such as a super capacitor. Vibrational harvesters and thermal-electric generators show potential, however, there is currently a gap between the generated and the required energy. Another issue of an in-flight SHM system is the generation of large amount of data, that could easily

reach rates of tens of MB/hour/channel. Transmission of such large amounts of data and especially full waveforms would be costly and power consuming (Anastasi et al. 2009). Therefore, intelligent processing and data management is needed to filter out non-essential data, something that would require integration of improved algorithms for damage localization and characterization into the hardware. Finally, another important point is the harsh environments that the wireless SHM system should operate in, meaning that any device on board must pass a series of tests ranging from temperature to vibration-based testing. Only combination and optimization of all above aspects will enable unlocking the potential the true potential of a SHM system, while the specific issues are dealt with in more detail in the respective chapters.

References

- Aggelis DG, Tsinopoulos SV, Polyzos D (2004) An iterative effective medium approximation (IEMA) for wave dispersion and attenuation predictions in particulate composites, suspensions and emulsions. *J Acoust Soc Am* 116:3443–3452. <https://doi.org/10.1121/1.1810273>
- Aggelis DG, Barkoula N-M, Matikas TE et al (2012) Acoustic structural health monitoring of composite materials: damage identification and evaluation in cross ply laminates using acoustic emission and ultrasonics. *Compos Sci Technol* 72:1127–1133. <https://doi.org/10.1016/j.compscitech.2011.10.011>
- Aggelis DG, Dassios KG, Kordatos EZ et al (2013) Damage accumulation in cyclically-loaded glass-ceramic matrix composites monitored by acoustic emission, the scientific world. 869467.
- Aggelis DG, El Kadi M, Tysmans T et al (2017) Effect of propagation distance on acoustic emission fracture mode classification in textile reinforced cement. *Constr Build Mater* 152:872–879. <https://doi.org/10.1016/j.conbuildmat.2017.06.166>
- Aki K, Richards PG (1980) Quantitative seismology, theory and methods. University Science Books, Sausalito
- Anastasi G, Conti M, Di Francesco M, Passarella A (2009) Energy conservation in wireless sensor networks: a survey. *Ad Hoc Netw* 7:537–568
- Anastassopoulos AA, Philippidis TP (1995) Clustering methodology for the evaluation of acoustic emission from composites. *J Acoust Emission* 13:11–21
- Anastassopoulos AA, Nikolaidis VN, Philippidis TP (1999) A comparative study of pattern recognition algorithms for classification of ultrasonic signals. *Neural Comput Appl* 8:53–66. <https://doi.org/10.1007/s005210050007>
- Baensch F, Sause MGR, Brunner AJ et al (2015a) Damage evolution in wood – pattern recognition based on acoustic emission (AE) frequency spectra. *Holzforschung* 69:357–365. <https://doi.org/10.1515/hf-2014-0072>
- Baensch F et al (2015b) Damage evolution in wood – pattern recognition based on acoustic emission (AE) frequency spectra. *Holzforschung* 69(3):1–9. <https://doi.org/10.1515/hf-2014-0072>
- Baxter MG, Pullin R, Holford KM et al (2007) Delta T source location for acoustic emission. *Mech Syst Signal Process* 21:1512–1520. <https://doi.org/10.1016/j.ymsp.2006.05.003>
- Bendat JS, Piersol AG (1993) Engineering applications of correlation and spectral analysis, 2nd edn. Wiley, New York
- Bianchetti R, Hamstad MA, Mukherjee AK (1976) Origin of burst-type acoustic emission in unflawed 7075-T6 aluminum. *J Test Eval* 4:313. <https://doi.org/10.1520/JTE10518J>
- Blom J, El Kadi M, Wastiels J et al (2014) Bending fracture of textile reinforced cement laminates monitored by acoustic emission: influence of aspect ratio. *Constr Build Mater* 70:370–378. <https://doi.org/10.1016/j.conbuildmat.2014.07.080>

- Bohse J, Chen J (2001) Acoustic emission examination of mode I, mode II and mixed-mode I/II interlaminar fracture of unidirectional fiber-reinforced polymers. *J Acoust Emission* 19:1–10
- Burks B, Kumosa M (2014) A modal acoustic emission signal classification scheme derived from finite element simulation. *Int J Damage Mech* 23:43–62. <https://doi.org/10.1177/1056789513484620>
- Chandarana N, Sanchez DM, Soutis C et al (2017) Early damage detection in composites during fabrication and mechanical testing. *Materials* 10:685. <https://doi.org/10.3390/ma10070685>
- Ciampa F, Meo M (2010a) A new algorithm for acoustic emission localization and flexural group velocity determination in anisotropic structures. *Compos A* 41:1777–1786. <https://doi.org/10.1016/j.compositesa.2010.08.013>
- Ciampa F, Meo M (2010b) Acoustic emission source localization and velocity determination of the fundamental mode A0 using wavelet analysis and a Newton-based optimization technique. *Smart Mater Struct* 19. <https://doi.org/10.1088/0964-1726/19/4/045027>
- Cousland SMK, Scala CM (1983) Acoustic emission during the plastic deformation of aluminium alloys 2024 and 2124. *Mater Sci Eng* 57:23–29. [https://doi.org/10.1016/0025-5416\(83\)90023-X](https://doi.org/10.1016/0025-5416(83)90023-X)
- Crivelli D, Guagliano M, Monici A (2014) Development of an artificial neural network processing technique for the analysis of damage evolution in pultruded composites with acoustic emission. *Compos Part B Eng* 56:948–959. <https://doi.org/10.1016/j.compositesb.2013.09.005>
- De Groot PJ, Wijnen PAM, Janssen RBF (1995) Real-time frequency determination of acoustic emission for different fracture mechanisms in carbon/epoxy composites. *Compos Sci Technol* 55:405–412. [https://doi.org/10.1016/0266-3538\(95\)00121-2](https://doi.org/10.1016/0266-3538(95)00121-2)
- De Oliveira R, Frazão O, Santos JL et al (2004) Optic fibre sensor for real-time damage detection in smart composite. *Comput Struct* 82:1315–1321. <https://doi.org/10.1016/j.compstruc.2004.03.028>
- Doan DD et al. (2014) Application of an unsupervised pattern recognition approach for AE data originating from fatigue tests on CFRP. In: 31st Conference of the European working group on acoustic emission. Dresden, Germany, pp 1–8.
- Eaton M, May M, Featherston C et al (2011) Characterisation of damage in composite structures using acoustic emission. *J Phys Conf Ser* 305:012086. <https://doi.org/10.1088/1742-6596/305/1/012086>
- Ebrahimkhanlou A, Salamone S (2018a) Single-sensor acoustic emission source localization in plate-like structures using deep learning. *Aerospace* 5:50. <https://doi.org/10.3390/aerospace5020050>
- Ebrahimkhanlou A, Salamone S (2018b) Single-sensor acoustic emission source localization in plate-like structures: a deep learning approach. In: Proceedings of the Volume 10600, health monitoring of structural and biological systems, XII. <http://www.ncbi.nlm.nih.gov/pubmed/1060010>.
- Elasha F, Greaves M, Mba D (2018) Planetary bearing defect detection in a commercial helicopter main gearbox with vibration and acoustic emission. *Struct Heal Monit* 17:1192–1212. <https://doi.org/10.1177/1475921717738713>
- Enoki M, Watanabe M, Chivavibul P et al (2000) Non-contact measurement of acoustic emission in materials by laser interferometry. *Sci Technol Adv Mater* 1:157–165. [https://doi.org/10.1016/S1468-6996\(00\)00017-6](https://doi.org/10.1016/S1468-6996(00)00017-6)
- Ernst R, Dual J (2013) Acoustic emission source detection using the time reversal principle on dispersive waves in beams. In: Proceedings of the 2013 international congress on ultrasonics (ICU 2013). Singapore, pp 87–92. <http://www.zfm.ethz.ch/pdf/13-Ernst-1.pdf>
- Esola S, Wisner BJ, Vanniamparambil PA et al (2018) Part qualification methodology for composite aircraft components using acoustic emission monitoring. *Appl Sci* 8:1490. <https://doi.org/10.3390/app8091490>
- Fidanboylyu K, Efendioglu HS (2009) Fiber optic sensor and their applications. In: 5th International advanced technologies symposium (IATS'09), May 13-15. Karabuk, Turkey

- Fowler TJ (1977) Acoustic emission testing of fiber reinforced plastics. ASCE Fall Convention, San Francisco
- Gallego A, Ono K (2012) An improved acousto-ultrasonic scheme with lamb wave mode separation and damping factor in CFRP plates. *J Acoust Emission* 2012:109–123
- Gao S, Dai X, Hang Y, Guo Y, Ji Q (2018) Airborne wireless sensor networks for airplane monitoring system. *Wireless Commun Mobile Comput* 2018. <https://doi.org/10.1155/2018/6025825>
- Gawronski M, Grabowski K, Russek P et al (2016) Acoustic emission source localization based on distance domain signal representation. *Proc SPIE 9805 Health Monit Struct Biol Syst* 2016:980501.
- Gianni C, Balsi M, Esposito S et al (2020) Low-power global navigation satellite system-enabled wireless sensor network for acoustic emission localisation in aerospace components. *Struct Control Heal Monit* 27:1–13. <https://doi.org/10.1002/stc.2525>
- Giordano M, Calabro A, Esposito C et al (1998) An acoustic-emission characterization of the failure modes in polymer-composite materials. *Compos Sci Technol* 58:1923–1928. [https://doi.org/10.1016/S0266-3538\(98\)00013-X](https://doi.org/10.1016/S0266-3538(98)00013-X)
- Giordano M, Condelli L, Nicolais L (1999) Acoustic emission wave propagation in a viscoelastic plate. *Compos Sci Technol* 59:1735–1743. [https://doi.org/10.1016/S0266-3538\(99\)00035-4](https://doi.org/10.1016/S0266-3538(99)00035-4)
- Godin N, Reynaud P, Fantozzi G (2018) Challenges and limitations in the identification of acoustic emission signature of damage mechanisms in composites materials. *Appl Sci* 8:article number 1267. <https://doi.org/10.3390/app8081267>
- Gorman MR (1991) Plate wave acoustic emission. *J Acoust Soc Am* 90:358–364. <https://doi.org/10.1121/1.401258>
- Gorman MR (2011) Modal AE analysis of fracture and failure in composite materials, and the quality and life of high pressure composite pressure cylinders. *J Acoust Emission* 29:1–28
- Gorman MR, Prosser WH (1991) AE source orientation by plate wave analysis. *J Acoust Emission* 9:283–288. <https://calhoun.nps.edu/handle/10945/40334>
- Gorman MR, Ziola SM (1991) Plate waves produced by transverse matrix cracking. *Ultrasonics* 29:245–251. [https://doi.org/10.1016/0041-624X\(91\)90063-E](https://doi.org/10.1016/0041-624X(91)90063-E)
- Grabowski K, Nakatani H, Gawronski M et al (2015) System reliability for verification and implementation. In: *Proceedings of the 10th international workshop on structural health monitoring optimization of acoustic source localization in large plates. IWSHM 2015*.
- Grabowski K, Gawronski M, Baran I et al (2016a) Time–distance domain transformation for acoustic emission source localization in thin metallic plates. *Ultrasonics* 68:142–149. ISSN 0041-624X
- Grabowski K, Gawronski M, Staszewski WJ et al (2016b) Acoustic emission source localization through excitability prediction and dispersion removal technique. IIIAE, Kyoto, p IAES-23 & ICAE-8, Kyoto, Japan
- Green ER (1995) Acoustic emission sources in a cross-ply laminated plate. *Compos Eng* 5:1453–1469. [https://doi.org/10.1016/0961-9526\(94\)00072-H](https://doi.org/10.1016/0961-9526(94)00072-H)
- Green ER (1998) Acoustic emission in composite laminates. *J Nondestruct Eval* 17:117–127
- Grosse CU, Linzer LM (2008) Ch. 5 Signal-based AE analysis, In: Grosse CU, Ohtsu M (ed) *Acoustic emission testing*, pp 53–99.
- Grosse CU, Ohtsu M (2008) *Acoustic emission testing*. Springer, Berlin Heidelberg. <https://doi.org/10.1007/978-3-540-69972-9>
- Haile MA, Bordick NE, Riddick JC (2017) Distributed acoustic emission sensing for large complex air structures. *Struct Heal Monit* 17:624–634. <https://doi.org/10.1177/1475921717714614>
- Hamstad MA (1986) A discussion of the basic understanding of the Felicity effect in fiber composites. *J Acoust Emission* 5:95–102
- Hamstad MA (2010) Frequencies and amplitudes of AE signals in a plate as a function of source rise time. In: *29th European conference on acoustic emission testing*. Vienna, Austria, pp 1–8.
- Hamstad MA, O’Gallagher A, Gary J (2002a) A wavelet transform applied to acoustic emission signals: part 1: source identification. *J Acoust Emission* 20:39–61

- Hamstad MA, O'Gallagher A, Gary J (2002b) A wavelet transform applied to acoustic emission signals: part 2: source location. *J Acoust Emission* 20:62–82
- Haselbach W, Lauke B (2003) Acoustic emission of debonding between fibre and matrix to evaluate local adhesion. *Compos Sci Technol* 63:2155–2162. [https://doi.org/10.1016/S0266-3538\(03\)00193-3](https://doi.org/10.1016/S0266-3538(03)00193-3)
- Holford KM, Eaton MJ, Hensman JJ et al (2017) A new methodology for automating acoustic emission detection of metallic fatigue fractures in highly demanding aerospace environments: an overview. *Prog Aerosp Sci* 90:1–11. <https://doi.org/10.1016/j.paerosci.2016.11.003>
- Huguet S, Godin N, Gaertner R et al (2002) Use of acoustic emission to identify damage modes in glass fibre reinforced polyester. *Compos Sci Technol* 62:1433–1444. [https://doi.org/10.1016/S0266-3538\(02\)00087-8](https://doi.org/10.1016/S0266-3538(02)00087-8)
- Kaiser J (1950) Untersuchung über das Auftreten von Geräuschen beim Zugversuch, PhD Thesis, Technische Hochschule Munich
- Kalafat S, Sause MG, GR (2015) Acoustic emission source localization by artificial neural networks. *Struct Health Monit* 14:633–647. <https://doi.org/10.1177/1475921715607408>.
- Kalteremidou K-A, Aggelis DG, Hemelrijck DV, Pyl L (2021) On the use of acoustic emission to identify the dominant stress/strain component in carbon/epoxy composite materials. *Mechanics Research Communications*, 111, art. no. 103663.
- Kalteremidou K-A, Murray BR, Tsangouri E et al (2018) Multiaxial damage characterization of carbon/epoxy angle-ply laminates under static tension by combining in situ microscopy with acoustic emission. *Appl Sci* 8. <https://doi.org/10.3390/app8112021>
- Kline RA, Green RE, Harvey Palmer CH (1978) A comparison of optically and piezoelectrically sensed acoustic emission signals. *J Acoust Soc Am* 64:1633–1639. <https://doi.org/10.1121/1.382129>
- Kolanu NR, Raju G, M R (2019) Damage assessment studies in CFRP composite laminate with cut-out subjected to in-plane shear loading. *Compos Part B Eng* 166:257–271. doi:<https://doi.org/10.1016/j.compositesb.2018.11.142>.
- Kostopoulos V, Loutas TH, Kotsos A et al (2003) On the identification of the failure mechanisms in oxide/oxide composites using acoustic emission. *NDT E Int* 36:571–580. [https://doi.org/10.1016/S0963-8695\(03\)00068-9](https://doi.org/10.1016/S0963-8695(03)00068-9)
- Kundu T (2012) A new technique for acoustic source localization in an anisotropic plate without knowing its material properties, In: 6th European workshop on structural health monitoring, Dresden, Germany, July 3–6 2012
- Kundu T (2014) Acoustic source localization. *Ultrasonics* 54:25–38ISSN 0041-624X. <https://doi.org/10.1016/j.ultras.2013.06.009>
- Kundu T, Yang X, Nakatani H et al (2015) A two-step hybrid technique for accurately localizing acoustic source in anisotropic structures without knowing their material properties. *Ultrasonics* 56:271–278. <https://doi.org/10.1016/j.ultras.2014.08.009>
- Li L, Lomov SV, Yan X et al (2014) Cluster analysis of acoustic emission signals for 2D and 3D woven glass/epoxy composites. *Compos Struct* 116:286–299. <https://doi.org/10.1016/j.compstruct.2014.05.023>
- Li L, Lomov SV, Yan X (2015) Correlation of acoustic emission with optically observed damage in a glass/epoxy woven laminate under tensile loading. *Compos Struct* 123:45–53. <https://doi.org/10.1016/j.compstruct.2014.12.029>
- Liang D, Yuan S, Liu M (2013) Distributed coordination algorithm for impact location of preciseness and real-time on composite structures. *Measurement* 46:527–536. <https://doi.org/10.1016/j.measurement.2012.08.011>
- Liu PF, Chu JK, Liu YL et al (2012) A study on the failure mechanisms of carbon fiber/epoxy composite laminates using acoustic emission. *Mater Des* 37:228–235. <https://doi.org/10.1016/j.matdes.2011.12.015>
- Lysak MV (1996) Development of the theory of acoustic emission by propagating cracks in terms of fracture mechanics. *Eng Fract Mech* 55:443–452. [https://doi.org/10.1016/0013-7944\(96\)00026-4](https://doi.org/10.1016/0013-7944(96)00026-4)

- Mabry N, Banks C, Toutanji H et al. (2011) Acoustic emission felicity ratio measurements in carbon composites laminates using fiber Bragg grating sensors. In: Proc SPIE. Singapore-M.I.T alliance for research and technology center, Sens. Phenom. Technol. Netw. Syst. 7982
- Mahdavi HR, Rahimi GH, Farokhabadi A (2016) Failure analysis of ($\pm 55^\circ$)₉ filament-wound GRE pipes using acoustic emission technique. *Eng Fail Anal* 62:178–187. <https://doi.org/10.1016/j.engfailanal.2015.12.004>
- Maillet E, Singhal A, Hilmas A, Gao Y, Zhou Y, Henson G, Wilson G (2019) Combining in-situ synchrotron X-ray microtomography and acoustic emission to characterize damage evolution in ceramic matrix composites. *J Eur Ceramic Soc* 39(13):3546–3556. <https://doi.org/10.1016/j.jeurceramsoc.2019.05.027>
- Marec A, Thomas J-H, El Guerjouma R (2008) Damage characterization of polymer-based composite materials: multivariable analysis and wavelet transform for clustering acoustic emission data. *Mech Syst Signal Process* 22:1441–1464. <https://doi.org/10.1016/j.ymssp.2007.11.029>
- Martin CA, Van Way CB, Lockyer AJ et al (1995) Acoustic emission testing on an F/A 18 E/F titanium bulkhead. *Smart Struct Mater* 2444:204–211. <https://doi.org/10.1117/12.207672>
- Martínez-Jequier J, Gallego A, Suárez E et al (2015) Real-time damage mechanisms assessment in CFRP samples via acoustic emission lamb wave modal analysis. *Compos Part B Eng* 68:317–326. <https://doi.org/10.1016/j.compositesb.2014.09.002>
- McBride SL, MacLachlan JW, Paradis BP (1981) Acoustic emission and inclusion fracture in 7075 aluminum alloys. *J Nondestr Eval* 2:35–41. <https://doi.org/10.1007/BF00614995>
- McLaskey GC, Glaser SD (2012) Acoustic emission sensor calibration for absolute source measurements. *J Nondestr Eval* 31:157–168. <https://doi.org/10.1007/s10921-012-0131-2>
- McLaskey GC, Glaser SD, Grosse CU (2010) Beamforming array techniques for acoustic emission monitoring of large concrete structures. *J Sound Vib* 329:2384–2394. <https://doi.org/10.1016/j.jsv.2009.08.037>
- Mirgal P, Pal J, Banerjee S (2020) Online acoustic emission source localization in concrete structures using iterative and evolutionary algorithms. *Ultrasonics* 108:106211. <https://doi.org/10.1016/j.ultras.2020.106211>
- Mistras (2013). 1284: The first multi channel wireless acoustic emission system. [Online] [http://www.mistrasgroup.com/products/company/Publications/2\\$Acoustic_Emission/1284_AE_Wireless_Node.pdf](http://www.mistrasgroup.com/products/company/Publications/2$Acoustic_Emission/1284_AE_Wireless_Node.pdf)
- Moore PO (ed) (2005) Nondestructive testing handbook, acoustic emission testing, vol 6. American Society for Nondestructive Testing
- Morscher GN (1999) Modal acoustic emission of damage accumulation in a woven SiC/SiC composite. *Vacuum* 59:687–697. [https://doi.org/10.1016/S0266-3538\(98\)00121-3](https://doi.org/10.1016/S0266-3538(98)00121-3)
- Murray BR, Kalteremidou KA, Carrella-Payan D et al (2020) Failure characterisation of CF/epoxy V-shape components using digital image correlation and acoustic emission analyses. *Compos Struct* 236. <https://doi.org/10.1016/j.compstruct.2019.111797>
- Nakatani H, Hajzargarbashi T, Ito K et al. (2012) Impact localization on a cylindrical plate by near-field beamforming analysis. In: Tomizuka M (ed) *Sensors and smart structures technologies for civil, mechanical, and aerospace*
- Neau G, Deschamps M, Lowe MJS (2001) Group velocity of Lamb waves in anisotropic plates: comparison between theory and experiments. In: AIP conf proc, pp 81–88.
- Njuhovic E, Bräu M, Wolff-Fabris F et al (2014) Identification of interface failure mechanisms of metallized glass fibre reinforced composites using acoustic emission analysis. *Compos Part B Eng* 66:443–452. <https://doi.org/10.1016/j.compositesb.2014.06.018>
- Ohtsu M, Ono K (1984) A generalized theory of acoustic emission and Green's function in a half space. *J Acoust Emission* 3:27–40
- Ohtsu M, Ono K (1986) The generalized theory and source representation of acoustic emission. *J Acoust Emission* 5:124–133
- Ono K (2017) On the piezoelectric detection of guided ultrasonic waves. *Materials* 10:1325. <https://doi.org/10.3390/ma10111325>

- Ono K, Gallego A (2012) Research and applications of AE on advanced composites. *J Acoust Emission* 30:180–229
- Osptia N, Aggelis DG, Tsangouri E (2020) Dimension effects on the acoustic behavior of TRC plates. *Materials* 13:955. <https://doi.org/10.3390/ma13040955>
- Ozevin D, Heidary Z (2011) Acoustic emission source orientation based on time scale. *J Acoust Emission* 29:123–132
- Ozevin D, Greve DW, Oppenheim IJ et al (2006) Resonant capacitive MEMS acoustic emission transducers. *Smart Mater Struct* 15:1863–1871. <https://doi.org/10.1088/0964-1726/15/6/041>
- Papalouros D, Bollas K, Kourousis D et al (2016) Acoustic emission monitoring of high temperature process vessels & reactors during cool down, emerging Technologies in non-destructive testing. In: *Proceedings of the 6th international conference on emerging technologies in nondestructive testing, ETNDT 2016, VI*, pp 197–201
- Park WH, Packo P, Kundu T (2017) Acoustic source localization in an anisotropic plate without knowing its material properties – a new approach. *Ultrasonics* 79:9–17. <https://doi.org/10.1016/j.ultras.2017.02.021>
- Pearson MR, Eaton M, Featherston C et al (2017) Improved acoustic emission source location during fatigue and impact events in metallic and composite structures. *Struct Heal Monit* 16:382–399. <https://doi.org/10.1177/1475921716672206>
- Philippidis TP, Nikolaidis VN, Anastassopoulos AA (1998) Damage characterisation of C/C laminates using neural network techniques on AE signals. *NDT E Int* 31:329–340. [https://doi.org/10.1016/S0963-8695\(98\)00015-2](https://doi.org/10.1016/S0963-8695(98)00015-2)
- Piotrkowski R, Gallego A, Castro E et al (2005) Ti and Cr nitride coating/steel adherence assessed by acoustic emission wavelet analysis. *NDT E Int* 38:260–267. <https://doi.org/10.1016/j.ndteint.2004.09.002>
- Pollock AA (1986) Classical wave theory in practical AE testing, In: *Proceedings of the 8th international AE symposium*. Tokyo, Japan, pp 708–721.
- Prieß T, Sause MG, Fischer D et al (2015) Detection of delamination onset in laser-cut carbon fiber transverse crack tension specimens using acoustic emission. *J Compos Mater* 49:2639–2647. <https://doi.org/10.1177/0021998314552003>
- Prosser WH (1996) Advanced AE techniques in composite materials research. *J Acoust Emission* 14:1–11. <http://ntrs.nasa.gov/search.jsp?R=20040110429>
- Prosser WH (2002) (Ch. 6) acoustic emission. In: Shull PJ (ed) *Nondestructive evaluation, theory, techniques and applications*. Marcel Dekker, New York, pp 369–446
- Prosser WH et al (1995) Advanced waveform-based acoustic emission detection of matrix cracking in composites. *Mater Eval* 53:1052–1058
- Prosser WH et al (1997) Evaluation of damage in metal matrix composites by means of acoustic emission monitoring. *NDT E Int* 30:108. [https://doi.org/10.1016/S0963-8695\(97\)85514-4](https://doi.org/10.1016/S0963-8695(97)85514-4)
- Prosser WH, Hamstad MA, Gary J et al (1999) Finite element and plate theory modeling of acoustic emission waveforms. *J Nondestruct Eval* 18:83–90. <https://doi.org/10.1023/A:1021888009896>
- Prosser WH, Gorman MR, Madaras E (2004) Acoustic emission detection of impact damage on space shuttle structures. In: *17th international acoustic emission symposium*. <https://doi.org/10.1063/1.1916797>.
- Ramirez-Jimenez CR, Papadakis N, Reynolds N et al (2004) Identification of failure modes in glass/polypropylene composites by means of the primary frequency content of the acoustic emission event. *Compos Sci Technol* 64:1819–1827. <https://doi.org/10.1016/j.compscitech.2004.01.008>
- Richardson JM, Elsley RK, Graham LJ (1984) Nonadaptive, semi-adaptive and adaptive approaches to signal processing problems in nondestructive evaluation. *Pattern Recogn Lett* 2:387–394. [https://doi.org/10.1016/0167-8655\(84\)90005-9](https://doi.org/10.1016/0167-8655(84)90005-9)
- Ritschel F et al. (2014) Acoustic emission (AE) signal classification from tensile tests on plywood and layered wood, In: *31st conference of the European working group on acoustic emission*. Dresden, Germany, pp 1–7.
- Sause M (2010) Identification of failure mechanisms in hybrid materials utilizing pattern recognition techniques applied to acoustic emission signals. mbv-Verlag, Berlin. <https://doi.org/10.13140/RG.2.1.4492.2088>.

- Sause MGR (2013) Acoustic emission signal propagation in damaged composite structures. *J Acoust Emission* 31:1–18
- Sause MGR (2016) In situ monitoring of fiber-reinforced composites. Springer, Cham. <https://doi.org/10.1007/978-3-319-30954-5>
- Sause M, Hamstad M (2018) Acoustic emission analysis. In: Beaumont PWR, Zweben CH (eds) *Comprehensive composite materials II*. Elsevier, Oxford, pp 291–326. <https://doi.org/10.1016/B978-0-12-803581-8.10036-0>
- Sause MGR, Horn S (2010a) Simulation of acoustic emission in planar carbon fiber reinforced plastic specimens. *J Nondestruct Eval* 29:123–142. <https://doi.org/10.1007/s10921-010-0071-7>
- Sause MGR, Horn SR (2010b) Influence of specimen geometry on acoustic emission signals in fiber reinforced composites: FEM-simulations and experiments. In: 29th European conference on acoustic emission testing. Vienna, Austria, pp 1–8.
- Sause MGR, Richler S (2015) Finite element modelling of cracks as acoustic emission sources. *J Nondestruct Eval* 34:4. <https://doi.org/10.1007/s10921-015-0278-8>
- Sause MGR, Schultheiß D, Horn S (2008) Acoustic emission investigation of coating fracture and delamination in hybrid carbon fiber reinforced plastic structures. *J Acoust Emission* 26:1–13
- Sause MGR, Haider F, Horn S (2009) Quantification of metallic coating failure on carbon fiber reinforced plastics using acoustic emission. *Surf Coatings Technol* 204:300–308. <https://doi.org/10.1016/j.surfcoat.2009.07.027>
- Sause MGR, Gribov A, Unwin AR et al (2012) Pattern recognition approach to identify natural clusters of acoustic emission signals. *Pattern Recogn Lett* 33:17–23. <https://doi.org/10.1016/j.patrec.2011.09.018>
- Sause MGR et al. (2014) Acoustic emission source localization in bearing tests of fiber reinforced polymers by neural networks. In: 16th international conference on experimental mechanics. Cambridge, UK, pp 1–3.
- Scholey JJ, Wilcox PD, Wisnom MR et al (2010) Quantitative experimental measurements of matrix cracking and delamination using acoustic emission. *Compos A* 41:612–623. <https://doi.org/10.1016/j.compositesa.2010.01.008>
- Scruby CB (1985) Quantitative acoustic emission techniques. *Non Destructive Test* 8:141–208
- Sen N, Gawronski M, Packo P et al (2020) Square-shaped sensor clusters for acoustic source localization in anisotropic plates by wave front shape-based approach. Submitted to MSSP 2020
- Shen, G. (2017), Progress of acoustic emission technology on pressure equipment in China. Proceedings of the world conference on acoustic Emission-2015. Springer Proceedings in Physics
- Surgeon M, Wevers M (1999) Modal analysis of acoustic emission signals from CFRP laminates. *NDT E Int* 32:311–322. [https://doi.org/10.1016/S0963-8695\(98\)00077-2](https://doi.org/10.1016/S0963-8695(98)00077-2)
- Talreja R, Phan N (2019) Assessment of damage tolerance approaches for composite aircraft with focus on barely visible impact damage. *Compos Struct* 219:1–7. <https://doi.org/10.1016/j.compstruct.2019.03.052>
- Tobias A (1976) Acoustic-emission source location in two dimensions by an array of three sensors. *Non Destructive Test* 9:9–12 ISSN 0029-1021. [https://doi.org/10.1016/0029-1021\(76\)90027-X](https://doi.org/10.1016/0029-1021(76)90027-X)
- Tsangouri E, Aggelis DG (2018) The influence of sensor size on acoustic emission waveforms-a numerical study. *Appl Sci* 8:168. <https://doi.org/10.3390/app8020168>
- Veloso GFC, Silva LD et al. (2006) Localization of partial discharges in transformers by the analysis of the acoustic emission. In: IEEE international symposium on industrial electronics, pp 537–541
- Vergeynst LL et al (2014a) Finite element modelling used to support wood failure identification based on acoustic emission signals. *Timber Bridges COST Conf* 2014:141–146
- Vergeynst LL, Sause MGR, Steppe K (2014b) Acoustic emission signal detection in drought-stressed trees: beyond counting hits. In: 31st Conference of the European working group on acoustic emission. Dresden, Germany, pp 1–8.
- Vi-Tong E, Gaillard P (1987) An algorithm for non-supervised sequential classification of signals. *Pattern Recogn Lett* 5:307–313. [https://doi.org/10.1016/0167-8655\(87\)90071-7](https://doi.org/10.1016/0167-8655(87)90071-7)
- Wadley HNG, Scruby CB (1981) Acoustic emission source characterization. *Advances in acoustic emission*. Dunhart Publishers, Knoxville

- Wang Y-B, Chang D-G, Fan Y-H et al (2017) Acoustic localization of partial discharge sources in power transformers using a particle-swarm-optimization-route-searching algorithm. *IEEE Trans Dielect Electr Insul* 24:3647–3656. <https://doi.org/10.1109/TDEI.2017.006857>
- Ward IM (1971) *Mechanical properties of solid polymers*. John Wiley & Sons Ltd., New York
- Wevers M (1997) Listening to the sound of materials: acoustic emission for the analysis of material behaviour. *NDT E Int* 30:99–106. [https://doi.org/10.1016/S0963-8695\(96\)00051-5](https://doi.org/10.1016/S0963-8695(96)00051-5)
- Wilcox PD et al (2006) Progress towards a forward model of the complete acoustic emission process. *Adv Mater Res* 13–14:69–75
- Wild, G., Hinckley, S. (2008) Acousto-Ultrasonic Optical Fiber Sensors: Overview and State-of-the-Art. *IEEE Sensors Journal*, Vol. 8, No. 7, 1184–1193
- Wisner B, Kotsos A (2018) Investigation of particle fracture during fatigue of aluminum 2024. *Int J Fatigue* 111:33–43. <https://doi.org/10.1016/j.ijfatigue.2018.02.001>
- Wisner BJ, Potstada P, Perumal VI et al (2019) Progressive failure monitoring and analysis in aluminium by in situ nondestructive evaluation. *Fatigue Fract Eng Mater Struct* 42:2133–2145. <https://doi.org/10.1111/ffe.13088>
- Wolfe JP (2005) *Imaging phonons: acoustic wave propagation in solids*. Cambridge University Press, Cambridge
- Wu Q, Okabe Y (2012) Novel acoustic emission sensor system based on two cascaded phase-shifted fiber Bragg gratings. In: *Proceedings of the SPIE international conference fiber sensation*, p 8421
- Xiao D, He T, Pan Q et al (2014) A novel acoustic emission beamforming method with two uniform linear arrays on plate-like structures. *Ultrasonics* 54:737–745. <https://doi.org/10.1016/j.ultras.2013.09.020>
- Yao WB, Dai CY, Mao WG et al (2012) Acoustic emission analysis on tensile failure of air plasma-sprayed thermal barrier coatings. *Surf Coatings Technol* 206:3803–3807. <https://doi.org/10.1016/j.surfcoat.2012.03.050>
- Yedavalli RK, Belapurkar RK (2011) Application of wireless sensor networks to aircraft control and health management systems. *J Control Theory Appl* 9:28–33
- Yin S, Cui Z, Kundu T (2018) Acoustic source localization in anisotropic plates with “Z” shaped sensor clusters. *Ultrasonics* 84:34–37. <https://doi.org/10.1016/j.ultras.2017.10.007>
- Yu P, Anastassopoulos V, Venetsanopoulos AN (1996) Pattern recognition based on morphological shape analysis and neural networks. *Math Comput Simul* 40:577–595. [https://doi.org/10.1016/0378-4754\(95\)00008-9](https://doi.org/10.1016/0378-4754(95)00008-9)
- Zhou W, Qin R, Han K-N, Wei Z-Y, Ma L-H (2021) Progressive damage visualization and tensile failure analysis of three-dimensional braided composites by acoustic emission and micro-CT. *Polym Test* 93:106881. <https://doi.org/10.1016/j.polymertesting.2020.106881>

Open Access This chapter is distributed under the terms of the Creative Commons Attribution 4.0 International License (<http://creativecommons.org/licenses/by/4.0/>), which permits use, duplication, adaptation, distribution and reproduction in any medium or format, as long as you give appropriate credit to the original author(s) and the source, a link is provided to the Creative Commons license and any changes made are indicated.

The images or other third party material in this chapter are included in the work’s Creative Commons license, unless indicated otherwise in the credit line; if such material is not included in the work’s Creative Commons license and the respective action is not permitted by statutory regulation, users will need to obtain permission from the license holder to duplicate, adapt or reproduce the material.



Chapter 8

Strain Monitoring



Steve Vanlanduit, Mario Sorgente, Aydin R. Zadeh, Alfredo Güemes,
and Nadimul Faisal

Abstract This chapter provides an overview of the use of strain sensors for structural health monitoring. Compared to acceleration-based sensors, strain sensors can measure the deformation of a structure at very low frequencies (up to DC) and enable the measurement of ultrasonic responses. Many existing SHM methods make use of strain measurement data. Furthermore, strain sensors can be easily integrated in (aircraft) structures. This chapter discusses the working principle of traditional strain gauges (Sect. 8.1) and different types of optical fiber sensors (Sect. 8.2). The installation requirements of strain sensors and the required hardware for reading out sensors are provided. We will also give an overview of the advantages and the limitations of commonly used strain sensors. Finally, we will present an overview of the applications of strain sensors for structural health monitoring in the aeronautics field.

8.1 Strain Gauges

A strain gauge (or gage) is a sensing device used to determine the directions and magnitudes of principal surface strains (ASTM E1561-93 2014) and residual stresses (ASTM E837-13a 2013) in conjunction with established algorithms. Once the surface on which the strain gauge is assembled is deformed, the strain gauge causes a change in length leading to a change in electrical resistance. The change in electrical

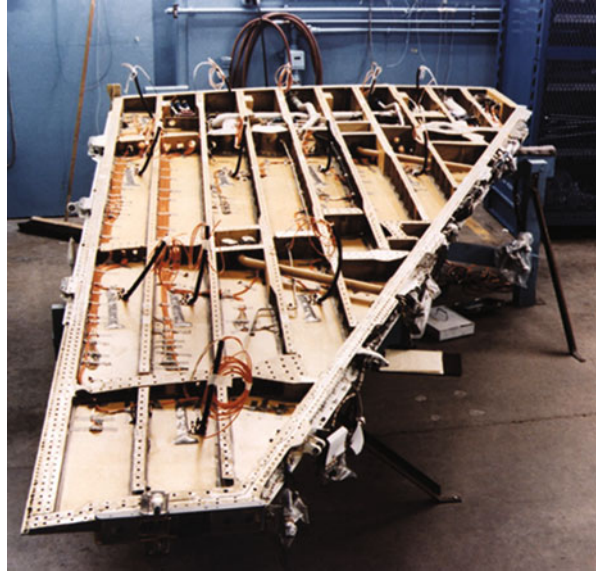
S. Vanlanduit (✉)
University of Antwerp, Antwerp, Belgium
e-mail: steve.vanlanduit@uantwerpen.be

M. Sorgente · A. R. Zadeh
Optics 11, Amsterdam, The Netherlands

A. Güemes
Technical University of Madrid, Madrid, Spain

N. Faisal
Robert Gordon University, Aberdeen, UK

Fig. 8.1 Strain gauge installation on metallic aircraft structures (installed in the interior of the AFTI/F-16 wing at NASA DFRC) (Anon. 1984)



resistance is measured using an electrical circuit (i.e. Wheatstone bridge), which is then related to strain by the quantity known as the gauge factor. The stress is force per unit of surface (i.e. pressure) that is acting on an infinitesimal area. The stress is a derived quantity that under some assumptions (e.g. single axis stress state and strain measured in the transverse direction) can be calculated from the strain (if the Young's modulus is known). In general the measured strain depends on the mechanical load as well as the thermal loading. When establishing the stress-strain relationship both contributions should be balanced. Furthermore in case of permanent or plastic deformation of a material setting up the relation between the measured strain and the stresses (including residual stress) is much more difficult (Faisal et al. 2019).

Figure 8.1 shows the strain gauge installation inside an aircraft wing structure (Anon. 1984). To prepare any surface or structure of interest to assemble the strain gauge, grit-based sandpaper is typically used to largely remove any debris or rust to increase the contact surface area of the surface face with the bonding agent sandwiched with the strain gauge (Anon. 1984). Following which, alcohol-based solutions are used to decontaminate the material surface. The adhesive glue for the strain gauge assembly is applied and let to cure in ambient conditions for a high bond strength. The adhesive type may affect the bonding quality with the test surface, and control measures may be necessary for verifying the installation features.

Even in the case of uni-axial loading, bi-directional strains often need to be measured. In the case of a purely compressive load of a beam for instance, tensile strain would be induced at 90° to the compressional strain direction. This is of interest in a number of aircraft structures; therefore, bi-element strain gauges are typically used during testing. Strain relief must be considered during testing. Typically, a thin plastic layer is glued on top of the components to relieve some of the

stress exerted. Excess plastic is then removed after the glue sets. A commercially available programmable automation controller (e.g. National Instruments, Vishay Precision Group) can be used to receive the signals created by strain gauges. The instrumentation includes strain indicators, signal conditioning amplifiers, and software for data recording. The strain gauge would normally come with a shorter lead cable length (e.g. recommended length of 1.5–2.5 m, (IPC/JEDEC 2005). Quarter-bridge strain gauges in a ‘three-wire connection’ are preferred over those in a ‘two-wire connection.’ The increase in the lead wire length increases the possibility of errors due to temperature variations, lead desensitization, and lead-wire resistance changes (ASTM E1561-93 2014). A slight change in the temperature can generate a measurement error of several microstrain. For the extension of strain gauge cables, a careful consideration is needed when extending to long lengths because the overall resistance of the strain gauge assembly will change (Takeuchi 2012).

For aircraft SHM, the complex geometry of the structures (specimen) leads to a complex strain analysis. Usually assumptions of a much simpler strain distribution are made in practice (e.g. by ignoring the strain in the thickness direction of a thin beam). Due to a combination of the high sensitivity of the strain gauge measurement equipment, outdoor environment, and necessity for extremely long data cables, the raw data could feature a high noise level. To minimise the effects of such noise and allow trends to be more clearly identified, the signals (for each strain gauge) can be smoothed by averaging over a window of data points using a computational code, thereby removing localised spikes that could potentially be seen in the raw data. Despite data smoothing, there can still be a fluctuation due to the low signal-to-noise ratio, which makes it difficult to identify significant events within the test from the strain gauge data alone.

8.2 Optical Fiber Sensors

8.2.1 Introduction

In a fiber optic sensor, light guided through the fiber core is affected by the measurand. Optical fiber sensors (OFS) are most frequently used to measure strain, temperature, or pressure, but they can also be used as chemical sensors, vibroacoustic detectors and refractometers for cure monitoring (Lee 2003). One of the main advantages of the optical fiber sensor is its thinness. It usually has a diameter of 125 μm , but OFS with a diameter of up to 12 μm have also been reported (Malik et al. 2016). This makes it easy to integrate them in materials like composite materials. In the last few decades, the OFS have been successfully used for damage detection in composite materials (Kinet et al. 2014).

In composite materials, OFS are sandwiched between two composite layers (Dawood et al. 2007). This process has been successfully applied to aircraft components at Airbus (Giraldo et al. 2017).

In metals, OFS are also being integrated in components (Saheb and Mekid 2015; He et al. 2019). In this case, fiber is inserted in a groove closed by melting subsequent powder layers on top of the fibers (Havermann et al. 2015). Metal melting is usually performed by laser cladding or high-power ultrasound (He et al. 2019). A metal (Grandal et al. 2018) or carbon (Nedjalkov et al. 2018) coating is applied to protect the fibers from high temperatures during the integration process.

In other applications, the OFS is not integrated in the material under test, but the sensors are applied at the surface of the part. This can be done by using a prepreg sample with an integrated optical fiber, of which the so-called fiber optic ribbon tape (FORT) is an example (Loutas et al. 2015). For aerospace applications, a specialty aerospace-grade coated fiber Bragg gratings (FBG) sensor with an adapted bonding procedure was developed (Goossens et al. 2019). Goossens et al. tested their sensor in in-flight conditions with realistic humidity, temperature, and pressure cycles, as well as hydraulic fluid and fatigue loading.

Optical fiber sensors can be used in harsh environments (Mihailov 2012). They are immune to electromagnetic interference (Druet et al. 2018) and can be used at very high temperatures. Silica glass allows the detection of strains in environments up to 1000 °C (Yu and Okabe 2017). Radiation-hardened sensors have been developed for space applications (Girard et al. 2018).

Another important advantage of OFS is the fact that they can be multiplexed. Several sensors can be inscribed in one optical fiber, and these sensors can be read out using one single interrogator. The interrogator is the hardware needed to acquire the measurand from the reflected or transmitted light that goes through the fiber. Time domain multiplexing has been used to realise up to 1000 ultra-weak FBG for distributed temperature sensing (Wang et al. 2012) and 100s of strain sensors (Dai et al. 2009; Cranch and Nash 2001). In addition to the point sensors, also distributed fiber optics sensors based on different principles are available: Rayleigh (Froggatt et al. 1998) and Brillouin scattering (Garus et al. 1996).

8.2.2 Types of Optical Fiber Sensors

Sensors vitally affect our life in multiple fields, such as IoT, structural health monitoring, smart structures, and digital twins. The necessity of tracking the material behavior has assumed a great, and not trivial importance in reducing maintenance costs and promoting prevention over replacement. In addition, the harsher the environment, the more challenging the measurement. The advantages of optical sensors come into play because of the fact that they are

- completely passive,
- lightweight,
- survive at critical temperature, dust, and ATEX (ATmosphere EXplosible) environment,
- immune to electromagnetic interference,

- not required to have pre-amplification, and
- capable of being interrogated from hundreds of meters of distance.

These features open up scenarios for more accurate, precise, and repeatable measurements (Pinet 2009). This study discusses some of the most common optical sensing techniques based on the interferometry principle.

8.2.3 Interferometry

Interferometry is a technique based on the wave interference phenomenon. In classic physics, this comes into play when two waves superimpose to generate a resultant wave of a greater (constructive interference) or lower amplitude (destructive interference). The former occurs when the phase difference of the two waves is an even multiple of π (180°), whereas the latter happens when the difference is an odd multiple of π . The phase differences with values between these two extremes will result in displacement magnitudes that range between the minimum and maximum values. Two conditions must be met to set up an interference pattern that is stable and clear (Hariharan 2007):

1. *Coherent light sources must be used*, meaning they emit waves with a constant phase difference.
2. The waves should be of a single wavelength, that is, monochromatic.

Several types of interferometers are available and have a wide-spread use in optical sensing applications. Interferometry based optical sensors can be easily scaled up to long ranges, used in satellite imaging of surface deformation, and scaled down to cell stiffness measurement in biological matters. Furthermore, the sensitivity of these sensors can be tuned by adjusting the interferometry arm lengths of the sensor. For these reasons, the interferometry principle has become a basis for numerous sensor designs in both academia and in the industry.

In this article, three of the most common interferometer types will be discussed, namely Mach–Zehnder, Michelson, and Fabry–Pérot.

8.2.4 Mach–Zehnder

In optics, the Mach–Zehnder interferometer is an optical device capable of determining the relative phase shift variation between the superposition of two collimated beams. Figure 8.2 shows the working principle. A light beam is shined on a beam splitter that divides it into two parts. The traveling different paths will be reflected on the mirrors and recombined on a second beam splitter, then directed on the photo-detectors to be acquired (Zetie et al. 2000).

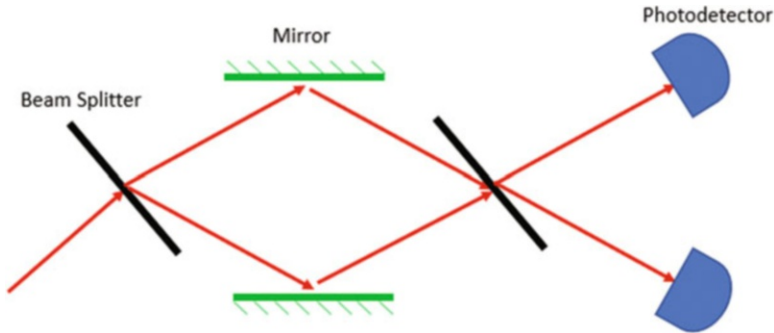


Fig. 8.2 Schematic of a Mach-Zehnder interferometer

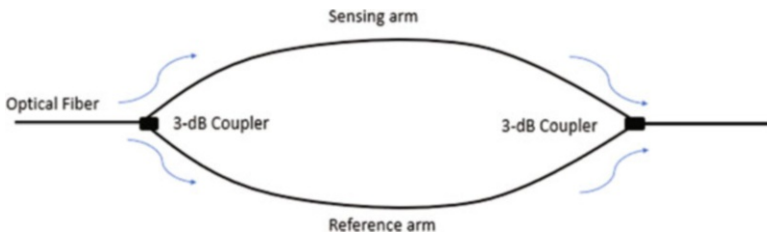


Fig. 8.3 Mach-Zehnder interferometer: integrated configuration

Mach-Zehnder interferometers (MZIs) have been implemented as optical devices in multiple sensing applications because of their flexible configurations (Bahrapour 2012). Their optical fiber integrated version is based on the same working principle using a different optical element (Fig. 8.3). The incident beam is split into two arms and recombined into one using two fiber couplers. For sensing applications, the reference arm is ideally isolated from the external variations, and only the sensitive arm experiences changes. The information is kept in the optical path difference between the two arms, which as discussed in the previous section, can be detected by calculating the interference signal variation.

The physical quantities that externally affect the sensing arm change its length, thereby generating a phase difference between the beams traveling the reference and the sensing arms. The optical phase delay \varnothing can be expressed as follows:

$$\varnothing = nkL \quad (8.1)$$

where, n is the refractive index, and L is the fiber length. The product nL represents the optical path length, and k is the wavenumber (Zahid et al. 2019).

8.2.5 Michelson Interferometer

Similar to the Mach–Zehnder interferometer, the Michelson interferometer (MI) compares two beams reflected from two mirrors on two configuration branches. An MI is considered as half of an MZI, where the main difference is the presence of two reflectors.

In the Michelson interferometer in Fig. 8.4, light is shined from a coherent light source on a beam splitter that splits the light into two different optical paths. The reflected and transmitted waves are recombined to let them interfere on a photodetector. The beam splitter placed at an angle of 45° with respect to the incoming laser beam distributes the light equally to both mirrors. The following relationship is valid on the photodetector:

$$2D = n\lambda \quad (8.2)$$

where, D distance of the movable; n number of interferometric fringes; λ beam wavelength.

Figure 8.5 depicts a fiber-based model of an MI. Light travels through the sensitive and reference arm, thereby being distributed and recombined by an optical coupler. The external physical quantity affects the sensitive arm that will modify its lengths accordingly. The output in terms of the phase change is processed at the port where the photodetector is connected (Zahid et al. 2019).

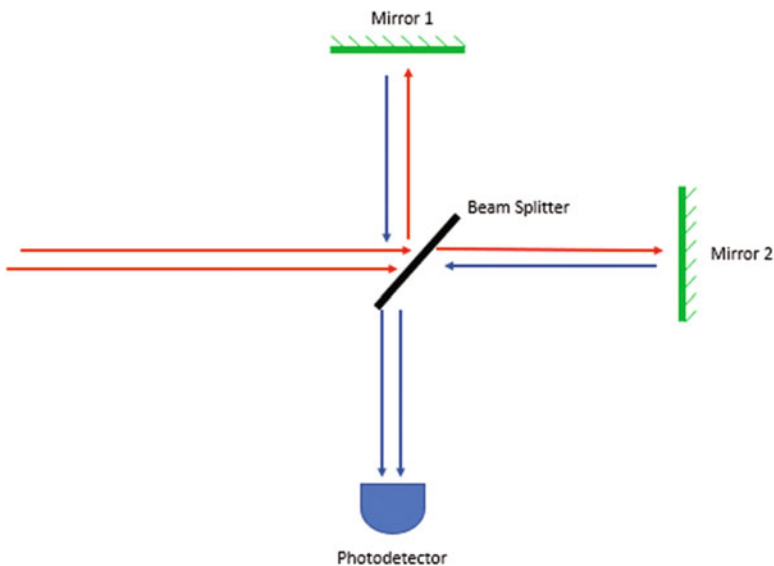


Fig. 8.4 Configuration of a Michelson interferometer

Fig. 8.5 Michelson interferometer: integrated configuration

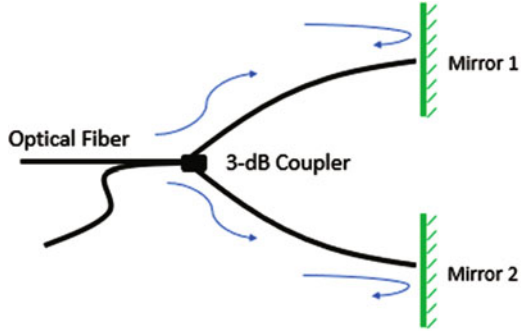
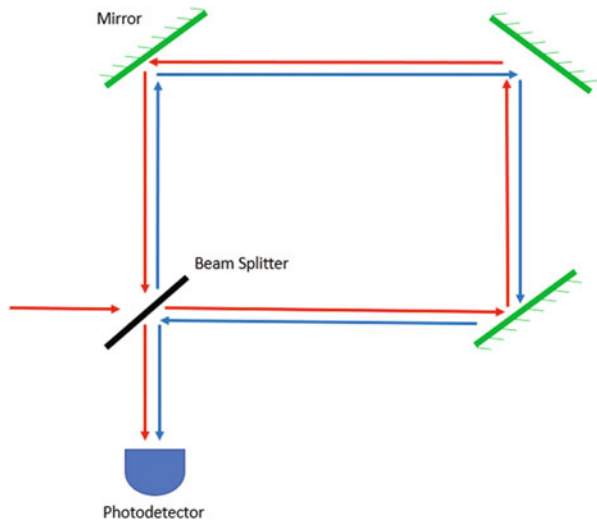


Fig. 8.6 Sagnac interferometer



8.2.6 Sagnac Interferometer

The Sagnac interferometer is based on the Sagnac effect. The phase difference between two counter propagating beams depends on the angular velocity of the rotating apparatus on which they are circulating.

Light is shined on the beam splitter that divides the wave into two counter propagating beams. They travel the same path on opposite directions and are then recombined on the exit point to interfere on the photodetector Fig. 8.6 (Kondrat et al. 2007).

The relation that links the rotating apparatus with the phase difference between the two beams is presented below:

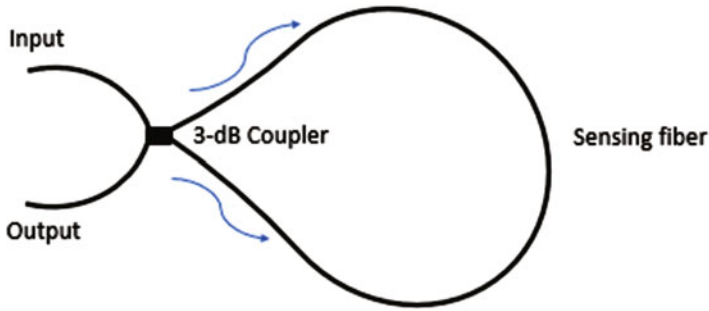


Fig. 8.7 Fiber-optic Sagnac interferometer

$$\Delta\phi = \frac{4\mathbf{A}\omega_{rot}}{\lambda v} \quad (8.3)$$

where, \mathbf{A} is the unit vector perpendicular to the surface area of the apparatus; ω_{rot} is the angular velocity of the apparatus; λ is the light wavelength; and v is the beam speed.

Figure 8.7 shows the fiber optic version of the Sagnac Interferometer. The setup comprises an optical fiber loop and a 3-dB coupler. The latter splits the shined light into two beams that circulate the former in opposite directions. As long as the setup is stable, the phase difference of optical path between both waves is constant and zero. Introducing a rotation around the axis perpendicular to the figure plane the optical path difference (OPD) is determined by the polarization-dependent propagating velocity of the light mode guided along the path (Lee 2003).

8.2.7 Fabry–Pérot

The Fabry–Pérot (FP) sensor bases its working principle on the Fabry–Pérot interferometer (FPI). This type of optical system comprises two reflective parallel surfaces spaced apart at a certain distance from each other (Wei 2013). The shined light from a light source beams on the two parallel reflective surfaces under transmission and reflection rules. The interference occurs due to the continuous superposition of both the transmitted and reflected beams (Lee 2003).

FP sensors can be categorised into intrinsic and extrinsic (Tsai 2001). The former has reflecting components within the fiber itself by using optical elements, fiber defects, and chemical etching. The latter manipulates the reflection from an external cavity. In general, the cavity is in between the cleaved fiber and a membrane modulated depending on the external physical quantity to be monitored. The majority part of FP optical sensors is based on the same principle: they have an FP interferometer, whose cavity length changes according to the physical parameter

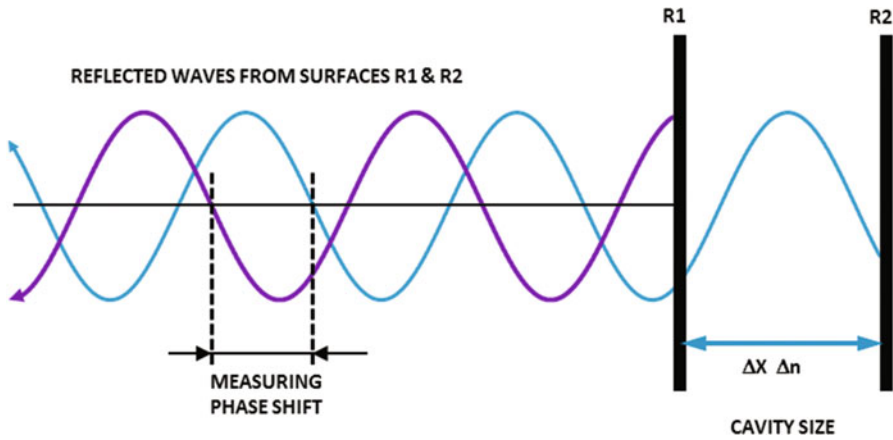


Fig. 8.8 Working principle of the FPI sensor, where ΔX is the change in length of the cavity and Δn is the change of the refractive index in the cavity

they are designed to measure. The cavity length is converted into the appropriate unit corresponding to the sensor type using appropriate sensor calibration (Pinet 2009).

The FP reflection (or transmission) spectrum is described as the wavelength-dependent intensity modulation of the input light source caused by the optical phase difference (wave imaginary part variation) between two reflected (or transmitted) beams. Constructive and destructive interference combines the maximum and minimum peaks in the 2π modulus. The phase difference is given as follows:

$$\Delta\phi_{FPI} = \frac{2\pi}{\lambda} n 2L \quad (8.4)$$

where, λ is the wavelength on the incident light; n is the refractive index of the cavity mode or cavity material; and L is the physical length of the cavity considering the light traveling back and forth (Rajan 2016).

Let us consider for instance a first fixed mirror and a second sensitive one (Fig. 8.8). Introducing an external perturbation to the sensor, the physical length of the cavity and/or the refractive index of the cavity material changes, producing a variation of the interferometer optical path difference (OPD). This affects the abovementioned phase difference. Applying a strain to the sensor, the cavity length and/or its optical property may change, thereby resulting in a phase variation.

8.2.8 Fiber Bragg Grating Sensors

FBG are the most common type of optical fiber sensors used in point strain or temperature measurement applications. FBG sensors are created by exposing the core of an optical fiber to a spatially modulated ultraviolet light pattern (Erdogan

1997). This exposed fiber length creates a refractive index modulation in the optical fiber core that partially reflects certain wavelengths of the input light to the fiber (Kersey et al. 1997). Different kinds of FBG sensors exhibit different behaviors based on how the refractive index modulation is realised. A few of the most common FBG types will be discussed in the next sections of this article, but in its most basic form, the grating period and the amplitude of the refractive index modulation are constant along the entire length of the FBG sensor. This is called a uniform FBG sensor, in which the peak wavelength of the reflected spectrum that is also called Bragg wavelength or λ_B linearly depends on the constant period (Λ) of the refractive index modulation and the effective refractive index of the fiber (n_{eff}) or

$$\lambda_B = 2\pi n_{\text{eff}}\Lambda. \quad (8.5)$$

From the above equation, the Bragg wavelength will shift toward higher wavelengths under tension and lower wavelengths under compression. The amount of strain or temperature change applied over the sensor length can be determined by tracking the shift of this peak wavelength of the reflection spectrum. In its simplified form, the relationship between the shift of the Bragg wavelength and the amount of strain or temperature change over the sensor length is presented as follows:

$$\Delta\lambda_{B_s} = k_s s \text{ and } \Delta\lambda_{B_T} = k_T \Delta T. \quad (8.6)$$

where s is the amount of strain change, k_s and k_T are constants determined by the optical fiber composition. For instance, in silica-based optical fibers operate at $\lambda_B = 1550 \text{ nm}$, $k_s \approx 1.209 \times 10^{-3} \text{ nm}/\mu\epsilon$, and $k_T = 10.075 \times 10^{-3} \text{ nm}/^\circ\text{C}$ (Kersey et al. 1997). Figure 8.9 depicts this linear behavior of FBG sensors under a uniform strain over its length.

The simplicity of the strain (or temperature) measurement algorithm, along with all the advantages of fiber optic sensing, has made FBG sensors an attractive alternative to electrical strain gauges and thermocouples.

8.2.9 Other FBG Grating Structures

If the grating period of the FBG has a uniform variation along its length, it will be called a linearly chirped FBG (LCFBG). Such chirped FBGs generally have a broader reflection spectrum and are mostly used as dispersive elements or filters in fiber optic communications (Xu et al. 1996), especially considering the fact that in ideal production conditions, they have a symmetrical reflection spectrum (Rajabzadeh 2018). However, they can also be used as sensors in strain or temperature demodulation, where instead of tracking the peak wavelength, the center of mass of the reflection spectrum is monitored (Erdogan 1997). Furthermore, they can be embedded within different composite structures for micro-crack detection

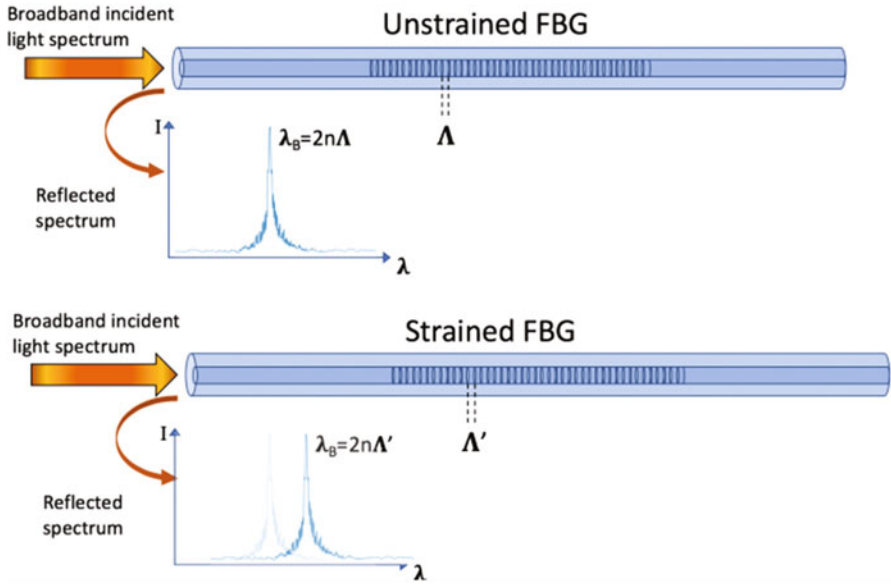


Fig. 8.9 Uniform FBG sensor under a uniform axial strain field

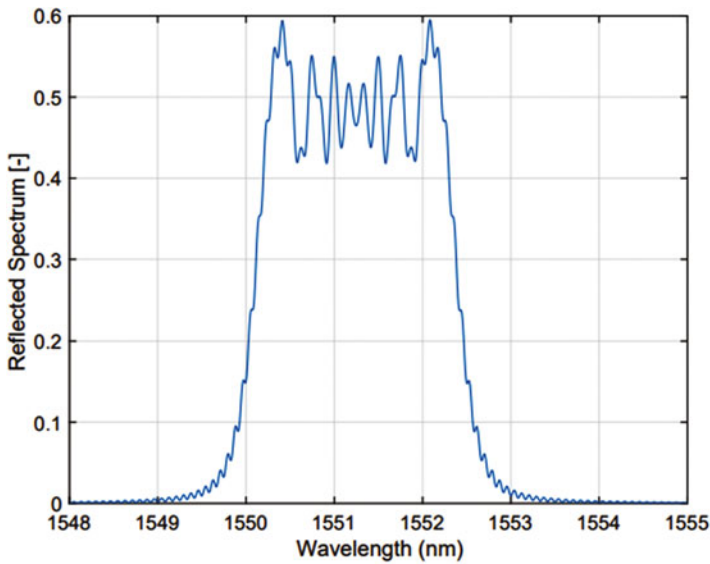


Fig. 8.10 Reflection spectrum from a linearly chirped FBG

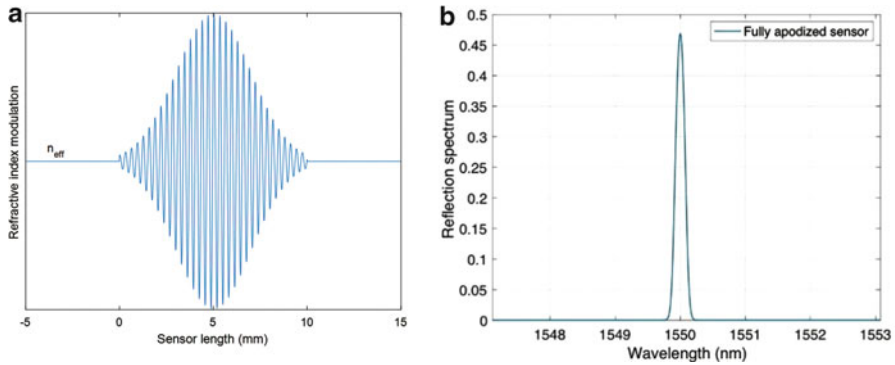


Fig. 8.11 (a) Gaussian apodization of the refractive index. (b) Apodised FBG sensor with fully suppressed side lobes

applications (Takeda et al. 2013). In Fig. 8.10 an example of the reflection spectrum of such a LCFBGs is given (with 10 mm length and a linear chirp rate of $\frac{d\lambda_B}{dz} = 2.5$ nm/cm).

In some FBG sensor applications, having side lobes in the reflection spectra is not ideal, and they must be suppressed as much as possible. A way of doing that is by apodizing the refractive index change along the sensor, which means the amplitude of the refractive index modulation follows a (Gaussian or raised cosine) pattern similar to that in Figure 8.11a. Figure 8.11b shows the suppressed side lobes of a Gaussian apodised FBG sensor.

Long-period gratings (LPGs) are another class of Bragg grating sensors, where the period of the grating is much larger than that of regular FBG sensors typically in the order of a few hundred nanometers to a few hundred micrometers (James and Tatam 2003). LPG sensors are mostly interesting for their transmission spectrum, where different attenuation bands correspond to different fiber cladding modes. These attenuation bands have different sensitivities to the different measurands applied over the sensor length, which allows them to be utilised for multi-parameter sensing elements capable of monitoring multiple environmental parameters independently.

Moreover, other kinds of FBG structures and types, such as tilted fiber Bragg gratings and phase-shifted FBGs, are also suitable for sensing a particular set of environmental parameters.

8.2.10 *State-of-the Art Damage Detection Systems*

In this paragraph three interrogators examples are reported. They make use of the optical interferometric principles and the readout techniques reported above in this chapter.



Fig. 8.12 DeltaSens interrogator by Optics11

DeltaSens: Fabry Perot Interrogator

The DeltaSens interrogator from Optics11 is a high-speed interrogation unit for reading Fabry–Pérot-type sensors. Optical sensors have to be properly coupled with DeltaSens, which will then communicate the sensed physical quantities to a computer to allow data processing. The readout must be equipped with the optical interface to manipulate and interpret the light.

DeltaSens (Fig. 8.12) interrogates multiple Fabry–Pérot-type sensors in an optical fiber network connected through standard optical splitters. The interferometer is formed by a broadband light source and a spectrometer. A spectral acquisition arrangement acquires successive spectral responses from the optical sensor arrangement during successive time intervals. All connected FP cavities with different cavity lengths result in specific footprints on the spectrometer. The spectral analysis arrangement detects a phase evolution of the periodicity throughout the successive spectral responses. The phase evolution of the periodicity provides a relatively precise measurement of a variation in an optical path length between the two reflective surfaces of the Fabry–Pérot structure. A variation in a physical quantity can cause optical path length variation. Accordingly, a relatively precise measurement of the physical quantity can be achieved (Grzegorz Gruca 2019).

The main application of such an interrogator is acceleration sensing using 1D and 3D optical accelerometers. The distances between each sensor and to the read-out can be kilometers (Rijnveld 2017). Further algorithms have been implemented to retrieve both the relative variation and the absolute value of the acceleration.

I4 Series: FBG Interrogators

Several methods can be used to interrogate FBG sensors, and a few of the most common techniques will be discussed herein. The most straightforward approach is to use a superluminescent diode (SLD) as a light source and a spectrometer to record the FBG-reflected spectrum (Alves 2003). However, the wavelength resolution and the accuracy offered by such spectrometers are usually above a few hundreds of picometers to a few nanometers, greatly limiting the strain and temperature resolution of the FBG sensor. Another approach is to use the fiber Fabry–Pérot tunable



Fig. 8.13 FAZT I4G interrogator

filter technology for a high-spatial resolution interrogation of the reflected spectrum. In this technique, a tunable laser and a high-precision synchronization system are used to scan the wavelength region of interest and sample the FBG-reflected spectrum (Ushakov 2015).

A similar alternative method is the interrogation of FBG sensors with the semiconductor tunable laser technology used in FAZ interrogators. This technology offers a sub-picometer wavelength accuracy that translates into micro-strain accuracy for strain measurements and temperature measurement accuracy of below $0.1\text{ }^{\circ}\text{C}$ or $\pm 1\text{ }\mu\text{e}$ at scanning frequencies between 1 and 8 kHz (Fig. 8.13).

The I4 series can sustain up to 30 sensing points per channel. Different channel versions are produced: 4 and 16 with a trade-off between the number of sensing points and the sampling frequency.

8.2.11 Acoustic Emission Interrogator (*OptimAE*)

Acoustic emission (AE) is a non-invasive technique that allows the detection of damage and crack formation in engineering structures in real time (see Chap. 7). As a crack forms in such structures, the energy release results in transient surface acoustic waves, which are also called Rayleigh waves, that propagate throughout the material (Park 2011). Electrical AE systems use piezo-electric sensors to acquire these high-frequency acoustic waves. However, piezo-electric sensors have some limitations that narrow down their application in harsh environments.

The OptimAE unit is the optical acoustic emission monitoring system (Fig. 8.14). The optical AE setup contains two optical fibers (i.e., one operating as a sensing arm and one as a reference arm), which together form an interferometry setup. The sensing fiber is densely coiled on a metallic mandrel and is in a direct contact with the material surface for the optimum transmission of the surface acoustic wave to the sensor. The elastic energy of the acoustic wave stretches the fiber that changes the



Fig. 8.14 OptimAE acoustic emission monitoring system

differential length of the fibers on the sensing and the reference arms of the interferometer. The resulting interferometric signal is transferred to the OptimAE readout for signal acquisition, demodulation, and communication to the computer. The optical AE sensors can be sampled at 1 MS/s and have a spectral noise density of $150 f\epsilon/\sqrt{Hz}$ (this term is the average amount of displacement noise per frequency bin which can be derived from power spectral analysis of the noise floor of the sensor response). They operate at a C-band wavelength range.

Performance tests showed that the optical acoustic emission sensors are a comparable alternative with respect to existing piezoelectric ones, opening new measurement scenarios in harsh environment conditions and extending the benefits of AE testing to new industries (Mario Sorgente 2020).

8.2.12 OFS Applications in Aeronautics

The optical fiber sensor technology and fiber Bragg gratings are evaluated as good tools for load monitoring and damage detection of aircraft structures (Guo et al. 2011; Mendoza et al. 2013) see overview in (Fig. 8.15). Di Sante gave a relatively recent overview of the major potential of OFS in the aeronautics industry (Di Sante 2015). Real-life OFS measurement campaigns on complete aircraft have been performed in the literature. A real-time analysis of wing deformations with a millimeter resolution allowed load interpretation during flight manoeuvres (Wada et al. 2019). Other researchers demonstrated the use of 780 FBG sensors to obtain out-of-plane loads and the wing deformations at various load levels (Nicolas, Sullivan and Richards 2016). OFS have also been used for wing shape deflection measurements of an ultralight carbon-composite aerial vehicle (Ma and Chen 2019).

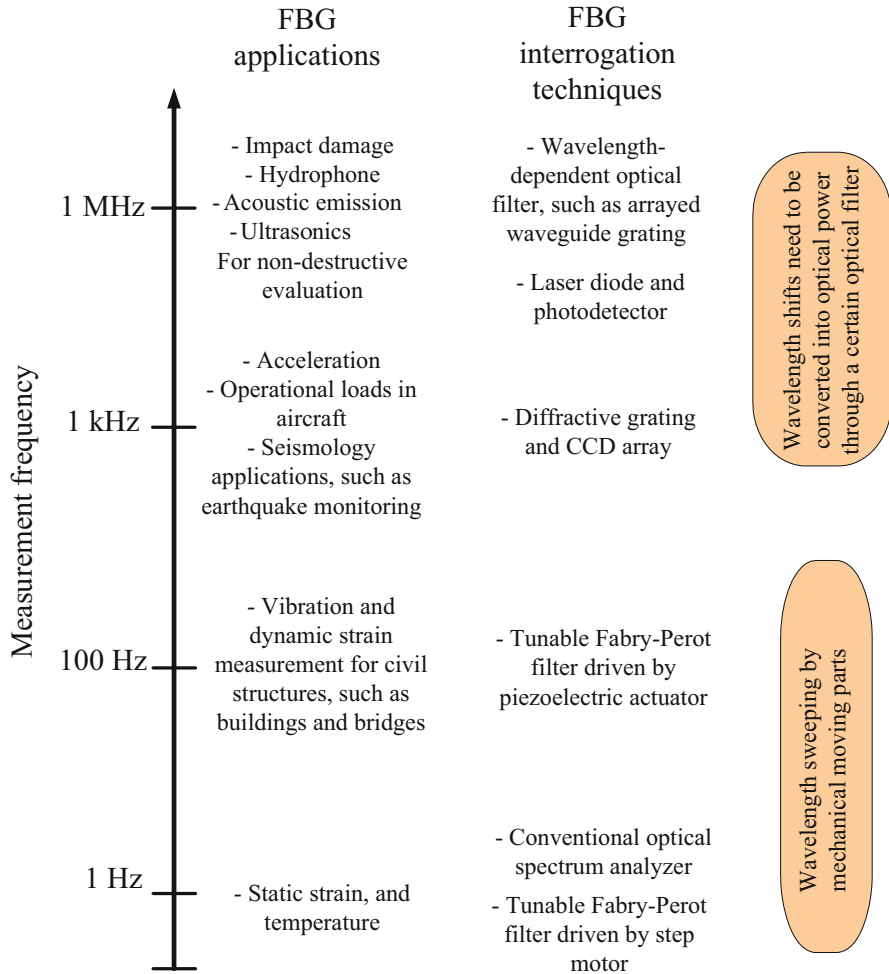


Fig. 8.15 Classification of FBG sensing techniques according to the frequency range (Guo et al. 2011)

Different types of embedded sensing solutions for the structural health monitoring of a helicopter blade, including FBG sensors and phased and discrete piezoelectric sensor arrays have been reported by Ghoshal et al. (2015). In addition to the potential use of OFS during operations and monitoring, these sensors also allow the production monitoring of aircraft components made from composite materials (Chiesura et al. 2016).

In addition to the vast opportunities in shell-type structures (wings, fuselage, etc.), OFS can also be used on solid components. García et al. (2015) used an intensity-modulated optical fiber sensor for tip clearance and tip timing measurements. Fiber sensors also enable load monitoring in landing gears (Iele et al. 2019).

Limitations and Challenges of Optical Fiber Sensors

Notwithstanding their immense application potential, optical fiber sensors also face some limitations, as is the case with any sensor type. Fiber integration is challenging, and care should be taken that debonding of the host composite material does not happen during the integration (Wang et al. 2012). Other researchers proposed the integration of a standard connector in the material (Sjögren 2000; Green and Shafir 1999). This facilitates the test process, but has an additional effect on the component strength (Sjögren 2001).

Another aspect related to the sensor integration is the fact that the optical response of the sensor might change after the embedding process (Luyckx et al. 2011). This generally does not pose any problem for the OFS operation, but in some situations like when the integration is poorly done, peak-splitting can occur. This peak-splitting can also occur because of a non-uniform loading (Kuang et al. 2001). In other words, a single Bragg peak will split in two separate peaks. In that case, the adapted signal processing algorithms should be used to consider the deformed state of the peak (Lamberti et al. 2014).

After integration in the material, the sensor is protected and can withstand high loads and temperatures. High-percentage strains can be reached in the case of polymer fiber (Zhou and Sim 2002; Peters 2011). However, the weakest point in the sensor system is the ingress or egress point where the fiber leaves the material. At this location, care should be taken not to apply high loads. In practice, a stress-relieve cover is often used to protect the fiber at the ingress/egress point. Accordingly, Missinne et al. (2017) proposed a special type of connector to detect a potential signal loss between the fiber and the connector.

Optical fiber sensors can be used to measure a variety of measurands (e.g., strain, pressure, temperature, etc.). However, it is not generally easy to separate these quantities if they appear simultaneously. One possible technique for simultaneously measuring strain and temperature is using so-called micro-structured optical fibers (Sonnenfeld et al. 2011).

8.3 Strain-Based SHM

Note that measuring strains is not the same as detecting damage. A local crack in a structure may significantly drop the failure loads, but until it grows toward the catastrophic failure, it produces negligible changes in most of the structure parameters (natural frequencies, global strain fields, etc.). The main difficulty for the SHM is identifying the 'features' or parameters sensitive to minor damages and distinguishing the response from natural and environmental disturbances.

If a crack does not change the strain field at the sensor location, it would not be detected, and the strain changes are quite small a few millimeters away from the crack tip, providing difficulties for a global SHM system based on strain monitoring. Figure 8.16 illustrates a few existing approaches:

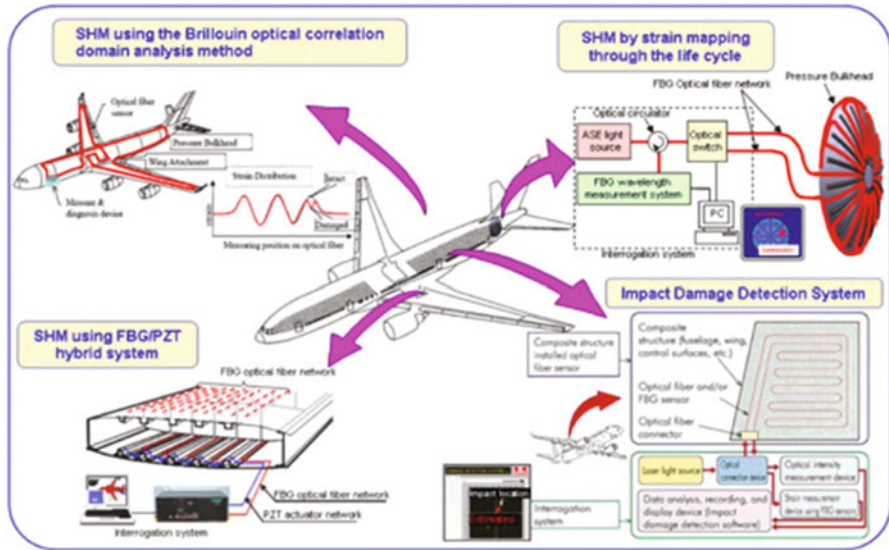


Fig. 8.16 Strain-based SHM systems in the METI Project (Takeda et al. 2013)

- Impact damage detection systems: by using FBGs as a high-frequency sensor for elastic waves, the impact location and its energy can be estimated similar to PZTs. Two main issues are the need of a wide structure coverage requiring a large number of sensors and the high sensitivity required in the interrogation system.
- Hybrid PZT–FBG sensors: similar to the former one, the elastic waves are produced by PZTs and detected by FBGs. Algorithms quite similar to those used for ultrasonics techniques are used.
- SHM by strain mapping: when the strains are measured at a very large number of points distributed throughout the structure and with adequate pattern recognition algorithms, the slight changes caused by a damage can be identified, even when the damage is not coincident with the sensor position. This is currently the most promising approach, even if the resolution is still not good enough (Sierra-Perez et al. 2013).
- SHM by distributed sensing: This is a procedure limited to optical fiber methods (either Brillouin or Rayleigh). When the optical fiber crosses a crack, this crack produces a local strain peak. Edge delamination in composite structures has been detected by this method (Güemes et al. 2018).

References

- Alves JA (2003) Fiber Bragg sensor interrogation system based on a CCD spectrometer. *Sensors*:909–913
- Anon. (1984) Strain gage instrumentation installed on the interior of the AFTI/F-16 wing NASA/Dryden Flight Research Center (NASA-DFRC) (p 1/1/1984)
- ASTM E1561-93 (2014) Standard practice for analysis of strain gage rosette data. ASTM International, West Conshohocken, PA
- ASTM E837-13a (2013) Standard test method for determining residual stresses by the hole-drilling strain-gage method. ASTM International, West Conshohocken, PA
- Bahrapour AR (2012) Optical fiber interferometers and their application. *Interferometry Res Appl Sci Technol*. <https://doi.org/10.5772/34346>
- Chiesura G, Lamberti A, Yang Y et al (2016) RTM production monitoring of the A380 hinge arm droop nose mechanism: a multi-sensor approach. *Sensors* 16. <https://doi.org/10.3390/s16060866>.
- Cranch GA, Nash PJ (2001) Large-scale multiplexing of interferometric fiber-optic sensors using TDM and DWDM. *J Lightwave Technol* 19:687–699. <https://doi.org/10.1109/50.923482>
- Dai Y, Liu Y, Leng J et al (2009) A novel time-division multiplexing fiber Bragg grating sensor interrogator for structural health monitoring. *Opt Lasers Eng* 47:1028–1033. <https://doi.org/10.1016/j.optlaseng.2009.05.012>
- Dawood TA, Sheno RA, Sahin M (2007) A procedure to embed fibre Bragg grating strain sensors into GFRP sandwich structures. *Compos A* 38:217–226. <https://doi.org/10.1016/j.compositesa.2006.01.028>
- Di Sante R (2015) Fibre optic sensors for structural health monitoring of aircraft composite structures: recent advances and applications. *Sensors (Switzerland)* 15:18666–18713. <https://doi.org/10.3390/s150818666>
- Druet T, Chapuis B, Jules M et al (2018) Passive guided waves measurements using fiber Bragg gratings sensors. *J Acoust Soc Am* 144:1198. <https://doi.org/10.1121/1.5054015>.
- Erdogan T (1997) Fiber grating spectra. *J Lightwave Technol* 15:1277–1294. <https://doi.org/10.1109/50.618322>
- Faisal NH et al (2019) Diametral compression test method to analyse relative surface stresses in thermally sprayed coated and uncoated circular disc specimens. *Surface Coatings Technol* 357:497–514
- Froggatt M et al (1998) High-spatial-resolution distributed strain measurement in optical fiber with Rayleigh scatter. *Appl Opt* 37(10):1735–1740
- García I, Zubia J, Durana G et al (2015) Optical fiber sensors for aircraft structural health monitoring. *Sensors (Switzerland)* 15:15494–15519. <https://doi.org/10.3390/s150715494>
- Garus D, Krebber K, Schliep F et al (1996) Distributed sensing technique based on Brillouin optical-fiber frequency-domain analysis. *Opt Lett* 21(17):1402–1404. <https://doi.org/10.1364/OL.21.001402>
- Ghoshal A, Ayers J, Gurvich M et al (2015) Experimental investigations in embedded sensing of composite components in aerospace vehicles. *Compos Part B Eng* 71:52–62. <https://doi.org/10.1016/j.compositesb.2014.10.050>
- Giraldo CM, Sagredo JZ, Gómez JS et al (2017) Demonstration and methodology of structural monitoring of stringer runs out composite areas by embedded optical fiber sensors and connectors integrated during production in a composite plant. *Sensors (Basel, Switzerland)* 17. <https://doi.org/10.3390/s17071683>.
- Girard S et al (2018) Recent advances in radiation-hardened fiber-based technologies for space applications. *J Opt (United Kingdom)* 9:20. <https://doi.org/10.1088/2040-8986/aad271>
- Goossens S, De Pauw B, Geernaert T et al (2019) Aerospace-grade surface mounted optical fibre strain sensor for structural health monitoring on composite structures evaluated against in-flight conditions. *Smart Mater Struct* 28. <https://doi.org/10.1088/1361-665X/ab1458>

- Grandal T, Zornoza A, Fraga S et al (2018) Laser cladding-based metallic embedding technique for fiber optic sensors. *J Lightwave Technol* 36:1018–1025. <https://doi.org/10.1109/JLT.2017.2748962>.
- Green AK, Shafir E (1999) Termination and connection methods for optical fibres embedded in aerospace composite components. *Smart Mater Struct* 8:269–273. <https://doi.org/10.1088/0964-1726/8/2/013>
- Grzegorz Gruca NR (2019). United States Patent No. US, 10, p 255 B2
- Güemes A, Fernández-López A, Díaz-Maroto PF et al (2018) Structural health monitoring in composite structures by fiber-optic sensors. *Sensors* 18:1094. <https://doi.org/10.3390/s18041094>
- Guo H, Xiao G, Mrad N et al (2011) Fiber optic sensors for structural health monitoring of air platforms. *Sensors* 11:3687–3705. <https://doi.org/10.3390/s110403687>.
- Hariharan P (2007) Basics of interferometry, Academic Presse, ISBN: 978-0-12-373589-8, <https://doi.org/10.1016/B978-0-12-373589-8.X5000-7>.
- Havermann D, Mathew J, MacPherson WN et al (2015) Temperature and strain measurements with fiber Bragg gratings embedded in stainless steel 316. *J Lightwave Technol* 33:2474–2479. <https://doi.org/10.1109/JLT.2014.2366835>.
- He XL, Wang ZQ, Wang DH et al (2019) Optical fiber sensor for strain monitoring of metallic device produced by very high-power ultrasonic additive Manufacturing. *IEEE Sensors J* IEEE 19:10680–10685. <https://doi.org/10.1109/JSEN.2019.2928966>.
- Iele A et al (2019) A fiber optic sensors system for load monitoring on aircraft landing Gears. In: Kalli K, Brambilla G, O'Keefe S (eds) *Opt Eng (proc SPIE) seventh European workshop on optical fibre sensors (EWOFS 2019)*. SPIE-International Society, Bellingham, WA, pp 98227–90010. <https://doi.org/10.1117/12.2541110>.
- IPC/JEDEC (2005) Printed wiring board strain gage test guideline JEDEC. IPC/JEDEC-9704
- James SW, Tatam RP (2003) Optical fibre long-period grating sensors: characteristics and application. *Meas Sci Technol* 14:R49–R61. <https://doi.org/10.1088/0957-0233/14/5/201>
- Kersey AD, Davis MA, Patrick HJ et al (1997) Fiber grating sensors. *J Lightwave Technol* 15:1442–1463. <https://doi.org/10.1109/50.618377>.
- Kinet D, Mégret P, Goossen KW et al (2014) Fiber Bragg grating sensors toward structural health monitoring in composite materials: challenges and solutions. *Sensors (Switzerland)* 14:7394–7419. <https://doi.org/10.3390/s140407394>
- Kondrat M et al (2007) A Sagnac-Michelson fibre optic interferometer: signal processing for disturbance localization. *Opto-Electronics Review* 15:127–132
- Kuang KSC, Kenny R, Whelan MP et al (2001) Embedded fibre Bragg grating sensors in advanced composite materials. *Compos Sci Technol* 61:1379–1387. [https://doi.org/10.1016/S0266-3538\(01\)00037-9](https://doi.org/10.1016/S0266-3538(01)00037-9).
- Lamberti A, Vanlanduit S, De Pauw B et al (2014) A novel fast phase correlation algorithm for peak wavelength detection of fiber Bragg grating sensors. *Opt Express* 22:7099–7112. <https://doi.org/10.1364/OE.22.007099>.
- Lee B (2003) Review of the present status of optical fiber sensors. *Opt Fiber Technol* 9:57–79. [https://doi.org/10.1016/S1068-5200\(02\)00527-8](https://doi.org/10.1016/S1068-5200(02)00527-8)
- Loutas TH, Charlaftis P, Airoidi A et al (2015) Reliability of strain monitoring of composite structures via the use of optical fiber ribbon tapes for structural health monitoring purposes. *Compos Struct* 134:762–771. <https://doi.org/10.1016/j.compstruct.2015.08.100>
- Luyckx G, Voet E, Lammens N et al (2011) Strain measurements of composite laminates with embedded fibre Bragg gratings: criticism and opportunities for research. *Sensors* 11:384–408. <https://doi.org/10.3390/s110100384>.
- Ma Z, Chen X (2019) Fiber Bragg gratings sensors for aircraft wing shape measurement: recent applications and technical analysis. *Sensors (Switzerland)* 19. <https://doi.org/10.3390/s19010055>
- Malik SA, Wang L, Curtis PT et al (2016) Self-sensing composites: in-situ detection of fibre fracture. *Sensors (Switzerland)* 16:1–18. <https://doi.org/10.3390/s16050615>

- Mario Sorgente AR (2020) Performance comparison between fiber-optic and piezoelectric acoustic emission sensors.
- Mendoza E et al (2013) In-flight fiber optic acoustic emission sensor (FAESense) system for the real time detection, localization, and classification of damage in composite aircraft structures. *Photon Appl Aerosp Comm Harsh Environ IV* 8720:87200K. <https://doi.org/10.1117/12.2018155>
- Mihailov SJ (2012) Fiber Bragg grating sensors for harsh environments. *Sensors* 12:1898–1918. <https://doi.org/10.3390/s120201898>
- Missinne J, Luyckx G, Voet E et al (2017) Low-loss connection of embedded optical fiber sensors using a self-written waveguide. *IEEE Photon Technol Lett* 29:1731–1734. <https://doi.org/10.1109/LPT.2017.2747630>.
- Nedjalkov A, Meyer J, Waltermann C et al (2018) Direct inscription and evaluation of fiber Bragg gratings in carbon-coated optical sensor glass fibers for harsh environment oil and gas applications. *Appl Opt* 57:7515–7525. <https://doi.org/10.1364/AO.57.007515>.
- Nicolas MJ, Sullivan RW, Richards WL (2016) Large scale applications using FBG sensors: determination of in-flight loads and shape of a composite aircraft wing. *Aerospace* 3. <https://doi.org/10.3390/aerospace3030018>
- Park S-JA-K (2011) *Interface science and composites*. Academic Press, Cambridge, MA
- Peters K (2011) Polymer optical fiber sensors - a review. *Smart Mater Struct* 20. <https://doi.org/10.1088/0964-1726/20/1/013002>
- Pinet É (2009) Fabry-Pérot fiber-optic sensors for physical parameters. *J Sens* 2009:1–9. <https://doi.org/10.1155/2009/720980>
- Rajabzadeh AA (2018) Analysis of FBG reflection spectra under anti-symmetrical strain distributions using the approximated transfer matrix model *Optical sensing and detection V* (p. 1068000). International Society for Optics and Photonics, Strasbourg
- Rajan G (2016) *Structural health monitoring of composite structures using fiber optic methods*. CRC Press, Boca Raton
- Rijnveld N (2017) *Optical fibre interferometry – new concepts and applications*. Mikroniek 18–21
- Saheb N, Mekid S (2015) Fiber-embedded metallic materials: from sensing towards nervous behavior. *Materials* 8:7938–7961. <https://doi.org/10.3390/ma8115435>
- Sjögren A (2000) Manufacturing technique for embedding detachable fiber-optic connections in aircraft composite components. *Smart Mater Struct* 9:855–858. <https://doi.org/10.1088/0964-1726/9/6/316>
- Sjögren BA (2001) Static strength of CFRP laminates with embedded fiber-optic edge connectors. *Compos A* 32:189–196. [https://doi.org/10.1016/S1359-835X\(00\)00138-X](https://doi.org/10.1016/S1359-835X(00)00138-X)
- Sonnenfeld C, Sulejmani S, Geernaert T et al (2011) Microstructured optical fiber sensors embedded in a laminate composite for smart material applications. *Sensors* 11:2566–2579. <https://doi.org/10.3390/s110302566>.
- Takeda NA et al (2013) Outline of the Japanese National Project on Structural Health Monitoring System for Aircraft Composite Structures and JASTAC Project. IWSHM2013, Stanford
- Takeda NA (2005) Development of smart composite structures with small-diameter fiber Bragg grating sensors for damage detection: quantitative evaluation of delamination length in CFRP laminates using lamb wave sensing. *Compos Sci Technol* 2005:2575–2587
- Takeuchi K (2012) Locations of strain gauges for fatigue analysis of welded joints (2). *Weld Int* 26:655–664. <https://doi.org/10.1080/09507116.2011.590680>
- Tsai W (2001) A novel structure for the intrinsic Fabry-Perot fiber-optic temperature sensor. *J Lightw Technol*
- Ushakov NA (2015) Utilization of NI PXIe-4844 interrogator for high resolution fiber intrinsic Fabry-Perot interferometric sensing. In: 2015 International Siberian conference on control and communications (SIBCON). IEEE, pp 1–4
- Wada D, Igawa H, Tamayama M et al (2019) Flight demonstration of aircraft wing monitoring using optical fiber distributed sensing system. *Smart Mater Struct* 28. <https://doi.org/10.1088/1361-665X/aae411>

- Wang Y, Gong J, Dong B et al (2012) A large serial time-division multiplexed Fiber Bragg grating sensor network. *J Lightwave Technol IEEE* 30:2751–2756. <https://doi.org/10.1109/JLT.2012.2205897>.
- Wei US (2013) *Fiber optic interferometric devices*. Springer Science, Cham
- Xu MG, Alavie AT, Maaskant R et al (1996) Tunable fibre bandpass filter based on a linearly chirped fibre Bragg grating for wavelength demultiplexing. *Electron Lett* 32:1918–1919. <https://doi.org/10.1049/el:19961242>
- Yu F, Okabe Y (2017) Fiber-optic sensor-based remote acoustic emission measurement in a 1000 °C environment. *Sensors (Switzerland)* 17. <https://doi.org/10.3390/s17122908>
- Zahid MN et al (2019) *Reflectometric and interferometric fiber optic sensor's principles and applications*. Springer, Cham
- Zetie KP, Adams SF, Tocknell RM (2000) How does a Mach-Zehnder interferometer work? *Westminster School Phys Educ* 35:46–48. <https://doi.org/10.1088/0031-9120/35/1/308>
- Zhou G, Sim LM (2002) Damage detection and assessment in fibre-reinforced composite structures with embedded fibre optic sensors-review. *Smart Mater Struct* 11:925–939. <https://doi.org/10.1088/0964-1726/11/6/314>

Open Access This chapter is distributed under the terms of the Creative Commons Attribution 4.0 International License (<http://creativecommons.org/licenses/by/4.0/>), which permits use, duplication, adaptation, distribution and reproduction in any medium or format, as long as you give appropriate credit to the original author(s) and the source, a link is provided to the Creative Commons license and any changes made are indicated.

The images or other third party material in this chapter are included in the work's Creative Commons license, unless indicated otherwise in the credit line; if such material is not included in the work's Creative Commons license and the respective action is not permitted by statutory regulation, users will need to obtain permission from the license holder to duplicate, adapt or reproduce the material.



Chapter 9

Data Reduction Strategies



**Basuraj Bhowmik, Said Quqa, Markus G. R. Sause, Vikram Pakrashi,
and Mohamad Ghazi Droubi**

Abstract Based on the variety of methods available for gathering data for the aircraft health status, the challenge is to reduce the overall amount of data in a trackable and safe manner to ensure that the remaining data are characteristic of the current aircraft status. This chapter will cover available data reduction strategies for this task and discuss the data intensity of the SHM methods of Chaps. 5 to 8 and established approaches to deal with the acquired data. This includes aspects of algorithms and legal issues arising in this context.

9.1 Introduction

In the framework of this publication, the term “signal processing” covers all processing steps with the goal of extracting information from a (received or measured) signal or preparing information for transmission from an information source to an information consumer. The important goals of signal processing are the acquisition of information about the structural health status, data reduction, and preparation for visualization. In this chapter we focus on the available data reduction strategies, their challenges in relation to wireless sensors and issues arising from the data management. From a broader sense, the chapter will not only deal with the theoretical development of the said concepts, but will also provide accurate applications, strategies for monitoring and future prospects of the algorithms—embedded

B. Bhowmik (✉) · V. Pakrashi
University College Dublin, Dublin, Ireland
e-mail: basuraj.bhowmik@ucd.ie

S. Quqa
University of Bologna, Bologna, Italy

M. G. R. Sause
Institute of Materials Resource Management, University of Augsburg, Augsburg, Germany

M. G. Droubi
Robert Gordon University, Aberdeen, UK

within the context of dynamical systems. While signal processing forms the building blocks of the chapter, the applicability of these methods—especially in data reduction strategies—provides significant evidence towards the practical implementation of monitoring from a real-time perspective.

9.2 Signal Processing

Traditionally, distinction is made between digital and analog signal processing. In the context of the SHM methods introduced in Chaps. 5 to 8, digital signal processing is becoming more and more important due to the following advantages:

- The analog signal may be affected by extraneous noise and coupling from other electrical systems nearby, which is intrinsically eliminated after digitization. This can be easily carried out in real-time using algorithms such as the recursive singular spectrum analysis (Bhowmik 2018).
- The desired data reduction steps can often be implemented more easily with digital processing steps (e.g. by programming microcontrollers).
- Digital signal processing allows for storage and simple further processing (transmission to other systems (e.g. visualization, storage, or control systems)).

Nevertheless, some distinct disadvantages are associated to digital signal processing:

- Analog-to-digital converters (ADCs) and/or digital-to-analog converters (DACs) temporally discretise information with a certain sampling rate and a certain “vertical” accuracy based on the bit depth of the system.
- In some cases, the digitization forms an intermediate processing step (analog→digital and later again digital→analog) in the implementation chain, which doubles potential conversion errors.
- The implementation of digital processing steps and their execution can sometimes be very time consuming and lead to information delays. This may make approximation methods necessary instead of using the full precision of available algorithms.

Basically, a distinction can be made between one- (e.g. ultrasonic and strain gauge signals) (1D), two- (e.g. images) (2D), and three-dimensional (3D) (e.g. moving images and video) signal processing. In the SHM framework in aircraft, Table 9.1 provides the first overview on the typical sensing techniques applied in aircraft monitoring. Based on this, all currently applied typical SHM methods deliver 1D information, which must be interpreted in terms of the aircraft status. Powerful approaches exist to combine the information provided by a network of 1D sensors to retrieve some 2D or 3D damage mapping on the structure. However, the limitation of signal information to essentially 1D data streams also addresses the requirement of data reduction for signal processing as far as today’s computational capabilities are concerned.

Table 9.1 Aircraft monitoring techniques

Monitoring technique		Type of sensor	Type of damage monitored	Mode of detection	Dimensionality
Strain		Fiber optical sensor	Impact	Passive	Scalar
Wave propagation	Guided waves	Piezoelectric sensor (PZT, PVDF, etc.)	Global/local damage	Active	Scalar
	Ultrasonics	Piezoelectric sensor and laser	Local damage	Active	Scalar
	Acoustic emission	Piezoelectric sensor	Global/local damage	Passive	Scalar
	Stress waves	Piezoelectric sensor	Impact and loads	Passive	Scalar
Electrical resistance		Resistance element	Local damage	Passive	Scalar
Electro-mechanical impedance		Piezoelectric sensor	Local damage	Active	Scalar

The cyclic step of converting analogue to digital signals and vice versa is mainly associated with the transmission costs that might arise during data transfer. For certain transmission systems, digital communication sources are preferred which generally require post processing in an offline mode. However, in recent times, methods using real-time fault detection approaches have strikingly lowered the transmission costs for a monitoring system and therefore, the cyclic conversion back into the analogue regime can sometimes prove beneficial. This aspect is also applicable to aerospace incorporations.

In the context of real-time SHM, recent literature has time and again illustrated the potential to identify system faults online. This is particularly helpful for aircraft machinery where the state of system health can be identified in real-time and mitigation measures can be correctly implemented. Real-time control of dynamic systems has never been more comprehensive when investigated under the auspices of eigen perturbation theories and higher order error stabilization. In the present context, the authors firmly believe that signal processing approaches have paved the way to online SHM contributions over the recent years. This is also systematically evidenced by the relevant inclusions of references throughout the text.

Although approaches such as digital filtering, lossless compression, and methods to increase SNR have been adopted by researchers and practitioners worldwide, the inherent difficulties in performing real-time impedes their possible applications. Cases where data needs to be transmitted from a monitored section to the processing site, the transmission should be at a capacity to transfer a bulk of data. However, in order to alleviate these drawbacks, recent works on perturbation theory have shed light on the in-situ approach of data-driven decision-based framework (Bhowmik et al. 2020a). Forming an evidence base around the topic are extensive numerical

simulations and experimental case studies which are supplemented by practical real-life scenarios.

9.3 Data Reduction Strategies

Traditional SHM systems employ coaxial wires for the communication and data transmission between sensors and the decision making (data interpretation) unit. As a result, traditional models and schemes developed for health monitoring are largely challenged by low-cost, quality-guaranteed, and real-time event monitoring. The data involved in many SHM systems are time-domain structural responses with large data sizes. Damage detection methods with a higher detection sensitivity are generally often associated with a higher sampling rate. It is not unusual for a wave propagation-based damage detection system to excite and sense wave motions at a megahertz range. High-frequency sampling and excitation pose multiple challenges to wireless sensor development, one of which is the timely transmission of a large amount of data. Although directly transmitting the original sensor data to the data interpretation unit can retain the signal fidelity for a comprehensive data analysis, this may lead to a prohibitive burden to the wireless data transmission, especially for applications that need near real-time decision making. One tempting idea is to perform data pre-processing at the local sensor level, such that the data can be greatly compressed/reduced while the critical features reflecting the damage effects can be preserved. If effectively established, such data reduction, which is also known as feature extraction, can alleviate the data transmission rate issue between the sensors and the data interpretation unit. On the contrary, it requires a higher computing capability and the associated power consumption at the local sensor level.

9.3.1 *Sampling Rates of Different SHM Methods*

Gaining a clear understanding of the structural behaviour to allow a reasonable assessment of its as-built condition requires high-fidelity sensor data to build accurate models (Nagayama et al. 2006). In addition, potentially problematic structural changes, such as corrosion, cracking, buckling, and fracture, all occur locally within a structure. Sensors are expected to be in close proximity to the damage to capture the resulting change in response, while sensors further from the damage are unlikely to observe measurable changes. A dense array of sensors is required to achieve an effective monitoring system capable of generating informative structural models and detecting critical structural changes. Such a dense instrumentation system is not practically realised with the traditional structural monitoring technology due to the cost of deployment and the potential for data inundation. Advances in the wireless technology and embedded processing have made much lower-cost wireless smart sensor networks (WSSNs) an attractive alternative to wired,

centralised data acquisition (DAQ) systems. The majority of the work using wireless smart sensors for structural monitoring has focused on using the sensors to emulate traditional wired sensor systems (Arms et al. 2004; Pakzad et al. 2008; Whelan and Janoyan 2009). These systems require that all data be sent back to a central DAQ system for further processing; hence, the amount of wireless communication required in the network can become costly in terms of excessive communication times and the associated power it consumes as the network size increases. For example, a wireless sensor network implemented on the Golden Gate Bridge that generated 20 MB of data (1600 s of data, sampling at 50 Hz on 64 sensor nodes) took over 9 h to complete the communication of the data back to a central location (Pakzad et al. 2008).

In the following we are presenting the sampling rate requirements for the main SHM systems discussed in this book to better differentiate between the different methods.

9.3.1.1 Ultrasonics

Ultrasonics are particularly a data-heavy and popular class of approach in this regard. Michaels (2008) reported how guided waves for large-area monitoring, diffuse waves in complex components (e.g. plates), and local ultrasonics for hotspot monitoring, change the demand. In this regard, local hotspot monitoring is of relevance, and the sampling rate can be as high as 10 MHz. The data intensity is often a question of orders of magnitude; thus, comparing such rates for other applications is worthwhile. Acousto-ultrasonics have been successfully utilised for detecting a notch on a plate (Smithard et al. 2017) with a 100–550 kHz range, while a central input frequency of 138 kHz was kept for rotor damage detection by Li et al. (2018). Damage detection in carbon fiber-reinforced plates (CFRP) is also observed at the 40–260 kHz range (Krishnaraj et al. 2012). Delamination (Krohn et al. 2002; Farrar et al. 2007) is a typical phenomenon for detection, and the kHz–MHz range is often used. Scruby and Drain (1990) indicated 3–5 MHz to be typical for laser ultrasonics, but recent studies went up to 250 MHz (Cavuto et al. 2015).

On the other end of this data intensity lies the fact that high-frequency ultrasonics do not have a deep penetration, and for the 500 kHz–1 MHz range, distinguishing differences in composites is hard.

9.3.1.2 Vibration-Based Methods

Vibration-based methods typically consider accelerometer-based global responses, and sampling is typically based on the type of accelerometer aligned to the needs of the system. This can vary from hundreds of Hertz (popularly sampled diadically as 256 Hz, 512 Hz, etc.) to thousands of Hz (Bhowmik et al. 2019a, 2019b; Noel et al. 2017; Zhu et al. 2018). Displacement sensors like linear variable differential transformers (Wang and Tang 2017) or radar-based ones (Li et al. 2015) can have a

similar sampling rate range compared to accelerometers, although image processing-based techniques are limited by the camera frames per second (O'Donnell et al. 2017; Yang and Nagarajaiah 2016). High-speed imaging can often come at the expense of pixel resolution and with an uncertainty related to the displacement measurement. Laser Doppler vibrometry measures velocity, but encoders in them can transfer such data to acceleration or displacement and have typical sampling rates wider than what has been discussed in this section (Schell et al. 2006).

9.3.1.3 Acoustic Emission

The typical bandwidth of frequencies reaches from a few kHz to 1 – 2 MHz due to the dynamic phenomena causing AE signals. Accordingly, this results in typical sampling rates in research applications that are well beyond 5 MSP/s (million samples per second) because of the required oversampling for adequate signal digitization. In particular, for composite materials, some AE sources exhibit high-frequency components that resemble very critical failure modes, such as fiber breakage (Grosse and Ohtsu 2008; Sause 2016). Based on sensor spacing, much of the high-frequency information is lost during propagation, which consequently may result in lesser sampling rates for practical structural health monitoring applications. Nevertheless, these will still reside in the range of several MSP/s required for data capture. With a reasonable number of sensors installed on the structure, this will result in a large amount of data generated during AE monitoring. From the beginning, this aspect has been considered in the development of the measurement equipment. With the lack of a real-time storage capacity for such “high-frequency” signals, some of the first commercially used systems started to focus on extracting features from the recorded waveforms instead of attempting to store full waveforms (Grosse and Ohtsu 2008). One of the most popular analysis routines considers the localization of AE sources by means of a sensor network (cf. Sect. 7.4). This is based on the respective time-of-flight between source and sensor and thus requires a precise, continuous synchronisation at ultrasonic timescales across multiple sensors. Otherwise, offsets or scatter in the synchronisation accuracy may lead to false source coordinates and thus may render this analysis routine completely useless. In this processing chain, the first step is adequate triggering to initiate any further processing, that is often taken as arrival time of the signal, although more dedicated methods have been developed (cf. Sect. 7.4). That is, the acquisition system detects the presence of a signature that exceeds the typical noise floor based on several criteria. Technically, this is implemented as an analysis of the currently recorded signal portion kept available in ring buffers. Based on this first analysis, the relevant portion of the signal stream is extracted and subject to further analysis, such as feature extraction. In this context, several representative features (e.g. amplitudes, frequencies, and more) are calculated from the signals (see Sect. 6.4.1 or standard literature on concise definition (Grosse and Ohtsu 2008; Sause 2016)). This well-established procedure is by far the most effective data reduction step in AE, turning a typical AE signal of 100 kB into a dataset of only 100–150 B. Nevertheless, it comes

with the cost of skipping the actual raw data early on, causing potential conflicts in later interpretation steps. With the availability of much more powerful computer systems within the last 20 years, storing at least the relevant portions of the signal streams in addition to the extracted features seems to be more and more desirable. This is based on several new capabilities that have emerged in the last decades regarding source interpretation, source localization, and for decision making.

It was identified early that, especially outside laboratory investigations, there is a high chance of presence of faulty AE sources, which could mess up the correct interpretation of AE measurements. In most application scenarios, there is a likelihood for “noise” sources being present, such as friction between components, signals from electrical or hydraulic systems, mechanical motion, or even from other (active) ultrasonic systems. For the passive operation of material defects, such as crack growth, the noise sources may mask useful signals and lead to a false interpretation on the actual health status of the structure. This forms one of the driving reasons for performing a more sophisticated signal analysis based on machine learning approaches, cross-correlation techniques, or advanced feature extraction in time-frequency space. All the latter have proven highly useful for improving the AE signal interpretation; however, they come with an additional computational complexity that must be covered by the processing chain. Ideally, this is done highly integrated inside the DSPs or FPGAs on actual acquisition systems, but this is not the standard. As an additional turn-back, this also comes with a higher energy demand that must be delivered by the on-site supply in an SHM application.

While acoustic emission approaches are less popular than ultrasonics, the sampling frequency remains high and in the MHz range. The damage detection in reinforced concrete at 5 MHz (Yoon et al. 2000) has been established over decades now. Detection using Lamb Wave is also performed in a MHz range. Smart composite laminate detection relevant to aerospace applications requires 5 MHz sampling (Masmoudi et al. 2013), while the recent detection of concrete damage uses 10 MHz sampling (Nor 2018). While such application has typically seen an overall increase in the data intensity by an order in the last two decades, challenges in underwater situations have catered to a lower (64 kHz) sampling rate (Walsh et al. 2017). Overall, the AE frequencies in material evaluation and characterization and in engineering asset health monitoring typically range between 100 kHz and 10 MHz (Tan 2016).

9.3.1.4 Strain Monitoring

While larger infrastructure systems typically consider more robust vibrating wire strain gauges, their application is limited, and the sampling rates are very low (typically one sample per minute) (Pakrashi et al. 2013). Such rates limit the abilities to perform frequency domain analyses, and time series techniques must be employed. Distributed fiber optic sensors increase this rate, but only to approximately 1–5 Hz (Berrocal et al. 2020). On the contrary, these gauges usually come

with thermal measurements. Bragg grating sensing or dynamic strain gauges can go up to tens or approximately 100 Hz (Moyo et al. 2005), but still several orders lower than the ultrasonic counterpart. Distributed fiber optic sensors are more prevalent for strain monitoring in composites (Jothibasu et al. 2018). Lower sampling rates lead to less demand on data analyses or storage, but come with the limitation of being able to accommodate low frequencies alone, which may be inadequate when trying to assess certain damage types. The other option is to create a dense network of strain sensors (Daichi and Tamayama 2019; dos Santos 2015; Lizotte and Lokos 2005; Świąch and Świąch 2020), which has been experimented on aircraft wings before, but come with the problem of cumbersome instrumentation and having to deal with several channels of simultaneous data. For example, Bombardier tested heavily instrumented strain gauges (Marsh 2011).

9.3.2 Established Approaches for Data Reduction

Aspects around data reduction were highlighted by Martin et al. (1997), and several techniques exist. While frequency domain transforms can reduce data, certain features can also be missed. The recent work around real- or near real-time approaches (Mucchielli et al. 2020; Bhowmik et al. 2020a; Krishnan et al. 2018), along with batch-processing assessments (Martinez-Luengo et al. 2016), has provided typical statistical methods for reducing the data intensity. Park et al. (2010) identified the need for data denoising as a primary step. A wavelet-based approach was primarily followed here. Bolandi et al. (2019) more recently approached this topic by interpreting the cumulative duration of strain events at different predefined strain levels. Techniques based on multivariate statistics (Worden and Manson 2000) and statistical process control (SPC) (Fugate et al. 2001) have recently been applied in structural damage detection. On the contrary, PCA (principal component analysis) has been used for performing data compression prior to the feature extraction process when data from multiple measurement points are available to enhance the discrimination between features from undamaged and damaged structures (Bhowmik et al. 2019a). This process transforms the time series from multiple measurement points into a single time series. Visualization and dimension reduction were implemented using the PCA for damage detection. The PCA technique has been used to condense the frequency response functions data and their projection onto the most significant principal components used as the artificial neural network input variables (Zang and Imregun 2001). Moreover, the PCA has also been recently used for several purposes, including model reduction, dynamic characterization (Feeny 2002), sensor validation (Friswell and Inman 1999), modal analysis (Feeny 2003), parameter identification (Lenaerts et al. 2001), or damage detection (Bhowmik et al. 2019a). Some nonlinear extensions of the PCA have been employed for SHM purposes.

With its advent, the wavelet theory has served as a useful approach for data compression where conventional techniques have not achieved the desired speed, accuracy, or efficiency. The wavelet transform principle lies in hierarchically

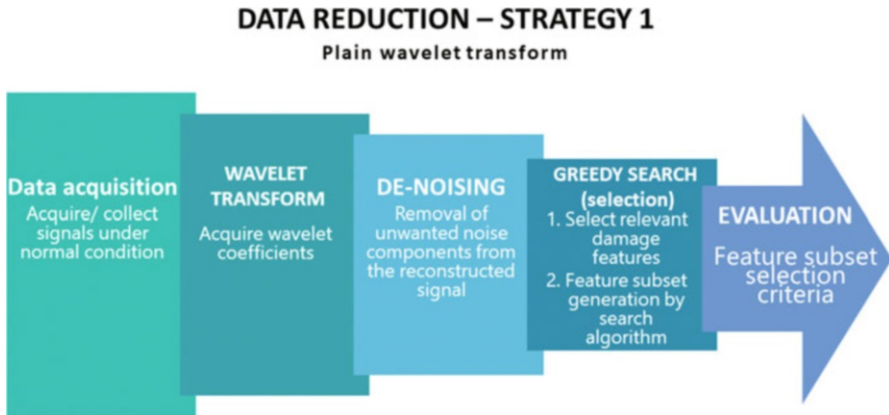


Fig. 9.1 Data reduction through wavelet transform approaches

decomposing an input signal into a series of successively lower resolution signals (Rioul and Vetterli 1991; Strang and Nguyen 1996). At each level, the decomposed signal contains the information needed to reconstruct the signal situated at the next higher resolution level. This concept owns its potential of extending to electric power quality issues (Santoso et al. 1997). For this application, the wavelet transform coefficients corresponding to a disturbance can be found larger than others unrelated. Therefore, we can store only those data related with the event. Using this method, the data of power quality disturbance can be compressed, while the original signal can be reconstructed with very little information loss. Figure 9.1 depicts an informative illustration of wavelet-based data reduction.

The data compression for SHM systems has attracted much interest in the recent years, especially for wireless monitoring systems, because data compression techniques can provide a method of improving the power efficiency and minimising the bandwidth during the transmission of structural response time histories from wireless sensors (Lynch 2004; Xu et al. 2004). Wavelet-based compression (Xu et al. 2004) and Huffman lossless compression (Lynch 2004) techniques have been developed. All these data compression methods belong to a conventional framework for sampling signals that follow the Nyquist–Shannon theorem: the sampling rate must be at least twice the maximum frequency present in the signal.

Compressive sensing (CS) (Candés and Wakin 2008; Donoho 2006) is a novel sampling technique for data acquisition, whose capability, when first met, seems surprising. It asserts that if certain signals are sparse in some orthogonal basis, one can accurately reconstruct these signals from far fewer measurements than what is usually considered necessary based on Nyquist–Shannon sampling. This new technique may become the main paradigm for simultaneously sampling and compressing data, thereby increasing the efficiency of data transfer and storage. Figure 9.2 shows a quick summary of data reduction through compressive sensing.

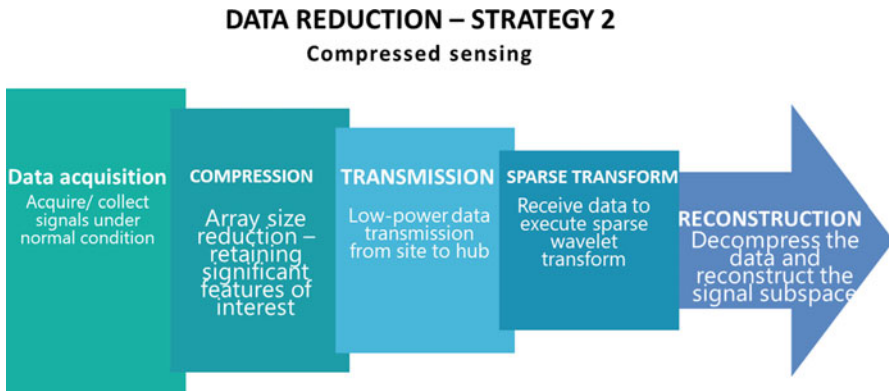


Fig. 9.2 Data reduction through compressive sensing strategies

9.3.3 Open Challenges for Data Reduction in SHM Systems

For ultrasonics, the protocols for quantifying the output of an SHM system are generally not available. The full 3D modeling of wave propagation is still prohibitive for several applications, but the numerics around this keeps improving. Validation against real defects in structures remains a problem. Environmental effects like temperature, load variations, and surface conditions are well known to cause significant changes in ultrasonic signals, often exceeding changes due to damage. Load changes, unlike temperature changes, are generally anisotropic; like temperature changes, they cause changes in the propagation times of individual ultrasonic echoes.

9.3.3.1 Ultrasonic Systems

For some SHM methods using ultrasonic signals to retrieve information, one of the key aspects in data reduction is how to deal with the raw data. As per the ultrasonic range definition, the typical sampling rates in the order of several MSP/s will produce a serious amount of data within a very short time of monitoring operation. For active methods, such as pulse-echo systems and guided wave monitoring, one can select pulsing intervals for the monitoring inspection and adjust the amount of data. For one active monitoring operation, the generated data will still require a certain share of data storage capacity. For passive systems, such as acoustic emission monitoring, skilled data reduction steps may be used to avoid storage of raw data streams. Nevertheless, the amount of data generated cannot be freely selected because it depends on the overall acoustic emission activity during the operation. Based on the likelihood of numerous noise sources being active, this will generate a serious amount of data during the aircraft operation, which needs to be interpreted.

9.3.3.2 Reliability Issues Related to Loss of Information Via Data Reduction

Every data reduction pipeline has an intrinsic issue related to the potential loss of relevant information due to skipping of signal portions, compression, selection, or other measures. While the actual (digital) raw signals may be properly reconstructed in some cases, many cases in presently used SHM data reduction steps require a significant reduction of the amount of data to come to a final decision regarding the actual status of the structure under monitoring. With much of the signal reduction steps still being under research, there is no expectation of established reliability schemes for all algorithms being applied. This considers the aspects of false alarm rates and the likelihood of false interpretation. In addition, for SHM systems to become a part of in-flight avionics, the aircraft operation standards request a certain reliability of the full chain because the SHM system will contribute to high-level decisions with the ultimate consequence of the risk of lives.

9.4 Wireless Sensing Considerations

Structural health monitoring (SHM) applications in the field of aerospace engineering generally involve a limited space for sensor installation and mechanical movements, which may damage parts of the monitoring system. Moreover, long cables may considerably increase the system cost and the overall aircraft weight. For these reasons, wireless communications are generally preferable, although several critical issues may arise using these technologies.

According to Logan and Sankareswaran (2015), aircraft electrical wiring problems have recently increased in the aircraft manufacturing industry. The Airbus A380, for example, has 40,000 sensor connectors and 98,000 wires consisting of over 530 km of wiring in each aircraft (Gao et al. 2018). All onboard safety systems are based on wired connections; hence, the wiring degradation might contribute to further issues and lead to terminated flight missions (Gao et al. 2018), which results in production and delivery delays. The US Navy spends approximately 1 to 2 million man-hours finding and fixing wiring problems. Replacing onboard wired sensing devices by wireless-based solutions can optimise maintenance and improve the safety of aircraft, reducing their weight. Less wires mean less chances of wiring problems, which is great for the most important factor in the aerospace industry, that is, safety. In terms of fuel efficiency, a lighter plane will use less fuel than a heavier one. Therefore, wireless communications and sensors can bring a host of economic benefits.

Several researchers (Logan and Sankareswaran 2015; Yedavalli and Belapurkar 2011) have conducted studies on the improvement in weight due to wireless systems, which has led to an improvement in the fuel efficiency. Moreover, Liu et al. (2008) suggested that the aerospace industry should consider replacing some aerial-vehicle

sensor wiring with wireless communications, thereby lowering the weight of the aerial-vehicle wiring and leading to an increased payload capacity. This thought has been shared by other researchers (Yedavalli and Belapurkar 2011; Zahmati et al. 2011) and become the utmost importance with the most recent developments in the aircraft industry because transportation systems and test facilities are becoming increasingly complex (Figueroa and Mercer 2002).

Nevertheless, some researchers believe that airborne wireless systems (AWSs) may negatively affect the overall reliability of aerial vehicles, jeopardizing their safety (Liu et al. 2008). For this reason, the field of research of wireless sensing systems faces continuous growth, proposing different network topologies and operative algorithms aimed at maximizing the monitoring system efficiency while preserving the robustness and reliability comparable to those of wired solutions.

9.4.1 *Network Topologies*

Dealing with dense wireless sensor networks is generally impractical if continuous and high-rate data streams are necessary. Accordingly, some studies (Cao and Liu 2016) proposed event-triggered sensing systems to collect high-fidelity data at the occurrence of particular events aimed at performing condition-based decision making with minimal data transmissions, while others (Montalvão et al. 2006) were simply based on periodic inspections. Although these systems are particularly effective in some cases, continuous real-time approaches are generally preferable in aerospace applications (Abdeljaber et al. 2017).

Neural networks are effectively used in real-time monitoring systems. However, unlike eigen perturbation methods for damage detection, CNN (or any deep learning-based approach, for that matter) is computationally more expensive (Bhowmik et al. 2019b, 2020a, 2020b). The reason for this placeholder in the present context is to make the reader aware of such methods that exist both in industry and in research practice. Numerous industries (including the tech giants such as Google and Apple) have taken up neural network-based modeling, fault identification, and system reliability as important pathways for product design and development (Marr 2017; Apple 2017). Even though real-time SHM is not mandatory for all SHM systems, as the present chapter focuses on data reduction strategies—and it has been time and again mentioned about the usefulness and lower resource involvement for real-time SHM systems—the authors strongly opine that the placement of this concept is apt. Recalling the concepts here—real-time SHM based monitoring systems can perform in-situ analysis, thereby lowering the transmission cost (Bhowmik et al. 2019a). As compared to conventional monitoring systems, these contemporary modules can lower the computational cost (about 75% lower) than traditional (Kalman filter based) systems (Bhowmik et al. 2019b). The importance of taking higher resolution, lower interval data reading is much more important when aircraft systems are involved. For monitoring such systems, it is usually desired that the readings are close and evenly spaced, such that preventive measures can be

adopted as soon as possible to prevent any disaster (Bhowmik 2018). For such cases, if the aircraft loses communication with the control tower, it is the onus of the crew to prepare for emergency evacuation and initiate mitigation protocols to save lives of the passengers. This can only happen if a real-time monitoring system is placed on the black box, and critical junctures of the aircraft. In the event of an impending disaster, these real-time monitoring stations will provide accurate, early and timely detection (and forecasting) to prevent any mishaps—and therefore, crucial in aircraft systems and for the aerospace industry.

Centralised networks (i.e., those consisting of sensing nodes connected with a central monitoring station through one-to-one connections) are among the most widely used in current SHM applications because they easily allow the application of traditional identification algorithms. In particular, the raw data collected at the instrumented locations are directly transmitted to the monitoring station, where centralised processes occur, thereby generally using algorithms for multivariate data. However, in this case, the amount of data to be centrally collected exceeds the network bandwidth as the number of nodes increases, regardless of the adopted data transmission method, posing a strict constraint on the network scalability. Therefore, this topology is suitable in the case of small or sparsely distributed sensor networks, where the throughput should be maximised without considering a large number of sensor locations.

In the last years, innovative sensing solutions, namely wireless smart sensor networks (WSSNs), have been introduced, disposing micro electro-mechanical system (MEMS) sensors and microcontrollers that can perform a simple onboard processing, such as digital signal processing, self-diagnosis, and self-adaption functions (Nagayama et al. 2009). Their modest computational footprint can be exploited through edge-computing, giving rise to decentralised systems (Abdulkarem et al. 2020; Avci et al. 2018; Quqa et al. 2020), in which part of the signal processing is performed at the node level to lighten data transfer, reduce the computational burden for real-time implementations, and improve the energy efficiency of the entire system. Sensing nodes capable of collecting and processing data independently from the others constitute decentralised networks.

Over the last two decades, different decentralised network configurations have been implemented in SHM applications, and the simpler of which consists of the star topology. Although the connections are similar to those of centralised networks, data processing and compression can be performed before transmitting to the central node (i.e., the sink). However, this configuration does not exploit the information gained from combining data from neighboring nodes (e.g. spatial information), making onboard pre-processing generally limited to simple operations. Filtering and downsampling are generally performed in onboard smart nodes in star configurations (Quqa et al. 2020). The first studies on SHM through decentralised networks in a star configuration were conducted by extending traditional techniques, such as the damage locating vector (DLV) (Gao et al. 2006; Nagayama et al. 2009), to allow their application in a decentralised fashion. Nevertheless, time-series representations (Long and Büyüköztürk 2017) and artificial neural networks (ANNs) (Avci et al.

2018) have recently been exploited to obtain damage sensitive features (DSFs) using small amounts of data.

Hierarchical systems usually organised in tree structures can resolve the limitations of both centralised and independent processing approaches. Smart nodes are divided into hierarchical levels performing different tasks. Leaves (i.e., end devices) are generally used for data collection and filtering, while at the higher levels, data are aggregated. Thus, lighter parameters are calculated at each level before transmitting the data to the monitoring station. In the study of Gao and Spencer (2008), a hierarchical configuration was used for the online evaluation of the flexibility matrix. Meanwhile in the study of Jindal and Liu (2012), the singular value decomposition was performed on the data collected on small groups of sensors, thereby generating a tree-structured identification process.

The other implementations of decentralised WSSNs include mesh topologies, which are still rarely used in SHM applications, due to the need for more power for redundant multi-hop transmissions and the requirement of a complex routing scheme (Abdulkarem et al. 2020). Nevertheless, Mechitov et al. (2004) developed a mesh-compatible algorithm with transmissions limited to extracted features only. Linear, bus, and clustered hierarchical configurations have recently emerged as choice topologies for WSSNs and could find applications in the field of SHM soon.

9.4.2 Data Rates

Dürager et al. (2013) performed a comparison of wireless signal measurement systems with regard to dimensions and weight, processor, wireless transmission system and its range, and energy supply. The sensor nodes discussed in the recent literature had one, four, or eight measuring channels each (Dong et al. 2015; Dürager et al. 2013). The signal resolution is usually 12 or 16 bits. Depending on the system, the sampling rate varies between approximately 100 kHz (Grosse et al. 2010) and 5 MHz (Wu et al. 2017) and the data transmission rate between approximately 40 kB/s (Dürager et al. 2013) and approximately 6 Mbit/s (Wu et al. 2017). The energy required for wireless signal transmission varies depending on the system and the operating mode (e.g. transmission or reception and active or inactive). Dürager et al. (2013) specified approximately 50 mW for “inactive” and 1.4 W for “active”/“transmit.”

A recently published review article (Ayaz et al. 2018) generally described the state of the art of wireless sensor technology, but did not deal with applications in the ultrasonic signal range, with the exception of acoustic methods for leak detection in pipelines (e.g. underwater hydrophones). Wireless underground networks were discussed by (Trang et al. 2018), but this was again without reference to ultrasonic signal measurements. In general, the possible data transmission rates faced in ultrasonic signal evaluation are a problem. Assuming a typical transmission capacity in the order of 100 Mbit/s (Alonso et al. 2018) and determining the required data transmission rate from the number of channels, sampling rate, and estimated

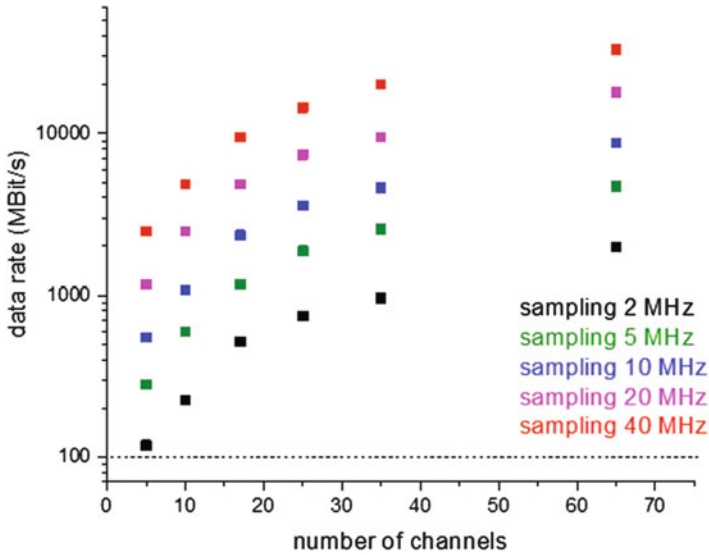


Fig. 9.3 Required data transmission rates in Mbit/s for ultrasonic signals with a 16-bit resolution for a different number of data acquisition channels and sampling rates, with a logarithmic scale of the y-axis. Technically possible: approximately 100 Mbit/s

maximum rates for signals of 10^3 s^{-1} , Figure 9.3 shows the result in diagrams. The wireless transmission of recorded waveforms in quasi real time practically requires data transmission rates of $>1 \text{ Gbit/s}$, which is not possible with existing systems.

One approach of solving this problem is locally implemented data storage, possibly data compression and optimised data transmission protocols (Wang et al. 2018). This can be useful if the average amount of data is limited (e.g. data acquisition is not continuously performed), but only during peak loads of a structure (e.g. using event-triggered systems). Therefore, intermediate storage only has to absorb the peak demand (e.g. in the case of short-term significant damage and the corresponding generation of signals for an active or passive inspection of the structure), but 100 Mbit/s may be sufficient.

Another approach is to reduce the amount of data locally (e.g. by extracting only relevant parameters for data transmission) during further evaluation, without using the actually recorded high-frequency signals. Figure 9.4 shows the possible scope of such parameter data sets for the corresponding number of channels, assuming that each channel generates a maximum of 1000 data sets per second. Under these assumptions, data sets of approximately 2 kB each can be transmitted wirelessly.

Typically, lower sampling rate sometimes creates issues with algorithms to analyse the data stream. Consider the algorithm singular spectrum analysis. First, this works solely on a single channel data available from monitored stations (Bhowmik et al. 2019a). Next, if the sampling is low, chances of aliasing can also prevail, with lower sample sizes. It becomes extremely difficult to analyse such a low

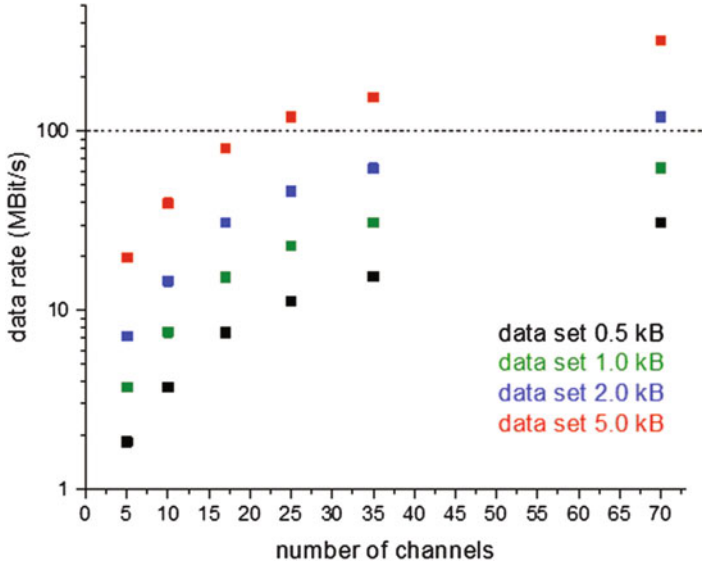


Fig. 9.4 Required data transfer rates for 1000 parameter sets per second and channel for different numbers of data acquisition channels and amount of data sets with the logarithmic scale of the y-axis. Technically possible: approximately 100 Mbit/s

number of samples in such cases. For AE signals, usually a greater bandwidth is approved—for easy analysis of the data, and therefore, this content is particularly helpful for such implementations. Depending on the system, the sampling rate varies between approximately 100 kHz and 5 MHz and the data transmission rate between approximately 40 kB/s and approximately 6 Mbit/s. The energy required for wireless signal transmission varies depending on the system and the operating mode (e.g. transmission or reception and active or inactive).

At this stage, there is inadequate evidence base around the topic and the above values are engineered to be application-specific—sometimes to an experiment—forming a lack of generality. This is due to paucity of extensive round robin experiments and also for this industry's reluctance around data sharing. Under such circumstances, these values are strongly related to:

- (a) the technology
- (b) the sampling rate
- (c) what is to be measured
- (d) the error allowed
- (e) the minimum size of event to be measured
- (f) the resolutions of the event changes to be measured
- (g) the definition and the extent and the structure of noise in the system
- (h) the operational conditions
- (i) the effect of extraneous variables

- (j) the measurement regime and
- (k) the data compression and signal fidelity.

A combination of so many makes it an extensive field which should be addressed - but before such values should be quoted with confidence (and confidence internals, to allow for uncertainties), the authors choose to resort to the previous format presented above.

9.4.3 Synchronization

In SHM applications, the data collected at different structure locations should usually be synchronised, especially when modal shapes are exploited for damage identification. The measured signals from sensing nodes with intrinsic local time differences can generate inaccuracies in the outcomes of the SHM process. The synchronization accuracy depends on the algorithm used to manage the data, the implemented communication layer, network topology, and specific application (e.g. due to the environmental conditions). Time synchronization errors may be caused by both clock offset and drift between sensor nodes. The first depends on the contemporaneous initialization of all the sensing nodes in a wireless sensor network (WSN), while the latter occurs due to the clock rate of the crystal oscillation, which may differ from design reference clocks.

Time synchronization is considered as an open challenge in scientific research (Abdulkarem et al. 2020). Several studies have addressed the effects of inaccurate synchronization on the monitoring process results (Abdaoui et al. 2017; Krishnamurthy et al. 2008; Nguyen et al. 2014). The effects of time synchronization on the ability to identify mode shapes through the well-known frequency domain decomposition (FDD) was evaluated by Krishnamurthy et al., which demonstrated that the error in the modal shapes due to inaccurate synchronization is dependent on both the time shift and the modal frequency.

A precise synchronization also enables the sensor nodes to transmit data in a scheduled time, preserving power and involving less collision and retransmission of the data. Hu et al. proposed an energy-balanced synchronization protocol for SHM applications (Hu et al. 2010).

However, the accurate time synchronization of the processed signal and synchronised sensing do not necessarily coincide. The precise sensing timing control based on synchronised clocks is challenging, especially when two or more tasks, including sensing, are simultaneously performed because it usually happens in smart systems. Accordingly, several solutions have been proposed involving both hardware and algorithms.

Huang et al. proposed a new design for the hardware cross-layer, achieving high-precision synchronization for single-hop transmission (Huang et al. 2015). Xiao et al. obtained a good performance for multi-hop communication (Xiao et al. 2017). Araujo et al. proposed a Zigbee-based solution directly involving the physical layer,

employing the synchronization clock pulses transmitted by the master device to all the end devices (Araujo et al. 2012). The global positioning system (GPS) has also been used with a considerable power consumption and a poor indoor performance. Sazonov et al. proposed a hierarchical architecture with beacon synchronization for local clusters of sensors using the GPS time reference (Sazonov et al. 2010).

The frequent implementation of time synchronization protocols or algorithms may mitigate synchronization errors. Two main families of synchronization protocols exist: (1) the sender–receiver protocol involves the synchronization of each sensing node with a reference node clock using bidirectional communication; and (2) the receiver–receiver synchronization employs broadband transmission from a reference node to a group of sensing devices. However, synchronization protocols typically require considerable power consumption. Recent studies (Abdaoui et al. 2017; Nguyen et al. 2014; Yan and Dyke 2010) proposed error-resilient algorithms aimed to reduce the influence of non-synchronous data on structural identification via software. This solution aims to reduce the power consumption by reducing the use of synchronization protocols.

The other algorithmic solutions presented in the literature involve resampling-based approaches (Nagayama and Spencer 2008) applied after collection without the need of strict timing control, which yielded an accuracy of approximately 30 μ s.

9.4.4 Power Management and Consumption

The longevity of WSNs is one of the main challenges for SHM applications using battery-powered sensing systems (Gao et al. 2018). Using a lithium-polymer (LiPo) battery (330 mA/h, 4.2 V), Dürager et al. (2013) concluded that a typical SHM system based on guided ultrasonic waves can operate for only 0.24 h in actuator mode and only 0.51 h when in sensing mode. For this reason, ambient energy is commonly used to self-power sensor networks. Moreover, within the aerospace industry, batteries may not be permitted in most structures; therefore, power must be managed through wireless methods or completely harvested, making this topic of utmost importance. However, the harvested source of power is typically not enough to completely supply wireless devices; hence, research studies in this topic have attempted to maximise the efficiency of WSNs from both the algorithmic and hardware viewpoints (Davidson and Mo 2014; Xu 2016).

Both dynamic power management (DPM) and dynamic voltage scaling (DVS) are suitable for optimizing the efficiency of WSNs. Figure 9.5 shows the DVS scaling effect on the power of a single processor, where the embedded system adjusts the supply voltage to place components into lower power states, which are idle at any given time by using various heuristics (Park et al. 2009).

In contrast to the DVS, the DPM selectively places idle components into lower power states, thereby decreasing the power consumption (Park et al. 2009). Figure 9.6 shows the relation between time and power of the DPM for a single device that has a shutdown and wake up delay in idle states, but drastically reduces the

Fig. 9.5 DVS scaling effect on the power of a single processor (Park et al. 2009)

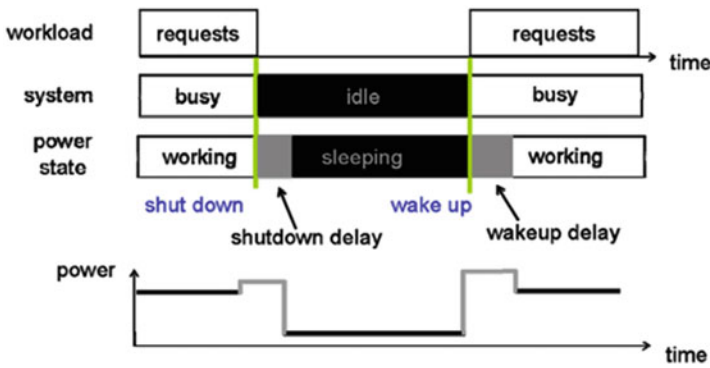
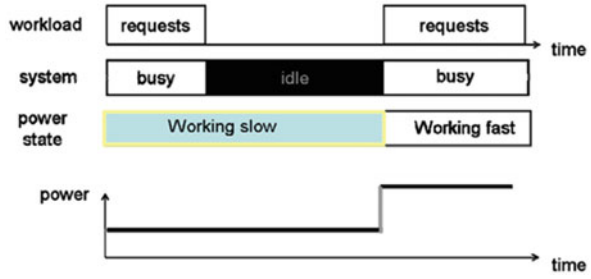


Fig. 9.6 Dynamic power management for a single device (Park et al. 2009)

Table 9.2 Drawn current and power consumption per mode (Farinholt et al. 2010)

Mode	Current (mA)	Power (mW)
Measurement	26	72.8
Data transmission	22	61.6
Sleep mode	0.075	0.21

power consumed in these states. The usage of the DPM compared to the DVS increases the power savings of the system by at least a factor of 10 (Park et al. 2009).

A method of interest in this context is the electromechanical impedance (EMI) technique, which uses a PZT transducer (bonded or embedded) that monitors the mechanical impedance of a structure by relating it directly to the electrical impedance sensed by the transducer (Neto et al. 2011). This theory is employed when constructing a wireless impedance device (WID). WID-3 (Farinholt et al. 2010), which was originally used for monitoring civil structures, is a low-powered sensor/transducer operating from 2.8 V. Its overall power consumption (Table 9.2) allows taking a single measurement per day for up to 5 years based on the power provided by two lithium AA batteries.

In an effort to minimise power consumption, the digital-to-analogue converter (DAC) for generating the excitation signal required for the EMI (Zhou et al. 2010) can be omitted by replacing the initial sinusoidal wave emission with a digital pulse

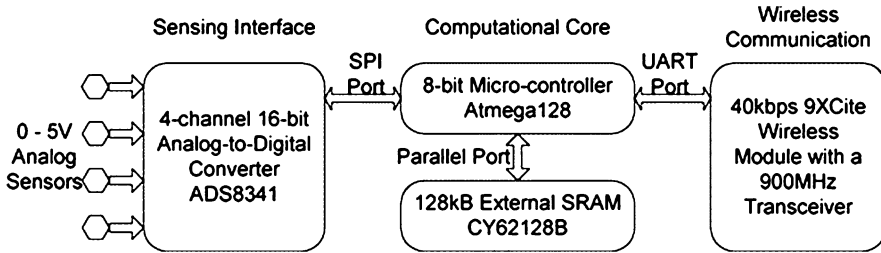


Fig. 9.7 Design of the wireless sensing unit (Wang et al. 2007)

train. A similarly wireless, but with integrated, multithreaded sensors design was suggested by Wang et al. (2007). Figure 9.7 depicts the schematic design of which. All components were programmed to 5 V, with both the active and standby currents per item detailed, giving a total active current for the unit of 77 mA and a resting current of 100 mA.

A connectivity-driven synchronization method was also proposed to reduce the power consumption of WSNs (Anastasi et al. 2009). Specific nodes were activated as “coordinators” and remained awake, while the other nodes were in the sleep mode. If two sleeping nodes cannot connect either directly or via one node, that node will become a coordinator, allowing for a minimization of the power consumption. This theory is common fold among WSNs. Liu et al. previously developed sensors that “wake up” at 3 mA power consumption, with full powering down at 0.5 A (Liu et al. 2005).

9.4.5 Future Developments in Energy Harvesting and Power Management

Several sources of energy may be exploited in aerospace structures (Fig. 9.8). However, the most promising are thermal gradients and vibration (Le et al. 2015). The research performed by the Cardiff School of Engineering found that average power levels may be produced by a thermoelectric generator between 5 and 30 mW. However, only up to 1 mW could be produced from a single vibrational energy harvester (Pearson et al. 2012). Moreover, using the quasi-static temperature difference in aerospace structures has shown great potential. Thermoelectric devices can be used to harvest energy in an aircraft, where hot and cold surfaces are available (Elefsiniotis et al. 2013).

Vibration may be used through electrostatic devices, such as capacitors, to harvest energy. The device capacitance varies with the vibration levels of the structure (Gilbert and Balouchi 2008). Research has shown that up to 40 μ W could be generated on a single device if the monitored structure vibrates at 2 Hz frequency (Naruse et al. 2009).

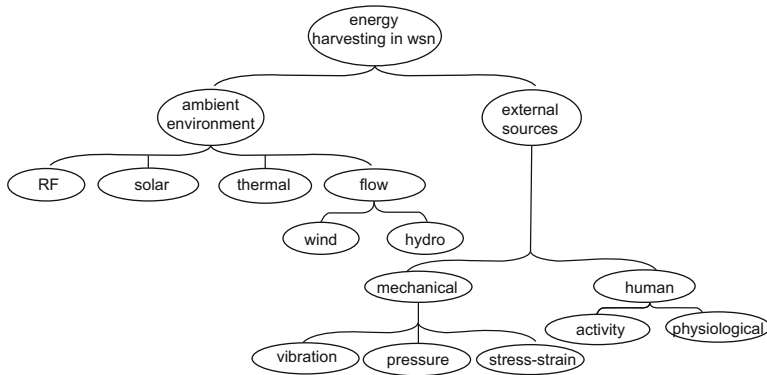


Fig. 9.8 Taxonomy of energy-harvesting sources in a WSN (Shaikh and Zeadally 2016)

Another method employed for energy harvesting involves the strain energy from the aircraft wing deformation. The experiments conducted by the University of Exeter found that power levels of up to 3.34 mW could be produced. An energy transfer efficiency of up to 80% was also possible. These experimental results give real promise to a fully developed system utilised in real-world applications (Chew et al. 2016).

However, a more extensive research into long-lasting self-sufficient energy harvesters is still needed. The biggest constraint that must be overcome for the development of aerospace energy harvesters is the creation of materials that can handle the extreme temperature fluctuations (Zhang and Yu 2011). For this aim, a more application-specific research with a focus on design is needed (Priya and Inman 2009). NASA is currently conducting studies on sensors that require low power for use on hypersonic aircraft where temperatures can reach in excess of 1000 °C. One method includes the use of chemical sensors, such as single-walled carbon nanotubes (SWNTs). SWNTs work due to their high responsiveness to chemicals, such as nitrogen dioxide, acetone, and ammonia. These sensors are one of the many research objects in the NASA roadmap that require the use of passive wireless in low-energy electronics (Wilson and Atkinson 2014). Promising results have been achieved in the mentioned study employing a system that involves wireless sensor nodes capable of making logic-based decisions, which are then transmitted to a central base station. However, powering such a system is troublesome.

The reliability of devices must also be improved. For example, many vibration-based devices operate at their natural frequency resonances and will eventually become unstable after long periods of use (Priya and Inman 2009).

Synchronised sensing. Measured signals from a smart sensor network with intrinsic local time differences need to be synchronised. If not appropriately addressed, time synchronization errors can cause inaccuracy in SHM applications, particularly in the mode shape phases.

9.5 Data Management

Flight data management systems are an essential part of mandatory flight reports, recording and analysis of flight data, improving operational safety, and aircraft maintenance. With the advent of modern computational techniques and the ability to process a massive amount of data in almost real time, several aircraft operators are already using advanced data processing routines to improve the rentability of their air fleet. The expectations for such systems are generally high because the processing of in-flight data can be used to perform a faster fault diagnosis, repair affected systems, reduce turn times by up to 50%, and reduce false alarms due to no-fault found equipment returned for repair. Generally, this is expected to lower the maintenance costs and provide higher on-time deliveries.

While much data from the regular flight avionics of the aircraft are already stored and processed, the integration of structural health monitoring systems faces several new challenges in providing reliable data storage, traceability, and liability. The specific types of SHM systems discussed in this work are considered onboard maintenance systems. Their primary function is to monitor the aircraft health (through a continuous monitoring of all acquired data) and quickly and accurately diagnose issues. The recorded data typically includes all aircraft avionics during flight and flight crew alerts, such as voice records and crew reports. The combined amount of data aims to diagnose the root cause fault behind symptoms, the correlation of the fault with crew reports, to quickly inform the maintenance crew of the required repair action.

9.5.1 Reliability

Digital sensors, processors, and data links have improved over time; hence, modern aircraft can produce huge amounts of data (cf. Sect. 9.1). These data are not completely processed in real time nor necessarily onboard an aircraft; thus, they need to be transferred outside the aircraft and stored for a certain amount of time. This is desired for any sort of offline analysis, but is also causing a cascade of reliability issues. First, the data transfer itself must be reliable enough to inhibit data corruption due to technical issues and the vulnerability of transmission protocols. Second, the data must be persistently stored to avoid data corruption over time and for potential liability issues.

In the future, the required level of security of airborne systems will require standard solutions as is also the case for ground-based security systems. The existing solutions assume that the personnel will not improperly handle keys or data. Some existing systems assume that opaque connections, by their specialised nature, prevent attacks or that system isolation is sufficient. These types of assumptions will not be acceptable to regulators or data users as data, and its use has become increasingly integrated into aircraft operations as in the case of an SHM system.

As a result, cryptographic systems will be required for all systems in the aircraft and for communication with the aircraft. These systems require a verified authentication method to enable host and client checks before data are sent. Several companies are already working toward an architecture that provides an appropriate level of security while improving data availability through hardware-based cryptography and isolation to enable fast data processing.

Onboard maintenance systems also include aircraft data loading hardware (wired or wireless) used to provide a secure connection between ground systems and aircraft avionics. Specifically, for critical flight tools, including navigation databases (charts and maps) and flight plans, this requires specifically certified hardware and software tools. Intentionally, the secured connection is used to download fault history database information from the aircraft's central maintenance computer.

9.5.2 *Liability Issues*

The current status of data usage in aerospace faces several emerging legal issues (Spreen 2019). New legal considerations with regard to aerospace as a technology are constantly emerging and changing society in the course of time. A topic of particular attention is the legal status and the effect of data resulting from the aircraft operation. Huge amounts of aircraft-related data are involved; thus, questions arise regarding data ownership, liability for errors or misuse, and how to control data distribution.

OEMs have developed systems for generating and collecting data concerning the maintenance, repair, and overhaul sector. OEMs have been said to abuse their privileged access to data to dominate the aftermarket by unjustifiable business from other businesses. This consideration raises potential antitrust issues. Other data-related issues include intellectual property rights and confidentiality laws. Business agreements involving aircraft operators are beginning to address, control, and use data and attempt to manage data access and their applications. The contractual limits of data use continue to evolve (Helland and Tabarrok 2012).

The security of aircraft-related data systems is not a legal issue in itself, but potential consequences of an insecure system open up numerous legal questions. The negative consequences for companies if data are lost or hacked could be serious. New EU laws allow fines of up to 4% of the worldwide turnover for operators of 'essential services' and 'digital service providers' if they are not able to adequately manage cyber-risk attacks. Aircraft manufacturers and operators have a clear legal liability in case of failure to take due account of the data system security. Digital systems permeate aircraft design and play a greater role in the actual control of aircraft in flight; thus, numerous questions of product liability arise. The two Boeing 737 MAX crashes in 2018 and 2019 suddenly brought the role of digital autopilots into the public consciousness and raised questions regarding the individual responsibility of the human pilot and the aircraft software. These issues are still the subject of lively discussions by regulators in courts and within the industry, which still has to be solved.

SHM systems intend to provide a decisional basis for grounding the airplane or for putting it back into service; therefore, similar legal issues are expected and must be addressed to provide a system that is not only technically feasible, but also ready for practice.

9.5.3 *Ground-Based Systems*

In addition to onboard management systems, the so-called ground-based tools are also used. These tools include loadable diagnostic information, report builders to help customise reports, and manage system updates based on the aircraft operators' preferences. In general, the same regulations regarding their technical reliability apply as for onboard systems; however, they do not suffer so much from other requirements. In particular, the system weight is not an issue; data transfer can be much higher and does not need to be specified for the harsh environments faced in-flight, but only the typical requirements for operating equipment on an airport.

9.6 Conclusions

From the viewpoint of an aircraft ready monitoring system, the data intensity provided by SHM systems still proves as a general challenge. Specifically, in the context of wireless sensing systems and their energy demand, technical solutions are already developed, but could benefit substantially from proper integration of modern data reduction strategies. The requirements for proper SHM integration completely depend on the desired monitoring application: the nature of potential structural damage; the operating environment; the consequences of failure to detect damage; the consequences of false positives; the frequency at which data is required; the regulatory environment; the economic case in terms of capital costs, operational costs, opportunity costs and many more. Therefore, as pointed out in Chaps. 2 and 4, the system operator does need to consider not solely the technical aspects, but also the complete framework required to safely operate a SHM system in an aerospace context.

References

- Abdaoui A, El Fouly TM, Ahmed MH (2017) Impact of time synchronization error on the mode-shape identification and damage detection/localization in WSNs for structural health monitoring. *J Netw Comput Appl* 83:181–189. <https://doi.org/10.1016/j.jnca.2017.01.004>
- Abdeljaber O, Avci O, Kiranyaz S et al (2017) Real-time vibration-based structural damage detection using one-dimensional convolutional neural networks. *J Sound Vib* 388:154–170. <https://doi.org/10.1016/j.jsv.2016.10.043>.

- Abdulkarem M, Samsudin K, Rokhani FZ et al (2020) Wireless sensor network for structural health monitoring: a contemporary review of technologies, challenges, and future direction. *Struct Health Monit* 19:693–735. <https://doi.org/10.1177/1475921719854528>.
- Alonso L, Barbarán J, Chen J et al (2018) Middleware and communication technologies for structural health monitoring of critical infrastructures: a survey. *Comput Stand Interfaces* 56:83–100. <https://doi.org/10.1016/j.csi.2017.09.007>.
- Anastasi G, Conti M, Di Francesco M et al (2009) Energy conservation in wireless sensor networks: a survey. *Ad Hoc Netw* 7:537–568. <https://doi.org/10.1016/j.adhoc.2008.06.003>.
- Apple Inc. (2017) An on-device deep neural network for face detection. <https://machinelearning.apple.com/research/face-detection>
- Araujo A, García-Palacios J, Blesa J et al (2012) Wireless measurement system for structural health monitoring with high time-synchronization accuracy. *IEEE Trans Instrum Meas* 61:801–810. <https://doi.org/10.1109/TIM.2011.2170889>.
- Arms SW, Galbreath JH, Newhard AT et al. (2004) Remotely reprogrammable sensors for structural health monitoring. Proceedings of the structural materials technology (SMT), September. NDE Publishing/NDT for Highways and Bridges, Buffalo, NY
- Avci O, Abdeljaber O, Kiranyaz S et al. (2018) Wireless and real-time structural damage detection: a novel decentralized method for wireless sensor networks. *J Sound Vib*. 424:158–172. <https://doi.org/10.1016/j.jsv.2018.03.008>
- Ayaz M, Ammad-Uddin M, Baig I et al (2018) Wireless sensor's civil applications, prototypes, and future integration possibilities: a review. *IEEE Sensors J* 18:4–30. <https://doi.org/10.1109/JSEN.2017.2766364>.
- Berrocal CG, Fernandez I, Rempling R (2020) Crack monitoring in reinforced concrete beams by distributed optical fiber sensors. *Struct Infrastruct Eng*:1–16. <https://doi.org/10.1080/15732479.2020.1731558>.
- Bhowmik B (2018) Online structural damage detection using first order eigen perturbation techniques (Doctoral dissertation)
- Bhowmik B, Krishnan M, Hazra B, Pakrashi V (2019a) Real-time unified single-and multi-channel structural damage detection using recursive singular spectrum analysis. *Struct Health Monit* 18 (2):563–589
- Bhowmik B, Tripura T, Hazra B et al (2019b) First order eigen perturbation techniques for real time damage detection of vibrating systems: theory and applications. *Appl Mech Rev* 71(6):060801
- Bhowmik B, Tripura T, Hazra B et al (2020a) Robust linear and nonlinear structural damage detection using recursive canonical correlation analysis. *Mech Syst Signal Process* 136:106499
- Bhowmik B, Tripura T, Hazra B et al (2020b) Real time structural modal identification using recursive canonical correlation analysis and application towards online structural damage detection. *J Sound Vib* 468:115101
- Bolandi H, Lajnef N, Jiao P et al (2019) A novel data reduction approach for structural health monitoring systems. *Sensors* 19:4823. <https://doi.org/10.3390/s19224823>.
- Candés EJ, Wakin MB (2008) An introduction to compressive sampling. *IEEE signal processing magazine*, 25(2):21–30
- Cao J, Liu X (2016) Enabling network-wide and event-triggered wakeup. Springer briefs in electrical and computer engineering. pp 13–35. https://doi.org/10.1007/978-3-319-29034-8_3
- Cavuto A, Martarelli M, Pandarese G et al (2015) Experimental investigation by laser ultrasonics for high speed train axle diagnostics. *Ultrasonics* 55:48–57. <https://doi.org/10.1016/j.ultras.2014.08.010>
- Chew ZJ, Ruan T, Zhu M (2016) Strain energy harvesting powered wireless sensor node for aircraft structural health monitoring. *Procedia Eng* 168:1717–1720. <https://doi.org/10.1016/j.proeng.2016.11.498>
- Daichi W, Tamayama M (2019) Wing load and angle of attack identification by integrating optical fiber sensing and neural network approach in wind tunnel test. *Applied Sciences* 9(7):461
- Davidson J, Mo C (2014) Recent advances in energy harvesting technologies for structural health monitoring applications. *Smart Mater Res* 2014:1–14. <https://doi.org/10.1155/2014/410316>

- Dong J, Lowenhar ED, Godinez V et al (2015) State-of-the-art wireless acoustic emission system for structural health monitoring. *Springer Proc Phys* 158:15–22. https://doi.org/10.1007/978-1-4939-1239-1_2
- Donoho DL (2006) Compressed sensing. *IEEE Trans Inform Theory* 52:1289–1306. <https://doi.org/10.1109/TIT.2006.871582>
- dos Santos FL (2015) The use of strain gauges in vibration-based damage detection. In: Marques, Bart Peeters, Jenny Lau, Wim Desmet, and Luiz Carlos Sandoval Goes (eds) *Journal of Physics: conference series*, vol. 628. IOP Publishing, p 012119
- Dürager C, Heinzelmann A, Riederer D (2013) A wireless sensor system for structural health monitoring with guided ultrasonic waves and piezoelectric transducers. *Struct Infrastruct Eng* 9:1177–1186. <https://doi.org/10.1080/15732479.2012.671833>
- Elefsiniotis A, Samson D, Becker T et al (2013) Investigation of the performance of thermoelectric energy harvesters under real flight conditions. *J Electron Mater* 42:2301–2305. <https://doi.org/10.1007/s11664-012-2411-0>.
- Farinholt KM, Miller N, Sifuentes W et al (2010) Energy harvesting and wireless energy transmission for embedded SHM sensor nodes. *Struct Health Monit* 9:269–280. <https://doi.org/10.1177/1475921710366647>.
- Farrar CR, Worden K, Todd MD et al (2007) Nonlinear system identification for damage detection (No. LA-14353-MS). Los Alamos NM, Los Alamos National Laboratory (LANL)
- Feeny BF (2002) On proper orthogonal co-ordinates as indicators of modal activity. *Journal of Sound and Vibration*, 255(5):805–817
- Feeny BF, Liang Y (2003) Interpreting proper orthogonal modes of randomly excited vibration systems. *Journal of Sound and Vibration* 265(5):953–966
- Figueroa F, Mercer CR (2002) Advancing sensor technology for aerospace propulsion. *Proceedings of the ASME international mechanical engineering congress and exposition*, pp 185–192
- Friswell MI, Inman DJ (1999) Sensor validation for smart structures. *J Intell Mater Syst Struct* 10:973–982. <https://doi.org/10.1106/GVD2-EGPN-C5B1-DPNX>
- Fugate ML, Sohn H, Farrar CR (2001) Vibration-based damage detection using statistical process control. *Mech Syst Signal Process* 15:707–721. <https://doi.org/10.1006/mssp.2000.1323>
- Gao Y, Spencer BF (2008) Structural health monitoring strategies for smart sensor networks.
- Gao Y, Spencer BF, Ruiz-Sandoval M (2006) Distributed computing strategy for structural health monitoring. *Struct Control Health Monit* 13:488–507. <https://doi.org/10.1002/stc.117>
- Gao S, Dai X, Hang Y et al (2018) Airborne wireless sensor networks for airplane monitoring system. *Wirel Commun Mob Comput* 2018:1–18. <https://doi.org/10.1155/2018/6025825>
- Gilbert JM, Balouchi F (2008) Comparison of energy harvesting systems for wireless sensor networks. *Int J Autom Comput* 5:334–347. <https://doi.org/10.1007/s11633-008-0334-2>
- Grosse CU, Ohtsu M (2008) Basics for research – applications in civil engineering. In: Grosse C, Ohtsu M (eds) *Acoustic emission testing*. Springer, Berlin, Heidelberg. <https://doi.org/10.1007/978-3-540-69972-9>.
- Grosse CU, Glaser SD, Krüger M (2010) Initial development of wireless acoustic emission sensor nodes for civil infrastructure state monitoring. *Smart Struct Syst* 6:197–209. <https://doi.org/10.12989/sss.2010.6.3.197>.
- Helland EA, Tabarrok A (2012) Product liability and moral hazard: evidence from general aviation. *J Law Econ* 55(3):593–630. <https://doi.org/10.1086/666363>
- Hu X, Wang B, Hu X (2010, November). A novel energy-balanced time synchronization protocol in wireless sensor networks for bridge structure health monitoring. In *2010 2nd International Workshop on Database Technology and Applications* (pp. 1–5). IEEE
- Huang Q, Tang B, Deng L (2015) Development of high synchronous acquisition accuracy wireless sensor network for machine vibration monitoring. *Measurement* 66:35–44. <https://doi.org/10.1016/j.measurement.2015.01.021>
- Jindal A, Liu M (2012) Networked computing in wireless sensor networks for structural health monitoring. *IEEE/ACM Trans Networking* 20:1203–1216. <https://doi.org/10.1109/TNET.2011.2175450>.

- Jothibasu S, Du Y, Anandan S et al. (2018) Strain monitoring using distributed fiber optic sensors embedded in carbon fiber composites. In: *Sensors and smart structures technologies for civil, mechanical, and aerospace systems*, vol. 10598. International Society for Optics and Photonics
- Li C, Chen W, Liu G, Yan R, Xu H, Qi Y (2015) A noncontact FMCW radar sensor for displacement measurement in structural health monitoring. *Sensors*, 15(4):7412–7433
- Krishnamurthy V, Fowler K, Sazonov E (2008) The effect of time synchronization of wireless sensors on the modal analysis of structures. *Smart Mater Struct* 17. <https://doi.org/10.1088/0964-1726/17/5/055018>
- Krishnan M, Bhowmik B, Hazra B et al (2018) Real time damage detection using recursive principal components and time varying autoregressive modeling. *Mech Syst Signal Process* 101:549–574. <https://doi.org/10.1016/j.ymssp.2017.08.037>
- Krishnaraj V, Prabukarthi A, Ramanathan A et al (2012) Optimization of machining parameters at high speed drilling of carbon fiber reinforced plastic (CFRP) laminates. *Compos Part B Eng* 43:1791–1799. <https://doi.org/10.1016/j.compositesb.2012.01.007>
- Krohn N, Stoessel R, Busse G (2002) Acoustic non-linearity for defect selective imaging. *Ultrasonics* 40(1-8):633–637. [https://doi.org/10.1016/s0041-624x\(02\)00188-9](https://doi.org/10.1016/s0041-624x(02)00188-9)
- Le MQ, Capsal JF, Lallart M et al (2015) Review on energy harvesting for structural health monitoring in aeronautical applications. *Prog Aerosp Sci* 79:147–157. <https://doi.org/10.1016/j.paerosci.2015.10.001>
- Lenaerts V, Kerschen G, Golinval JC (2001) Proper orthogonal decomposition for model updating of non-linear mechanical systems. *Mech Syst Signal Process* 15:31–43. <https://doi.org/10.1006/mssp.2000.1350>
- Li M, Meng G, Li H et al (2018) Online structural health monitoring of rotating machinery via ultrasonic guided waves. *Shock Vib* 2018:1–12. <https://doi.org/10.1155/2018/8142371>
- Liu L, Yuan FG, Zhang F (2005) Development of wireless smart sensor for structural health monitoring *Smart structures and materials 2005: sensors and smart structures technologies for civil, mechanical, and aerospace systems*. 5765:176.
- Liu J, Demirkiran I, Yang T et al. (2008) Communication schemes for aerospace wireless sensors. *AIAA IEEE digit avionics Syst Conf proc*.
- Lizotte A, Lokos W (2005) Deflection-based aircraft structural loads estimation with comparison to flight. In: *46th AIAA/ASME/ASCE/AHS/ASC structures, structural dynamics and materials conference*, p 2016
- Logan S, Sankareswaran UM (2015) Performance analysis of wireless sensors for aircraft control. *Journal of Vibration and Control* 21(2):211–216
- Long J, Büyüköztürk O (2017) Decentralised one-class kernel classification-based damage detection and localisation. *Struct Control Health Monit* 24:1–22. <https://doi.org/10.1002/stc.1930>
- Lynch JP (2004) Overview of wireless sensors for real-time health monitoring of civil structures. In: *Proceedings of the 4th international workshop on structural control*, pp 189–194
- Marr B (2017) Forbes: the amazing ways google uses deep learning AI. [Press release]. <https://www.forbes.com/sites/bernardmarr/2017/08/08/the-amazing-ways-how-google-uses-deep-learning-ai/?sh=6ae9e2753204>
- Marsh G (2011) Bombardier throws down the gauntlet with CSeries airliner. *Reinf Plast* 55:22–26. [https://doi.org/10.1016/S0034-3617\(11\)70181-3](https://doi.org/10.1016/S0034-3617(11)70181-3)
- Martin RR, Stroud IA, Marshall AD (1997) Data reduction for reverse engineering. RECCAD, Deliverable Document 1 COPERNICUS project, No 1068:111
- Martinez-Luengo M, Kolios A, Wang L (2016) Structural health monitoring of offshore wind turbines: a review through the statistical pattern recognition paradigm. *Renew Sust Energ Rev* 64:91–105. <https://doi.org/10.1016/j.rser.2016.05.085>
- Masmoudi S, El Mahi A, Turki S et al (2013) Structural health monitoring by acoustic emission of smart composite laminates embedded with piezoelectric sensor. In: *Lecture notes in mechanical engineering*. Springer, Berlin, Heidelberg, pp 307–314. https://doi.org/10.1007/978-3-642-37143-1_37.

- Mechitov K, Kim W, Agha G, Nagayama T (2004) June. High-frequency distributed sensing for structure monitoring. In Proc. First Intl. Workshop on Networked Sensing Systems (INSS 04) (pp. 101–105)
- Michaels JE (2008) Ultrasonic structural health monitoring: strategies, issues, and progress. In: Smart sensor phenomena, technology, networks, and systems, vol. 6933, p 69330Z. International Society for Optics and Photonics
- Montalvão D, Maia NMM, Ribeiro AMR (2006) A review of vibration-based structural health monitoring with special emphasis on composite materials. *Shock Vib Digest* 38(4):295–324
- Moyo P, Brownjohn JMW, Suresh R et al (2005) Development of fiber Bragg grating sensors for monitoring civil infrastructure. *Eng Struct* 27:1828–1834. <https://doi.org/10.1016/j.engstruct.2005.04.023>.
- Mucchielli P, Bhowmik B, Hazra B et al (2020) Higher-order stabilised perturbation for recursive eigen-decomposition estimation. *ASME J Vib Acoust* 142. <https://doi.org/10.1115/1.4047302>
- Nagayama T, Spencer BF (2008) Structural health monitoring using smart sensors.
- Nagayama T, Rice JA, Spencer BF Jr (2006) Efficacy of Intel's Imote2 wireless sensor platform for structural health monitoring applications. In: Proceedings of the Asia-Pacific workshop on structural HealthMonitoring. Yokohama, Japan
- Nagayama T, Spencer BF, Rice JA (2009) Autonomous decentralized structural health monitoring using smart sensors. *Struct Control Health Monit* 16. <https://doi.org/10.1002/stc.352>
- Naruse Y, Matsubara N, Mabuchi K et al (2009) Electrostatic micro power generation from low-frequency vibration such as human motion. *J Micromech Microeng* 19:94002. <https://doi.org/10.1088/0960-1317/19/9/094002>
- Neto FRM, Steffen Jr, V, Rade DA, Gallo C A, Palomino LV (2011) A low-cost electromechanical impedance-based SHM architecture for multiplexed piezoceramic actuators. *Structural Health Monitoring* 10(4):391–402
- Nguyen T, Chan THT, Thambiratnam DP (2014) Effects of wireless sensor network uncertainties on output-only modal analysis employing merged data of multiple tests. *Adv Struct Eng* 17:319–329. <https://doi.org/10.1260/1369-4332.17.3.319>
- Noel AB, Abdaoui A, Elfouly T et al (2017) Structural health monitoring using wireless sensor networks: a comprehensive survey. *IEEE Commun Surv Tutor* 19:1403–1423. <https://doi.org/10.1109/COMST.2017.2691551>
- Nor NM (2018) Structural health monitoring through acoustic emission. In: Eco-efficient repair and rehabilitation of concrete infrastructures. Woodhead Publishing, pp 123–146.
- O'Donnell D, Wright R, O'Byrne M et al. (2017) Modelling and testing of a historic steel suspension footbridge in Ireland. In: Proceedings of the institution of civil engineers-bridge engineering (Vol. 170, No. 2, pp 116–132). Thomas Telford Ltd
- Pakrashi V, Kelly J, Harkin J et al (2013) Hurst exponent footprints from activities on a large structural system. *Phys A* 392:1803–1817. <https://doi.org/10.1016/j.physa.2012.11.004>.
- Pakzad SN, Fenves GL, Kim S et al (2008) Design and implementation of scalable WirelessSensor network for structural monitoring. *J Infrastruct Syst* 14:89–101. [https://doi.org/10.1061/\(ASCE\)1076-0342\(2008\)14:1\(89\)](https://doi.org/10.1061/(ASCE)1076-0342(2008)14:1(89)).
- Park G, Farinholt KM, Farrar CR et al (2009) Powering wireless SHM sensor nodes through energy harvesting. *Energy Harvesting Technol*:493–506
- Park C, Tang J, Yu D (2010) Aggressive data reduction for damage detection in structural health monitoring. *Struct Health Monit* 9:59–74. <https://doi.org/10.1177/1475921709341017>
- Pearson MR, Eaton MJ, Pullin R et al (2012) Energy harvesting for aerospace structural health monitoring systems. *J Phys Conf Ser* 382. <https://doi.org/10.1088/1742-6596/382/1/012025>
- Priya S, Inman DJ (2009) Energy harvesting technologies. *Energy Harvest Technol* 2009:1–517
- Quqa S, Landi L, Diotallevi PP (2020) Instantaneous modal identification under varying structural characteristics: a decentralized algorithm. *Mech Syst Signal Process* 142:106750
- Rioul O, Vetterli M (1991) Wavelets and signal processing. *IEEE Signal Process Mag* 8:14–38. <https://doi.org/10.1109/79.91217>

- Santoso S, Powers EJ, Grady WM (1997) Power quality disturbance data compression using wavelet transform methods. *IEEE Trans Power Delivery* 12:1250–1257. <https://doi.org/10.1109/61.637001>
- Sause MGR (2016) Acoustic emission. *Mater Sci* 2016:131–359. https://doi.org/10.1007/978-3-319-30954-5_4.
- Sazonov E, Krishnamurthy V, Schilling R (2010) Wireless intelligent sensor and actuator network – a scalable platform for time-synchronous applications of structural health monitoring. *Struct Health Monit* 9:465–476. <https://doi.org/10.1177/1475921710370003>.
- Schell J, Johansmann M, Schüssler M et al (2006) Three dimensional vibration testing in automotive applications utilizing a new non-contact scanning method. *SAE Trans*:1025–1032
- Scruby CB, Drain LE (1990) *Laser ultrasonics techniques and applications*. CRC Press, Boca Raton
- Shaikh FK, Zeadally S (2016) Energy harvesting in wireless sensor networks: a comprehensive review. *Renew Sust Energ Rev* 55:1041–1054. <https://doi.org/10.1016/j.rser.2015.11.010>
- Smithard J, Norman P, van der Velden S et al (2017) The Acousto ultrasonic structural health monitoring array module (AUSAM+) for damage detection in structures. *Procedia Eng* 188:448–455. <https://doi.org/10.1016/j.proeng.2017.04.507>.
- Spren W (2019) *The aerospace business*. Routledge. <https://doi.org/10.4324/9780429299452>.
- Strang G, Nguyen T (1996) *Wavelets and filter banks*.
- Świąch SIAM, Świąch Ł (2020) Calibration of a load measurement system for an unmanned aircraft composite wing based on fibre Bragg gratings and electrical strain gauges. *Aerospace* 7:27. <https://doi.org/10.3390/aerospace7030027>
- Tan ACC (2016) How can acoustic emission signals be used in condition monitoring and diagnosis of diesel engine condition? *Adv Automobile Eng S*, 1. <https://doi.org/10.4172/2167-7670.S1-002>
- Trang HTH, Dung LT, Hwang SO (2018) Connectivity analysis of underground sensors in wireless underground sensor networks. *Ad Hoc Netw* 71:104–116. <https://doi.org/10.1016/j.adhoc.2018.01.002>
- Walsh J, Bashir I, Garrett JK et al (2017) Monitoring the condition of marine renewable energy devices through underwater acoustic emissions: case study of a wave energy converter in Falmouth Bay, UK. *Renew Energy* 102:205–213. <https://doi.org/10.1016/j.renene.2016.10.049>.
- Wang T, Tang Y (2017) Dynamic displacement monitoring of flexural structures with distributed long-gage macro-strain sensors. *Adv Mech Eng* 9. <https://doi.org/10.1177/1687814017698885>.
- Wang Y, Lynch JP, Law KH (2007) A wireless structural health monitoring system with multithreaded sensing devices: design and validation. *Struct Infrastruct Eng* 3:103–120. <https://doi.org/10.1080/15732470600590820>
- Wang Z, Wang L, Liu S et al (2018) Encoding-decoding-Based control and filtering of networked systems: insights, developments and opportunities. *IEEE/CAA J Autom Sinica* 5:3–18. <https://doi.org/10.1109/JAS.2017.7510727>
- Whelan MJ, Janoyan KD (2009) Design of a robust, high-rate wireless sensor network for static and dynamic structural monitoring. *J Intel Mat Syst Str* 20:849–863. <https://doi.org/10.1177/1045389X08098768>
- Wilson WC, Atkinson GM (2014) Passive wireless sensor applications for NASA’s extreme aeronautical environments. *IEEE Sensors J* 14:3745–3753. <https://doi.org/10.1109/JSEN.2014.2322959>
- Worden K, Manson G (2000) Damage identification using multivariate statistics: kernel discriminant analysis. *Inverse Probl Eng* 8:25–46. <https://doi.org/10.1080/174159700088027717>
- Wu Y, Liu W, Li K (2017) A novel wireless acoustic emission sensor system for distributed wooden structural health monitoring. *Int J Innov Comput Inf Control* 13:1289–1306
- Xiao X, Tang B, Deng L (2017) High accuracy synchronous acquisition algorithm of multi-hop sensor networks for machine vibration monitoring. *Measurement* 102:10–19. <https://doi.org/10.1016/j.measurement.2017.01.036>
- Xu TB (2016) Energy harvesting using piezoelectric materials in aerospace structures. *Struct Health Monit (SHM) Aerosp Struct* 2016:175–212

- Xu N, Rangwala S, Chintalapudi K et al (2004) A wireless sensor network for structural monitoring. In: Proceedings of the ACM conference on embedded networked sensor systems, Baltimore, MD, pp 13–24
- Yan G, Dyke SJ (2010) Structural damage detection robust against time synchronization errors. *Smart Mater Struct* 19. <https://doi.org/10.1088/0964-1726/19/6/065001>
- Yang Y, Nagarajaiah S (2016) Dynamic imaging: real-time detection of local structural damage with blind separation of low-rank background and sparse innovation. *J Struct Eng* 142:04015144. [https://doi.org/10.1061/\(ASCE\)ST.1943-541X.0001334](https://doi.org/10.1061/(ASCE)ST.1943-541X.0001334).
- Yedavalli RK, Belapurkar RK (2011) Application of wireless sensor networks to aircraft control and health management systems. *J Control Theory Appl* 9:28–33. <https://doi.org/10.1007/s11768-011-0242-9>
- Yoon DJ, Weiss WJ, Shah SP (2000) Assessing damage in corroded reinforced concrete using acoustic emission. *J Eng Mech* 126:273–283. [https://doi.org/10.1061/\(ASCE\)0733-9399\(2000\)126:3\(273\)](https://doi.org/10.1061/(ASCE)0733-9399(2000)126:3(273))
- Zahmati AS, Fernando X, Kojori H (2011) Emerging wireless applications in aerospace: benefits, challenges, and existing methods. In: 4th Annual Caneus Fly-by-wireless workshop. FBW, vol 11, pp 87–90
- Zang C, Imregun M (2001) Structural damage detection using artificial neural networks and measured FRF data reduced via principal component projection. *J Sound Vib* 242:813–827. <https://doi.org/10.1006/jsvi.2000.3390>
- Zhang S, Yu F (2011) Piezoelectric materials for high temperature sensors. *J Am Ceram Soc* 94:3153–3170. <https://doi.org/10.1111/j.1551-2916.2011.04792.x>
- Zhou D, Ha DS, Inman DJ (2010) Ultra low-power active wireless sensor for structural health monitoring. *Smart Struct Syst* 6:675–687. https://doi.org/10.12989/sss.2010.6.5_6.675.
- Zhu L, Fu Y, Chow R et al (2018) Development of a high-sensitivity wireless accelerometer for structural health monitoring. *Sensors* 18:262. <https://doi.org/10.3390/s18010262>.

Open Access This chapter is distributed under the terms of the Creative Commons Attribution 4.0 International License (<http://creativecommons.org/licenses/by/4.0/>), which permits use, duplication, adaptation, distribution and reproduction in any medium or format, as long as you give appropriate credit to the original author(s) and the source, a link is provided to the Creative Commons license and any changes made are indicated.

The images or other third party material in this chapter are included in the work's Creative Commons license, unless indicated otherwise in the credit line; if such material is not included in the work's Creative Commons license and the respective action is not permitted by statutory regulation, users will need to obtain permission from the license holder to duplicate, adapt or reproduce the material.



Chapter 10

Conclusions



**Elena Jasiūnienė, Markus G. R. Sause, Vykintas Samaitis,
Dimitrios G. Aggelis, Maria Pina Limongelli, and Steve Vanlanduit**

Abstract The state of the art of structural health monitoring damage detection systems reviewed in this book shows that it is a promising area of technologies. SHM damage detection systems in civil aviation are still mostly limited to lab applications because there are still issues, which need to be solved for such systems to be integrated in an aircraft structure. Therefore, further research is needed to solve the current drawbacks/limitations of the existing SHM approaches such that this technology can be used in aircrafts.

Despite the current limitations, SHM application for damage detection in aircrafts would make the flying safer and the structure lifetime longer and reduce the maintenance time and costs considering that the maintenance could be performed not at the predetermined intervals, but upon the need based on the condition that would be determined by the SHM systems used. We conclude some of the important differences and the common challenges to the methods reviewed in this book and provide an outlook on the next steps to a successful implementation.

E. Jasiūnienė (✉)

Prof. K. Baršauskas Ultrasound Research Institute, Kaunas University of Technology,
Kaunas, Lithuania
e-mail: elena.jasiuniene@ktu.lt

M. G. R. Sause

Institute of Materials Resource Management, University of Augsburg, Augsburg, Germany

V. Samaitis

Kaunas University of Technology, Kaunas, Lithuania

D. G. Aggelis

Vrije Universiteit Brussel, Brussels, Belgium

M. P. Limongelli

Politecnico di Milano, Milano, Italy

S. Vanlanduit

University of Antwerp, Antwerp, Belgium

© The Author(s) 2021

M. G. R. Sause, E. Jasiūnienė (eds.), *Structural Health Monitoring Damage Detection Systems for Aerospace*, Springer Aerospace Technology,
https://doi.org/10.1007/978-3-030-72192-3_10

273

10.1 Overview of the SHM Methods for Aerospace Integration

As outlined in detail throughout Chaps. 5, 6, 7, and 8, various SHM methods are readily used in aerospace research and applications. Recently, an SAE industrial committee presented an International Aerospace Recommended Practices document SAE ARP 6461 “Guidelines for Implementation of Structural Health Monitoring on Fixed Wing Aircraft”. With its focus on the integration of SHM methods into aircraft maintenance procedures, generic requirements and advice on validation, verification and airworthiness, it does not have a strong focus on the actual methods as outlined in the previous chapters. Thus, in the following, a quick overview regarding some selected technological aspects with high relevance for practical applications is provided. It is necessary to evaluate/compare, even quantify the capabilities of different SHM methods. Unfortunately, no strict guidelines are yet available for quantitatively assessing and comparing the performance of SHM systems. Table 10.1 lists several technological aspects for the comparison of four primary SHM approaches discussed in this book, namely monitoring using ultrasonic guided waves, vibration, acoustic emission, and strain. Nevertheless, there are certainly more SHM technologies proposed and demonstrated in operational aircraft, such as Comparative Vacuum Monitoring (CVM) for crack detection or leakage monitoring by percolation sensors, but the scope of this chapter is limited to the primary approaches presented throughout Chaps. 5 to 8.

System reliability is understood as the combination of reliability under normal operation mode and susceptibility to external factors of influence, such as arising from climate changes, as well as operation of nearby technical systems. As established in non-destructive testing approaches, reliability can be assessed in terms of the probability of detection (POD), but this is not directly transferable in the same fashion to the SHM methods discussed herein.

Integration readiness considers all aspects of the measurement chain to properly integrate the system inside an aircraft, as well as the ease of sensor and wire integration in the context of production technologies.

As *maturity*, the overall technological readiness of the method, including the factors of traceability to physical principles and the capability and repeatability of the involved algorithms to retrieve information from the sensing system is considered.

Under *power consumption*, the methods with respect to the electrical power required to operate the system for SHM are compared.

In the category *form factor*, the SHM methods with respect to their size and weight, including the aspects of bulk attachments vs. sensor solutions fully integrated into the aircraft components is compared.

Finally, under *costs*, the SHM methods relative to each other in terms of investment and operation costs of the required measurement chain are compared. The latter may solely provide a first estimate because the overall number of sensors required to

Table 10.1 Overview of the selected technological aspects for SHM integration

SHM method	System reliability	Integration readiness	Maturity	Power consumption	Form factor	Costs
Ultrasonic guided wave monitoring	Limited (For screening applications can be high, for small defect detection low)	Good	Medium	Medium, active pulsing required	Medium	Medium cost, depends on complexity of the system (sensors, instrumentation and applications)
Vibration-based monitoring	Sensitive to environmental conditions and noise in sensors; both can be reduced through bespoke processing, but not eliminated	Good	Good	Medium, sensors can be wired or wireless	Reasonable, but depends on the sensors; MEMS can be very small; piezoelectric have higher dimensions	Depends on the sensors (MEMS can be low cost)
Acoustic emission monitoring	Good for some aspects like detection and localization, but limited for characterization	Medium	Medium	Low	Good	Low
Strain monitoring	Good in case the sensors are protected (coated)	Very good for optical fiber sensors, good for strain gauges	Good (optical fiber sensors) to very good (strain gauges)	Low	Very good, compact and light-weight	Low

cover a certain area strictly depends on the required probability of detection, type of monitoring (e.g., type of defect), and material.

The capabilities of each of the four SHM methods are summarized in Table 10.1 to provide more details.

10.1.1 Ultrasonic Guided Wave Based Monitoring

Ultrasonic guided waves (GW) could serve as a promising tool for the assessment of aerospace components. Guided waves are sensitive to the change in the mechanical properties of the material and possess relatively minor attenuation; thus, different defects can be detected from the single transducer position, which makes them essentially attractive for structural health monitoring applications. However, the development progress of guided wave methods is still limited because many external factors must be suppressed to obtain a response that is not influenced by temperature, loads, geometrical variations, structural boundaries, or coupling of the sensor. Guided waves have emerged as a powerful tool due to their ability to screen large areas and overcome the existing limitations of point-wise bulk wave inspections. GW possess multiple modes and through-thickness distributions, meaning that the defects of different size, type, depth, and orientation can be interrogated. On the contrary, this technique suffers from its own complexity. Many methods are being developed by various research groups to isolate specific modes of interest or extract and visualize weak responses of flaws. The reflections from the defects are usually concealed within the multimodal and quite noisy signals; hence, such developments usually include approaches to minimize the number of modes propagating in the structure and specific processing, such as filtering, summation, and various signal transformations. The scaling of existing methods from the laboratory to in-situ is still quite limited due to the complexity of the signal analysis, which itself becomes even more complicated with multi-layered and anisotropic structures in addition to stiffeners and bolt holes. With the advent of machine learning methods and increasing computational capabilities, GW inspections are expected to overcome some of their existing limitations and used to a larger extent with more confidence.

10.1.2 Vibration-Based Monitoring

Vibration-based monitoring allows the identification of damage due to changes of structural stiffness, mass or energy dissipation capacity. Damages that usually affect aeronautical structures usually cause stiffness variation. Modal frequency variations are features sensitive to this type of damage; thus, their variation can provide useful information for its detection. The advantage of this method is that it enables damage detection at a global level using sensors not necessarily located in the proximity of the damaged location. For this reason, vibration-based damage detection does not

require prior knowledge of the so-called ‘hot spot,’ which is a location where damage is likely to develop. Sensors must be installed at locations that enable the most accurate, precise, and complete identification of modal parameters, discarding any consideration about the location where damage will happen. The only exception is damages at locations where one or more modes have a node and are not affected by that damage. Sensor location must be chosen to account for this. A further issue to consider when using modal frequencies as damage features is their sensitivity to the variations of environmental parameters, such as temperature or humidity. This means that changes of modal frequencies may occur due to damage or variation of environmental sources. Therefore, these effects must be accounted for or eliminated to obtain a reliable identification of damage. Alternative or further damage features may be defined in terms of other modal parameters, which are less sensitive to environmental sources and/or more sensitive to the damage location, to address this issue and enrich the description of damage (e.g., through information about its location). Modal shapes are extensively used for this aim. One drawback of vibration-based methods for damage identification is their scarce sensitivity to small damages. This is the reverse side of the advantage related to the global nature of these features: on one side, this enables the identification of damage without any prior knowledge about its location; on the other side, it limits their sensitivity to small localized changes. This issue is worsened by modelling and measurement errors, which increase the uncertainty in the identified modal parameters and the reliability of damage identification in real-world applications.

10.1.3 Acoustic Emission Monitoring

The condition monitoring of aeronautic components is extremely important for flight safety. Due to its sensitivity, AE allows the detection of crack nucleation and propagation earlier than other NDT techniques. The main advantages of AE are the aforementioned sensitivity, ability to localize active sources even without visual contact, inspection of a large area with limited sensors, and the possibility for fracture mode evaluation, which is very useful, especially in composites. It is applied without influencing the object under monitoring while wireless sensor solutions are gaining ground. One of the disadvantages of AE is related to its sensitivity because it makes it prone to noise, either environmental or anyway unrelated to structural health monitoring. This may not be uncommon in real flight conditions and require specialized filtering techniques and sophisticated pattern recognition approaches that are helpful for classification, while compressing data could be an extra burden. Another disadvantage is the influence from experimental conditions like sample geometry, sensor separation distance, and sensitivity. While laboratory studies have greatly advanced in interpretation and accuracy, this is not reflected in in-situ studies due to the aforementioned limitations. Issues that are relatively reliable and mature are detection and localization. An exact characterization (size, orientation, mode of defect) can be achieved mostly in laboratory conditions, while this would facilitate

decision on the maintenance action and, possibly, prediction of the remaining life in reality. Nevertheless, the currently faced lack of standardization does not allow engineers and scientists to share more robust conclusions.

10.1.4 Strain-Based Monitoring

Both strain gauges and optical fiber sensors can be used to measure the local strain of aircraft components and systems. Strain gauges are extensively used during the flight testing of new aircraft types to measure loads during a flight operation. In addition to the low frequency strains, strain sensors (strain gauges and optical fiber sensors) can also be used to measure the dynamic vibration response of components. As such, vibration-based monitoring techniques, as described in Sect. 10.1.2, can be used in combination with strain sensors. Moreover, optical fiber sensors like fiber Bragg gratings also allow measurements at very high frequencies of up to several MHz. Therefore, these strain sensors can be used for acoustic emission monitoring (Sect. 10.1.3).

Optical fiber sensors are lightweight and compact (diameter: typically 125 μm). They are easy to integrate in composite materials and metals (by using grooves in which the fibers are laser cladded). One single fiber in a Fibre Bragg Grating can easily contain several tens of sensors. By using adapted interrogation principles, it is even possible to continuously realize distributed sensor systems.

10.2 Defect Detectability

Based on the review of different defect types in Chap. 3, Table 10.2 lists the primary categories of defects encountered in aircrafts distinguished by the top-level categories of metals, composites, coatings, and joints. In this context, the different methods in their capabilities of detecting the defect type are ranked. Focus is given to these defects, which are not due to manufacturing deficiencies (e.g., bad curing, foreign inclusions, etc.), but on those defects that may occur inside a flight-ready qualified aircraft as a result from detrimental operation conditions (e.g., overloading, weather conditions, accidents, etc.) or even as a result from a system malfunction under regular operation conditions.

We use a scale ranging from good to medium to poor to rank the methods in case they are able to detect the defect.

Table 10.2 Comparison of the defect sensitivities of different SHM methods

Defects	Ultrasonic guided waves monitoring	Vibration-based monitoring	Acoustic emission monitoring	Strain-based monitoring
<i>Metals</i>				
Fatigue	Poor	Good	Good	Good
Corrosion	Good	Good	Medium	Poor
Wear	Medium	Poor		
Creep deformation	Poor	Poor	Poor	Good
(Micro-)cracks	Poor	Poor	Good	Good
<i>Composites</i>				
Disbonds (Sandwiches)	Good	Good	Medium	Good
Core crushing/buckling (sandwiches)	Medium	Medium	Medium	Good
Delamination	Good	Good	Good	Good
Matrix cracking	Medium	Medium	Good	Medium
Fibre breakage	Poor	Medium	Good	Good
Moisture absorption	Medium	Poor	Poor	Medium
Temperature induced degradation	Medium	Poor	Poor	Good
Fatigue cracks	Poor	Good	Good	Good
<i>Coatings</i>				
Corrosion	Good	Poor	Medium	Poor
Wear	Good	Poor	Medium	Medium
(Micro-)cracks	Medium	Poor	Medium	Medium
Delamination	Good	Poor	Medium	Medium
<i>Joints</i>				
Wear	Poor	Poor	Medium	Good
Disbond	Good	Medium	Poor	Good
Voids	Medium	Medium	Poor	Medium
(Micro-)cracks	Poor	Medium	Good	Medium
Kissing bond	Poor	Poor	Poor	Medium
Moisture absorption	Poor	Poor	Poor	Poor
Temperature-induced degradation	Poor	Poor	Poor	Poor

10.3 Advantages and Disadvantages of SHM Techniques

In this section, we focus on the distinct advantages and disadvantages that originate from the principles of different methods. We attempt to objectively discuss the strength and the weakness of each SHM approach because this provides some further background to the suitability of a method for a given task. Furthermore, Table 10.3 includes some of the current challenges associated with the use of each method.

Table 10.3 SHM techniques: advantages and disadvantages

SHM method	Advantages	Disadvantages
Ultrasonic guided wave monitoring	Directly sensitive to the change of the structural properties of the material; can be used to screen large areas with a small amount of sensors; sensitive to both surface and internal defects of various kinds; can be used to inspect almost any kind of large components, including metals and composites; can be used to inspect inaccessible parts located under the ground or coatings; and various parameters of the flaws, such as size, position, and depth can be extracted	Requires sophisticated methods to avoid generation of multiple modes; interpretation of the structural responses is usually nontrivial and requires deep understanding about the structure and additional modelling; complicated verification, calibration of the inspection techniques, and scaling from the laboratory to the in-situ environment; and many surrounding factors influence the result of structural response
Vibration-based monitoring	Provides global damage features that do not require prior knowledge and accessibility of the damage location. They can detect damage with a very small number (ideally just one) of sensors. They can be used for any material and enable detection, localization, and quantification of damage	Vibration-based damage features are affected by environmental sources that can hide erroneous damage identification. Modal frequencies are global quantities, scarcely affected by local damages. The noise level in available sensing systems usually decreases with the cost; hence, low-cost sensors have still high noise levels that furtherly reduce the sensitivity to small damages. POD concept was not used for vibration-based tests. Recent studies have investigated the extension of the POD concept for vibration-based monitoring. Currently this is possible only for small laboratory specimens since the definition of the POD requires data measured in the damaged configuration which might not be always possible when working on large structural components
Acoustic emission monitoring	Capacity to detect active damage; localization; high sensitivity; global inspection with necessary access only at specific points on the surface; ability to characterize the type/mode of damage; and passive, not necessary to inject signal	Prone to noise; influenced by sample size and sensor distance and sensitivity; transfer of conclusions from the laboratory to real size and interpretation not straightforward
Strain-based monitoring	Strains allow the measurement of the loads of an aircraft component or system; Optical fibers sensors for strain measurement can be fully integrated in a component, especially in composite materials	Strain sensors (gauges and OFS) are brittle and should be protected (with a coating)

10.4 Roadmap for SHM Integration in Future Aircraft

The modern aircraft manufacturing technology aims to further increase the production rates to the amount of 60–100 planes a month (at least 2 planes a day) with even more serious reduction in weight, cost, waste, environmental impact and assembly time. To achieve this, a composite manufacturing technology is changing rapidly, going from hand layup and automated fibre placement (AFP) technologies to resin transfer molding (RTM), high pressure HP-RTM, thermoplastic composites, hybrid metal-composite structures and 3D printed parts. The more advanced technologies like HP-RTM are already implemented in some parts of an aircraft, i.e. manufacturing of Airbus A330/A340 spoilers, Airbus A350 passenger doors and surrounding frames. Such manufacturing technology allow to achieve approx. 30% cost reduction and increase of the production efficiency by 10–20%. The production efficiency can also be increased with thermoplastic composite technology which allow greater integration of structural elements by using thermoplastic joining technologies like overmolding and welding. This will reduce the amount of assembly steps, eliminate some rivets and fasteners, resulting in reduced overall manufacturing cost. Thermoplastic composite materials are up to 10 times lighter than metals, are temperature, chemical and corrosion resistant, have better design flexibility and fatigue properties. Another example of the automation is the emerging additive manufacturing (AM) technology. The new Boeing 777X aircraft will have GE9X engine which consists of 304 separate additively manufactured parts like low pressure turbine blades, heat exchanger, combustor mixer, fuel nozzle etc. The AM technology allowed to combine multiple parts into single one since the shape of the part is no longer limited like in the conventional manufacturing methods such as stamping and casting. The production of the modern aircraft clearly seeks faster, cheaper production, increased automation, reduced weight and fuel consumption of an aircraft. Inevitably this can be achieved by using composites and modern manufacturing technologies only. This drastically changes the design process, meaning that the NDT technologies will have to adapt.

As a result of the comprehensive assessment of different methods presented in this book, several targets must be achieved that are common to all methods and individually for each method. For all methods, the roadmap to SHM implementation in aircrafts should start at the hotspots, implementing sensors with a minimum of changes to the structure first. One should think about simple, but effective solutions because complex integration solutions will require time and contribute to weight, and the operation of such solutions might be error-prone and not cost-effective, even requiring additional maintenance needs. The first approach could be to use off-line sensor systems, being able to upgrade later to on-line sensor systems and perspective to fully integrated sensors. Smart structures with integrated sensing capabilities should be developed to reduce weight and cost. SHM approaches must be standardized, including sensors, sensor application, and integration into the systems, as well as subsequent algorithms. Last but not the least, certification costs are an important factor as well.

Guided waves offer many advantages over other existing techniques to be used in SHM. They involve a rather complex technique that requires much a-priori knowledge about the structure and the propagation of guided waves. Consequently, it offers tremendous sensitivity to structural changes and may be used for a huge variety of objects. To simplify the guided wave inspection, additional tools are required, which can monitor environmental factors or adjust inspection parameters dynamically. Hence, the guided wave inspection may be seen as a part of a smart inspection system that uses different sensors and signal processing algorithms that communicate with each other. The creation of an inspection ecosystem with wireless communications, real-time signal processing boards, and regulations for calibration, verification, and reference cases (baselines) are the main development areas for a successful integration of guided wave techniques.

Vibration-based methods provide a tool for damage detection at a global level, which does not require prior knowledge of the damage location. Currently, the uncertainty connected with measurements and modeling errors still hinder their large-scale application under operational environmental conditions. The development of low-cost wireless sensors and procedures for real-time processing is a requirement, as well as standardization, for their further development.

The potential of contribution of AE technique in SHM is high. AE analyses may provide a relatively simple and fast platform for damage detection. However, difficulties with interfering noise, data interpretation, inability to understand the underlying physical mechanism in real applications, and the lack of standardization prevent widespread application. Wireless systems may be a potential direction to reduce the whole system weight, which is a crucial factor for aviation. Recording whole waveforms for an elaborate analysis for source identification may require much memory power and time, but will greatly upgrade the assessment. Basic features like damage detection and localization are more mature because they can go forward only with a representative reduced dataset.

Apart from typical applications, such as load monitoring and low-frequency vibration monitoring, strain-based structural health monitoring can be used for shape sensing and prognosis of damage-based on the fatigue behavior of the component. Some implementations of shape sensing have been performed in the morphing wings of aircrafts using fiber optic strain sensors, where a long length of optical fiber covers the wing area and measures the strain behavior of the wing during flight and disturbances. By monitoring this strain behavior, the fatigue life of the wings can be assessed and used to optimize scheduled maintenances. In this example, the optical fibers were surface mounted on the wing structure. However, the installation of the electrical strain gauges or fiber optics can be improved by embedding them either in the internal layers of the structure or its walls. Furthermore, technological advances in increasing the signal acquisition rates and improving the signal-to-noise ratio of acquired strain values, as well as improvements in big data management can also boost the relevance of these methods.

10.5 Future Research Directions

Finally, we would like to summarize the key items identified for a further development of the SHM methods discussed in this book.

One of the key objectives for all methods are automated data analysis systems, which require advanced signal processing algorithms. As elaborated in Chap. 9, this will enable the diagnosis of problems and the initiation of high-level decisions.

With the advent of machine learning methods, the large amounts of data generated by guided wave SHM systems can be exploited in trying to estimate features and dependencies between the parameters of guided waves and properties of defects that cannot be observed by a human. This will gradually open new horizons for guided wave inspection and data interpretation. The risks of biased predictions will remain high, and the in-situ performance of such models will have to be carefully verified. Another development area is the extraction of more advanced defect features, such as through thickness positions, severity of damage, and remaining lifetime of the structure, which would allow the implementation of a true condition-based inspection of engineering assets in aircrafts.

For vibration-based monitoring, the identification of features more sensitive to damage and less affected by environmental sources is a stringent research need. The development of low-cost wireless sensors systems is another important aspect necessary for their application to inflight monitoring. Standardization is another requirement to pave the way to a larger usage of these techniques.

An interesting research direction for acoustic emission monitoring is the prediction of the type of damage before severe defects actually occur. Past research has shown that the developed strain, even at a low load, leaves its signature to the AE recordings, even before the actual crack manifestation. This demonstrates the huge potential of the method. However, an important point is the compensation of the signal against the distortion caused by the long propagation through heterogeneous, dispersive media like composite or metal plates, as used in aeronautics. This would allow a clearer assessment of the source, the elimination of a large amount of error that is now included in the waveforms, masking the original source content. Technical issues like wireless transmission speed and capacity and power requirements are also open for optimization.

Strain-based structural health monitoring can benefit from in-depth research in several aspects. On the mechanical side, optimizing the sensor placement and concentrating them on the more sensitive areas, along with optimizing the embedment procedure to avoid risking the health of sensors and changing the aerodynamics of the structures, can be among the most relevant research topics. On the data-processing part, the reliability of the prognosis algorithms and big data management, along with improvements in signal processing algorithms, can be investigated. Incorporating machine learning approaches can also be beneficial in this area and is certainly an interesting research topic.

While each method has acquired technological development within many decades, much potential is left for further research. With some current mega-trends out of the field of artificial intelligence, as well as microfabrication of sensor systems and electronics, there is a huge playground to push SHM methods beyond the current limits. Ultimately, these shall provide highly integrated system solutions and a true benefit for the safe operation of aircraft.

Open Access This chapter is distributed under the terms of the Creative Commons Attribution 4.0 International License (<http://creativecommons.org/licenses/by/4.0/>), which permits use, duplication, adaptation, distribution and reproduction in any medium or format, as long as you give appropriate credit to the original author(s) and the source, a link is provided to the Creative Commons license and any changes made are indicated.

The images or other third party material in this chapter are included in the work's Creative Commons license, unless indicated otherwise in the credit line; if such material is not included in the work's Creative Commons license and the respective action is not permitted by statutory regulation, users will need to obtain permission from the license holder to duplicate, adapt or reproduce the material.

